

2013

# Cyclic block copolypeptoids : synthesis, self-assembly and macroscopic properties

Chang-Uk Lee

Louisiana State University and Agricultural and Mechanical College, clee59@lsu.edu

Follow this and additional works at: [https://digitalcommons.lsu.edu/gradschool\\_dissertations](https://digitalcommons.lsu.edu/gradschool_dissertations)



Part of the [Chemistry Commons](#)

---

## Recommended Citation

Lee, Chang-Uk, "Cyclic block copolypeptoids : synthesis, self-assembly and macroscopic properties" (2013). *LSU Doctoral Dissertations*. 1964.

[https://digitalcommons.lsu.edu/gradschool\\_dissertations/1964](https://digitalcommons.lsu.edu/gradschool_dissertations/1964)

This Dissertation is brought to you for free and open access by the Graduate School at LSU Digital Commons. It has been accepted for inclusion in LSU Doctoral Dissertations by an authorized graduate school editor of LSU Digital Commons. For more information, please contact [gradetd@lsu.edu](mailto:gradetd@lsu.edu).

CYCLIC BLOCK COPOLYPEPTOIDS:  
SYNTHESIS, SELF-ASSEMBLY AND MACROSCOPIC PROPERTIES

A Dissertation

Submitted to the Graduate Faculty of the  
Louisiana State University and  
Agricultural and Mechanical College  
in partial fulfillment of the  
requirements for the degree of  
Doctor of Philosophy

in

The Department of Chemistry

by  
Chang-Uk Lee  
B.S., Pusan National University, 2004  
M.S., University of Tennessee, 2006  
May 2013

## ACKNOWLEDGMENTS

I would like to thank Professor Donghui Zhang for her supervision and help to make this research possible. I thank my advisory committee, Professor Paul Russo, Professor David Spivak, Professor Jayne Garno, and Professor James Oard for their time and assistance. I would like to thank my lab colleagues, Dr. Li Guo, Sam Lahasky, Wayne Huberty, Brandon Chan, Lu Lu, Jinbao Cao, Ang Li, Sunting Xuan, Jessica Simpson, Ashley Taylor, Albert Chao, Monika Lavan, and Kushal Ghale, for their camaraderie and discussions during this research. Special thanks to Sam, Wayne, and Brandon for proofreading chapters of this dissertation.

I thank Dr. Rafael Cueto for helping me to do DSC, TGA, DLS, and SEC experiments. I thank Dr. Thomas Smart and Professor Thomas Epps, III at the University of Delaware for conducting Cryo-TEM and light scattering experiments and for helpful discussions. I thank Dr. Jihua Chen at Oak Ridge National Laboratory for conducting SAED experiments. I thank Professor Vince LiCata in the Department of Biological Sciences for allowing me to use the VP-DSC instrument and helpful discussions. I thank Professor Qinglin Wu in School of Renewable Natural Resources for allowing me to use a rheometer. Many thanks to Melissa Collins for helping me to do WAXS and SAXS experiments. I thank staffs, Andrew Weber and Henning Lichtenberg in the SAXS beamline at CAMD.

I would like to thank my family. I thank my parents, Byungmun Lee and Jungja Doh for their love and support. I thank my sisters, Kyungmi Lee, Sunhwa Lee, and Kyunga Lee who always give me confidence. I thank my parents in law, Donghyuk Park and Mirang Hwang for their love and support. I thank my brother in law, Jegwan Park, for his encouragement.

Finally, I thank my wife, Soyoung Park, for supporting and trusting me during time for my Ph.D. studies. Without her, this work would not be possible. I thank my son, Seojun Lee, for being with me and my wife and his smile.

## TABLE OF CONTENTS

ACKNOWLEDGMENTS .....	ii
LIST OF TABLES .....	vii
LIST OF FIGURES .....	viii
LIST OF SCHEMES .....	xiv
TABLE OF ABBREVIATIONS .....	xv
ABSTRACT .....	xvii
<b>CHAPTER 1. INTRODUCTION TO CYCLIC BLOCK COPOLYPEPTOIDS</b> .....	<b>1</b>
1.1 Introduction to cyclic polymers .....	1
1.1.1 Cyclic polymers: distinct properties and benefits over linear counterparts .....	1
1.1.2 Synthetic strategies to prepare cyclic polymers .....	3
1.2 Introduction to peptoids and polypeptoids .....	6
1.2.1 Peptoids as a peptidomimetic material: benefits over peptides.....	6
1.2.2 Synthesis of oligomeric peptoids and polypeptoids .....	7
1.2.3 Structures and physical properties of peptoids and polypeptoids .....	9
1.3 Introduction to block copolymers .....	10
1.3.1 Self-assembly of block copolymers in dilute solution .....	11
1.4 Synthesis of cyclic block copolymers .....	14
1.5 Synthesis of cyclic peptoids .....	15
1.6 Investigation on cyclic block copolypeptoids .....	16
<b>CHAPTER 2. CYCLIC DIBLOCK COPOLYPEPTODIS: SYNTHESIS, SELF-ASSEMBLY AND MACROSCOPIC PROPERTIES</b> .....	<b>23</b>
2.1 Synthesis and characterization of cyclic poly( <i>N</i> -methyl-glycine)- <i>b</i> -poly( <i>N</i> -decyl-glycine) diblock copolymers .....	23
2.1.1 Experimental .....	23
2.1.1.1 Materials .....	23
2.1.1.2 Instrumentations and sample preparation .....	23
2.1.1.3 Synthesis of monomers .....	25
2.1.1.4 Synthesis of polymers .....	27
2.1.2. Results and discussion.....	30
2.1.2.1 Synthesis and characterization of cyclic poly( <i>N</i> -decyl-glycine)s ( <i>c</i> -PNDGs) .....	30
2.1.2.2 Synthesis and characterization of <i>c</i> -PNMG- <i>b</i> -PNDG diblock copolymers .....	41
2.2 Self-Assembly of <i>c</i> -PNMG- <i>b</i> -PNDG diblock copolymers in dilute solution: crystallization-driven formation of cylindrical micelles from spherical micelles over time .....	46
2.2.1 Experimental .....	46
2.2.2 Results and discussion.....	48

2.2.2.1 Cryo-TEM and light scattering .....	48
2.2.2.2 Selected area electron diffraction (SAED) .....	52
2.2.2.3 Ultrasensitive microcalorimetry differential scanning calorimetry (US-DSC) .....	52
2.2.2.4 Variable-temperature NMR spectroscopy .....	53
2.3 Crystallization-driven, thermo-reversible gelation from <i>c</i> -PNMG- <i>b</i> -PNDG diblockcopolypeptoids .....	55
2.3.1 Introduction .....	55
2.3.2 Experimental .....	57
2.3.2.1 Synthesis of cyclic or linear PNMG- <i>b</i> -PNDGs .....	57
2.3.2.2 Synthesis of cyclic poly( <i>N</i> -methyl-glycine)- <i>b</i> -poly( <i>N</i> -2-ethyl-1-hexyl -glycine) diblock copolymers ( <i>c</i> -PNMG- <i>b</i> -PNEHG) .....	58
2.3.2.3 Preparation for gels from PNMG- <i>b</i> -PNDGs .....	59
2.3.2.4 Instrumentations .....	60
2.3.3 Results and discussion .....	62
2.3.3.1 Thermo-reversible gelation from PNMG- <i>b</i> -PNDG .....	62
2.3.3.2 Viscoelastic properties of gels .....	63
2.3.3.3 Variable-temperature <sup>1</sup> H NMR analysis of gels .....	66
2.3.3.4 POM of gels .....	69
2.3.3.5 DSC of gels .....	70
2.3.3.6 WAXS of gels .....	71
2.3.3.7 SAXS of gels .....	72
2.3.3.8. Variable-time WAXS and SAXS analyses of gels .....	74
2.3.3.9 AFM of gels .....	75
2.3.3.10 Effect of crystallization of core-forming hydrophobic segments on the gelation .....	77

CHAPTER 3. CYCLIC TRIBLOCK TERPOLYPEPTOIDS: SYNTHESIS AND SELF- ASSEMBLY .....	78
3.1 Introduction .....	78
3.2 Cyclic poly( <i>N</i> -methyl-glycine)- <i>b</i> -poly( <i>N</i> -allyl-glycine)- <i>b</i> -poly( <i>N</i> -benzyl-glycine) triblock terpolypeptoids .....	82
3.2.1 Experimental .....	82
3.2.2 Results and discussion .....	83
3.2.2.1 Synthesis of cyclic PNMG-PNAG-PNBnG triblock terpolymers with controlled chain length and compositions .....	83
3.3 Cyclic [poly( <i>N</i> -ethyl-glycine)- <i>ran</i> -poly( <i>N</i> -butyl-glycine)]- <i>b</i> -poly( <i>N</i> -methyl-glycine)- <i>b</i> - poly( <i>N</i> -decyl-glycine) triblock terpolypeptoids .....	86
3.3.1 Experimental .....	86
3.3.1.1 Synthesis of cyclic [P(NEG- <i>ran</i> -NBG)]-PNMG-PNDG triblock terpolymers .....	86
3.3.1.2 Sample preparation for DLS and TEM .....	87
3.3.2 Results and discussion .....	88
3.3.2.1 Synthesis and characterization of thermo-responsive triblock terpolypeptoids .....	88
3.3.2.2 Micellar aggregation from cyclic [P(NEG <sub>20</sub> - <i>ran</i> -NBG <sub>15</sub> )]-PNMG <sub>16</sub> -PNDG <sub>5</sub>	

triblock terpolymers.....	90
CHAPTER 4. CRYSTALLIZATION AND MELTING BEHAVIOR OF CYCLIC OR LINEAR POLYPEPTOIDS WITH VARIOUS ALKYL SIDE CHAINS.....	93
4.1 Introduction.....	93
4.2 Experimental.....	95
4.2.1 Synthesis of monomers and their NMR spectra.....	95
4.2.2 Synthesis of cyclic or linear poly( <i>N</i> -alkyl-glycine)s.....	100
4.2.3 Instrumentations and sample preparation for characterization .....	104
4.3 Results and discussion.....	105
4.3.1 DSC of cyclic or linear polypeptoids with various <i>n</i> -alkyl side chains .....	105
4.3.1.1 Effect of architecture of polymers, i.e. cyclic or linear on melting and crystallization of polypeptoids.....	114
4.3.2 WAXS of cyclic or linear polypeptoids with various <i>n</i> -alkyl side chains .....	115
4.3.3 Effect of branching of side groups on melting and crystallization of polypeptoids .....	119
4.3.4 Effect of annealing temperature on molecular packing of polypeptoids .....	121
4.3.5 Decomposition temperatures of cyclic or linear polypeptoids.....	123
CHAPTER 5. CONCLUSIONS AND FUTURE WORK.....	125
REFERENCES .....	129
VITA.....	137

## LIST OF TABLES

Table 2.1. NHC-mediated zwitterionic polymerizations of decyl-NCA ( $M_1$ ). <sup>a</sup> .....	32
Table 2.2. Melting temperature and heat of fusion of <i>c</i> -PNDGs with different MWs. ....	39
Table 2.3. Crystallization temperature and heat of fusion of <i>c</i> -PNDGs with different MWs. ....	39
Table 2.4. Compositions and molecular weights of <i>c</i> -PNMG- <i>b</i> -PNDG block copolymers. <sup>a</sup> .....	45
Table 2.5. Molecular parameters of <i>c/l</i> -PNMG- <i>b</i> -PNDG diblock copolymers presented in section 2.3.....	58
Table 3.1. Compositions and molecular weights of cyclic PNMG-PNAG-PNBnG triblock terpolymers. <sup>a</sup> .....	85
Table 3.2. Compositions and polymer MWs of cyclic [P(NEG- <i>ran</i> -NBG)]-PNMG-PNDG triblock terpolymers. <sup>a</sup> .....	89
Table 4.1. Alkyl side chains of polypeptoids studied in chapter 4. ....	101
Table 4.2. DSC results of cyclic or linear polypeptoids with various alkyl side chains: melting temperature ( $T_m$ ), crystallization temperature ( $T_c$ ), enthalpy change during melting ( $\Delta H_m$ ), enthalpy change during crystallization ( $\Delta H_c$ ), decomposition temperature ( $T_d$ ), and glass transition temperature ( $T_g$ ). .....	107



## LIST OF FIGURES

Figure 1.1. Electron micrograph of polyoma DNA, naturally-occurring cyclic macromolecules (copied from reference 2).....	1
Figure 1.2. Scheme of synthetic strategies to prepare cyclic polymers (reproduced from reference 18). .....	4
Figure 1.3. N-heterocyclic carbene(NHC)-mediated zwitterionic polymerization of lactide (copied from reference 8).....	5
Figure 1.4. Molecular structure of polypeptides and various polypeptoids.....	6
Figure 1.5. A stepwise method to prepare oligomeric peptoids (reproduced from reference 30 and 31). .....	7
Figure 1.6. Self-assembly of diblock copolymers as spherical, cylindrical, and bilayer micelles in a selective solvent for one block (modified from reference 52). .....	11
Figure 1.7. Schematic illustration of contributing forces to formation of micelles from block copolymers and the packing parameter discussed in the text (modified from reference 53 and 54). .....	12
Figure 1.8. An illustration to summarize investigation on cyclic block copolypeptoids in this dissertation. ....	18
Figure 2.1. $^1\text{H}$ and $^{13}\text{C}\{^1\text{H}\}$ NMR spectra of (A) 2-( <i>n</i> -decylamino)acetic acid hydrochloride (1) in <i>d</i> -DMSO and of (B) 2-( <i>N,N</i> - <i>tert</i> -butoxycarbonyl- <i>n</i> -decylamino)acetic acid (2) in $\text{CDCl}_3$ .....	30
Figure 2.2. $^1\text{H}$ and $^{13}\text{C}\{^1\text{H}\}$ NMR spectra of decyl-NCA in $\text{CDCl}_3$ .....	31
Figure 2.3. $^1\text{H}$ and $^{13}\text{C}\{^1\text{H}\}$ NMR spectra of high MW <i>c</i> -PNDGs in $\text{CDCl}_3/\text{CF}_3\text{COOD}$ . .....	33
Figure 2.4. Representative ESI MS spectra of a low MW cyclic PNDG sample synthesized from NHC-mediated ring-opening polymerization of decyl-NCA. ....	34
Figure 2.5. SEC chromatograms of (A) high MW <i>c</i> -PNDGs ( $M_n = 20.4 \text{ kg}\cdot\text{mol}^{-1}$ , PDI = 1.20) and (B) <i>l</i> -PNDGs ( $M_n = 20.8 \text{ kg}\cdot\text{mol}^{-1}$ , PDI = 1.09) that were independently prepared from the NHC-mediated and $\text{BuNH}_2$ -initiated polymerization of decyl-NCA. ....	35
Figure 2.6. SEC chromatograms of <i>c</i> -PNDGs prepared from NHC-mediated polymerization of decyl ( $[\text{M}]_0:[\text{NHC}]_0 =$ (A) 25:1, (B) 50:1, (C) 100:1, and (D) 200:1).....	36
Figure 2.7. $^1\text{H}$ NMR spectrum of a low MW <i>c</i> -PNDG in $\text{CDCl}_3/\text{CF}_3\text{COOD}$ where proton resonances of the NHC are notably visible.....	36

Figure 2.8. Representative  $^1\text{H}$  NMR spectrum of a NHC-mediated polymerization of  $M_1$  at  $70\text{ }^\circ\text{C}$  in toluene- $d_8$  showing the formation of *c*-PNDG and unreacted  $M_1$  ( $[\text{M}_1]_0:[\text{NHC}]_0 = 50:1$ ,  $[\text{M}_1]_0 = 0.4\text{ M}$ , reaction time = 62 min). ..... 37

Figure 2.9. (A) Plots of  $\ln([\text{M}_1]_0/[\text{M}_1])$  as a function of the reaction time and their linear fits for the NHC-mediated polymerizations of decyl-NCA at  $70\text{ }^\circ\text{C}$  in toluene- $d_8$  at three different initial NHC concentrations (i.e.,  $[\text{NHC}]_0 = 3$  (●),  $8$  (▲),  $16\text{ mM}$  (■)), and a constant initial monomer to NHC concentration (i.e.,  $[\text{M}_1]_0:[\text{NHC}]_0 = 50:1$ ). (B) Plot of the observed rate constant ( $k_{\text{obs}}$ ) as a function of the initial NHC concentration and its linear fit. .... 37

Figure 2.10. The plot of polymer molecular weights ( $M_n$ ) (■) determined by SEC-MALS-DRI or  $M_n$  (▲) by  $^1\text{H}$  NMR analysis and PDI (●) of *c*-PNDGs as a function of conversion for the NHC-mediated polymerization of decyl-NCA in THF at  $70\text{ }^\circ\text{C}$  ( $[\text{M}_2]_0:[\text{I}]_0 = 150:1$  or  $50:1$ ,  $[\text{M}_2]_0 = 0.4\text{ M}$ ). Note: aliquots of the polymerization solution ( $[\text{M}_2]_0:[\text{I}]_0 = 150:1$ ) was taken, filtered and directly injected into SEC columns for the MW determination over the course of reaction. 38

Figure 2.11. (A) DSC thermograms of *c*-PNDGs having different molecular weights from the second heating cycle. (B) Plots of two melting points ( $T_{m,1}$ ,  $T_{m,2}$ ) as a function of molecular weights of the polymers. .... 39

Figure 2.12. DSC thermograms of *c*-PNDGs having different molecular weights collected from the first cooling cycle. .... 39

Figure 2.13. (A) WAXS diffractogram of a thermally annealed *c*-PNDG sample in the solid state ( $M_n = 7.7\text{ kg}\cdot\text{mol}^{-1}$ ,  $\text{PDI}=1.26$ ) at room temperature and (B) the proposed crystalline packing of *c*-PNDGs based on WAXS data. .... 41

Figure 2.14. SEC traces of (A) *c*-PNMG<sub>105</sub>, and (B) *c*-PNMG<sub>105</sub>-*b*-PNDG<sub>15</sub>. .... 42

Figure 2.15.  $^1\text{H}$  NMR spectra of a series of cyclic diblock copolymers with various compositions: (1) PNMG<sub>105</sub>-*b*-PNDG<sub>10</sub> in  $\text{CD}_3\text{OD}$ , and (2) PNMG<sub>105</sub>-*b*-PNDG<sub>25</sub>, (3) PNMG<sub>105</sub>-*b*-PNDG<sub>50</sub>, and (4) PNMG<sub>105</sub>-*b*-PNDG<sub>125</sub> in  $\text{CDCl}_3/\text{CF}_3\text{COOD}$ . .... 44

Figure 2.16.  $^{13}\text{C}\{^1\text{H}\}$  NMR spectra of *c*-PNMG<sub>105</sub>-*b*-PNDG<sub>50</sub> in  $\text{CDCl}_3/\text{CF}_3\text{COOD}$ . .... 44

Figure 2.17.  $^1\text{H}$  NMR spectrum of *c*-PNMG<sub>72</sub>-*b*-PNDG<sub>8</sub> diblock copolymers in MeOD, where proton resonances of the NHC are notably visible. .... 45

Figure 2.18. Turbidity measurements of both linear and cyclic PNMG<sub>105</sub>-*b*-PDMG<sub>10</sub> solutions in methanol over the first two days after preparation. .... 49

Figure 2.19. Representative cryo-TEM images obtained from dilute methanol solutions of cyclic PNMG<sub>105</sub>-*b*-PNDG<sub>10</sub> block copolypeptoids after (A) 1 h, (B) 2 h, and (C) 15 d, and linear PNMG<sub>112</sub>-*b*-PNDG<sub>16</sub> block copolypeptoids after (D) 1 h, (E) 2 h, and (F) 7 d in methanol. .... 49

Figure 2.20. SEC-DRI chromatograms of (A) cyclic PNMG <sub>105</sub> - <i>b</i> -PNDG <sub>15</sub> diblock copolymers obtained after 17 days in methanol (---) and the original sample (—). .....	51
Figure 2.21. SAED patterns of (A) spherical and (B) cylindrical micelles obtained by the self-assembly of <i>c</i> -PNMG <sub>100</sub> - <i>b</i> -PNDG <sub>10</sub> in methanol (1.0 mg·mL <sup>-1</sup> ) after aging for 15 min and 14 d at room temperature, respectively.....	52
Figure 2.22. Microcalorimetric endotherms for <i>c</i> -PNMG <sub>100</sub> - <i>b</i> -PNDG <sub>10</sub> diblock copolymers in methanol (1 mg·mL <sup>-1</sup> ) during heating, after aging (A) for 15 min and (B) for 2 weeks at room temperature. ....	53
Figure 2.23. <sup>1</sup> H NMR spectra of <i>c</i> -PNMG <sub>100</sub> - <i>b</i> -PNDG <sub>10</sub> in CD <sub>3</sub> OD (0.2 wt %) after aging for 2 weeks at 25, 45 and 65 °C, the ratio of integration from PNDG methyl protons to that of PNMG methyl protons as a function of temperature, and a sigmoidal fit of the data.....	54
Figure 2.24. Thermo-responsive gelation from <i>c/l</i> -PNMG <sub>100</sub> - <i>b</i> -PNDG <sub>10</sub> diblock copolymers in methanol at a concentration of 2, 5, and 10 wt %.....	62
Figure 2.25. Storage modulus (G') and loss modulus (G'') of gels from <i>c</i> -PNMG <sub>100</sub> - <i>b</i> -PNDG <sub>10</sub> diblock copolymers in methanol (2, 5 or 10 wt %) as a function of angular frequency (ω) at a strain amplitude of γ = 1.0 % at 25 °C.....	64
Figure 2.26. G' and G'' of gels from <i>c/l</i> -PNMG <sub>100</sub> - <i>b</i> -PNDG <sub>10</sub> diblock copolymers in methanol at a concentration of (A) 5 wt % and (B) 2 wt % as a function of angular frequency (ω) at a strain amplitude of γ = 1.0 % at 25 °C.....	65
Figure 2.27. (A) Storage modulus (G') and loss modulus (G'') of gels from <i>c</i> -PNMG <sub>100</sub> - <i>b</i> -PNDG <sub>10</sub> diblock copolymers in methanol (5 wt %) as a function of strain amplitude (γ <sub>0</sub> ) at a frequency of 10 (rad·s <sup>-1</sup> ) at 25 °C, (B) the calculated elastic stress (σ' = G'γ) as a function of strain.....	65
Figure 2.28. Steady-state flow rheological data of gels from cyclic or linear PNMG <sub>100</sub> - <i>b</i> -PNDG <sub>10</sub> diblock copolymers in methanol (2 wt or 5 wt %)......	66
Figure 2.29. <sup>1</sup> H NMR spectra of gels from (A) <i>c</i> -PNMG <sub>100</sub> - <i>b</i> -PNDG <sub>10</sub> and (B) <i>l</i> -PNMG <sub>100</sub> - <i>b</i> -PNDG <sub>10</sub> in CD <sub>3</sub> OD (5 wt %) at 25, 45, and 65 °C.....	67
Figure 2.30. The ratio of integration of methyl protons of PNDGs ( <i>a</i> in Figure 2.29) to that of methyl protons of PNMGs ( <i>b</i> in Figure 2.29) in gels from cyclic or linear PNMG <sub>100</sub> - <i>b</i> -PNDG <sub>10</sub> as a function of temperature, and sigmoidal fits from experimental data.....	67
Figure 2.31. Full <sup>1</sup> H NMR spectra of gels from <i>c</i> -PNMG <sub>100</sub> - <i>b</i> -PNDG <sub>10</sub> diblock copolymers in CD <sub>3</sub> OD (5 wt %) at 25 (bottom), 45, and 65 °C. ....	69
Figure 2.32. POM images of gels from <i>c</i> -PNMG <sub>100</sub> - <i>b</i> -PNDG <sub>10</sub> diblock copolymers in methanol (5 wt %) (A) at room temperature and (B) at 55 °C.....	70

Figure 2.33. DSC of *c*-PNMG<sub>100</sub>-*b*-PNDG<sub>10</sub> diblock copolymer gels in methanol (10 wt %) (A) during first heating, and (B) during first cooling. .... 71

Figure 2.34. WAXS diffractograms of gels from (A) *c*-PNMG<sub>100</sub>-*b*-PNDG<sub>10</sub> and (B) *l*-PNMG<sub>100</sub>-*b*-PNDG<sub>10</sub> in methanol at 10 wt %. .... 72

Figure 2.35. (A) SAXS diffractograms of gels from cyclic or linear PNMG<sub>100</sub>-*b*-PNDG<sub>10</sub> (10 wt % in methanol), (B) the Guinier plot ( $\ln[I(q)q]$  as a function of  $q^2$ ) of the SAXS data of gels from the copolymers. (The inset graphs are the linear fits of the data in the Guinier region,  $q < 0.03 \text{ \AA}^{-1}$ ), and (C) the plot of  $\log I(q)$  as a function of  $q^2$ . .... 74

Figure 2.36. (A) WAXS diffractograms of gels from *c*-PNMG<sub>100</sub>-*b*-PNDG<sub>10</sub> in methanol (10 wt %) after 15 m, 40 m, 2 h and 20 h (B) SAXS diffractograms after 10 m, 70 m and 20 h after heating to 70 °C and cooling to room temperature. .... 75

Figure 2.37. Gels from cyclic PNMG<sub>100</sub>-*b*-PNDG<sub>10</sub> (1 wt %) viewed with tapping-mode AFM. (a) Topograph  $3 \times 3 \text{ \mu m}^2$ ; and (b) corresponding phase image. (c) Zoom-in topograph ( $1.5 \times 1.5 \text{ \mu m}^2$ ) and (d) corresponding phase image. .... 76

Figure 2.38. Gels from linear PNMG<sub>100</sub>-*b*-PNDG<sub>10</sub> (5 wt %) viewed with tapping-mode AFM. (a) Topograph  $6 \times 6 \text{ \mu m}^2$ ; (b) corresponding phase image. .... 76

Figure 2.39. Poly(*N*-methyl-glycine)<sub>100</sub>-*b*-poly(*N*-2-ethyl-1-hexyl-glycine)<sub>15</sub> diblock copolymers in methanol at 10 wt %. .... 77

Figure 3.1. <sup>1</sup>H and <sup>13</sup>C{<sup>1</sup>H} NMR spectra of cyclic PNMG<sub>144</sub>-PNAG<sub>25</sub>-PNBnG<sub>25</sub> triblock terpolymers in CDCl<sub>3</sub>/CF<sub>3</sub>COOD. .... 84

Figure 3.2. SEC traces of (A) cyclic PNMG<sub>144</sub>, (---), (B) cyclic PNMG<sub>144</sub>-*b*-PNAG<sub>25</sub> diblock copolymers (---), and (C) cyclic PNMG<sub>144</sub>-PNAG<sub>25</sub>-PNBnG<sub>25</sub> triblock terpolymers (—). .... 86

Figure 3.3. <sup>1</sup>H NMR spectrum of [P(NEG<sub>20</sub>-*ran*-NBG<sub>15</sub>)]-PNMG<sub>48</sub>-PNDG<sub>10</sub> triblock terpolymers in CDCl<sub>3</sub>. .... 89

Figure 3.4. SEC traces of (A) cyclic P(NEG<sub>47</sub>-*ran*-NBG<sub>21</sub>) (---), (B) [P(NEG<sub>47</sub>-*ran*-NBG<sub>21</sub>)]-PNMG<sub>128</sub>(---), and (C) [P(NEG<sub>47</sub>-*ran*-NBG<sub>21</sub>)]-PNMG<sub>128</sub>-PNDG<sub>13</sub> triblock terpolymers (—). 90

Figure 3.5. TEM image from cast film prepared from aqueous solution of cyclic [P(NEG<sub>20</sub>-*ran*-NBG<sub>15</sub>)]-PNMG<sub>16</sub>-PNDG<sub>5</sub> triblock terpolymer (1.0 mg·mL<sup>-1</sup>) at room temperature. (A TEM sample was negatively stained with uranyl formate aqueous solution.) .... 91

Figure 3.6. Apparent micelle size distributions of cyclic P(NEG<sub>20</sub>-*ran*-NBG<sub>15</sub>)-PNMG<sub>16</sub>-PNDG<sub>5</sub> triblock copolymers in water (1.0 mg·mL<sup>-1</sup>) (A) while heating after filtering through a 20 nm filter, (B) cooling, and (C) reheating after aging for 2 days at room temperature. .... 91

Figure 3.7. (A) $R_h$ and (B) PDI (broadness of $R_h$ distribution) of cyclic [P(NEG <sub>20</sub> - <i>ran</i> -N BG) <sub>15</sub> ]-PNMG <sub>16</sub> ]-PNDG <sub>5</sub> triblock terpolymer micelles as a function of temperature.....	92
Figure 4.1. <sup>1</sup> H NMR spectra of (A) hexyl-NCA, (B) octyl-NCA, (C) dodecyl-NCA, and (D) tetradecyl-NCA in CDCl <sub>3</sub> . .....	96
Figure 4.2. <sup>1</sup> H NMR spectra of (A) (2-ethyl-1-hexylamino)acetate (1) and (B) (2-ethyl-1-hexylamino)acetic acid hydrochloride (2). .....	98
Figure 4.3. <sup>1</sup> H and <sup>13</sup> C{ <sup>1</sup> H} NMR spectra of 2-ethyl-1-hexyl-NCA in CDCl <sub>3</sub> . .....	99
Figure 4.4. <sup>1</sup> H and <sup>13</sup> C{ <sup>1</sup> H} NMR spectra cyclic poly( <i>N</i> -2-ethyl-1-hexyl-glycine)s in CDCl <sub>3</sub> . ..	102
Figure 4.5. <sup>1</sup> H NMR spectra of (A) <i>c</i> -PNEG, (B) <i>c</i> -PNHG, and (C) <i>c</i> -PNOG in CDCl <sub>3</sub> .....	104
Figure 4.6. <sup>1</sup> H NMR spectra of (A) <i>c</i> -PNDDG and (B) <i>c</i> -PNTG in CDCl <sub>3</sub> . .....	104
Figure 4.7. DSC thermograms of (I) cyclic or (II) linear poly( <i>N</i> - <i>n</i> -alkyl-glycine)s during second heating ( <i>n</i> in the Figure is the number of carbons on <i>n</i> -alkyl side chains). .....	108
Figure 4.8. DSC thermograms of (I) cyclic or (II) linear poly( <i>N</i> - <i>n</i> -alkyl-glycine)s during first cooling ( <i>n</i> in the Figure is the number of carbons on <i>n</i> -alkyl side chains). .....	109
Figure 4.9. (A) $T_{m,1}$ and $T_{m,2}$ , and (B) $T_{c,1}$ and $T_{c,2}$ of of cyclic or linear poly( <i>N</i> - <i>n</i> -alkyl-glycine)s with various <i>n</i> -alkyl side chains.....	113
Figure 4.10. (A) $\Delta H_{m,1}$ and $\Delta H_{m,2}$ , and (B) $\Delta H_{c,1}$ and $\Delta H_{c,2}$ of cyclic or linear poly( <i>N</i> - <i>n</i> -alkyl-glycine)s with various <i>n</i> -alkyl side chains. ....	113
Figure 4.11. WAXS diffractograms of cyclic poly( <i>N</i> - <i>n</i> -alkyl-glycine)s ( <i>n</i> is the number of carbons on the side chains). .....	116
Figure 4.12. Domain spacing ( <i>d</i> ) calculated from the primary peak ( $q^*$ ) of WAXS experiment as a function of the number of carbons on <i>n</i> -alkyl side chains. The straight line indicates double length of fully extended alkyl side chains.....	119
Figure 4.13. (A) DSC thermograms and (B) WAXS diffractograms of cyclic PNEHGs along with those of PNHGs and PNOGs, respectively.....	120
Figure 4.14. (A) WAXS diffractograms of <i>c</i> -PNOGs annealed at 150 °C ( $T_{m,1} < T < T_{m,2}$ ) or 210 °C ( $T > T_{m,2}$ ), and (B) of <i>c</i> -PNTGs annealed at 120 °C ( $T_{m,1} < T < T_{m,2}$ ) or 170 °C ( $T > T_{m,2}$ ). ..	122
Figure 4.15. Schematic illustration of molecular packing of polypeptoid chains (A) below $T_{m,1}$ , (B) between $T_{m,1}$ and $T_{m,2}$ , and (C) above $T_{m,2}$ . .....	122

Figure 4.16. (A) Decomposition temperature ( $T_d$ ) of cyclic or linear polypeptoids with  $n$ -alkyl side chains as a function of the number of carbons on the side chains, (B) TGA of *c*-PNDGs and *l*-PNDGs..... 124

## LIST OF SCHEMES

Scheme 2.1. Synthetic procedure to prepare decyl-NCA. ....	30
Scheme 2.2. NHC-mediated zwitterionic polymerization of decyl-NCA .....	31
Scheme 2.3. Procedure to synthesize <i>c</i> -PNMG- <i>b</i> -PNDG diblock copolymers. ....	42
Scheme 2.4. Synthetic procedure to prepare <i>c/l</i> -PNMG- <i>b</i> -PNDG diblock copolymers. ....	57
Scheme 2.5. Synthetic procedure for cyclic <i>c</i> -PNMG- <i>b</i> -PNEHG diblock copolymers. ....	59
Scheme 3.1. Synthetic procedure to prepare cyclic PNMG-PNAG-PNBnG triblock terpolymers. ....	83
Scheme 3.2. Synthetic procedure to prepare cyclic [P(NEG- <i>ran</i> -NBG)]-PNMG-PNDG triblock terpolymers. ....	87
Scheme 4.1. Synthetic procedure to prepare 2-ethyl-1-hexyl NCAs. ....	97
Scheme 4.2. Synthesis of cyclic or linear poly( <i>N</i> - <i>n</i> -alkyl-glycine)s. ....	100

## TABLE OF ABBREVIATIONS

ATRP	atom transfer radical polymerization
<i>c</i> -PNDG	cyclic poly( <i>N</i> -decyl-glycine)
<i>c</i> -PNMG- <i>b</i> -PNDG	cyclic poly( <i>N</i> -methyl-glycine)- <i>b</i> -poly( <i>N</i> -decyl-glycine) diblock copolymers
cryo-TEM	cryogenic transmission electron microscopy
decyl-NCA	<i>N</i> -decyl <i>N</i> -carboxyanhydride
DLS	dynamic light scattering
DP <sub>(n)</sub>	(number average) degree of polymerization
DRI	differential refractive index
DSC	differential scanning calorimetry
G'	dynamic storage modulus
G''	dynamic loss modulus
<i>l</i> -PNDG	linear poly( <i>N</i> -decyl-glycine)
<i>l</i> -PNMG- <i>b</i> -PNDG	linear poly( <i>N</i> -methyl-glycine)- <i>b</i> -poly( <i>N</i> -decyl-glycine) diblock copolymers
methyl-NCA	<i>N</i> -methyl <i>N</i> -carboxyanhydride
M <sub>n</sub>	number average molecular weights
MWs	molecular weights
NCA	<i>N</i> -carboxyanhydride
NHC	<i>N</i> -heterocyclic carbene
NMR	nuclear magnetic resonance
PDI	polydispersity index
PEGylated	poly(ethylene glycine)-grafted
PNDG	poly( <i>N</i> -decyl-glycine)
PNMG	poly( <i>N</i> -methyl-glycine)
POM	polarized optical microscope
RAFT	reverse addition fragmentation chain transfer
R-NCA	<i>N</i> -substituted <i>N</i> -carboxyanhydride



$R_g$	radius of gyration
$R_h$	hydrodynamic radius
SAXS	small angle X-ray scattering
SEC	size exclusion chromatography
$T_{cp}$	cloud point temperature
US-DSC	ultrasensitive microcalorimetry DSC
WAXS	wide angle X-ray scattering

## ABSTRACT

This dissertation presents the first experimental efforts for synthesizing a new class of peptidomimetic polymers, cyclic block copolypeptoids, studying their self-assembly in dilute solution, and examining their macroscopic properties. Cyclic poly(*N*-methyl-glycine)-*b*-poly(*N*-decyl-glycine) (PNMG-*b*-PNDG) diblock copolymers were synthesized via sequential, *N*-heterocyclic carbene (NHC)-mediated ring-opening polymerization of NCA monomers with controlled chain length and compositions. Cryo-TEM shows that PNMG<sub>105</sub>-*b*-PNDG<sub>10</sub> copolymers in methanol (1 mg/mL) form spherical micelles that organize to form cylindrical micelles over time. The formation of cylindrical micelles is attributed to the crystallization of PNDG chains, as revealed by SAED and microDSC analyses. Cyclic PNMG<sub>100</sub>-*b*-PNDG<sub>10</sub> copolymers form thermo-reversible, free-standing gels at a concentration of 5 wt %. Rheological measurements of the gels reveal that cyclic copolymers produce harder gels than their linear counterparts. Variable-temperature <sup>1</sup>H NMR suggests that thermo-reversible gelation is related to any transitions of morphologies formed from the copolymers upon heating and cooling. Analyses by WAXS and SAXS suggest that the cyclic copolymers favor to form cylindrical micelles more than the linear copolymers, leading to formation of harder gels due to more transient networking among the cylindrical micelles.

The second part focuses on the synthesis of cyclic triblock terpolypeptoids and their self-assembly in solution. Cyclic poly(*N*-methyl-glycine)-*b*-poly(*N*-allyl-glycine)-*b*-poly(*N*-benzyl-glycine) triblock terpolypeptoids were synthesized via sequential addition of monomers. Studies by SEC and NMR suggest block copolymer compositions can be controlled by varying molar ratios of each monomer to NHC. Similarly, cyclic [poly(*N*-ethyl-glycine)-*ran*-poly(*N*-butyl-glycine)]-*b*-poly(*N*-methyl-glycine)-*b*-poly(*N*-decyl-glycine) triblock terpolypeptoids were

synthesized. Analysis by DLS suggests that this terpolymer forms micelles with broad size distributions below the cloud point temperature ( $T_{cp}$ ) of PNEG-*ran*-PNBG blocks, and it may form well-defined, larger micellar aggregates above the  $T_{cp}$ .

The third part presents systematic studies of the melting and crystallization of cyclic or linear polypeptoids with various *n*-alkyl side groups. Studies by DSC show that polypeptoids with butyl or longer side groups have two endothermic melting transitions ( $T_{m,1} < T_{m,2}$ ).  $T_{m,1}$  increases and  $T_{m,2}$  decreases, as the length of *n*-alkyl side groups increases. Studies by WAXS show that polypeptoids with butyl or longer side groups are well ordered.  $T_{m,1}$  is attributed to side chain packing and  $T_{m,2}$  to main polypeptoid packing.

## CHAPTER 1. INTRODUCTION TO CYCLIC BLOCK COPOLYPEPTOIDS

### 1.1 Introduction to cyclic polymers

#### 1.1.1 Cyclic polymers: distinct properties and benefits over linear counterparts

Cyclic macromolecules in biological systems have attracted much attention since 1965. Vinograd et al.<sup>1,2</sup> reported that the architecture of double-stranded polyoma DNA viruses was cyclic, as shown by electron microscopy (Figure 1.1). These cancer-causing viruses were shown to retain their biological activities even after the loss of helical conformation at 100 °C. This was attributed to their unique cyclic topology.

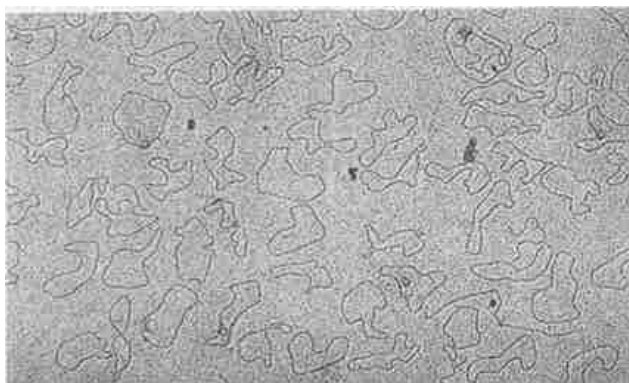


**Figure 1.1.** Electron micrograph of polyoma DNA, naturally-occurring cyclic macromolecules (copied from reference 2).

Synthetic cyclic polymers also possess distinct properties in the solid state or solution due to the lack of chain ends. For example, cyclic polymers have smaller radius of gyration ( $R_g$ ) than their linear counterparts in both good and theta solvents. The ratio of  $R_g$  of cyclic polymers to that of linear ones is theoretically predicted as 0.707 in a theta solvent,<sup>3</sup> and as 0.718 for good solvent.<sup>4</sup> These predictions were experimentally studied for polystyrene by Ohta et al.<sup>5</sup>, and they reported the ratio as 0.85 in cyclohexane (theta solvent) and 0.81 in benzene (good solvent). Additionally, polymer chains become more mobile without chain ends.<sup>6</sup> This mobility may provide less resistance to flow under the same conditions such as solvent, concentration, or

temperature. Lower intrinsic viscosity of cyclic polymers have been theoretically predicted,<sup>6</sup> and experimentally reported for several polymers, including poly(octenamer),<sup>7</sup> cyclic poly(lactide)s,<sup>8</sup> and cyclic poly( $\alpha$ -peptoid)s.<sup>9</sup>

Cyclic block copolymers have been shown to self-assemble in solution to form nanostructures that are distinctly different from those of their linear counterparts.<sup>10-12</sup> For example, Minatti et al.<sup>11</sup> reported that cyclic poly(styrene)-*b*-poly(isoprene) (PS-*b*-PI) diblock copolymers form giant worm-like micelles in heptane while their linear analogs with identical molecular weights form spherical micelles. The topological constraint of cyclic PS-*b*-PIs may first lead to the formation of individual “sunflower-like” micelles. The micelles then self-assemble to form worm-like micelles.<sup>11</sup> In addition to the micellar morphologies, thermal stability of micelles formed from block copolymers was affected by their topology. For example, Honda et al.<sup>13</sup> reported that both linear poly(butyl acrylate)-poly(ethylene oxide)-poly(butyl acrylate) triblock terpolymers and cyclic poly(butyl acrylate)-poly(ethylene oxide) diblock copolymers with identical molecular weights form flower-like micelles, but the cloud point temperature ( $T_{cp}$ ) of micelles formed from the cyclic copolymers was enhanced by 40 °C, as compared to that from the linear triblock terpolymers. In their studies, the  $T_{cp}$  of the micelles was controlled by co-assembling linear and cyclic polymers. Furthermore, cyclic topology of polymers affects the properties in bulk such as rates of crystallization. Shin et al.<sup>14</sup> reported the synthesis of cyclic poly( $\epsilon$ -caprolactone)s (PCL) with high molecular weights (up to 114,000 g·mol<sup>-1</sup>) by the *N*-heterocyclic carbene-initiated zwitterionic polymerization of  $\epsilon$ -caprolactones. Cyclic PCLs were crystallized faster than their linear counterparts in the melt, as studied by small angle X-ray scattering (SAXS) and differential scanning calorimetry (DSC).

Additionally, cyclic polymers are beneficial in drug delivery systems, because they provide slower, pharmacokinetic properties than their linear analogs. Nasongkla et al.<sup>15</sup> reported that cyclic PEGylated poly(caprolactone)s with high molecular weights (30 kD) had longer plasma circulation times than linear counterparts with identical molecular weights. This can be rationalized in that linear polymers with chain ends may pass through the nanopores in the glomeruli with less topological constraint than cyclic polymers.<sup>15</sup> Similarly, Chen et al.<sup>16</sup> reported that cyclic PEGylated poly(acrylic acid)s showed longer circulation time and higher tumor accumulation than their linear counterparts. Raskatov et al.<sup>17</sup> further reported cyclic pyrrole-imidazole polyamides had a slower bloodstream accumulation/excretion profile in animals than their linear analogs.

### **1.1.2 Synthetic strategies to prepare cyclic polymers**

Cyclic polymers can be prepared by several synthetic approaches including “ring-closure techniques” and “ring-expansion techniques.”<sup>18</sup> Ring-closure techniques involve the coupling of the functional groups on chain ends of linear, telechelic precursors. High dilution conditions are usually required to enhance intramolecular cyclization and to prevent intermolecular coupling, reaction of one polymer chain with another polymer chain. This method can be divided into two approaches. The first approach is the “ring-closure of  $\alpha,\omega$ -homodifunctional polymers” with two, identical chain ends (Figure 1.2 (a)).<sup>18</sup> An example of this method is to utilize anionic polymerization to generate two active anions at the chain ends, which are further coupled with a linking agent such as  $\alpha,\alpha'$ -dichloro-*p*-xylene.<sup>19</sup> Various vinyl monomers including styrene and its derivatives were polymerized by this method to prepare cyclic polymers.<sup>18</sup> The second approach is the “ring-closure of  $\alpha,\omega$ -heterodifunctional polymers” with two distinct chain ends (Figure 1.2 (b)). Controlled polymerizations such as ATRP (atom transfer radical polymerization) and RAFT

(reverse addition fragmentation chain transfer) polymerization were utilized to prepare linear, heterodifunctional precursors, due to relatively facile functionalization of terminal groups as well as controlled chain length. For example, Laurent et al.<sup>20</sup> prepared cyclic polystyrene by converting bromine-terminated polystyrene prepared by ATRP into an azide-functionalized polystyrene, followed by cyclization between the alkyne pendent group from the initiator and an azide chain end by click chemistry.

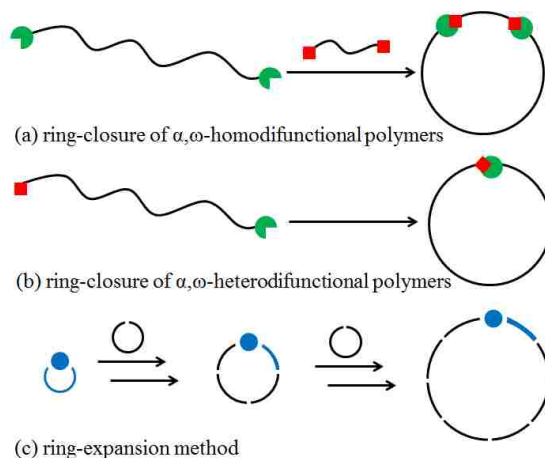


**Figure 1.2.** Scheme of synthetic strategies to prepare cyclic polymers (reproduced from reference 18).

Alternatively, ring-expansion techniques require the initiation of appropriate cyclic monomers (usually 4-8 member rings) by a catalyst or initiator, which generates cyclic propagating polymers possessing reactive chain ends such as organometallic or electrostatic bonds (Figure 1.2 (c)).<sup>18</sup> Polymer chains further grow by the insertion of monomers to the propagating species at the reactive sites. This method attracted much attention, because high dilution conditions for the ring-closure techniques are not required, so large-scale synthesis can be readily accomplished.<sup>18</sup> Additionally, high molecular weights of cyclic polymers can be achieved as cyclic architecture of the propagating species is maintained throughout polymerization.<sup>18</sup> Polymerization by this method, however, is affected by the rates of

polymerization, depolymerization, and back-biting of the propagating species, so the selection of monomers and catalysts for this method are limited.<sup>18</sup> Kricheldorf et al.<sup>21</sup> first reported synthesis of cyclic poly( $\beta$ -butyrolactone) by initiating  $\beta$ -butyrolactone (4-member ring) monomers by utilizing a cyclic tin oxide catalyst. The cyclic polymers were expanded by adding the monomers to the tin-oxide bonds of the propagating species. Additionally, ring-opening metathesis catalysts were utilized to prepare cyclic polymers by ring-expansion reactions.<sup>7,22-24</sup> For example, Bielawski et al.<sup>7</sup> reported synthesis of cyclic poly(octenamer) with molecular weights up to 1200 kg·mol<sup>-1</sup> using a cyclic Ru catalyst. In this study, the Ru catalyst was inserted to the *cis*-cyclic octene monomers, resulting in the propagation of a cyclic species. Recently, N-heterocyclic carbene (NHC) was utilized as a catalyst or an initiator to synthesize cyclic polymers with controlled molecular weights and relatively narrow molecular weight distributions. For example, Culkin et al.<sup>8</sup> reported synthesis of cyclic poly(lactide)s by zwitterionic ring-opening polymerization of lactides using N-heterocyclic carbene as a catalyst (Figure 1.3). They reported cyclic poly(lactide)s with molecular weights up to 26 kg·mol<sup>-1</sup> and moderate polydispersity index (PDI) (< 1.3). In this case, NHC inserts into the carbonyl groups of lactide monomers. As a result, zwitterionic polymeric species are generated, which are composed of the alkoxide anion and imidazolium cation (2 in Figure 1.3). The coulombic interaction between the ion pair keeps them close enough to induce back-biting, and thus a cyclic architecture was constructed (3 in Figure 1.3).<sup>8,18</sup>

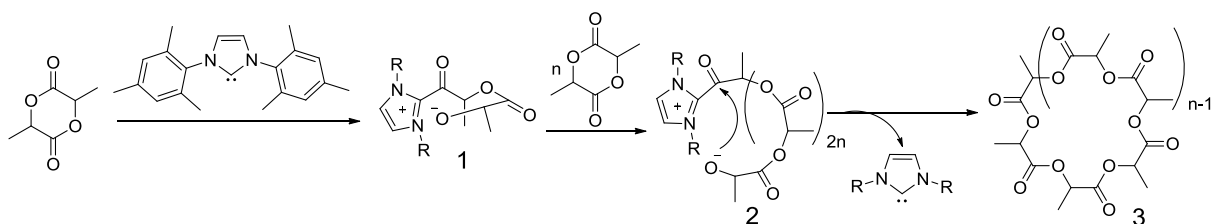


**Figure 1.3.** N-heterocyclic carbene(NHC)-mediated zwitterionic polymerization of lactide (copied from reference 8).



## 1.2 Introduction to peptoids and polypeptides

### 1.2.1 Peptoids as a peptidomimetic material: benefits over peptides

Peptoids, oligomeric N-substituted glycines, have attracted much attention as bio-inspired, or peptidomimetic materials, since their first report by Simon et al. in 1992.<sup>25</sup> As shown in Figure 1.4, peptoid lacks extensive hydrogen bonding due to the substitution of alkyl groups (R) on the nitrogen. This N-substitution may provide peptoids with benefits in biological or pharmacological applications over peptides. For example, peptoids showed enhanced proteolytic stability as they were resistant against degradation by cellular enzymes.<sup>26,27</sup> This proteolytic stability motivated researchers to design peptoids to control protein-protein interactions. For example, Hara et al.<sup>28</sup> investigated peptoids as inhibitors of interactions between p53, the tumor suppressor protein, and human double minute 2 (HDM2), which binds to and inactivates p53. They revealed that peptoids without helical conformations bind more HDM2, and thus are better inhibitors than helical peptoids. Additionally, peptoids can pass through cell membrane more readily than peptides. For example, Kwon et al.<sup>29</sup> quantitatively studied the relative cell permeability of peptoids and peptides by in vitro Glucocorticoid Receptor (GR) ligand-binding affinity and luciferase (oxidative enzymes) induction. They reported that the peptoid conjugates can be more than 20 times more permeable through the cell by than analogous peptides. This study suggests that peptoids may have enhanced lipophilicity, affinity with fats, oils or lipids, than peptides.<sup>29</sup>

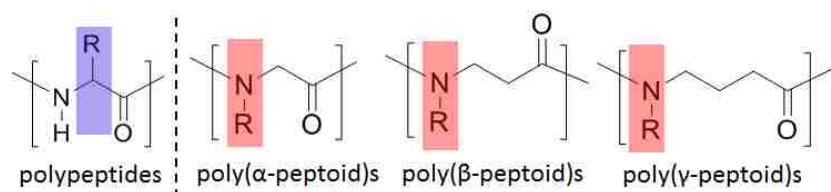


**Figure 1.4.** Molecular structure of polypeptides and various poly-peptoids.

### 1.2.2 Synthesis of oligomeric peptoids and polypeptoids

Synthesis of oligomeric peptoids was first reported by Zuckermann et al.<sup>30</sup> They synthesized peptoids by coupling bromoacetic acid to the solid support of Rink amide polystyrene resin by *N,N*-diisopropylcarbodiimide (DIC)-mediated acylation (Figure 1.5). A primary amine was added to form peptoids by an amination step. By repeating those two steps with a variety of primary amines, sequence-specific peptoids were prepared with precisely-controlled chain length. Peptoids were then cleaved from the solid support using trifluoroacetic acid to obtain peptoids with primary amide chain ends.<sup>31</sup> The sequence-specificity that is readily achieved by this method provides researchers with a variety of opportunities to investigate biomedical applications. A limiting factor of this method is that the chain length of peptoids is limited to a degree of polymerization (DP) of 30.

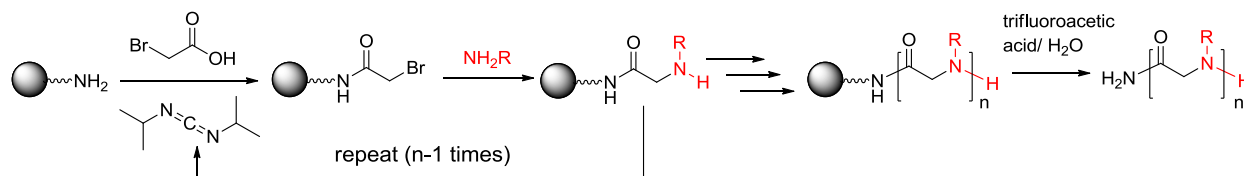


**Figure 1.5.** A stepwise method to prepare oligomeric peptoids (reproduced from reference 30 and 31).

It has been of great interest to synthesize polypeptoids with high molecular weights, as has been done with other structural mimics of polypeptides including poly(2-oxazoline)s and poly(*N*-substituted acrylamide)s. As early as 1948, Waley et al.<sup>32,33</sup> synthesized poly(*N*-methylglycine)s (polysarcosine, polypeptoids with methyl side groups) and investigated the kinetics and mechanism of nucleophilic ring-opening polymerization of *N*-carboxyanhydride (NCA).<sup>34</sup> Recently, Fetsch et al.<sup>35</sup> synthesized well-defined, linear polypeptoids with various side groups including methyl, ethyl, propyl, butyl, and isobutyl groups by primary amine-initiated ring-opening polymerizations of the corresponding *N*-substituted NCAs (R-NCA). They reported that

polymerizations occurred in a controlled manner, which enabled them to synthesize block copolypeptoids by sequential addition of monomers. Guo et al. has reported the controlled synthesis of cyclic poly(*N*-butyl-glycine)s by NHC-mediated ring-opening polymerization of butyl-NCAs.<sup>9</sup> This polymerization method was developed, as NHC-mediated polymerization of heterocyclic monomers such as lactide,  $\gamma$ -caprolactone,  $\beta$ -butyrolactone,  $\delta$ -valerolactone, and ethylene oxide was found to yield polymers with molecular weights and molecular weight distribution in a controlled manner.<sup>36</sup>

Additionally, polypeptoids were synthesized by the metal-catalyzed copolymerization of carbon monoxide (CO) and monomers. Sun et al.<sup>37</sup> reported successful synthesis of poly( $\alpha$ -peptoids) by alternating copolymerization of CO and imines by using acylcobalt complex, tetracarbonyl(phenylacetyl)cobalt, as a catalyst. This method was beneficial in that one may design polypeptoids with bulky side groups, such as phenyl groups, onto the  $\alpha$ -carbons in polypeptoids. They found that this method was not suitable to prepare block copolypeptoids by adding other imine monomers because of the rapid deactivation of the catalytic species which inhibits continued growth of the second monomers after consumption of the first monomers.<sup>36,37</sup> Similarly, Jia et al.<sup>38</sup> reported synthesis of poly( $\beta$ -peptoid)s (structure shown in Figure 1.4) by copolymerization of CO of such monomers as *N*-methylaziridine or *N*-ethylaziridine using  $\text{BnCOCo}(\text{CO})_4$  as a catalyst. They reported that this polymerization possesses living characteristics with controlled chain length, and the end groups of the polymers can be converted to functional groups such as thiols. Jia and co-workers further utilized those benefits to generate anti-fouling materials on the gold substrate to exhibit protein resistance.<sup>39</sup> Additionally, Jia and co-workers<sup>40,41</sup> reported synthesis of poly( $\gamma$ -peptoid)s (structure shown in Figure 1.4) by

copolymerization of *N-n*-butylazetidine or *N-isobutylazetidine*, CO, and THF using a Co-based catalyst.

### 1.2.3 Structures and physical properties of peptoids and polypeptoids

Recently, molecular structures of peptoids or polypeptoids with various side groups in solution and solid state have been widely investigated. Studies reveal that unlike polypeptides whose secondary structures ( $\alpha$ -helices or  $\beta$ -sheets) are largely determined by hydrogen bonding interaction, conformations of peptoids or polypeptoids are dominantly affected by steric and stereoelectronic interactions of the side groups on the nitrogen.<sup>9,42</sup> For example, Wu et al.<sup>43,44</sup> reported that peptoid oligomers (up to 20-mers) with  $\alpha$ -chiral, aromatic side chains in an organic or aqueous solution form helices. Helices were also observed from cyclic or linear polypeptoids with the molecular weight of 4 – 15 kg·mol<sup>-1</sup> with  $\alpha$ -chiral aromatic side groups.<sup>45</sup> In addition to helices, Guo et al.<sup>9</sup> reported that polypeptoids form random coils, when the side groups are alkyl (i.e. butyl) pendent groups. Furthermore, it was reported that diblock copolypeptoids without any chiral side groups may form super helices. Murnen et al.<sup>46</sup> revealed that partially charged diblock copolypeptoid 30-mer,  $[N-(2\text{-phenylethyl})\text{glycine}]_{15}\text{-}b\text{-}[N-(2\text{-carboxyethyl})\text{glycine}]_{15}$ , in aqueous solution at pH 6.8 form helices with diameters of  $624 \pm 69$  nm. The formation of these huge helices is attributed to the self-assembly of amphiphilic diblock copolypeptoids in aqueous solution. The interplay between hydrophobic interactions from 2-phenylethyl side groups and electrostatic interactions from 2-carboxylethyl side groups played an important role to form such complex helical structures.

Crystalline structures and physical properties of peptoids were also examined by several groups. For example, Nam et al.<sup>47</sup> investigated crystalline structures of oligomeric, sequence-specific peptoids by preparing free-floating, 2.7 nm-thick bimolecular-layered sheets from

mixtures of two oppositely charged peptoids. They revealed the interchain distance between peptoids chains as 4.5 Å and distance between the repeating units of peptoid chains as 3.6 Å, as characterized by aberration-corrected transmission electron microscopy (TEM) and X-ray diffraction (XRD). In addition to the crystalline structures, Rosales et al.<sup>48</sup> reported crystallization and melting behavior of linear, sequence-specific oligomeric peptoids (15-mers) as well as homopeptoids with *n*-alkyl side chains including *n*-butyl, *n*-hexyl, and *n*-octyl groups. They observed a melting transition at 170, 155, and 140 °C from peptoids with *n*-butyl, *n*-hexyl, and *n*-octyl side groups, respectively. In their studies, thermogravimetric analysis of the synthesized peptoids revealed that peptoids are thermally stable up to 260 °C, providing a temperature window for thermal processability. They further revealed that those alkyl side chains, even *n*-butyl groups, are highly ordered, as X-ray diffraction shows multiple reflections from them. Finally, solubility of polypeptoids in water is also affected by side groups. Fetsch et al.<sup>35</sup> reported that poly(*N*-methyl-glycine)s and poly(*N*-ethyl-glycine)s with methyl and ethyl side groups, respectively, are soluble in water, poly(*N*-propyl-glycine)s with propyl side groups have limited solubility, and polypeptoids with longer side groups than propyl one are insoluble in water.

### **1.3 Introduction to block copolymers**

Block copolymers are composed of blocks, or sequences of chemically-distinct repeating units connected by covalent bonds.<sup>49,50</sup> Two individual, chemically-incompatible polymer chains with high molecular weights are generally immiscible due to small negative entropic contribution ( $\Delta S$ ) and large positive enthalpic contribution ( $\Delta H$ ) to the total energy of mixing ( $\Delta G$ ), encompassing macroscopic phase separation.<sup>51,52</sup> The architecture of a block copolymer based on the covalent linkages of distinct polymer chains leads to phase separation on the length scale of

chain dimensions of each block (5 – 50 nm), which is called microphase separation.<sup>52</sup> By this small-scale phase separation, block copolymers spontaneously self-assemble to form various nanostructures in the solid state or solution. In the solid state or concentrated solution, block copolymers self-assemble to highly ordered morphologies, such as lamellae, hexagonally-packed cylinders, or body-centered cubic spheres. These structures can be obtained by manipulating the volume of fractions of the blocks.<sup>49</sup> Self-assembly of block copolymers in solution is detailed in the following section.

### 1.3.1 Self-assembly of block copolymers in dilute solution

In dilute solution, block copolymers may form micelles or vesicles in a selective solvent. Figure 1.6 shows illustration of self-assembly of block copolymers in solution. As can be seen, solvent-soluble blocks form coronas, and solvent-insoluble cores.<sup>52</sup> Spheres are a typical shape of micelles with a diameter of about 20 nm, which are composed of 50 - 200 molecules.<sup>52</sup> Under certain circumstances, block copolymers may form micelles of other shapes such as cylinders or even flat bilayers, which can become vesicles when they close the open layers.<sup>52</sup>

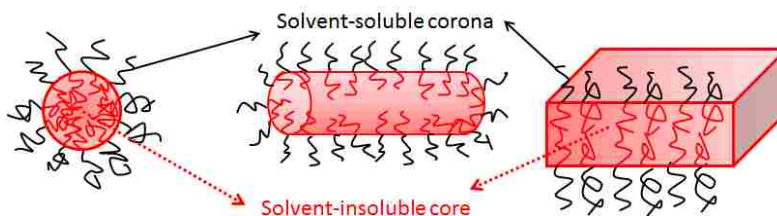


**Figure 1.6.** Self-assembly of diblock copolymers as spherical, cylindrical, and bilayer micelles in a selective solvent for one block (modified from reference 52).

Investigation of the mechanism and kinetics of micellization from block copolymers has been of great interest among researchers. Israelachvili and co-workers<sup>53</sup> predicted the shape of block copolymer micelles by geometric approaches.<sup>54</sup> More specifically, the dominant forces that determine the morphologies of micelles can be considered as the following two forces: the

solvophobic attractions between core-forming solvophobic chains, and the solvophilic repulsions between corona-forming solvophilic chains due to electrostatic or steric interactions. They suggest that three geometric parameters based on the two forces needs to be considered to determine the morphologies of micelles: the optimal interface ( $a_0$ ), the volume ( $v$ ) occupied by the solvophobic chains, and the maximum length ( $l_c$ ) of those solvophobic chains, as shown in Figure 1.7. These parameters are correlated to produce the packing parameter ( $p$ , equation 1.1). Smaller  $p$  values, spheres are more favored: when  $p < 0.3$ , spheres are favored, when  $0.3 < p < 0.5$ , cylinders are favored, and when  $0.5 < p < 1$ , vesicles or bilayers are favored.<sup>54</sup>

$$p = \frac{v}{a_0 l_c} \quad (1.1)$$

**Figure 1.7.** Schematic illustration of contributing forces to formation of micelles from block copolymers and the packing parameter discussed in the text (modified from reference 53 and 54).

In addition to the geometric approaches, it was reported that morphologies formed from block copolymer micelles are kinetically controlled. One of the most dominant differences in physical behavior between micelles formed from block copolymers and those from low molecular weight amphiphiles can be described as “ergodicity.”<sup>55,56</sup> While small molecules show rapid exchange of molecules between micelles and unimers, block copolymers with high molecular weights rarely exchange their chains over long time periods. Due to this non-ergodic characteristic, which can be defined as irreversible dynamics of polymer chains after forming micelles, the morphologies that block copolymers form are kinetically stable, and thus various

nanostructures can be constructed via different paths.<sup>56</sup> For example, Cui et al.<sup>57</sup> reported that poly(acrylic acid)<sub>94</sub>-*block*-poly(methyl acrylate)<sub>103</sub>-*block*-polystyrene<sub>44</sub> triblock copolymers (subscript numbers denote degree of polymerization) form spherical micelles in at the 1:4 ratio of THF to water in the presence of multiamine. Once the copolymer forms micelles, molecular exchange between the copolymers and micelles is not favorable. Consequently, as they further added THF into the solution of micelles up to the 2:1 ratio of THF to water, they observed a change of the spherical micelles to disk-like micelles, which ultimately results in anisotropic stacking of the disk-like micelles. Additionally, the non-ergodic characteristic may affect the epitaxial growth of micelles from block copolymers with crystalline cores. Wang et al.<sup>58</sup> reported that polyferrocenylsilane<sub>53</sub>-*b*-polyisoprene<sub>320</sub> (PFS<sub>53</sub>-*b*-PI<sub>320</sub>) diblock copolymers with crystalline core PFS segments form cylindrical micelles in hexane, and the length of the cylindrical micelles increases by the addition of the identical copolymers in solution. Furthermore, they revealed the formation of triblock co-micelles by adding different copolymers, PFS-*b*-polymethylvinylsiloxane (PFS-*b*-PMVS), to the cylindrical micelles from PFS-*b*-PI.

One may prepare micelles from block copolymers in dilute solution by the following two methods. One route is to dissolve polymers in a selective solvent for one block. This method is simple, but the fraction of solvophobic blocks, i.e. block copolymer compositions, should be limited due to the solubility of copolymers in a selective solvent. This method was utilized to prepare micelles from cyclic or linear block copolypetoids in methanol in this study, as the molar fraction of hydrophobic blocks is limited to about 10 %, compared to that of hydrophilic blocks. The other is to dissolve polymers in a good solvent for both blocks. Selective solvent for one of the blocks is then added to the solvent. As the solvent quality of one of the blocks decreases, micelles or aggregates can be formed. Broader windows of block copolymer compositions can be



available compared to the method by direct dissolution, and thus a variety of morphologies from identical copolymers can be achieved. Zhang et al.<sup>59,60</sup> showed pioneering work on the preparation of block copolymer micelles by this method. They dissolved polystyrene-*b*-poly(acrylic acid) with various compositions in DMF (a good solvent for both blocks), added water (a selective solvent for poly(acrylic acid) blocks), and removed DMF by dialysis. They achieved six different morphologies including spheres, rods, lamellae, vesicles, reverse micelle-like aggregates, and micrometer-size spheres composed of the reverse micelle-like aggregates.

#### **1.4 Synthesis of cyclic block copolymers**

Cyclic block copolymers would be an interesting material to study their morphologies in solution, solid-state, or thin films in that they may exhibit unique properties due to the combination of their unusual architecture and microstructures. Synthesis of cyclic block copolymers with high purity of cyclic architecture and controlled chain length has been challenging among researchers. The ring closure techniques of linear block copolymer precursors were widely utilized to prepare cyclic block copolymers. The advantage of this approach is that a variety of cyclic block copolymers can be prepared. The disadvantage is that the high dilution condition is required for the linear-to-cyclic coupling. In addition, the cyclic products often contain topological contaminants such as catenates and olympic rings, which are very difficult to separate. For example, polystyrene-based cyclic diblock copolymers, such as cyclic polystyrene-*b*-poly(dimethylsiloxane),<sup>59,60</sup> polystyrene-*b*-poly(2-vinylpyridine),<sup>59</sup> and polystyrene-*b*-poly(butadiene)<sup>61</sup>, were prepared by the synthesis of ABA-type linear triblock terpolymers via anionic polymerization, followed by cyclization using dichlorodimethylsilane as a coupling agent under highly dilute conditions.<sup>62</sup> In this method, successful intramolecular cyclization between active anions from polymers and the coupling agent is critical to minimize

producing linear polymer impurities. Recently, researchers attempted to obtain high purity of cyclic architecture by such a specific click coupling reaction. For instance, Eugene et al.<sup>62</sup> prepared cyclic poly(methyl acrylate)-*b*-poly(styrene) diblock copolymers by combination of ATRP, end-group functionalization, and cyclization of the “click” coupling between an azide and alkyl group from difunctional, linear diblock copolymers. Additionally, Poelma et al.<sup>63</sup> reported synthesis of cyclic polystyrene-*b*-poly(ethylene oxide) (PS-*b*-PEO) diblock copolymers by coupling two, distinct linear difunctional polymers, PEO with propargyl end groups and PS with azide end groups via the “click” reaction under dilute conditions. They further studied self-assembly in thin film from the copolymers, and reported that domain spacing from cyclic polymers reduced by 30%, compared to that of their linear counterparts. Synthesis of cyclic block copolymers with controlled molecular weights and narrow molecular weight distributions still remains challenging, and thus studies on self-assembly and macroscopic properties of such polymers have rarely been reported.

### **1.5 Synthesis of cyclic peptoids**

Cyclization of peptoids has been of particular interest, because the structural constraint may induce distinct conformations and biological activities of the peptidomimetic materials. For example, Shin et al.<sup>64</sup> synthesized cyclic oligo-peptoids of various peptoid sequences including methoxyethyl, phenylmethyl, or azidopropyl groups by intramolecular head-to-tail cyclization of linear oligomeric peptoids synthesized in the solid state. In their study, the cyclic architecture was achieved by coupling terminal groups of linear, telechelic peptoids in dilute conditions. They reported efficient cyclization to synthesize cyclic pentamers to 20mers with high yields (> 90%) within 5 minutes at room temperature. Structural confinement by cyclization was found to enhance conformational ordering, resulting in crystallization of cyclic hexamers and octamers.

They further presented that cyclic peptoids form reverse-turn secondary structures, which are observed from proteins, as studied by X-ray crystallography. Also, intramolecular cyclization from pendent side groups is another method to accomplish a ring structure of peptoids. For example, Holub et al.<sup>65</sup> reported cyclization of azide and alkyne side chains of linear oligopeptoids by the Cu-catalyzed [3+2] cycloaddition reaction. They studied the effects of cyclization on the conformational heterogeneity of peptoids by circular dichroism (CD) and two-dimensional heteronuclear single quantum coherence (2D-HSQC) NMR spectrometry, which provides information of the resonance of both protons and heteronucleus such as <sup>13</sup>C or <sup>15</sup>N. Reduced conformational heterogeneity in cyclic peptoids was further supported by increased ellipticity at a certain wavelength in CD. Additionally, the distribution of <sup>1</sup>H-<sup>13</sup>C cross-peaks from side or main chains of the linear peptoids was broader than that of the cyclic ones. This study suggests that structural constraints by cyclization increase conformational homogeneity.

### **1.6 Investigation on cyclic block copolypeptoids**

Cyclic block copolypeptoids are a new class of peptidomimetic polymers with novel architectures and molecular structures. This new class of polymers would be a good model polymer to investigate the effect of topological or architectural parameters, i.e. cyclic or linear architecture, on their self-assembly in solution or solid state and on the macroscopic properties such as mechanical properties of polypeptoid-based materials. This investigation can be realized by precisely controlling the chain length of such polymers. Synthesis of cyclic block copolypeptoids with controlled chain length, however, has rarely been reported. This dissertation presents the first experimental efforts for the synthesis of a new class of peptidomimetic polymers, cyclic block copolypeptoids. Furthermore, the first studies for the self-assembly of

cyclic block copolypeptoids in dilute solution and their thermo-reversible gelation at a concentration of 5 wt % are presented.

As discussed in sections 1.4 and 1.5, synthesis of block copolypeptoids remains challenging in terms of available monomers and efficient cyclization of linear precursors. Additionally, synthesis of cyclic polypeptoids with high molecular weights remains a challenge. Solid state synthesis can only provide access to short chain peptoids with up to 30 repeating units, and cyclization should be conducted under dilute condition (5 – 70 mM). Recently, it was reported by Guo et al.<sup>9</sup> that the zwitterionic ring-opening polymerization of *N*-substituted NCAs using NHC as an initiator provides a useful, synthetic pathway to access cyclic polypeptoids and cyclic block copolypeptoids. The molecular weights of cyclic polypeptoids were controlled from 3 to 30 kg·mol<sup>-1</sup> with narrow molecular weight distribution (1.04 – 1.12) under a relatively concentrated condition (0.4 M or 0.8 M). The cyclic structure was confirmed by matrix-assisted laser desorption-ionization time-of-flight (MALDI-TOF) and electrospray ionization (ESI) mass spectroscopy (MS), which suggest that the majority of polymers possess no terminal groups. The cyclic architecture was further supported by the lower intrinsic viscosity of cyclic polymers than that of linear ones. They further reported characteristics of controlled polymerization by the linear relationship of molecular weights with the consumption of monomers. This characteristic provides a useful way to synthesize block copolypeptoids by sequential addition of different monomers. In their studies, cyclic poly(*N*-methyl-glycine)-*b*-poly(*N*-butyl-glycine) diblock copolymers were successfully synthesized by sequential addition of *N*-methyl *N*-carboxyanhydride (methyl-NCA) and *N*-butyl *N*-carboxyanhydride (butyl-NCA).

In this study, cyclic block copolypeptoids with controlled molecular weights and compositions were synthesized by adapting the synthetic procedure by Guo et al. Chapter 2

presents experimental studies on the synthesis, self-assembly, and macroscopic properties of particular cyclic block copolypeptides, cyclic poly(*N*-methyl-glycine)-*b*-poly(*N*-decyl-glycine) (PNMG-*b*-PNDG) diblock copolymers. Figure 1.8 summarizes studies on PNMG-*b*-PNDG in this dissertation. To have a better understanding of the copolymer, cyclic poly(*N*-decyl-glycine) (PNDG) homopolymers were first synthesized by NHC-mediated ring-opening polymerization of *N*-decyl *N*-carboxyanhydride (decyl-NCA). Section 2.1 details synthesis and characterization of cyclic PNDGs including molecular weight control, chain conformation, polymerization kinetics, melting and crystallization transitions, and crystalline packing by nuclear magnetic

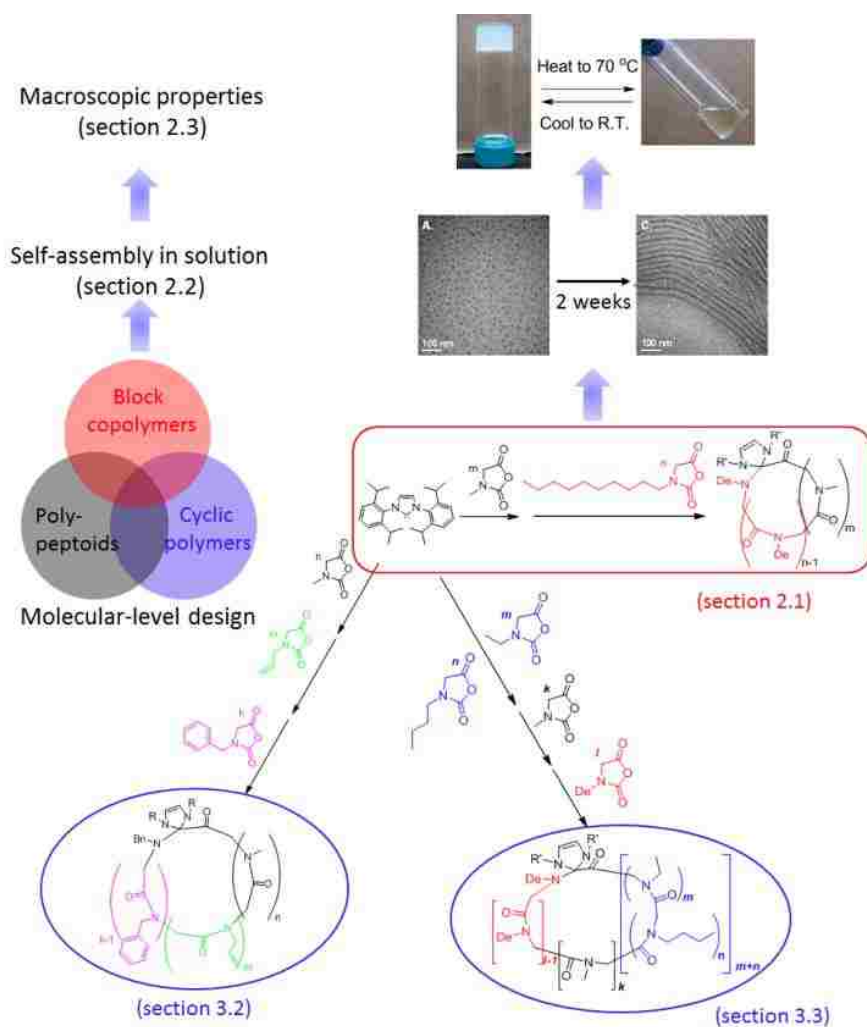


**Figure 1.8.** An illustration to summarize investigation on cyclic block copolypeptides in this dissertation.

resonance (NMR) spectroscopy, size exclusion chromatography (SEC), ESI-MS, DSC, and wide angle X-ray scattering (WAXS). ESI-MS suggests that the majority of synthesized species are cyclic. SEC analysis suggests that molecular weights of the polymers can be controlled by altering the molar ratio of NHC to monomers. Molecular weights of the polymers increase linearly with conversion, which is the characteristic of controlled polymerization. DSC shows that PNDGs have two, endothermic melting transitions at 72 - 79 °C ( $T_{m,1}$ ) and 166 – 177 °C ( $T_{m,2}$ ). The low-temperature melting transition ( $T_{m,1}$ ) was attributed to side chain melting, and high-temperature one ( $T_{m,2}$ ) to main chain melting. WAXS reveals that PNDGs are highly crystalline.

Cyclic PNMG-*b*-PNDG diblock copolymers were synthesized via sequential, NHC-mediated ring-opening polymerization of the corresponding methyl-NCA and decyl-NCA monomers.  $^1\text{H}$  NMR analysis reveals that adjusting the initial monomer to NHC molar ratio can readily control the chain length and composition of the copolymers, as presented in section 2.1.2.2. This particular diblock copolymer was designed for a polypeptoid to be composed of hydrophilic and amorphous PNMG chains and hydrophobic and semi-crystalline PNDG chains.

Self-assembly of the synthesized copolymers in solution was further investigated and presented in section 2.2. For this study, the copolymer was designed to have relatively long, hydrophilic PNMG blocks compared to hydrophobic PNDG blocks such that PNMGs form coronas and PNDGs cores in water or methanol. More specifically, cyclic PNMG<sub>105</sub>-*b*-PNDG<sub>10</sub> diblock copolymers in methanol at a concentration of 1.0 mg·mL<sup>-1</sup> self-assemble to form spherical micelles, which evolve to form cylindrical micelles with a diameter of 12.2 (1.8) nm and length of micrometers over 2 weeks, as revealed by cryogenic transmission electron microscopy (cryo-TEM) and time-lapsed light scattering. The formation of cylindrical micelles

was attributed to the crystallization of core-forming solvophobic PNDG segments. To examine the crystallization-driven morphological transition, the cast film of PNMG<sub>100</sub>-*b*-PNDG<sub>10</sub> diblock copolymer solution was characterized by selected area electron diffraction (SAED). Periodic diffraction rings were observed from cylindrical micelles. Microcalorimetric studies on the copolymer solution reveal that an endothermic peak at 58 °C was shown after aging the copolymer solution for 2 weeks at room temperature. Those two studies support the crystallization-driven formation of cylindrical micelles from the copolymers in methanol.

Additionally, macroscopic properties of cyclic or linear PNMG<sub>100</sub>-*b*-PNDG<sub>10</sub> diblock copolymers in methanol were investigated, and are presented at section 2.3. The copolymers at elevated concentrations (i.e. 5 or 10 wt %) form thermo-reversible, free-standing gels. They form free-standing gels at room temperature and a free-flowing liquid at 60 °C. This sol-gel transition is completely reversible. The viscoelastic properties of the gels were investigated by rheological measurements, which revealed that gels from the cyclic copolymers are harder than those from the linear counterparts. Variable-temperature <sup>1</sup>H NMR studies on cyclic or linear copolymers were conducted to gain insights into the change of solvation of the copolymers during the thermo-reversible gelation. These studies indicate that the solvation and mobility of solvophobic PNDGs of the copolymers are enhanced at elevated temperature at which the free-standing gels become free-flowing liquid. This suggests that the dissolution of gels at high temperature is related to any transitions of morphologies formed from the copolymers in gels. Polarized optical microscopy (POM) and WAXS analyses suggest that the gelation of the copolymers is driven by crystallization of core-forming PNDG segments. Additionally, SAXS and WAXS results of the gels from cyclic and linear copolymers are discussed to investigate the origin of the formation of harder gels from cyclic copolymers than linear ones.

In addition to cyclic diblock copolypeptoids, synthesis and characterization of cyclic triblock terpolypeptoids were presented in chapter 3 (Figure 1.8). Non-linear triblock terpolymers including such as miktoarm star terpolymers, hyperbranched star-block copolymers, and cyclic triblock terpolymers have attracted much attention, as such architectures of polymers may lead to the formation of more complex nanostructures than those from linear triblock terpolymers. Among them, cyclic triblock terpolymers with controlled chain length and compositions have rarely been reported yet. In this study, cyclic triblock terpolymers were synthesized by sequential, NHC-mediated ring-opening polymerization of three different NCA monomers. Synthesis of a particular copolymer, cyclic poly(*N*-methyl-glycine)-*b*-poly(*N*-allyl-glycine)-*b*-poly(*N*-benzyl-glycine) triblock terpolymer, is presented in section 3.2. <sup>1</sup>H NMR analysis of this copolymer suggests that its compositions can be readily controlled by altering the molar ratio of each monomer. Another particular copolymer, cyclic [poly(*N*-ethyl-glycine)-*ran*-poly(*N*-butyl-glycine)]-*b*-poly(*N*-methyl-glycine)-*b*-poly(*N*-decyl-glycine) triblock terpolypeptoid, is synthesized, and detailed in section 3.3. This copolymer is particularly interesting because it contains thermoresponsive poly(*N*-ethyl-glycine)-*ran*-poly(*N*-butyl-glycine) (PNEG-*ran*-PNBG) blocks, as reported by Lahasky et al.<sup>66</sup> Initial studies on this copolymer by dynamic light scattering (DLS) suggest that the triblock terpolymer forms micelles with broad size distributions below the  $T_{cp}$  of PNEG-*ran*-PNBG blocks. DLS further suggests that this copolymer forms well-defined micellar aggregates with much narrower distributions above  $T_{cp}$  of the thermoresponsive blocks.

Finally, this dissertation presents systematic studies on the crystallization and melting behavior of polypeptoids in chapter 4. A series of cyclic or linear polypeptoids with various *n*-alkyl side chains (*n* = 2, 4, 6, 8, 10, 12, and 14) was synthesized by NHC- or benzylamine-



mediated ring opening polymerizations of NCAs, respectively, and their crystallization and melting behavior were systematically studied by DSC and WAXS. It was revealed that cyclic or linear poly(*N*-ethyl-glycine)s with ethyl side groups are amorphous. On the other hand, polypeptoids with alkyl side chains of butyl ( $n = 4$ ) or longer side groups to tetradecyl groups ( $n = 14$ ) highly crystallized and are well-ordered. DSC results show that they have two, distinct endothermic or exothermic transitions. The first melting temperature ( $T_{m,1}$ ) increases from  $-65\text{ }^{\circ}\text{C}$  to  $100\text{ }^{\circ}\text{C}$ , and second one ( $T_{m,2}$ ) decreases from  $230\text{ }^{\circ}\text{C}$  to  $140\text{ }^{\circ}\text{C}$ , as the length of side chains increases from cyclic poly(*N*-butyl-glycine)s ( $n = 4$ ) to poly(*N*-tetradecyl-glycine)s ( $n = 14$ ). Additionally, the first crystallization ( $T_{c,1}$ ) increases from  $-110\text{ }^{\circ}\text{C}$  to  $89\text{ }^{\circ}\text{C}$ , and second one ( $T_{c,2}$ ) decreases from  $199\text{ }^{\circ}\text{C}$  to  $105\text{ }^{\circ}\text{C}$ . The low-temperature transitions are attributed to the crystallization and melting of alkyl side chains, and the high-temperature transitions to those of polypeptoid main chains. WAXS studies show that polypeptoids with butyl or longer side groups are well ordered, as the primary peak and multiple higher order reflections were observed. These results from the DSC and WAXS reveal that short side groups as butyl groups attached on polypeptoid backbones form well-ordered crystalline domains. Additionally, effects of architecture of main chains (i.e. cyclic or linear) and side chain (i.e. linear or branched) on their crystallization and melting behavior are discussed. Finally, the crystalline packing of polypeptoids at different temperatures is proposed based on WAXS data obtained from samples annealed at different temperatures.

## CHAPTER 2. CYCLIC DIBLOCK COPOLYPEPTODIS: SYNTHESIS, SELF-ASSEMBLY AND MACROSCOPIC PROPERTIES

### 2.1 Synthesis and characterization of cyclic poly(*N*-methyl-glycine)-*b*-poly(*N*-decyl-glycine) diblock copolymers

#### 2.1.1 Experimental

##### 2.1.1.1 Materials

All the solvents used in this study were purchased from Sigma-Aldrich and purified by passing through alumina columns under argon. Other chemicals were purchased from Sigma-Aldrich, and used as received.  $^1\text{H}$  and  $^{13}\text{C}\{^1\text{H}\}$ NMR spectra were recorded on a Bruker AV-400 spectrometer, and the chemical shifts in parts per million (ppm) were referenced relative to protic impurities or the  $^{13}\text{C}$  isotopes of  $\text{CDCl}_3$ ,  $\text{CD}_3\text{OD}$ ,  $\text{C}_6\text{D}_5\text{CD}_3$ , or  $\text{CF}_3\text{COOD}$  respectively. *N*-decyl *N*-carboxyanhydride (decyl-NCA,  $\text{M}_1$ ), *N*-methyl *N*-carboxyanhydride (methyl-NCA,  $\text{M}_2$ ) and 2,6-diisopropylphenylimidazol-2-ylidene (NHC) were synthesized by adapting literature procedures.<sup>9,67</sup>

##### 2.1.1.2 Instrumentations and sample preparation

ESI MS spectra were collected using a Waters Synapt HDMS quadrupole/time-of-flight (Q/TOF) mass spectrometer (Waters, Milford, MA) under the following experimental conditions: ESI capillary voltage, 3.5 kV; sample cone voltage, 35 V; extraction cone voltage, 3.2 V; desolvation gas flow,  $500 \text{ L}\cdot\text{h}^{-1}$  ( $\text{N}_2$ ); trap collision energy (CE), 6 eV; transfer CE, 4 eV; trap gas flow,  $1.5 \text{ mL}\cdot\text{min}^{-1}$  (Ar); IM gas flow,  $22.7 \text{ mL}\cdot\text{min}^{-1}$  ( $\text{N}_2$ ); sample flow rate,  $5 \mu\text{L}\cdot\text{min}^{-1}$ ; source temperature, 40 or 100 °C; desolvation temperature, 60 or 150 °C. The sprayed solutions were prepared by dissolving 0.3 mg of sample in 1 mL of  $\text{CHCl}_3/\text{MeOH}$  (v/v, 50/50). Data analysis was conducted using Waters MassLynx 4.1.

SEC analyses for the poly(*N*-methyl-glycine)s (PNMGs) were conducted using an Agilent 1200 system equipped with three Phenomenex  $5 \mu\text{m}$ ,  $300\times 7.8 \text{ mm}$  columns, Wyatt

DAWN EOS multi-angle light scattering (MALS) detector (GaAs 30 mW laser at  $\lambda=690$  nm), and Wyatt Optilab rEX differential refractive index (DRI) detector with a 690 nm light source. DMF containing 0.1 M LiBr was used as the eluent at a flow rate of  $1.0 \text{ mL}\cdot\text{min}^{-1}$ . The column temperature was  $50 \text{ }^\circ\text{C}$ , and the detector temperature was  $25 \text{ }^\circ\text{C}$ . All data analyses were conducted using Wyatt Astra V 5.3 software. The molecular weights (MWs) and PDI of polymers were obtained by the Zimm model fit of the MALS-DRI data. The absolute molecular weights of the cyclic and linear PNMGS were determined using the reported  $dn/dc$  values [i.e.,  $0.0991 \text{ mL}\cdot\text{g}^{-1}$  and  $0.0987 \text{ mL}\cdot\text{g}^{-1}$  in DMF/0.1 M LiBr, respectively].<sup>9</sup>

SEC analyses for the poly(*N*-decyl-glycine)s (PNDGs) were conducted using an Agilent 1100 system (a Gastorr 704 degasser, isocratic pump, and Agilent 1100 auto sampler) equipped with two Phenomenex  $10 \text{ }\mu\text{m}$ ,  $300\times 7.8$  mm columns [ $10^5 \text{ \AA}$ , linear MXM, and guard column], Wyatt DAWN DSP-F multi-angle light scattering (MALS) detector (a He-Ne 5 mW laser at  $\lambda = 632.8$  nm), and Agilent 1200 differential refractive index (DRI) detector. THF containing 250 ppm BHT (2,6-di-*tert*-butyl-4-methylphenol) was used as the elution solvent at a flow rate of  $1.0 \text{ mL}\cdot\text{min}^{-1}$ . The columns were kept at room temperature. The temperatures of the MALS and DRI detector were room temperature and  $35 \text{ }^\circ\text{C}$ , respectively. All data analyses were performed using Wyatt Astra V 4.7 software. The MWs and PDI of polymers were obtained by the Zimm model fit of MALS-DRI data. The absolute molecular weights of the cyclic and linear PNDGs were determined using the experimentally measured  $dn/dc$  values [i.e.,  $0.0876$  and  $0.0863 \text{ mL}\cdot\text{g}^{-1}$  in THF at  $35 \text{ }^\circ\text{C}$ , respectively].

The refractive index increment ( $dn/dc$ ) of cyclic or linear PNDGs was measured using Wyatt's rEX DRI detector and Astra software  $dn/dc$  template. The polymers were purified twice by dissolving in THF and precipitating in methanol. Six THF solutions with precisely known

PNDG concentrations (0.25-2.0 mg·mL<sup>-1</sup>) were prepared and injected to the DRI detector. The  $dn/dc$  value was obtained from the linear fit to a plot of refractive index versus polymer concentration.

DSC studies of a series of cyclic PNDGs were conducted using a TA DSC 2920 calorimeter under nitrogen. Powder samples sealed into the aluminum pans were first heated from room temperature to 250 °C at 10 °C·min<sup>-1</sup>, cooled to 0 °C at 5 °C·min<sup>-1</sup>, and second heated to 250 °C at 10 °C·min<sup>-1</sup>.

WAXS experiments were conducted on the synchrotron beamline at the Center for Advanced Microstructures and Devices (CAMD, Baton Rouge, LA). Solid samples were annealed at 200 °C under vacuum for 4 days. X-ray scattering patterns were collected under vacuum for 20 to 30 min using an image plate with a resolution of 200 μm per pixel (Molecular Dynamics storage phosphor screen with an active area of 20×25 cm). The wavelength of the X-ray beam was 1.55 Å. The sample-to-detector distance was 193.1 mm, giving a  $q$  range of 0.1 Å<sup>-1</sup> to 2.5 Å<sup>-1</sup>. WAXS data were reduced using FIT2D 12.077 developed by Dr. Andy Hammersley with the European Synchrotron Radiation Facility (ESRF).<sup>68</sup> The domain spacing,  $d_{Bragg}$ , was calculated using Bragg's law:  $d = 2\pi/q$ ,  $q = 4\pi\sin(\theta)/\lambda$ , where  $\theta$  is the angle between the incident beam and the scattering planes.

### 2.1.1.3 Synthesis of monomers

**Synthesis of 2-(*n*-decylamino)acetic acid hydrochloride (1 in Scheme 2.1)** Glyoxylic acid (14.8 g, 161 mmol) was stirred with *n*-decylamine (16 mL, 80.5 mmol) in CH<sub>2</sub>Cl<sub>2</sub> (400 mL) for 24 h at room temperature. The solvent was removed under vacuum to yield a yellow viscous liquid to which aqueous HCl (400 mL, 1 M) was added. The reaction mixture was heated at reflux for 20 h. The water was removed by rotary evaporation to afford a white solid which was

further purified by recrystallization from methanol/diethyl ether at 0 °C (14.2 g, 70 % yield). <sup>1</sup>H NMR (δ in DMSO, 400 MHz, ppm): 0.85 ppm (t, CH<sub>3</sub>(CH<sub>2</sub>)<sub>7</sub>CH<sub>2</sub>CH<sub>2</sub>-); 1.24 ppm (m, CH<sub>3</sub>(CH<sub>2</sub>)<sub>7</sub>CH<sub>2</sub>CH<sub>2</sub>-); 1.61 ppm (m, CH<sub>3</sub>(CH<sub>2</sub>)<sub>7</sub>CH<sub>2</sub>CH<sub>2</sub>-); 2.86 ppm (m, CH<sub>3</sub>(CH<sub>2</sub>)<sub>7</sub>CH<sub>2</sub>CH<sub>2</sub>-); 3.81 ppm (s, -COCH<sub>2</sub>-); 9.22 ppm (s, HNHCl). <sup>13</sup>C{<sup>1</sup>H} NMR (δ in DMSO, 100 MHz, ppm): 14.0 (CH<sub>3</sub>(CH<sub>2</sub>)<sub>8</sub>CH<sub>2</sub>-); 22.1 (CH<sub>3</sub>CH<sub>2</sub>(CH<sub>2</sub>)<sub>7</sub>CH<sub>2</sub>-); 25.2 (CH<sub>3</sub>CH<sub>2</sub>CH<sub>2</sub>(CH<sub>2</sub>)<sub>6</sub>CH<sub>2</sub>-); 26.0 (CH<sub>3</sub>(CH<sub>2</sub>)<sub>2</sub>CH<sub>2</sub>(CH<sub>2</sub>)<sub>5</sub>CH<sub>2</sub>-); 28.5 (CH<sub>3</sub>(CH<sub>2</sub>)<sub>3</sub>CH<sub>2</sub>(CH<sub>2</sub>)<sub>4</sub>CH<sub>2</sub>-); 28.7 (CH<sub>3</sub>(CH<sub>2</sub>)<sub>4</sub>CH<sub>2</sub>(CH<sub>2</sub>)<sub>3</sub>CH<sub>2</sub>-); 28.8 (CH<sub>3</sub>(CH<sub>2</sub>)<sub>5</sub>CH<sub>2</sub>(CH<sub>2</sub>)<sub>2</sub>CH<sub>2</sub>-); 28.9 (CH<sub>3</sub>(CH<sub>2</sub>)<sub>6</sub>CH<sub>2</sub>CH<sub>2</sub>CH<sub>2</sub>-); 31.3 (CH<sub>3</sub>(CH<sub>2</sub>)<sub>7</sub>CH<sub>2</sub>CH<sub>2</sub>-); 46.7 (CH<sub>3</sub>(CH<sub>2</sub>)<sub>7</sub>CH<sub>2</sub>CH<sub>2</sub>- & -COCH<sub>2</sub>-); 168.0 (HOCO-).

**Synthesis of 2-(*N,N*-*tert*-butoxycarbonyl-*n*-decylamino)acetic acid (2 in Scheme 2.1)**

A mixture of **1** (13 g, 52 mmol), di-*tert*-butyl dicarbonate (28.2 g, 129 mmol) and triethylamine (36 mL, 258 mmol) in distilled water (200 mL) was stirred at room temperature for 20 h. The reaction mixture was extracted with hexane (2×200 mL) to remove any unreacted di-*tert*-butyl dicarbonate. The aqueous phase was separated, acidified with aqueous HCl (50 mL, 4 M), and extracted with ethyl acetate (3×100 mL). The organic phase was then separated, washed with brine, and dried over anhydrous MgSO<sub>4</sub>. Subsequent filtration and solvent removal afforded a pale yellow oil (11.7 g, 72 % yield). <sup>1</sup>H NMR (δ in CDCl<sub>3</sub>, 400 MHz, ppm): 0.75 (t, CH<sub>3</sub>(CH<sub>2</sub>)<sub>7</sub>CH<sub>2</sub>CH<sub>2</sub>-); 1.15 (m, CH<sub>3</sub>(CH<sub>2</sub>)<sub>7</sub>CH<sub>2</sub>CH<sub>2</sub>-); 1.29 & 1.34 (s, -(CH<sub>3</sub>)<sub>3</sub>); 1.38 (m, CH<sub>3</sub>(CH<sub>2</sub>)<sub>7</sub>CH<sub>2</sub>CH<sub>2</sub>-); 3.13 (m, CH<sub>3</sub>(CH<sub>2</sub>)<sub>7</sub>CH<sub>2</sub>CH<sub>2</sub>-); 3.86 & 3.76 (s, -COCH<sub>2</sub>-). <sup>13</sup>C{<sup>1</sup>H} NMR (δ in CDCl<sub>3</sub>, 100 MHz, ppm): 14.1 (CH<sub>3</sub>(CH<sub>2</sub>)<sub>8</sub>CH<sub>2</sub>-); 22.7 (CH<sub>3</sub>CH<sub>2</sub>(CH<sub>2</sub>)<sub>7</sub>CH<sub>2</sub>-); 26.8 (CH<sub>3</sub>CH<sub>2</sub>CH<sub>2</sub>(CH<sub>2</sub>)<sub>6</sub>CH<sub>2</sub>-); 28.1 (CH<sub>3</sub>(CH<sub>2</sub>)<sub>2</sub>CH<sub>2</sub>(CH<sub>2</sub>)<sub>5</sub>CH<sub>2</sub>-); 28.3 & 28.4 (-(CH<sub>3</sub>)<sub>3</sub>); 29.3 (CH<sub>3</sub>(CH<sub>2</sub>)<sub>3</sub>CH<sub>2</sub>(CH<sub>2</sub>)<sub>4</sub>CH<sub>2</sub>-); 29.4 (CH<sub>3</sub>(CH<sub>2</sub>)<sub>4</sub>CH<sub>2</sub>(CH<sub>2</sub>)<sub>3</sub>CH<sub>2</sub>-); 29.6 (CH<sub>3</sub>(CH<sub>2</sub>)<sub>5</sub>CH<sub>2</sub>(CH<sub>2</sub>)<sub>2</sub>CH<sub>2</sub>-); 29.7 (CH<sub>3</sub>(CH<sub>2</sub>)<sub>6</sub>CH<sub>2</sub>CH<sub>2</sub>CH<sub>2</sub>-); 31.9 (CH<sub>3</sub>(CH<sub>2</sub>)<sub>7</sub>CH<sub>2</sub>CH<sub>2</sub>-); 48.4 & 49.0

(CH<sub>3</sub>(CH<sub>2</sub>)<sub>7</sub>CH<sub>2</sub>CH<sub>2</sub>- & -COCH<sub>2</sub>-); 80.5 (-OC(CH<sub>3</sub>)<sub>3</sub>); 155.4 & 156.3 (-NCOO-); 175.2 & 175.5 (HOOC-).

**Synthesis of *N*-decyl *N*-carboxyanhydride (M<sub>1</sub> in Scheme 2.1)** Compound **2** (10.3g, 32.8 mmol) was dissolved in anhydrous CH<sub>2</sub>Cl<sub>2</sub> (250 mL) under a nitrogen atmosphere. The solution was cooled to 0 °C and phosphorous trichloride (2.5 mL, 26.2 mmol) was added dropwise. The reaction mixture was stirred at 0 °C for 2 h, and then the volatiles were removed under vacuum. Inside the glovebox, the solid residue was extracted with anhydrous CH<sub>2</sub>Cl<sub>2</sub> (15 mL) and filtered. The filtrate was concentrated and layered with hexane to recrystallize at -20 °C overnight. White crystals were isolated by filtration and further purified by sublimation (4.5 g, 57 % yield). <sup>1</sup>H NMR (δ in CDCl<sub>3</sub>, ppm): 0.87 (t, CH<sub>3</sub>(CH<sub>2</sub>)<sub>7</sub>CH<sub>2</sub>CH<sub>2</sub>-); 1.25 (m, CH<sub>3</sub>(CH<sub>2</sub>)<sub>7</sub>CH<sub>2</sub>CH<sub>2</sub>-); 1.58 (m, CH<sub>3</sub>(CH<sub>2</sub>)<sub>7</sub>CH<sub>2</sub>CH<sub>2</sub>-); 3.38 (t, CH<sub>3</sub>(CH<sub>2</sub>)<sub>7</sub>CH<sub>2</sub>CH<sub>2</sub>-); 4.09 (s, -COCH<sub>2</sub>-). <sup>13</sup>C{<sup>1</sup>H} NMR (δ in CDCl<sub>3</sub>, 100 MHz, ppm): 14.2 (CH<sub>3</sub>(CH<sub>2</sub>)<sub>8</sub>CH<sub>2</sub>-); 22.8 (CH<sub>3</sub>CH<sub>2</sub>(CH<sub>2</sub>)<sub>7</sub>CH<sub>2</sub>-); 26.6 (CH<sub>3</sub>CH<sub>2</sub>CH<sub>2</sub>(CH<sub>2</sub>)<sub>6</sub>CH<sub>2</sub>-); 27.4 (CH<sub>3</sub>(CH<sub>2</sub>)<sub>2</sub>CH<sub>2</sub>(CH<sub>2</sub>)<sub>5</sub>CH<sub>2</sub>-); 29.2 (CH<sub>3</sub>(CH<sub>2</sub>)<sub>3</sub>CH<sub>2</sub>(CH<sub>2</sub>)<sub>4</sub>CH<sub>2</sub>-); 29.4 (CH<sub>3</sub>(CH<sub>2</sub>)<sub>4</sub>CH<sub>2</sub>(CH<sub>2</sub>)<sub>3</sub>CH<sub>2</sub>-); 29.6 [CH<sub>3</sub>(CH<sub>2</sub>)<sub>5</sub>CH<sub>2</sub>(CH<sub>2</sub>)<sub>2</sub>CH<sub>2</sub>-, CH<sub>3</sub>(CH<sub>2</sub>)<sub>6</sub>CH<sub>2</sub>CH<sub>2</sub>CH<sub>2</sub>-]; 32.0 (CH<sub>3</sub>(CH<sub>2</sub>)<sub>7</sub>CH<sub>2</sub>CH<sub>2</sub>-); 43.8 (CH<sub>3</sub>(CH<sub>2</sub>)<sub>8</sub>CH<sub>2</sub>-); 49.0 (-COCH<sub>2</sub>-); 152.2 (-NCOOCO-); 165.9 (-NCOOCO-).

#### 2.1.1.4 Synthesis of polymers

##### Representative synthetic procedure for the cyclic poly(*N*-decyl-glycine)s (*c*-PNDGs).

In the glovebox, M<sub>1</sub> (270 mg, 1.1 mmol, [M<sub>1</sub>]<sub>0</sub>=0.4 M) was dissolved in anhydrous THF (2.5 mL). A known volume of NHC/THF stock solution (246 μL, 11 μmol, 45.5 mM, [M<sub>1</sub>]:[NHC]<sub>0</sub> = 100:1) was added to the monomer solution. Polymerization was allowed to proceed at 70 °C for 24 h under nitrogen and then quenched by the addition of cold methanol. The white precipitate was collected and washed with ample methanol and hexane to remove any

unreacted monomer or initiator. Drying under vacuum yielded a white solid (180 mg, 82% yield).

$^1\text{H}$  NMR ( $\delta$  in  $\text{CDCl}_3/\text{CF}_3\text{COOD}$ , 400 MHz, ppm): 0.87 ( $\text{CH}_3(\text{CH}_2)_7\text{CH}_2\text{CH}_2^-$ ); 1.25 ( $\text{CH}_3(\text{CH}_2)_7\text{CH}_2\text{CH}_2^-$ ); 1.60 ( $\text{CH}_3(\text{CH}_2)_7\text{CH}_2\text{CH}_2^-$ ); 2.95-3.29 ( $\text{CH}_3\text{N}^-$ ); 3.28 ( $\text{CH}_3(\text{CH}_2)_7\text{CH}_2\text{CH}_2^-$ ); 4.00 ( $-\text{COCH}_2^-$ ).  $^{13}\text{C}\{^1\text{H}\}$  NMR ( $\delta$  in  $\text{CDCl}_3/\text{CF}_3\text{COOD}$ , 100MHz, ppm): 14.2 ( $\text{CH}_3(\text{CH}_2)_8\text{CH}_2^-$ ); 22.8 ( $\text{CH}_3\text{CH}_2(\text{CH}_2)_7\text{CH}_2^-$ ); 26.8 ( $\text{CH}_3\text{CH}_2\text{CH}_2(\text{CH}_2)_6\text{CH}_2^-$ ); 28.1 ( $\text{CH}_3(\text{CH}_2)_2\text{CH}_2(\text{CH}_2)_5\text{CH}_2^-$ ); 29.4 & 29.7 [ $\text{CH}_3(\text{CH}_2)_3\text{CH}_2(\text{CH}_2)_4\text{CH}_2^-$ ,  $\text{CH}_3(\text{CH}_2)_4\text{CH}_2(\text{CH}_2)_3\text{CH}_2^-$ ]; 32.1 ( $\text{CH}_3(\text{CH}_2)_7\text{CH}_2\text{CH}_2^-$ ); 48.2 ( $\text{CH}_3(\text{CH}_2)_8\text{CH}_2^-$ ); 49.7 ( $-\text{NCOCH}_2^-$ ); 170.2 ( $-\text{NCOCH}_2^-$ ).

### **Representative synthetic procedure for the cyclic poly(*N*-methyl-glycine)-*b*-poly(*N*-decyl-glycine) block copolymers (*c*-PNMG-*b*-PNDGs)**

In the glovebox, methyl-NCA ( $\text{M}_2$ ) (118 mg, 1.02 mmol,  $[\text{M}_2]_0=0.4$  M) was dissolved in anhydrous acetonitrile (2.5 mL). A known volume of NHC/THF stock solution (450  $\mu\text{L}$ , 20  $\mu\text{mol}$ , 45.5 mM,  $[\text{M}_2]_0:[\text{NHC}]_0 = 50:1$ ) was added using a syringe. Polymerization was allowed to proceed for 24 h at room temperature under a nitrogen atmosphere. Aliquots of the reaction mixture were taken and analyzed for conversion by  $^1\text{H}$  NMR and polymer MW by SEC. An acetonitrile solution (2.5 mL) containing decyl-NCA ( $\text{M}_1$ ) (247 mg, 1.02 mmol,  $[\text{M}_1]_0=0.4$  M,  $[\text{M}_1]_0:[\text{NHC}]_0=50:1$ ) was then added into the above reaction mixture, which was heated at 70  $^\circ\text{C}$  for additional 48 h to reach complete conversion. The polymer product was then precipitated by the addition of methanol and collected by filtration. The polymer was further washed with ample methanol and followed by THF to remove any unreacted monomers or homopolymers, and dried under vacuum (218 mg, 79% yield). For the copolymers that contain high molar fractions of PNMGs (e.g.,  $[\text{M}_2]_0:[\text{M}_1]_0:[\text{NHC}]_0 = 100:10:1$ ), the polymer products were obtained by precipitating in hexane and by washing with ample THF.  $^1\text{H}$  NMR ( $\delta$  in  $\text{CDCl}_3/\text{CF}_3\text{COOD}$ , 400 MHz, ppm): 0.87 ( $\text{CH}_3(\text{CH}_2)_7\text{CH}_2\text{CH}_2^-$ ); 1.25 ( $\text{CH}_3(\text{CH}_2)_7\text{CH}_2\text{CH}_2^-$ ); 1.60 ( $\text{CH}_3(\text{CH}_2)_7\text{CH}_2\text{CH}_2^-$ );

2.9-3.2 ( $\text{CH}_3\text{N-}$ ); 3.28 ( $\text{CH}_3(\text{CH}_2)_7\text{CH}_2\text{CH}_2\text{-}$ ); 4.09-4.45 ( $-\text{COCH}_2\text{-}$ ).  $^{13}\text{C}\{^1\text{H}\}$  NMR ( $\delta$  in  $\text{CDCl}_3/\text{CF}_3\text{COOD}$ , 100 MHz, ppm): 14.0 ( $\text{CH}_3(\text{CH}_2)_8\text{CH}_2\text{-}$ ); 22.6 ( $\text{CH}_3\text{CH}_2(\text{CH}_2)_7\text{CH}_2\text{-}$ ); 26.6 ( $\text{CH}_3\text{CH}_2\text{CH}_2(\text{CH}_2)_6\text{CH}_2\text{-}$ ); 27.9 ( $\text{CH}_3(\text{CH}_2)_2\text{CH}_2(\text{CH}_2)_5\text{CH}_2\text{-}$ ); 29.2 [ $\text{CH}_3(\text{CH}_2)_3\text{CH}_2(\text{CH}_2)_4\text{CH}_2\text{-}$ ,  $\text{CH}_3(\text{CH}_2)_4\text{CH}_2(\text{CH}_2)_3\text{CH}_2\text{-}$ ]; 29.4 [ $\text{CH}_3(\text{CH}_2)_5\text{CH}_2(\text{CH}_2)_2\text{CH}_2\text{-}$ ,  $\text{CH}_3(\text{CH}_2)_6\text{CH}_2\text{CH}_2\text{CH}_2\text{-}$ ]; 31.8 ( $\text{CH}_3(\text{CH}_2)_7\text{CH}_2\text{CH}_2\text{-}$ ); 36.1 ( $\text{CH}_3\text{N-}$ ); 47.8 ( $\text{CH}_3(\text{CH}_2)_8\text{CH}_2\text{-}$ ); 49.3-50.4 ( $-\text{NCOCH}_2\text{-}$ ); 170.0 ( $-\text{NCOCH}_2\text{-}$ ).

**Synthetic procedure for the linear poly(*N*-methyl-glycine)<sub>112</sub>-*b*-poly(*N*-decyl-glycine)<sub>16</sub> block copolymers (*l*-PNMG<sub>112</sub>-*b*-PNDG<sub>16</sub>)**

The butylamine initiator used in this synthesis was stirred over  $\text{CaH}_2$  for 24 h and distilled under vacuum (at room temperature and ca. 100 mmHg). In the glovebox, methyl-NCA ( $\text{M}_2$ ) (156 mg, 1.36 mmol,  $[\text{M}_2]_0 = 0.4 \text{ M}$ ) was dissolved in anhydrous acetonitrile (3.3 mL). A known volume of  $\text{BuNH}_2/\text{THF}$  stock solution (134  $\mu\text{L}$ , 14  $\mu\text{mol}$ , 101.2 mM,  $[\text{M}_2]_0:[\text{NHC}]_0 = 100:1$ ) was added using a syringe. Polymerization was allowed to proceed for 24 h at room temperature under a nitrogen atmosphere. Aliquots of the reaction mixture were taken and analyzed for conversion by  $^1\text{H}$  NMR and MWs of polymers by SEC. An acetonitrile solution (0.5 mL) containing Decyl-NCA ( $\text{M}_1$ ) (49 mg, 0.2 mmol,  $[\text{M}_1]_0 = 0.4 \text{ M}$ ,  $[\text{M}_1]_0:[\text{NHC}]_0 = 15:1$ ) was then added into the above reaction mixture, which was heated at 70 °C for an additional 48 h to reach complete conversion. The polymer products were precipitated by the addition of hexane and collected by filtration. The polymers were further washed with ample THF and MeOH to remove any unreacted monomers or homopolymers and dried under vacuum (105 mg, 77 % yield). The  $^1\text{H}$  and  $^{13}\text{C}\{^1\text{H}\}$  NMR spectra of linear PNMG-*b*-PNDGs appear identical to those of their cyclic counterparts.



## Kinetic studies of NHC-mediated ring-opening polymerization of decyl-NCA.

Polymerization was conducted in toluene- $d_8$  at 70 °C inside a sealed J-Young NMR tube.  $^1\text{H}$  NMR spectra were collected at a constant time interval for more than four half-lives.

### 2.1.2. Results and discussion

#### 2.1.2.1 Synthesis and characterization of cyclic poly(*N*-decyl-glycine)s (*c*-PNDGs)

Decyl-NCA has been synthesized in good overall yield (50-60%) by adapting a previously reported procedure (Scheme 2.1)<sup>9</sup> and purified by sublimation prior to polymerization. The desired structures of precursors to decyl-NCA and final products of decyl-NCA have been unambiguously verified by  $^1\text{H}$  and  $^{13}\text{C}\{^1\text{H}\}$  NMR spectroscopy, as shown in Figure 2.1 and 2.2, respectively.

**Scheme 2.1.** Synthetic procedure to prepare decyl-NCA.

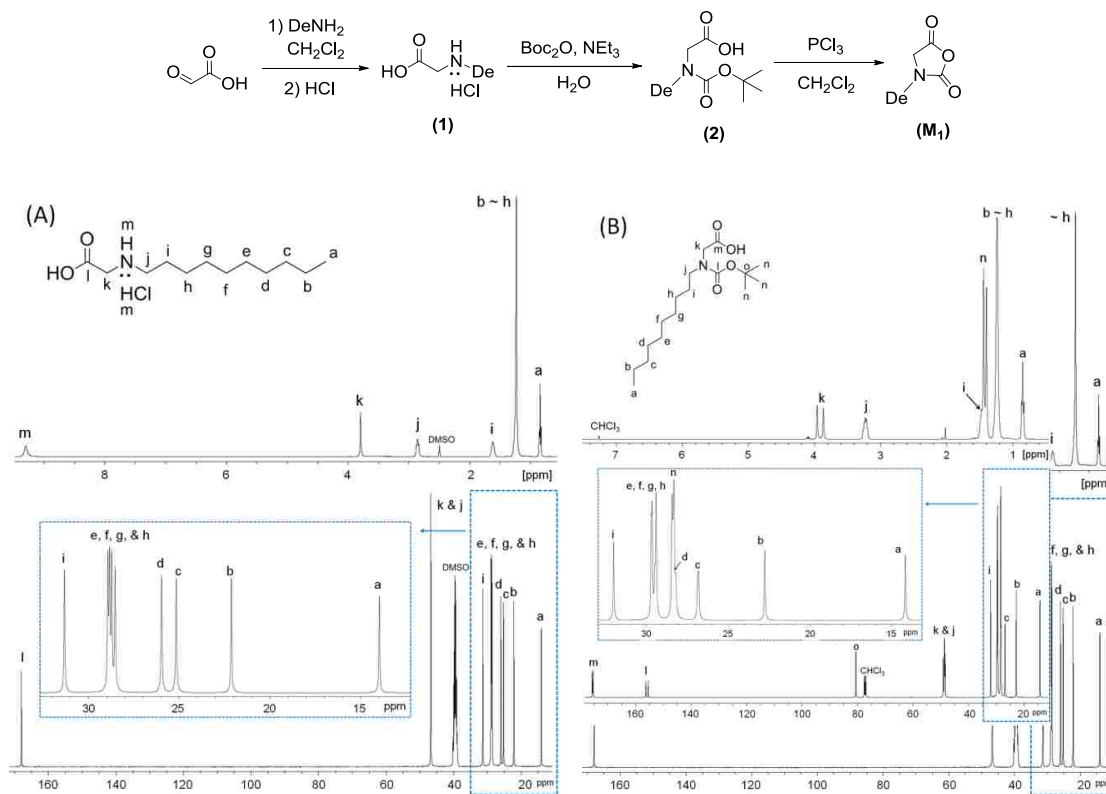


**Figure 2.1.**  $^1\text{H}$  and  $^{13}\text{C}\{^1\text{H}\}$  NMR spectra of (A) 2-(*n*-decylamino)acetic acid hydrochloride (1) in *d*-DMSO and of (B) 2-(*N,N*-*tert*-butoxycarbonyl-*n*-decylamino)acetic acid (2) in  $\text{CDCl}_3$ .

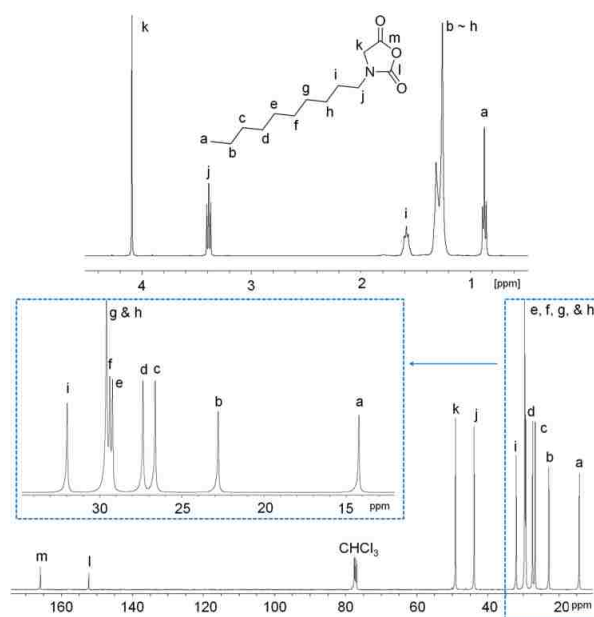


**Figure 2.2.**  $^1\text{H}$  and  $^{13}\text{C}\{^1\text{H}\}$  NMR spectra of decyl-NCA in  $\text{CDCl}_3$ .

It was previously demonstrated that NHC can mediate the zwitterionic polymerization of butyl-NCA in a quasi-living manner to yield cyclic poly(*N*-butyl-glycine)s.<sup>9</sup> To ascertain that the polymerization of decyl-NCA ( $M_1$ ) occurs in a controlled manner, polymerization of  $M_1$  with various  $[M_1]_0:[\text{NHC}]_0$  ratios have been conducted. Scheme 2.2 shows NHC-mediated zwitterionic polymerization of decyl-NCA. The reactions were allowed to proceed in THF at 70 °C under a nitrogen atmosphere until all of the monomers were consumed. The aliquots were taken and analyzed by  $^1\text{H}$  NMR spectroscopy to verify the conversion. Final polymer products were isolated by precipitation in cold methanol and dried under vacuum prior to further analysis. Table 2.1 summarizes results of polymerization of decyl-NCA.

**Scheme 2.2.** NHC-mediated zwitterionic polymerization of decyl-NCA

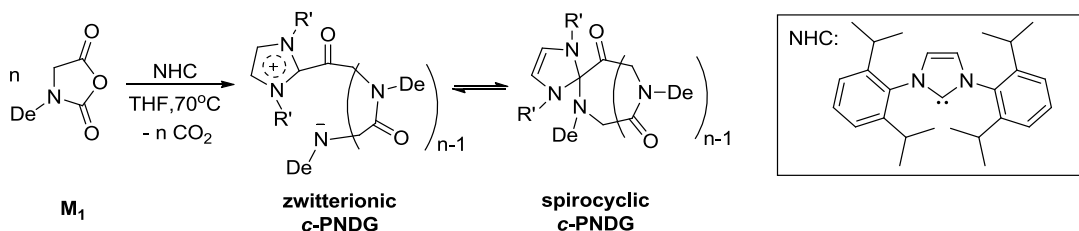


**Table 2.1.** NHC-mediated zwitterionic polymerizations of decyl-NCA ( $M_1$ ).<sup>a</sup>

Entry #	$[M_1]_0/[NHC]_0$	Reaction time (h)	Conv. (%)	$M_n(\text{theor.})^b$ (kg·mol <sup>-1</sup> )	$M_n(\text{SEC})^c$ (kg·mol <sup>-1</sup> )	$M_n(\text{NMR})^d$ (kg·mol <sup>-1</sup> )	PDI <sup>c</sup>
1	25	8	89	4.8	4.8	5.6	1.14
2	50	16	93	9.6	10.2	11.1	1.03
3	100	16	91	18.3	20.4	20.0	1.15
4	200	21	83	33.1	31.0	-	1.09

<sup>a</sup> Polymerizations were conducted in THF at 70 °C with  $[M_1]_0 = 0.4$  M. SEC analyses were conducted by directly injecting the polymerization solutions into SEC columns after the designated reaction time; <sup>b</sup> theoretical molecular weights were calculated based on conversion and the  $[M_1]_0:[NHC]_0$  ratio; <sup>c</sup> determined by a tandem SEC-MALS-DRI system using the  $dn/dc$  [0.0876(9) mL·g<sup>-1</sup>] at a concentration of 5 mg·mL<sup>-1</sup> in THF at room temperature; <sup>d</sup> determined by <sup>1</sup>H NMR analysis. Entry 4: The NHC content of the high MW PNDG is too low to be accurately integrated and hence its MW cannot be reliably determined by <sup>1</sup>H NMR.

Structures of the synthesized polymers were characterized by <sup>1</sup>H and <sup>13</sup>C{<sup>1</sup>H} NMR spectroscopy (Figure 2.3) and ESI MS spectrometry (Figure 2.4). The solubility of the dry polymer in CDCl<sub>3</sub> is limited and can be substantially improved by a few drops of CF<sub>3</sub>COOD. All proton resonances appear broad and their relative integrations are consistent with the desired polymer backbone structure shown in Scheme 2.2. ESI MS analysis of a low MW sample reveals one major (*e* in Figure 2.4) and four minor (*a-d* in Figure 2.4) envelopes of doubly charged ions. The mass of the major set of ion corresponds to the sum of an integer number of the PNDG repeating unit mass (197.18), one NHC mass (388.29) and two proton ion masses (2.02), consistent with the zwitterionic or spirocyclic PNDG with a NHC affixed to the chain end (Scheme 2.2).<sup>9,69</sup> One minor set of ions (*c* in Figure 2.4) corresponds to the same *c*-PNDG structure that is ionized by a potassium ion. Mass analysis of the other three minor sets of ions reveals several PNDG species with different end-groups (*a*, *b*, and *d* in Figure 2.4). The PNDGs

bearing carboxyl and amino chain ends (*a* in Figure 2.4) are likely to be formed by  $M_1$  polymerization that is initiated by residual water, whereas the species *b* in Figure 2.4 is presumably formed by end-to-end cyclization of the zwitterionic propagating species prior to  $\text{CO}_2$  liberation (Scheme 2.2). While it has been demonstrated that NHC moieties can be readily eliminated from the NHC-terminated poly(ethylene oxide) zwitterions by reaction with nucleophiles (e.g., water or alcohol) in the NHC-mediated polymerization of ethylene oxide,<sup>70</sup> we have found that treatment of NHC–polypeptoid adduct (*c*-PNDG in Scheme 2.2) with excess water did not result in increased formation of linear PNDGs (*a* in Figure 2.4).

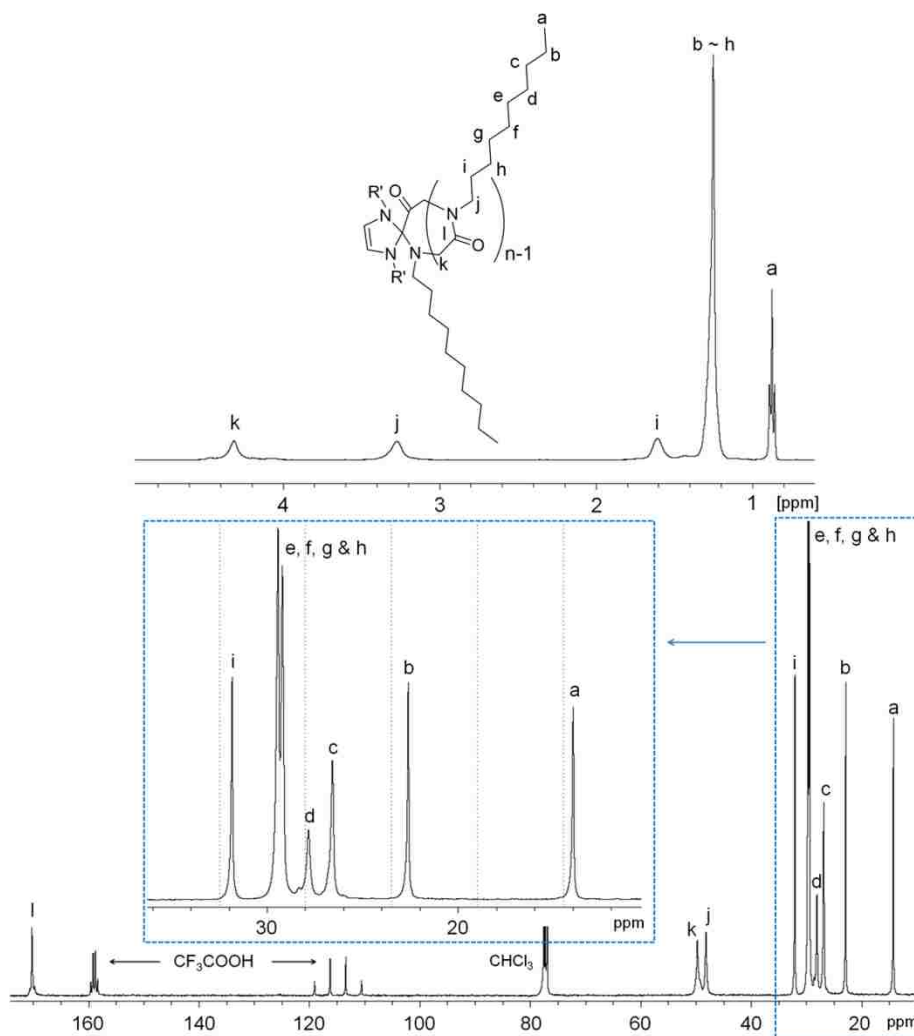


**Figure 2.3.**  $^1\text{H}$  and  $^{13}\text{C}\{^1\text{H}\}$  NMR spectra of high MW *c*-PNDGs in  $\text{CDCl}_3/\text{CF}_3\text{COOD}$ .

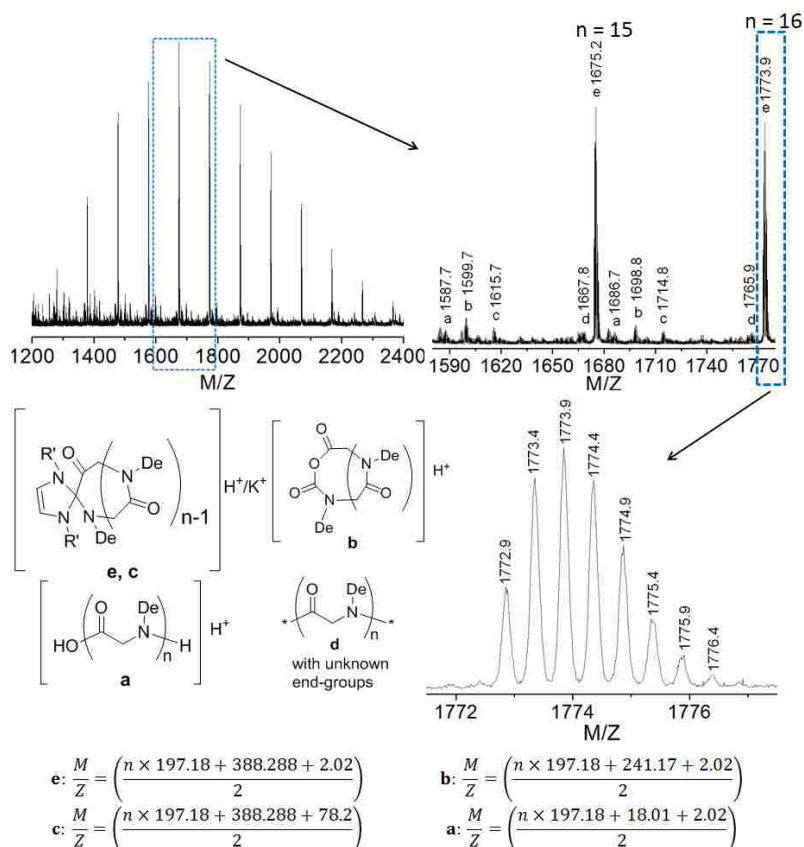


**Figure 2.4.** Representative ESI MS spectra of a low MW cyclic PNDG sample synthesized from NHC-mediated ring-opening polymerization of decyl-NCA.

Though the ESI MS results suggest that the cyclic PNDGs with one NHC affixed to the chain end are the dominant species from the NHC-mediated polymerization of  $M_1$ , high MW polymers cannot be analyzed by this method due to their poor ionization efficiency. To verify the architecture of high MW PNDG samples, SEC analysis of *c*-PNDGs ( $M_n = 20.4 \text{ kg}\cdot\text{mol}^{-1}$ , PDI = 1.20) and their linear analogs ( $M_n = 20.8 \text{ kg}\cdot\text{mol}^{-1}$ , PDI = 1.09) has been conducted (Figure 2.5). Both samples exhibit mono-modal SEC chromatograms with the *c*-PNDG sample eluting with a longer retention time than its linear analog. This suggests that the former has smaller hydrodynamic volume than the latter, consistent with the former having a cyclic architecture.

The PNDGs prepared from the NHC-mediated polymerization of  $M_1$  with different  $[M_1]_0:[\text{NHC}]_0$  ratio have been analyzed by SEC-MALS-DRI. We note that it is difficult to

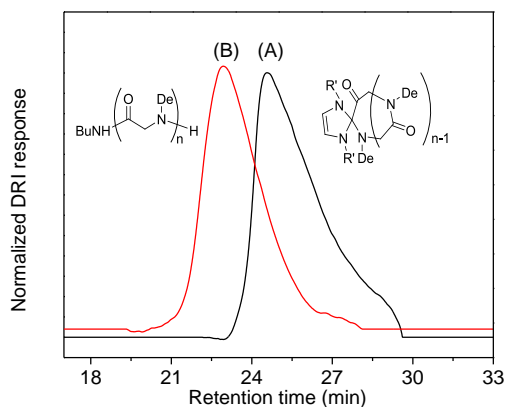


**Figure 2.5.** SEC chromatograms of (A) high MW *c*-PNDGs ( $M_n = 20.4 \text{ kg}\cdot\text{mol}^{-1}$ , PDI = 1.20) and (B) *l*-PNDGs ( $M_n = 20.8 \text{ kg}\cdot\text{mol}^{-1}$ , PDI = 1.09) that were independently prepared from the NHC-mediated and  $\text{BuNH}_2$ -initiated polymerization of decyl-NCA.

completely redissolve the dry polymer in THF even with heating. Additionally, a strong tendency of the polymer to aggregate causes erroneous and irreproducible SEC results. However, the aggregation is greatly diminished when the polymerization solution in THF is directly injected into SEC columns, which leads to reproducible SEC chromatograms (Figure 2.6). SEC-MALS-DRI analysis of the polymers reveals a systematic increase of molecular weights of polymers as the  $[\text{M}_1]_0:[\text{NHC}]_0$  ratio is raised (Table 2.1 and Figure 2.6). Furthermore, the experimental MWs determined by SEC are in good agreement with the theoretical MWs based on NHC-initiated controlled polymerization. The SEC chromatograms are mono-modal for all polymer MWs ( $4.8\text{-}31 \text{ kg}\cdot\text{mol}^{-1}$ ), and the molecular weight distributions remain reasonably narrow (PDI = 1.03-1.15). The molecular weights of the synthesized polymers also have been determined by  $^1\text{H}$  NMR analysis. More specifically, integration of the two methylene proton resonances of the PNDG repeating unit ( $j$  in Figure 2.7) relative to the four methine proton resonances of the NHC ( $m$  in Figure 2.7) yields the number average degree of polymerization, assuming each polymer chain has one affixed NHC. The MWs obtained by  $^1\text{H}$  NMR analysis also agree reasonably well with the theoretical MWs based on single-site initiation by NHCs (Table 2.1).

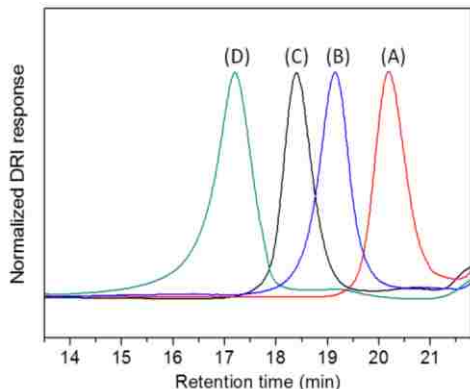


**Figure 2.6.** SEC chromatograms of *c*-PNDGs prepared from NHC-mediated polymerization of decyl ( $[M]_0:[NHC]_0 =$  (A) 25:1, (B) 50:1, (C) 100:1, and (D) 200:1).

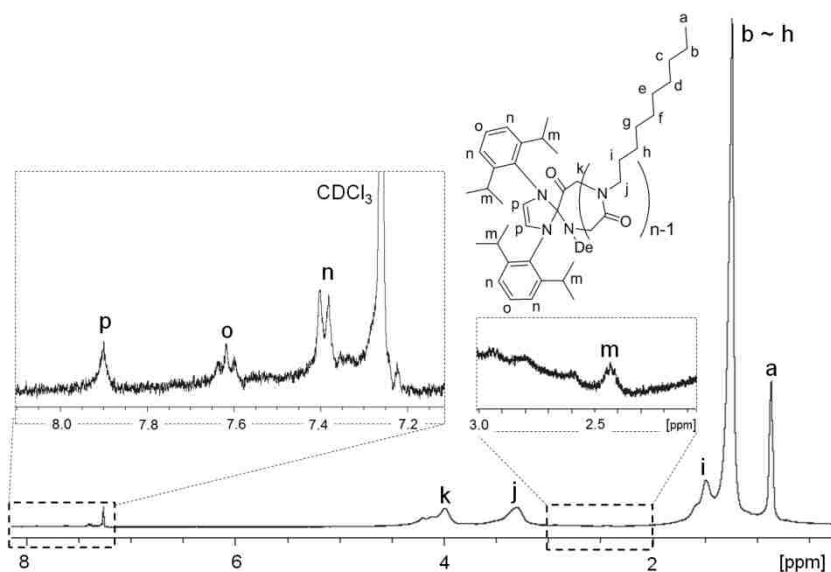


**Figure 2.7.**  $^1\text{H}$  NMR spectrum of a low MW *c*-PNDG in  $\text{CDCl}_3/\text{CF}_3\text{COOD}$  where proton resonances of the NHC are notably visible.

Polymerization kinetics were investigated at three initial NHC concentrations (i.e.,  $[\text{NHC}]_0 = 3, 8$  and  $16$  mM) and a constant, initial monomer to initiator ratio ( $[M]_0:[\text{NHC}]_0 = 50:1$ ). Conversions were determined by integrating the four methylene proton resonances of the monomer at 2.7-3.0 ppm (*k* and *j* in Figure 2.8) against those of the polymer at 3.4-3.7 and 4.0-4.2 ppm (*k'* and *j'* in Figure 2.8). Kinetic experiments were repeated twice for each polymerization condition. Figure 2.9 (A) shows the conversion of monomers to polymers ( $\ln([M]_0/[M]_1)$ ) as a function of reaction time, and Figure 2.9 (B) shows the observed rate

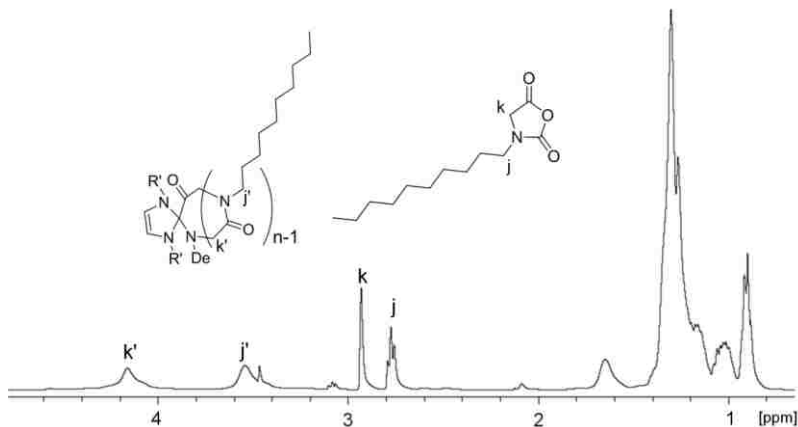


**Figure 2.8.** Representative  $^1\text{H}$  NMR spectrum of a NHC-mediated polymerization of  $\text{M}_1$  at  $70\text{ }^\circ\text{C}$  in toluene- $d_8$  showing the formation of *c*-PNDG and unreacted  $\text{M}_1$  ( $[\text{M}_1]_0:[\text{NHC}]_0 = 50:1$ ,  $[\text{M}_1]_0 = 0.4\text{ M}$ , reaction time = 62 min).

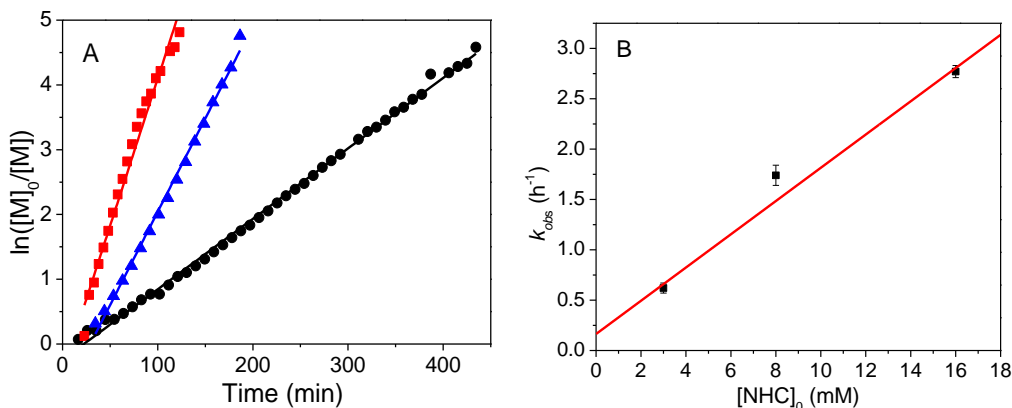


**Figure 2.9.** (A) Plots of  $\ln([\text{M}_1]_0/[\text{M}_1])$  as a function of the reaction time and their linear fits for the NHC-mediated polymerizations of decyl-NCA at  $70\text{ }^\circ\text{C}$  in toluene- $d_8$  at three different initial NHC concentrations (i.e.,  $[\text{NHC}]_0 = 3$  ( $\bullet$ ),  $8$  ( $\blacktriangle$ ),  $16\text{ mM}$  ( $\blacksquare$ )), and a constant initial monomer to NHC concentration (i.e.,  $[\text{M}_1]_0:[\text{NHC}]_0 = 50:1$ ). (B) Plot of the observed rate constant ( $k_{\text{obs}}$ ) as a function of the initial NHC concentration and its linear fit.

constant ( $k_{\text{obs}}$ ) as a function of the initial NHC concentration. As can be seen, all reactions exhibit a first-order dependence on the monomer concentration (i.e.,  $d[\text{M}_1]/dt = k_{\text{obs}}[\text{M}_1]$ ), consistent with controlled polymerization. As the initial NHC concentration ( $[\text{NHC}]_0$ ) increases from 3 to 8 to 16 mM, the observed rate constant ( $k_{\text{obs}}$ ) increases from 0.62(5) to 1.74(10) and 2.77(6)  $\text{h}^{-1}$  (Figure 2.9 (B)). The plot of  $k_{\text{obs}}$  against the initial NHC concentration reveals a linear relationship (i.e.,  $k_{\text{obs}} = k_p[\text{NHC}]_0$ , propagation rate constant  $k_p = 165(16)\text{ M}^{-1}\cdot\text{h}^{-1}$ ), indicative of



single-site initiation by the NHC. Additionally, the plot of polymer MWs as a function of conversion gives a linear relationship (Figure 2.10), suggesting a constant concentration of propagating species, consistent with controlled polymerization. The molecular weight distribution (PDI = 1.03-1.22) also remains narrow throughout the reaction.

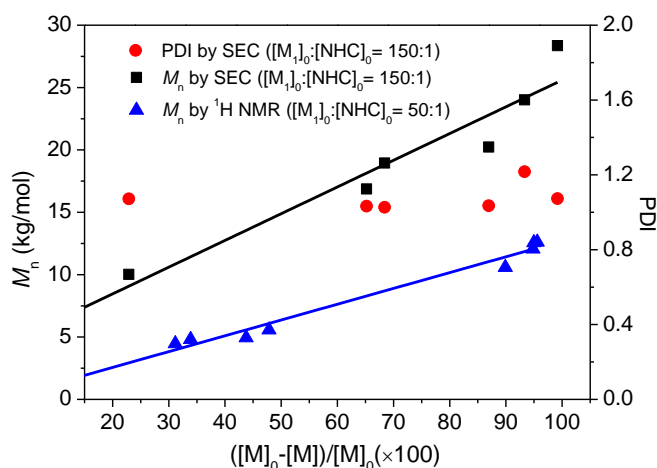


**Figure 2.10.** The plot of polymer molecular weights ( $M_n$ ) (■) determined by SEC-MALS-DRI or  $M_n$  (▲) by  $^1\text{H}$  NMR analysis and PDI (●) of *c*-PNDGs as a function of conversion for the NHC-mediated polymerization of decyl-NCA in THF at 70 °C ( $[\text{M}_2]_0:[\text{I}]_0 = 150:1$  or  $50:1$ ,  $[\text{M}_2]_0 = 0.4$  M). Note: aliquots of the polymerization solution ( $[\text{M}_2]_0:[\text{I}]_0 = 150:1$ ) was taken, filtered and directly injected into SEC columns for the MW determination over the course of reaction.

Figure 2.11 (A) shows DSC thermograms of *c*-PNDGs with different molecular weights during the second heating cycle. As can be seen, *c*-PNDGs have two, first-order endothermic transitions: one ( $T_{m,1}$ ) at 72-79 °C, and another ( $T_{m,2}$ ) at 166-176 °C. Figure 2.11 (B) shows  $T_{m,1}$  and  $T_{m,2}$  as a function of molecular weights of *c*-PNDGs. Table 2.2 summarizes melting temperatures and enthalpy change during each melting transition ( $\Delta H_{m,1}$  and  $\Delta H_{m,2}$ ). Additionally, Figure 2.12 shows DSC thermograms of the *c*-PNDGs during the cooling cycle. As can be seen, *c*-PNDGs have two, first-order exothermic transitions: one ( $T_{c,1}$ ) at 47-51 °C, another ( $T_{c,2}$ ) at 135-141 °C. Table 2.3 summarizes crystallization temperatures and enthalpy change during each

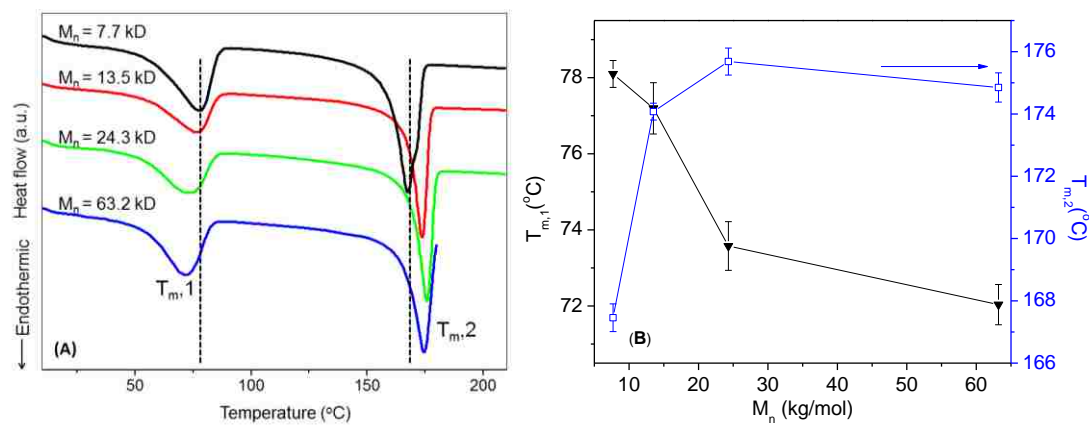


**Figure 2.11.** (A) DSC thermograms of *c*-PNDGs having different molecular weights from the second heating cycle. (B) Plots of two melting points ( $T_{m,1}$ ,  $T_{m,2}$ ) as a function of molecular weights of the polymers.

**Table 2.2.** Melting temperature and heat of fusion of *c*-PNDGs with different MWs.

Entry #	$M_n$ (kg·mol <sup>-1</sup> )	$T_{m,1}$ (°C)	$T_{m,2}$ (°C)	$\Delta H_{m,1}$ (J·g <sup>-1</sup> )	$\Delta H_{m,2}$ (J·g <sup>-1</sup> )
1	7.7	78	167	39	49
2	13.5	77	174	39	55
3	24.3	73	176	35	42
4	63.2	72	175	37	42

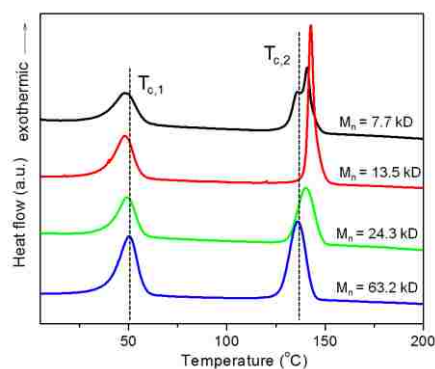


**Figure 2.12.** DSC thermograms of *c*-PNDGs having different molecular weights collected from the first cooling cycle.

**Table 2.3.** Crystallization temperature and heat of fusion of *c*-PNDGs with different MWs.

$M_n$ (kg·mol <sup>-1</sup> )	$T_{c,1}$ (°C)	$T_{c,2}$ (°C)	$\Delta H_{c,1}$ (J·g <sup>-1</sup> )	$\Delta H_{c,2}$ (J·g <sup>-1</sup> )
7.7	48.8	140.8	37.3	44.6
13.5	47.7	145.6	40.5	50.8
24.3	49.5	139.7	36.7	42.8
63.2	49.8	135.8	37.4	39.8

crystallization transition ( $\Delta H_{c,1}$  and  $\Delta H_{c,2}$ ). No notable secondary transitions were found in each cycle under the experimental conditions. Based on the magnitude of the enthalpic change ( $\Delta H_{m,1} = 35\text{-}39 \text{ J}\cdot\text{g}^{-1}$  and  $\Delta H_{m,2} = 42\text{-}55 \text{ J}\cdot\text{g}^{-1}$ ) associated with the transitions, these are attributed to melting and crystallization from the polymers. The two melting transitions ( $T_{m,1}$  and  $T_{m,2}$ ) are attributed to the crystalline packing from the side chains and main chains of *c*-PNDGs, respectively. Furthermore, the two melting transitions exhibit clear dependence on molecular weights, with the melting transition due to side chain packing ( $T_{m,1}$ ) moving to lower temperature and the melting transition due to main chain packing ( $T_{m,2}$ ) shifting to higher temperature as the MWs of polymer increases (Figure 2.11 (B)). This suggests that increasing the polymer chain length promotes the packing of the main chains and inhibits the packing of the side chains. The low-temperature melting or crystallization transitions have been rarely reported from peptoids. To have a better understanding on these transitions, systematic studies on melting and crystallization behavior from cyclic or linear polypeptoids with various *n*-alkyl side groups including ethyl, *n*-butyl, *n*-hexyl, *n*-octyl, *n*-decyl, *n*-dodecyl, and *n*-tetradecyl groups were conducted, and are presented in chapter 4.

The highly crystalline nature of the *c*-PNDGs also has been confirmed by WAXS analysis. Figure 2.13 (A) shows that a sharp primary scattering peak at  $q^*$  of  $0.26 \text{ \AA}^{-1}$  (domain spacing,  $d = 24 \text{ \AA}$ ) together with second and third order reflections are found for the thermally annealed *c*-PNDGs ( $M_n = 7.7 \text{ kg}\cdot\text{mol}^{-1}$ , PDI = 1.26), attesting to a lamellar packing of the crystalline domains. The domain spacing of  $24 \text{ \AA}$  is approximately twice the length of a fully extended decyl group (i.e.,  $12.4 \text{ \AA}$ ), consistent with the lamellar axis being parallel with the carbon chains on the decyl group (Figure 2.13 (B)). The peaks at  $q = 1.40 \text{ \AA}^{-1}$  ( $4.5 \text{ \AA}$ ) and  $q = 1.75 \text{ \AA}^{-1}$  ( $3.6 \text{ \AA}$ ) have been assigned to the in-plane diffractions off the polypeptoid main chains,

where the interchain distance is 4.5 Å and the distance between adjacent repeating units is 3.6 Å, in agreement with those previously reported for oligomeric peptoids.<sup>46,47</sup> The peak at  $q = 2.2 \text{ \AA}^{-1}$  (2.7 Å) is thereby assigned to the (110) diffraction of an orthorhombic cell ( $a = 4.5 \text{ \AA}$ ,  $b = 3.6 \text{ \AA}$ ,  $c = 24 \text{ \AA}$ ).<sup>47</sup>

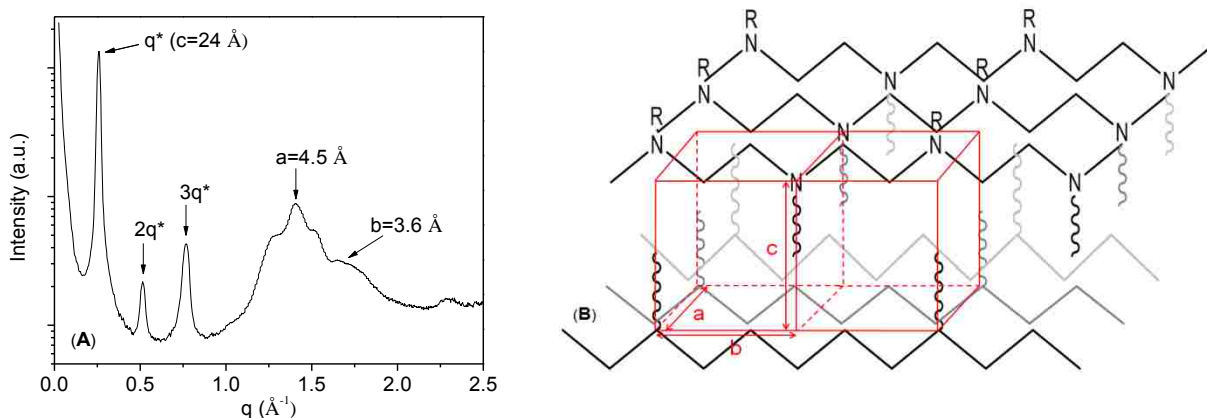


**Figure 2.13.** (A) WAXS diffractogram of a thermally annealed *c*-PNDG sample in the solid state ( $M_n = 7.7 \text{ kg}\cdot\text{mol}^{-1}$ , PDI=1.26) at room temperature and (B) the proposed crystalline packing of *c*-PNDGs based on WAXS data.

### 2.1.2.2 Synthesis and characterization of *c*-PNMG-*b*-PNDG diblock copolymers

Sequential NHC-mediated polymerizations of methyl-NCA ( $M_2$ ) and decyl-NCA ( $M_1$ ) were conducted to generate *c*-PNMG-*b*-PNDGs (Scheme 2.3). The PNMG homopolymers have poor solubility in THF and toluene, the solvents commonly used in NHC-mediated polymerizations of *N*-substituted NCAs. While acetonitrile appears to be a good solvent for PNMGs, the solubility of the polymers decreases as their MWs increases. To ensure that polymerization occurs in a homogeneous fashion, we targeted a series of *c*-PNMG-*b*-PNDG block copolymers where the PNMG block length was kept constant [ $M_n(\text{SEC-MALS-DRI}) = 10.6 \text{ kg}\cdot\text{mol}^{-1}$ ,  $\text{DP}_n(^1\text{H NMR}) = 105$ , PDI = 1.04] and the length of the PNDG blocks was systematically increased. The NHC-mediated polymerization of  $M_2$  in acetonitrile ( $[\text{M}_2]_0:[\text{NHC}]_0 = 100:1$ ,  $[\text{M}_2]_0 = 0.4 \text{ M}$ ) required 24 h at room temperature for quantitative conversion. Aliquots of the reaction mixture were taken to verify the conversion and  $\text{DP}_n$  by  $^1\text{H NMR}$  spectroscopy,

and polymer MWs and PDI by SEC-MALS-DRI. Variable amounts of  $M_1$  were subsequently introduced to the above reaction mixture, and the reaction was allowed to continue at 70 °C for another 48 h to reach full conversion. The diblock copolymers were isolated by precipitation with methanol and purified by washing with a mixture of methanol and THF. It was noted that *c*-PNMG-*b*-PNDGs with high PNDG contents become sparingly soluble in common organic solvents once they were isolated and dried. This enables the removal of any homopolymer impurities by washing with selective solvents, i.e., methanol for PNMG and THF for PNDGs. SEC-DRI analysis of a *c*-PNMG-*b*-PNDG sample with low PNDG content reveals an increase in the hydrodynamic size in comparison to the *c*-PNMG precursors, confirming successful enchainment by sequential addition of distinct monomers (Figure 2.14).

**Scheme 2.3.** Procedure to synthesize *c*-PNMG-*b*-PNDG diblock copolymers.

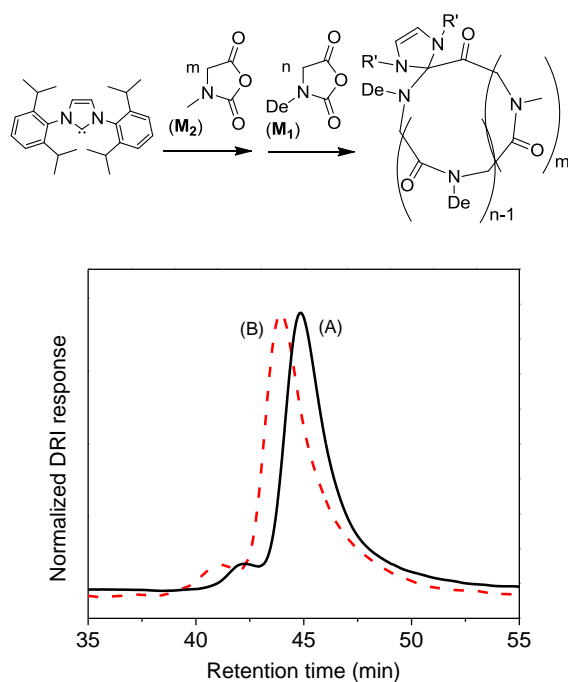


**Figure 2.14.** SEC traces of (A) *c*-PNMG<sub>105</sub>, and (B) *c*-PNMG<sub>105</sub>-*b*-PNDG<sub>15</sub>.

<sup>1</sup>H and <sup>13</sup>C{<sup>1</sup>H} NMR spectra of the purified products are consistent with the desired backbone structure of the *c*-PNMG-*b*-PNDG block copolymers (Figure 2.15 and Figure 2.16).

The NHC moieties remain attached to the block copolymers, as evidenced by the  $^1\text{H}$  NMR analysis of *c*-PNMG-*b*-PNDG with low molecular weights (Figure 2.17). Polymer MWs of *c*-PNMG-*b*-PNDG diblock copolypeptoids with high PNDG contents cannot be directly determined by SEC-MALS-DRI alone due to limited solubility and by the strong tendency to aggregate in many common organic solvents (e.g., THF,  $\text{CHCl}_3$ , methanol, or DMF). As a result,  $^1\text{H}$  NMR spectroscopy has been used in conjunction with SEC-MALS-DRI to determine the molecular weight ( $M_n$ ) of the block copolymers. More specifically, the molar ratios of the PNMG and PNDG repeating units were determined by integrating the methyl proton resonance of PNMGs (*k* in Figure 2.15) against the methyl proton resonance of PNDGs (*a* in Figure 2.15). As the absolute MWs of the PNMG blocks can be determined by SEC-MALS-DRI and  $^1\text{H}$  NMR analyses,<sup>9</sup> the  $M_n$  of the block copolymers can be deduced. All  $^1\text{H}$  NMR spectra of the block copolymers were collected either in  $\text{CDCl}_3/\text{CF}_3\text{COOD}$  or  $\text{CD}_3\text{OD}$  to ensure their complete solubility.

Table 2.4 summarizes the experimentally-determined MWs and compositions of *c*-PNMG-*b*-PNDG block copolymers. It is evident that *c*-PNMG-*b*-PNDGs with variable lengths of PNDG chains can be readily prepared by adjusting the ratio of  $[\text{M}_2]_0:[\text{M}_1]_0:[\text{NHC}]_0$ . The copolymer MWs and the relative weight fractions of the two blocks agree well with the theoretical predictions based on  $[\text{M}_2]_0:[\text{M}_1]_0:[\text{NHC}]_0$  and conversion. The deviation of molecular weights from the theoretical values is more pronounced for high MW polymers, with the copolymer having longer PNDG blocks than theoretically predicted values (entry 4 in Table 2.4). This increased deviation suggests the possibility of incomplete chain extension from the first PNMG block, presumably due to its limited solubility in the reaction medium.

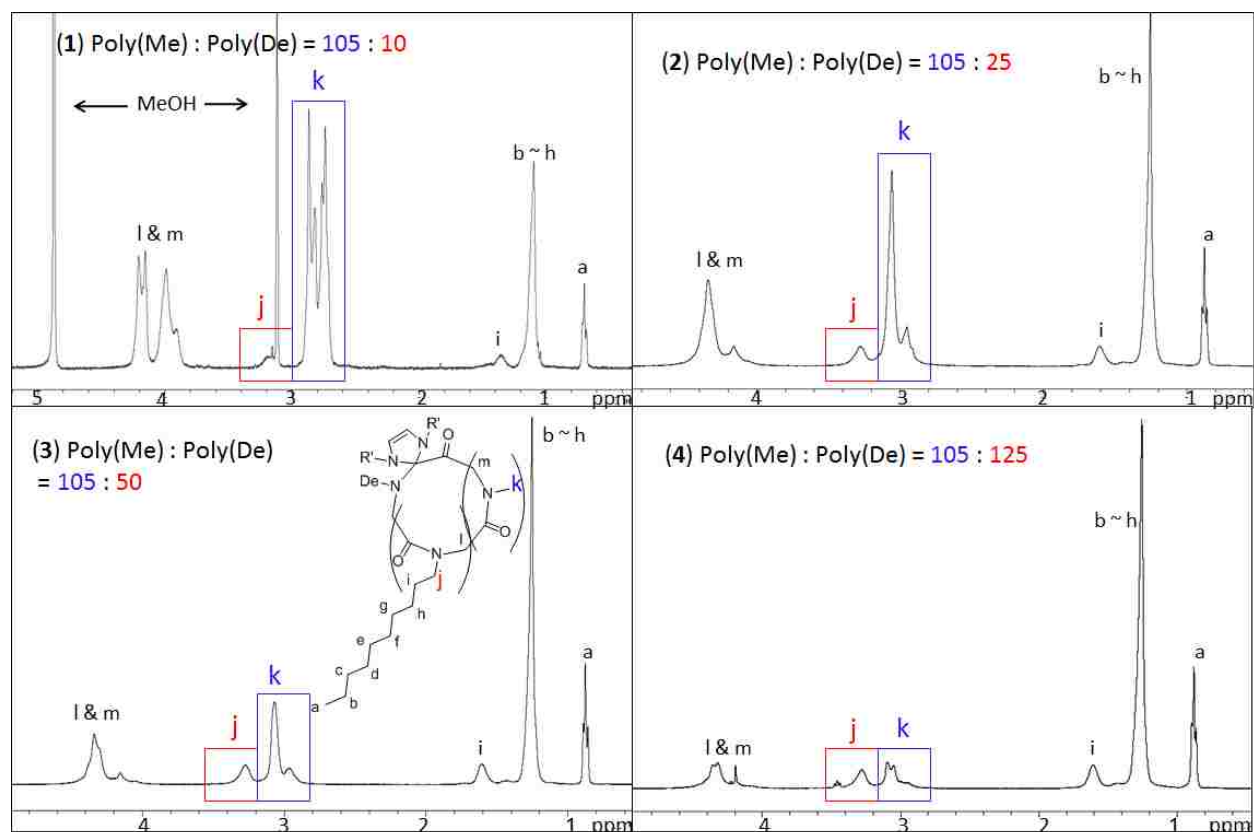


**Figure 2.15.**  $^1\text{H}$  NMR spectra of a series of cyclic diblock copolymers with various compositions: (1)  $\text{PNMG}_{105}\text{-}b\text{-PNDG}_{10}$  in  $\text{CD}_3\text{OD}$ , and (2)  $\text{PNMG}_{105}\text{-}b\text{-PNDG}_{25}$ , (3)  $\text{PNMG}_{105}\text{-}b\text{-PNDG}_{50}$ , and (4)  $\text{PNMG}_{105}\text{-}b\text{-PNDG}_{125}$  in  $\text{CDCl}_3/\text{CF}_3\text{COOD}$ .

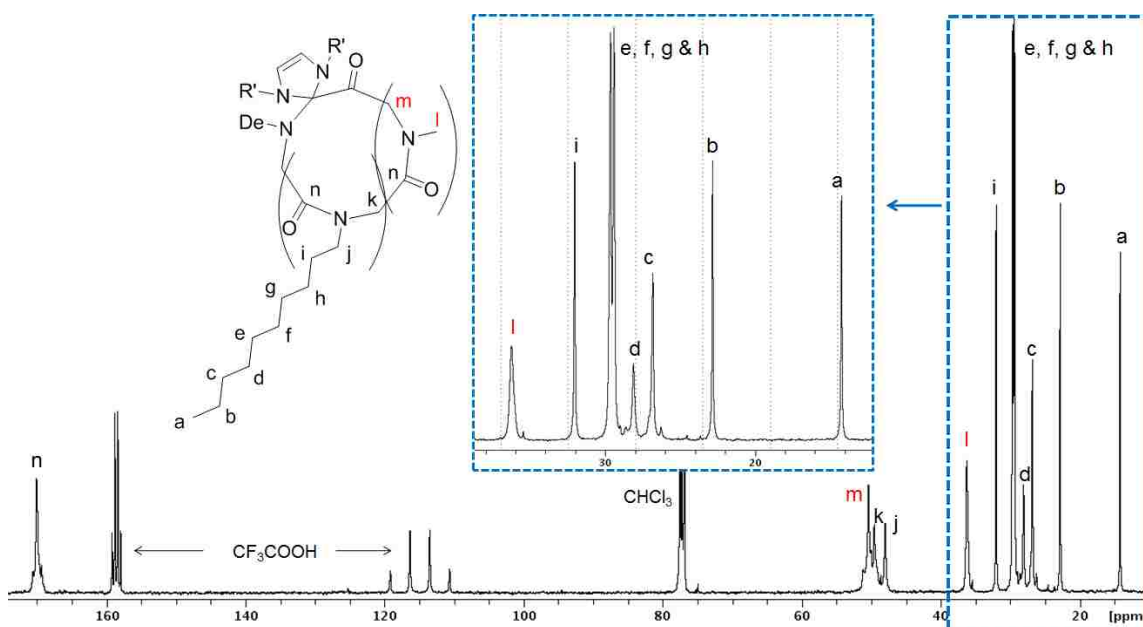


**Figure 2.16.**  $^{13}\text{C}\{^1\text{H}\}$  NMR spectra of  $c\text{-PNMG}_{105}\text{-}b\text{-PNDG}_{50}$  in  $\text{CDCl}_3/\text{CF}_3\text{COOD}$ .

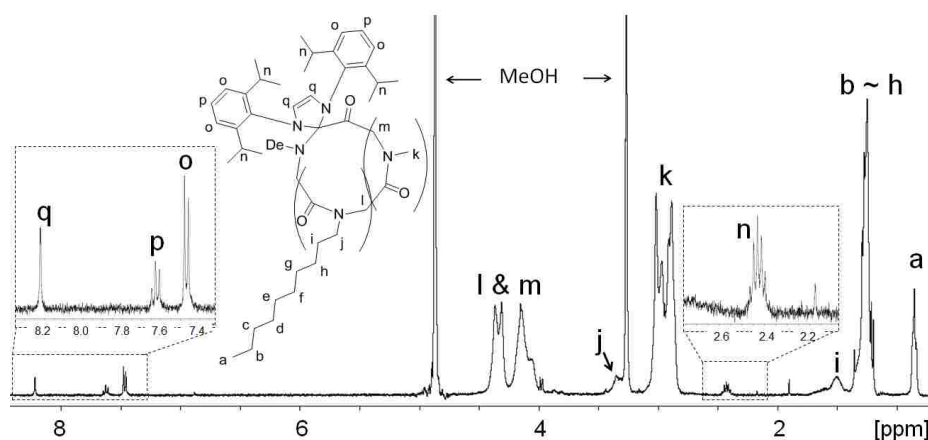


**Figure 2.17.**  $^1\text{H}$  NMR spectrum of *c*-PNMG<sub>72</sub>-*b*-PNDG<sub>8</sub> diblock copolymers in MeOD, where proton resonances of the NHC are notably visible.

**Table 2.4.** Compositions and molecular weights of *c*-PNMG-*b*-PNDG block copolymers.<sup>a</sup>

Entry #	$[\text{M}_2]_0:[\text{M}_1]_0$ : $[\text{NHC}]_0$	Experimental composition <sup>b</sup>	$M_n$ (theor.) ( $\text{kg}\cdot\text{mol}^{-1}$ ) <sup>c</sup>	$M_n$ (expt.) ( $\text{kg}\cdot\text{mol}^{-1}$ ) <sup>b</sup>	$W_{\text{PNMG}}$ (theor.) <sup>d</sup>	$W_{\text{PNMG}}$ (expt.) <sup>e</sup>	Yield (%)
1	100:10:1	PNMG <sub>105</sub> - <i>b</i> - PNDG <sub>10</sub>	9.5	9.8	0.78	0.79	85
2	100:25:1	PNMG <sub>105</sub> - <i>b</i> - PNDG <sub>25</sub>	12.4	12.8	0.59	0.60	84
3	100:50:1	PNMG <sub>105</sub> - <i>b</i> - PNDG <sub>50</sub>	17.4	17.7	0.42	0.43	85
4	100:100:1	PNMG <sub>105</sub> - <i>b</i> - PNDG <sub>125</sub>	27.2	32.5	0.26	0.23	82

<sup>a</sup> Polymerization of  $\text{M}_2$  and  $\text{M}_1$  were both allowed to reach full conversion; <sup>b</sup> the number average degree of polymerization ( $\text{DP}_n$ ) of the PNMG block was determined by  $^1\text{H}$  NMR analysis, from which the PNMG molecular weights were deduced; the block copolymer compositions were determined by  $^1\text{H}$  NMR analysis of *c*-PNMG-*b*-PNDGs, from which the copolymer molecular weights were deduced; <sup>c</sup> the theoretical molecular weights were determined from the  $[\text{M}_2]_0:[\text{M}_1]_0:[\text{NHC}]_0$  ratio; <sup>d</sup> the theoretical weight fractions of the PNMG block were determined from the  $[\text{M}_2]_0:[\text{M}_1]_0:[\text{NHC}]_0$  ratio; <sup>e</sup> the experimental weight fractions of the PNMG block were determined from the experimental compositions of the copolymers.



## **2.2 Self-Assembly of *c*-PNMG-*b*-PNDG diblock copolymers in dilute solution: crystallization-driven formation of cylindrical micelles from spherical micelles over time**

### **2.2.1 Experimental**

Cryo-TEM experiments were conducted on a Tecnai G2 12 Twin TEM operating at 120 keV, with a Gatan digital camera, and analyzed using Gatan DigitalMicrograph software. Samples were prepared on holey carbon coated 400 mesh copper grids, glow discharged in a plasma cleaner to render the carbon film hydrophilic. Grids were prepared using a FEI Vitrobot. The polymer solution (1 mg·mL<sup>-1</sup>, 2-4 μL) was pipetted onto the carbon-coated side. The grids were then blotted to remove excess solution and plunged into liquid ethane near its freezing point, resulting in a vitrified thin film (~100-300 nm). Grids were then transferred to a Gatan cryo-stage for analysis. A representative procedure for cryo-TEM sample preparation is as follows. The block copolymer was mixed in methanol at 1 mg·mL<sup>-1</sup>. The mixture was then heated to 70-80 °C and held at the temperature for 40 min in an oil bath; the opaque suspension became transparent upon heating. The solution was cooled in an oil bath to room temperature (5 °C·min<sup>-1</sup>). The copolymer solution was passed through a 0.2 μm filter (Whatman, PTFE membrane), and centrifuged at 14,000 rpm for 30 min. Finally the solution was passed through a 0.02 μm filter (Anotop 25) and analyzed at varying time intervals over a period of 0-15 days (sample incubated at room temperature).

Light scattering measurements were taken using a Lexel Laser Inc. 488 nm laser operating at 100 mW coupled with a Brookhaven Instruments Corporation goniometer. Data were collected at 90°, and the scattered intensity was measured over the first 2 days after sample preparation.

Selected area electron diffraction is conducted with a Zeiss Libra 120 with an in-column energy filter at 120 kV. An emission current as small as 5×10<sup>-6</sup> A and a 1-micron-diameter

selected area aperture are used with Al (111) (0.234 nm) standards as calibration. Typical exposure time and illumination angle are 0.6 s and 60  $\mu$ rad, respectively. A drop from a solution of cyclic PNMG-*b*-PNDGs in methanol (1 mg·mL<sup>-1</sup>) was deposited on carbon films with copper grids for TEM. Excess solution on the TEM grids was removed by filter paper, and the solution was dried in the air.

Ultrasensitive microcalorimetry differential scanning calorimetry (US-DSC) measurements were conducted by VP-DSC manufactured by MicroCal. The volume of the cell is 0.52 mL. The reference cell was filled with pure methanol. Dilute solution of *c*-PNMG<sub>100</sub>-*b*-PNDG<sub>10</sub> in methanol (1 mg mL<sup>-1</sup>) was prepared by dissolving the copolymer in methanol, heating to 70 °C, and cooling to room temperature slowly in an oil bath. This solution was filtered through a 0.02  $\mu$ m filter (Anotop 25), before aging at room temperature for VP-DSC experiment. The heat capacity of the sample after aging for 15 min or 2 weeks were recorded during heating from 25 °C to 70 °C at 0.5 °C·min<sup>-1</sup>, and cooling to 25 °C at the same rate.

<sup>1</sup>H NMR spectra were recorded on a Bruker AV-400 spectrometer, and the chemical shifts in parts per million (ppm) were referenced relative to protio impurities of CD<sub>3</sub>OD. Temperature-dependent spectra of dilute solution from cyclic or linear PNMG-*b*-PNDG in methanol (0.2 wt %) were obtained from 10 °C to 65 °C. The dilute solution sample was sealed in a J-Young NMR tube. It would be important to note that the relaxation delay of each experiment was set to be 30 seconds to allow complete relaxation. It was found that short relaxation delay (i.e. 2 seconds) caused less molar fraction of PNDG chains under identical conditions. At each temperature, the sample was stabilized for at least 10 min. The molar ratio of core-forming PNDG chains to PNMG chains in the copolymer ( $I_{PNDG}/I_{PNMG}$ ) was calculated by

integrating the methyl proton resonance of PNDGs ( $I_{PNDG}$ ) at around 0.9 ppm and the methyl proton resonance of PNMGs ( $I_{PNMG}$ ) at around 3 ppm.

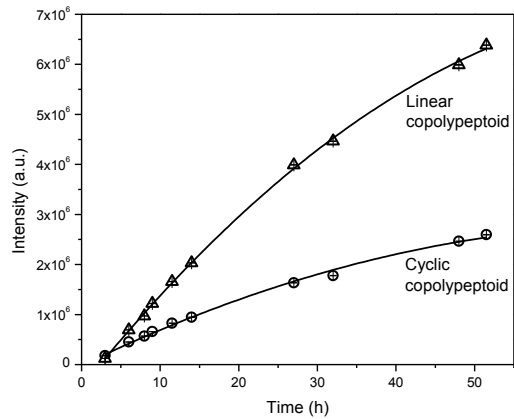
## 2.2.2 Results and discussion

### 2.2.2.1 Cryo-TEM and light scattering

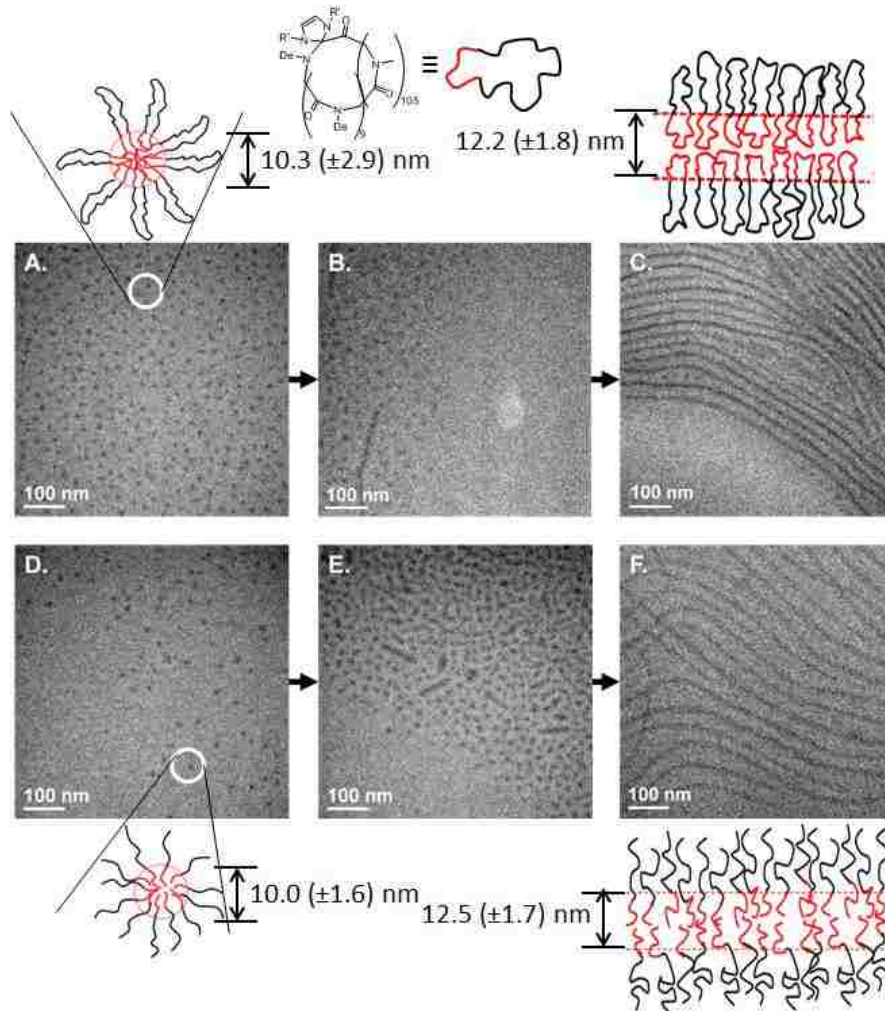
The PNMG-*b*-PNDG block copolypeptoids exhibit strong tendencies for aggregation in common solvents. It was noted that turbid methanol or aqueous suspension of *c*-PNMG<sub>105</sub>-*b*-PDMG<sub>10</sub> becomes clear upon gentle heating and remains so for an extended period of time (> 6 months) after cooling to room temperature. To investigate the aggregate structures of the block copolypeptoids in methanol, a dilute methanol solution of *c*-PNMG<sub>105</sub>-*b*-PDMG<sub>10</sub> (1.0 mg·mL<sup>-1</sup>) was characterized by both light scattering and cryo-TEM over a period of 15 days.

Figure 2.18 shows light scattering analysis of *c*-PNMG<sub>105</sub>-*b*-PDMG<sub>10</sub> solutions in methanol. It reveals an increase in intensity over the first 2 days, suggesting an increase in size of the self-assembled structures. The linear copolypeptoid solution showed a more rapid increase in turbidity compared to the cyclic copolypeptoid solution.

A kinetic cryo-TEM study of *c*-PNMG<sub>105</sub>-*b*-PDMG<sub>10</sub> reveals the initial formation of spherical micelles in methanol at room temperature within 30 min of sample preparation (Figure 2.19 A). After 1 h the spherical micelles remained; however, after 2 h the appearance of cylindrical micelles was evident (Figure 2.19 B), which appeared to increase in length over time (Figure 2.19 C). Over the course of the first 24 h the solution remained a mixture of spherical and cylindrical micelles as the spherical micelles continued to aggregate and form longer cylindrical micelles. After 7 days, cylindrical micelles were the dominant species, which continued to increase in length over the course of the next 15 days. After 15 days, the formation of mostly micron-long cylindrical micelles were evident with a very small fraction of spherical



**Figure 2.18.** Turbidity measurements of both linear and cyclic PNMG<sub>105</sub>-*b*-PDMG<sub>10</sub> solutions in methanol over the first two days after preparation.



**Figure 2.19.** Representative cryo-TEM images obtained from dilute methanol solutions of cyclic PNMG<sub>105</sub>-*b*-PNDG<sub>10</sub> block copolypeptides after (A) 1 h, (B) 2 h, and (C) 15 d, and linear PNMG<sub>112</sub>-*b*-PNDG<sub>16</sub> block copolypeptides after (D) 1 h, (E) 2 h, and (F) 7 d in methanol.

micelles remaining (Figure 2.19 C). The darker areas in the cryo-TEM images correspond to the PNDG-rich regions as a result of their higher electron density relative to that of the solvated PNMG blocks. Being solvophobic and highly crystalline, the PNDG blocks constitute the cores of the micelles in methanol, whereas the solvophilic and amorphous PNMG blocks constitute the coronas of the micelles, which is shown in structural schemes in Figure 2.19. The average core diameter of the spherical micelles is 10.3 ( $\pm 2.9$ ) nm (Figure 2.19 A). Over the course of 15 days, the spherical micelles slowly reorganize into micron-long cylindrical micelles with a uniform core diameter of 12.2 ( $\pm 1.8$ ) nm (Figure 2.19 C).

Additionally, the evolution of spherical micelles into cylindrical micelles was observed for the linear diblock copolypeptoid (*l*-PNMG<sub>112</sub>-*b*-PNDG<sub>16</sub>) that was prepared from sequential BuNH<sub>2</sub>-initiated polymerization of methyl-NCA and decyl-NCA. Cryo-TEM analysis of *l*-PNMG<sub>112</sub>-*b*-PNDG<sub>16</sub> reveals the morphological transition from spherical micelles with the diameter of 10.0 ( $\pm 1.6$ ) nm (Figure 2.19 D) into cylindrical micelles with the diameter of 12.5 ( $\pm 1.7$ ) nm (Figures 2.19 E and F) over a faster time scale than the cyclic copolypeptoids. The analysis of *l*-PNMG<sub>112</sub>-*b*-PNDG<sub>16</sub> revealed the cylindrical micelles were the dominant species after only 8 days, with no spherical micelles remaining in solution after the full 15 days. The different rates of transition in the cyclic and linear copolypeptoid solutions revealed by cryo-TEM (Figure 2.19) are consistent with the results of light scattering experiments (Figure 2.18) where a faster increase in total light scattering intensity was measured for the linear copolypeptoid relative to its cyclic counterpart. The morphological transition is attributed to the crystallization of the hydrophobic PNDG chains, which is retarded in the cyclic copolypeptoid aggregates, leading to the slower structural transitions. The following sections discuss the origin of the formation of cylindrical micelles.

Previous studies on the self-assembly of amorphous-crystalline diblock copolymers [i.e. polyisoprene-*b*-polyferrocenylsilane,<sup>71-74</sup> poly(3-hexylthiophene)-*b*-poly(dimethylsiloxane),<sup>75</sup> poly(lactide)-*b*-poly(acrylic acid)<sup>76</sup>] have shown that the formation of cylindrical micelles is the result of maximizing the packing of the short crystalline blocks. The cylindrical micelles undergo epitaxial growth in a living manner with the addition of the block copolymer unimers.<sup>71-74</sup> In contrast, cryo-TEM images of the block copolypeptoid samples taken between 1 hr and 15 days reveal that spherical micelles are initially formed before merging into one another to generate the cylindrical micelles (Figures 2.19 B and E) that continue to grow in length (Figures 2.19 C and F), suggesting an aggregation-induced morphological transition. This transition to eventually form cylindrical micelles can be explained by energy balance between energy penalty from stretching PNMG chains and favor from folding crystalline PNDG chains.<sup>71</sup> While hydrophilic PDMGs chains stretch out in methanol, resulting in entropic penalty in the system, crystalline PNDG chains favorably make folds in the lamellar domains.

Finally, Figure 2.20 shows that the SEC-DRI chromatogram of a cyclic copolypeptoid (i.e., *c*-PNMG<sub>105</sub>-*b*-PDMG<sub>15</sub>) obtained after 17 days in methanol at room temperature is identical to that of the original sample. This SEC analysis suggests that the cyclic copolypeptoids keep their cyclic architecture intact in methanol for more than 2 weeks.

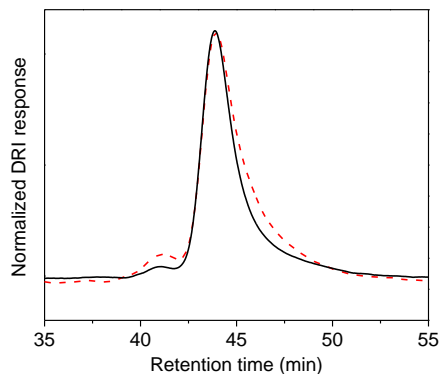


**Figure 2.20.** SEC-DRI chromatograms of (A) cyclic PNMG<sub>105</sub>-*b*-PNDG<sub>15</sub> diblock copolymers obtained after 17 days in methanol (---) and the original sample (—).

### 2.2.2.2 Selected area electron diffraction (SAED)

The formation of cylindrical micelles from the copolymers over time is attributed to crystallization of core-forming PNDG chains. To verify this crystallization-driven self-assembly, the spherical and cylindrical micelles obtained from  $\text{PNMG}_{100}\text{-}b\text{-PNDG}_{10}$  at the concentration of  $1.0 \text{ mg}\cdot\text{mL}^{-1}$  after aging for 15 min and 14 d in methanol at room temperature were analyzed by selected area electron diffraction (SAED) technique. As shown in Figure 2.21 (A), the spherical micelles do not show any distinct SAED reflection, suggesting the amorphous nature of the micelles. In contrast, Figure 2.21 (B) shows the cylindrical micelles exhibit a distinct ring with  $0.29 \text{ nm}$  spacing and uneven intensity in the azimuthal direction. The uneven intensity is due to the different orientation of cylindrical micelles in the SAED focal plane. Based on the crystal structure of lower paraffins,<sup>77</sup> the  $0.29 \text{ nm}$  spacing corresponds well to (01-7) diffraction in nonane. This result further supports the presence of alkyl-chain packed, crystalline domains in the cylindrical micelles.

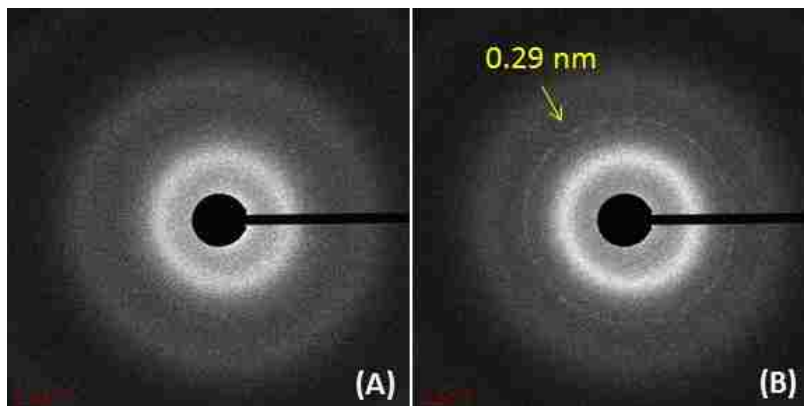


**Figure 2.21.** SAED patterns of (A) spherical and (B) cylindrical micelles obtained by the self-assembly of  $c\text{-PNMG}_{100}\text{-}b\text{-PNDG}_{10}$  in methanol ( $1.0 \text{ mg}\cdot\text{mL}^{-1}$ ) after aging for 15 min and 14 d at room temperature, respectively.

### 2.2.2.3 Ultrasensitive microcalorimetry differential scanning calorimetry (US-DSC)

Figure 2.22 shows microcalorimetric endotherms for  $c\text{-PNMG}_{100}\text{-}b\text{-PNDG}_{10}$  diblock copolymers in methanol at a concentration of  $1 \text{ mg}\cdot\text{mL}^{-1}$  at different aging times. An

endothermic peak at 58 °C with an enthalpic change ( $\Delta H_m$ ) of 3.8 cal·g<sup>-1</sup> (16 J·g<sup>-1</sup>) was developed after aging for 2 weeks at room temperature, while no peaks were observed after aging for 15 min. This endothermic transition is attributed to melting or disordering of crystalline domains formed from crystalline PNDG chains of the copolymers in methanol over sufficient time. Figure 2.22 further shows that the heat capacity ( $C_p$ ) increased by 0.75 cal·g<sup>-1</sup>·°C<sup>-1</sup> after the melting transition. This increased heat capacity suggests any morphological transitions from the copolymers, as the solvophobic PNDG segments become more exposed to the solvent at the elevated temperature. Similar behaviors are well documented for the denaturing of proteins where the hydrophobic interiors become increasingly exposed to water as the proteins unfold.<sup>78-</sup>

80

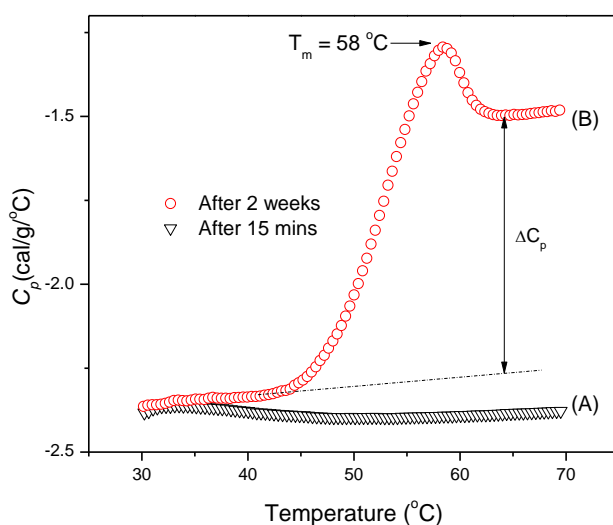


**Figure 2.22.** Microcalorimetric endotherms for *c*-PNMG<sub>100</sub>-*b*-PNDG<sub>10</sub> diblock copolymers in methanol (1 mg·mL<sup>-1</sup>) during heating, after aging (A) for 15 min and (B) for 2 weeks at room temperature.

#### 2.2.2.4 Variable-temperature NMR spectroscopy

To detect any morphological transitions of the copolymer in solution at a concentration of 0.2 wt % at different temperatures, variable-temperature NMR experiment was conducted. Figure 2.23 shows <sup>1</sup>H NMR spectra at temperatures between 10 °C and 65 °C collected from *c*-



PNMG<sub>100</sub>-*b*-PNDG<sub>10</sub> in deuterated methanol after aging for 2 weeks, molar ratio of PNMG chains to PNDG chains as a function of temperature, and its sigmoidal fit. As can be seen, a sigmoidal curve was observed for the plot of <sup>1</sup>H NMR integration of the methyl protons from PNDGs relative to those of the PNMGs as a function of temperature. As the temperature increases, the ratio increases from 0.090 to 0.15 with a two state-transition and a transition temperature at 45 °C. This indicates that solvophobic PNDG chains are more solvated at high temperature. This may lead to increased mobility, and thus curvature of the copolymers in dilute solution,<sup>81</sup> suggesting a morphological transition from cylindrical micelles to spherical micelles upon heating presumably due to a melting of crystallized PNDG chains.

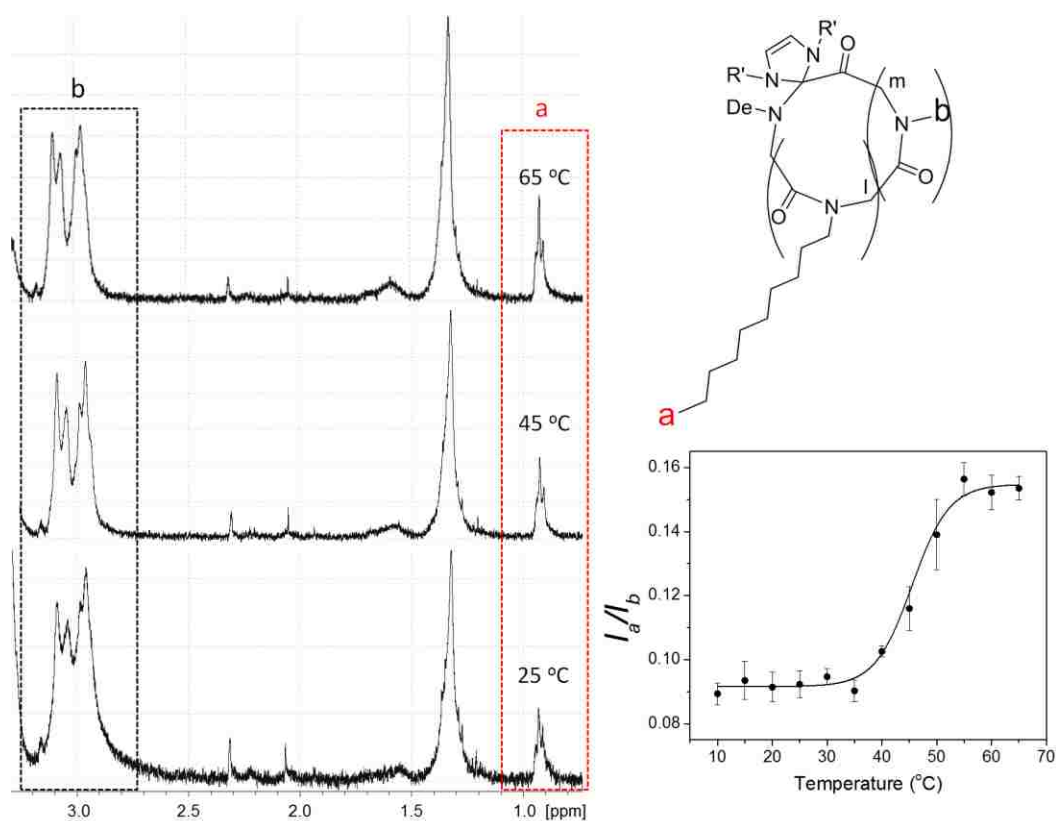


**Figure 2.23.** <sup>1</sup>H NMR spectra of *c*-PNMG<sub>100</sub>-*b*-PNDG<sub>10</sub> in CD<sub>3</sub>OD (0.2 wt %) after aging for 2 weeks at 25, 45 and 65 °C, the ratio of integration from PNDG methyl protons to that of PNMG methyl protons as a function of temperature, and a sigmoidal fit of the data.

## 2.3 Crystallization-driven, thermo-reversible gelation from *c*-PNMG-*b*-PNDG diblock copolypeptoids

### 2.3.1 Introduction

Gels are defined as “a substantially dilute system that does not exhibit steady-state flow.”<sup>82</sup> A material to fulfill this definition includes 3D networks of molecules that can immobilize substantial amount of solvent.<sup>83</sup> Hydro- (water as solvent) or organo- (organic solvent) gels from polymeric materials have attracted much attention in recent decades. Chemical gels can be prepared by cross-linking a polymer matrix, but networks from the cross-linked polymers are irreversible, meaning that gels may not be self-healed, after broken.<sup>83,84</sup> Physical gels are of growing interest, as they can be formed by intermolecular networks or entanglement of polymeric microdomains, or by supramolecular, non-covalent bonding interactions such as hydrophobic interactions, hydrogen bonding, ionic interactions, host-guest interactions of macrocyclic hosts,<sup>84</sup> and metal-ligand interactions.<sup>83-88</sup> As a result, physical gels may provide broad applications of tissue engineering and drug delivery, as the sol-gel transition can be reversible to external stimuli including temperature, pH, or light. It was reported that thermo-responsive, biocompatible hydrogels provide benefits including solubilization of low-molecular-weight hydrophobic drugs, controlled release, prolonged circulation time and site-specific delivery.<sup>89-92</sup>

Amphiphilic block copolymers are widely considered as gelators to generate physical gels, because they self-assemble to form micelles of various morphologies including spheres, cylinders, or vesicles in dilute solution. These micelles may form gels when the concentration of the solution exceeds critical gel concentration. Block copolymers provide advantages such that one may tune physical properties and responsibility of the gels by altering polymer structures, molecular weights, concentrations, compositions, and architectures.<sup>86</sup> Recently, stimuli

(temperature, pH, or light)-responsive polymers were widely selected as a building block in block copolymers to generate responsive gels to those stimuli.<sup>91</sup> For example, thermo-responsive hydrogels were reported from block copolymers composed of hydrophilic, thermoresponsive poly(ethylene glycol) (PEG or PEO)<sup>93</sup> and such hydrophobic polymers as poly(propylene oxide) (PPO),<sup>94</sup> poly(L-lactic acid),<sup>95</sup> poly(D,L-lactide-*co*-glycolide) (PLGA),<sup>96</sup> and poly( $\epsilon$ -caprolactone) (PCL).<sup>91,97</sup> Thermoresponsive hydrogels were also reported from ABA-type,<sup>98,99</sup> and ABC-type triblock copolymers<sup>86</sup> composed of thermoresponsive poly(*N*-isopropylacrylamide) (PNIPAM) as end blocks. Hydrogels responsive to more than one stimulus were further prepared by selecting the polymers responsive to multiple stimuli. For example, Nguyen et al.<sup>99</sup> reported thermo- and pH-responsive hydrogels from ABA triblock copolymers composed of hydrophilic poly(ethylene glycol) (PEG) blocks, and thermo- and pH-responsive poly(amidoamine) (PAA) blocks, (PAA-PEG-PAA). Jiang et al.<sup>98</sup> reported sol-gel-sol transitions from thermo- and light-responsive AB-type diblock copolymers composed of hydrophilic poly(ethylene oxide) blocks and random copolymers of thermoresponsive poly(ethoxytri(ethylene glycol) acrylate) blocks and light-responsive poly(nitrobenzyl acrylate) as responsive hydrophobic blocks.

However, thermoreversible gelation from amphiphilic block copolymers composed of semi-crystalline, hydrophobic blocks has rarely been reported. Furthermore, peptoid or polypeptoid gelators have not been reported yet. This section presents the formation of free-standing gels from cyclic or linear PNMG<sub>100</sub>-*b*-PNDG<sub>10</sub> diblock copolymers at a concentration of 5 wt % or 10 wt %. Viscoelastic properties of gels from cyclic or linear PNMG-*b*-PNDG were studied by rheological measurements. Temperature-variable NMR studies of the gels were conducted to investigate any temperature-induced morphological change of the gels from the copolymers. Thermo-reversible gelation of cyclic PNMG-*b*-PNDG was studied by DSC.

Morphologies of the gels from cyclic copolymers were observed by polarized optical microscopy (POM). The gels were analyzed by WAXS and SAXS to probe the origin of formation of harder gels from cyclic copolymers than linear ones. To investigate the role of the core-forming crystalline blocks for the gelation of the copolymers, cyclic poly(*N*-methyl-glycine)-*b*-poly(*N*-2-ethyl-1-hexyl-glycine) diblock copolymers (*c*-PNMG-*b*-PNEHG) were synthesized and examined for thermoreversible gelation.

## 2.3.2 Experimental

### 2.3.2.1 Synthesis of cyclic or linear PNMG-*b*-PNDGs

*c*-PNMG-*b*-PNDGs were synthesized by the procedure presented in section 2.1.1.4. *l*-PNMG-*b*-PNDGs were synthesized by using benzylamine as an initiator. The degree of polymerization (DP) of PNMG blocks was determined by  $^1\text{H}$  NMR, and relative DP of PNDGs was also determined by  $^1\text{H}$  NMR. Scheme 2.4 shows a synthetic route to prepare *c/l*-PNMG-*b*-PNDG diblock copolymers. Table 2.5 summarizes molecular parameters of the copolymers studied in this section.

**Scheme 2.4.** Synthetic procedure to prepare *c/l*-PNMG-*b*-PNDG diblock copolymers.

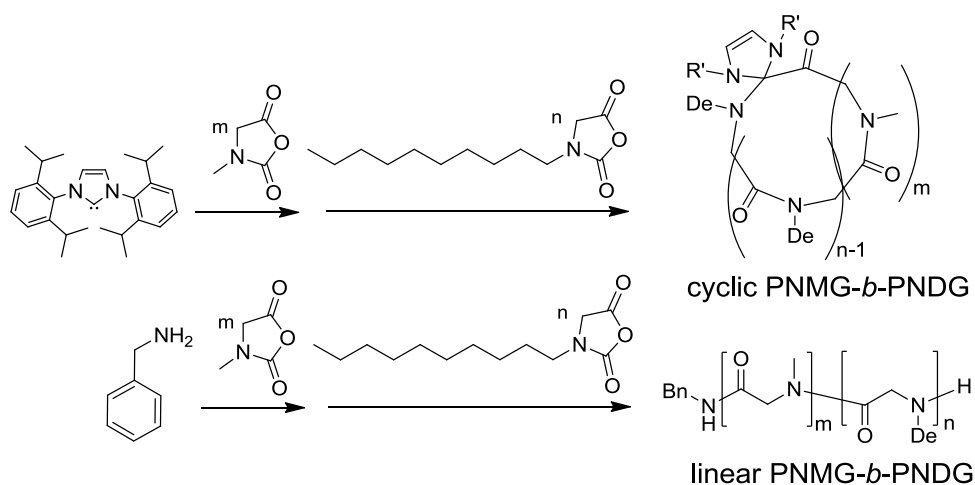


**Table 2.5.** Molecular parameters of *c/l*-PNMG-*b*-PNDG diblock copolymers presented in section 2.3.

sample <sup>a</sup>	$N_{\text{PNMG}}^b$	$N_{\text{PNDG}}^c$	$M_n^d$ ( $\text{kg}\cdot\text{mol}^{-1}$ )	$M_n^e$ ( $\text{kg}\cdot\text{mol}^{-1}$ )	$PDI^f$	$f_{\text{PNDG}}^g$
<i>c</i> -PNMG <sub>100</sub> - <i>b</i> -PNDG <sub>10</sub>	100	10	9.5	14.7	1.21	0.09
<i>l</i> -PNMG <sub>100</sub> - <i>b</i> -PNDG <sub>10</sub>	100	10	9.2	12.5	1.05	0.09

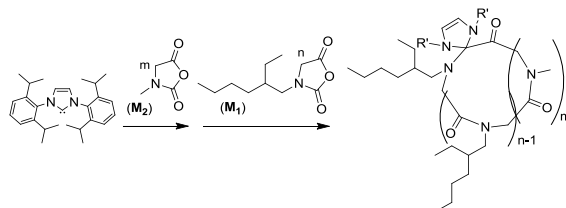
<sup>a</sup>The numbers in subscripts correspond to number average degree of polymerization ( $DP_n$ ) as determined by <sup>1</sup>H NMR spectroscopy. <sup>b</sup>Number average degree of polymerization of PNMG blocks was determined by end-group analysis using <sup>1</sup>H NMR in CD<sub>3</sub>OD. <sup>c</sup>Relative degree of polymerization was determined by <sup>1</sup>H NMR in CDCl<sub>3</sub>/CF<sub>3</sub>CO<sub>2</sub>D. <sup>d</sup>Number average molecular weights were calculated as determined by <sup>1</sup>H NMR. <sup>e,f</sup>The relative number average molecular weights and polydispersity index were determined by SEC-DRI using polystyrene standards in DMF/LiBr(0.01M). <sup>g</sup>The molar fraction of PNDG block was calculated from DP of each block.

### 2.3.2.2 Synthesis of cyclic poly(*N*-methyl-glycine)-*b*-poly(*N*-2-ethyl-1-hexyl-glycine) diblock copolymers (*c*-PNMG-*b*-PNEHGs)

Scheme 2.5 shows a synthetic procedure to prepare *c*-PNMG-*b*-PNEHGs. In the glovebox, methyl-NCA ( $M_2$ ) (86 mg, 0.74 mmol,  $[M_2]_0 = 0.4$  M) was dissolved in anhydrous acetonitrile (1.9 mL). A known volume of NHC/THF stock solution (168  $\mu$ L, 11  $\mu$ mol, 63.2 mM,  $[M_2]_0:[\text{NHC}]_0 = 70:1$ ) was added using a syringe. Polymerization was allowed to proceed for 24 h at room temperature under a nitrogen atmosphere. Aliquots of the reaction mixture were taken and analyzed for conversion by <sup>1</sup>H NMR and molecular weights by SEC. An acetonitrile solution (2.5 mL) containing 2-ethyl-1-hexyl-NCA ( $M_1$ ) (23 mg, 0.11 mmol,  $[M_1]_0 = 0.4$  M,  $[M_1]_0:[\text{NHC}]_0 = 10:1$ ) was added into the above reaction mixture, which was heated at 70 °C for additional 24 h to reach complete conversion. The polymer product was precipitated by the

addition of cold hexanes and collected by filtration. Following filtration, the polymer was washed with ample hexanes and followed by THF to remove any unreacted monomers or homopolymers, and dried under vacuum (45 mg, 63% yield).

**Scheme 2.5.** Synthetic procedure for cyclic *c*-PNMG-*b*-PNEHG diblock copolymers.



### 2.3.2.3 Preparation for gels from PNMG-*b*-PNDGs

Polymers as a slightly yellow powder for cyclic copolymers and a white one for linear ones were dissolved in methanol at a designated concentration (2, 5, or 10 wt %), and heated to 70 °C for 15 min. The cloudy solution became clear upon heating. Then the solution was slowly cooled to room temperature in an oil bath. At a concentration of 5 wt % or 10 wt %, cyclic or linear PNMG-*b*-PNDGs formed free-standing gels, but the cyclic ones behaves differently from the linear ones. For cyclic PNMG-*b*-PNDGs, free-standing gels formed from 10 wt % solution in about 3 h after cooling to room temperature, and 5 wt % overnight (ca. 20 h). Free standing gels did not form from 2 wt %, but rheological studies indicates they are “soft gels,”<sup>86</sup> as  $G'$  is higher than  $G''$  as a function of angular frequency in the linear viscoelastic region. For linear PNMG-*b*-PNDGs, 10 wt % solution formed free-standing gels overnight (ca. 20 h). Solution of a 5 wt % concentration formed gels, but did not stand by its weight well. Solution of 2 wt % did not form free-standing gels. Rheological studies on the 5 wt % and 2 wt % solution show that  $G'$  is higher than  $G''$ , indicating that they are “soft gels.”<sup>86</sup> These “soft gels” are not gels by the definition of gels by Ferry,<sup>82</sup> which was pointed out earlier in this section. Rather, they are a viscoelastic liquid which has higher solid-like character than liquid-like character.

#### 2.3.2.4 Instrumentations

$^1\text{H}$  NMR spectra were recorded on a Bruker AV-400 spectrometer, and the chemical shifts in parts per million (ppm) were referenced relative to protio (lightest isotope of hydrogen) impurities of  $\text{CD}_3\text{OD}$ . Temperature-dependent spectra of cyclic or linear PNMG-*b*-PNDG gels in  $\text{CD}_3\text{OD}$  (5 wt %) were obtained from 10 °C to 65 °C. The copolymers were dissolved in methanol at a certain concentration, and heated to 70 °C. When the copolymers in methanol form a free-flowing liquid, the solution was sealed in a J-Young NMR tube. This solution was cooled to room temperature to form gels. This experiment was done by the same procedure for variable-temperature NMR of PNMG-*b*-PNDG at a concentration of 0.2 wt %, as described in section 2.1.1.2.

Rheological experiments were conducted using a TA AR 2000ex rheometer. A parallel-plate geometry of 40 mm diameter was used. In each experiment, approximately 0.3 mL of the sample was loaded between the plates with a gap of 200  $\mu\text{m}$ . The plate cover was then put on the plates that were sealed with highly viscous oil to minimize evaporation of the solvent. Dynamic storage modulus ( $G'$ ) and loss modulus ( $G''$ ) of PNMG-*b*-PNDG gels in methanol (10, 5, or 2 wt %) were measured by oscillatory shear experiments. Dynamic strain sweep experiments were conducted at a frequency of 1 or 10 ( $\text{rad s}^{-1}$ ) at 25 °C to determine the linear viscoelastic regime. Dynamic frequency sweep experiments were conducted within the linear viscoelastic regime (at a strain amplitude of  $\gamma = 1.0\%$ ) at 25 °C as a function of angular frequency from 0.1 to 100 ( $\text{rad}\cdot\text{s}^{-1}$ ). Steady-state flow experiments were conducted by a shear rate ramp from 0.1 to 100  $\text{s}^{-1}$  for equilibrium duration of 10 min at 25 °C to measure apparent viscosity and shear stress as a function of shear rate.

Morphologies of *c*-PNMG<sub>100</sub>-*b*-PNDG<sub>10</sub> gels were observed by a polarized optical microscopy equipped with a hot stage (Mettler) under crossed polarizers. Polymers were dissolved in methanol, and heated to 70 °C until the solution became clear. Then this solution was sealed in a capillary tube, and aged at room temperature for 20 h. Upon cooling to room temperature and aging, the free-flowing liquid became a free-standing gel. POM micrographs of the gels were taken by a Canon digital camera during heating from room temperature (ca. 21 °C) to 60 °C.

DSC studies of *c*-PNMG<sub>100</sub>-*b*-PNDG<sub>10</sub> gels in methanol (10 wt %) were conducted using a TA DSC 2920 calorimeter under nitrogen. The gel sample of 10.9 mg was hermetically sealed between an aluminum pan and lid. This DSC sample was heated from 10 °C to 65 °C at 2 °C·min<sup>-1</sup>, and cooled from 65 °C to 10 °C at the same rate. Heat flow was recorded during heating and cooling cycles, and normalized by the mass (g) of the sample.

For WAXS and small angle X-ray scattering (SAXS) experiments, cyclic or linear copolymers were dissolved in methanol (10 wt %), and heated to 70 °C. This solution was sealed in a capillary tube with a diameter of 1 mm (Charles Supper Company, Natick, MA), and aged for 20 h at room temperature. SAXS data were collected using a Gabriel style 2D multiwire gas proportional counter with 200 mm active diameter in a 1024×1024 array.<sup>68</sup> The resolution of the detector is 200 – 250 μm FWHM at 8 keV with a *q* range from 0.0015 to 0.44 Å<sup>-1</sup>.

Atomic force microscopy (AFM) analysis was conducted to investigate the structures of gels from cyclic or linear PNMG<sub>100</sub>-*b*-PNDG<sub>10</sub>. Gels samples were characterized using a model 5500 scanning probe microscope from Agilent Technologies (Chandler, AZ) equipped with Picoview v1.12.4 software. Images were acquired using tapping-mode with probes from AppNano (Santa Clara, CA). The tip was driven to oscillate at a driving frequency of 339 kHz.



Images were processed using Gwyddion open source software, which is supported by the Czech Metrology Institute.<sup>100</sup> AFM samples were prepared by the following procedure. Polymers were dissolved in methanol at a concentration of 1 wt % for cyclic copolymers and 5 wt % for linear copolymers, heated to 70 °C, and cooled to room temperature. A 5  $\mu$ L drop of the soft gel was placed on freshly cleaved mica(0001). The samples were dried and stored in a desiccator for 24 h before AFM analysis. Different concentrations were used to achieve sufficient dilution for surface characterizations with AFM.

### 2.3.3 Results and discussion

#### 2.3.3.1 Thermo-reversible gelation from PNMG-*b*-PNDG

*c*-PNMG<sub>100</sub>-*b*-PNDG<sub>10</sub> and *l*-PNMG<sub>100</sub>-*b*-PNDG<sub>10</sub> copolymers in methanol form opaque and free-standing gels at room temperature at elevated concentrations at 5 wt % and 10 wt %, respectively (Figure 2.24). The gels dissolve upon heating to 70 °C to form a transparent and free-flowing liquid. Gelation and dissolution of the gels are thermally reversible upon repeated cooling to room temperature and heating. The origin of gelation and dissolution was investigated and is presented in the following sections.

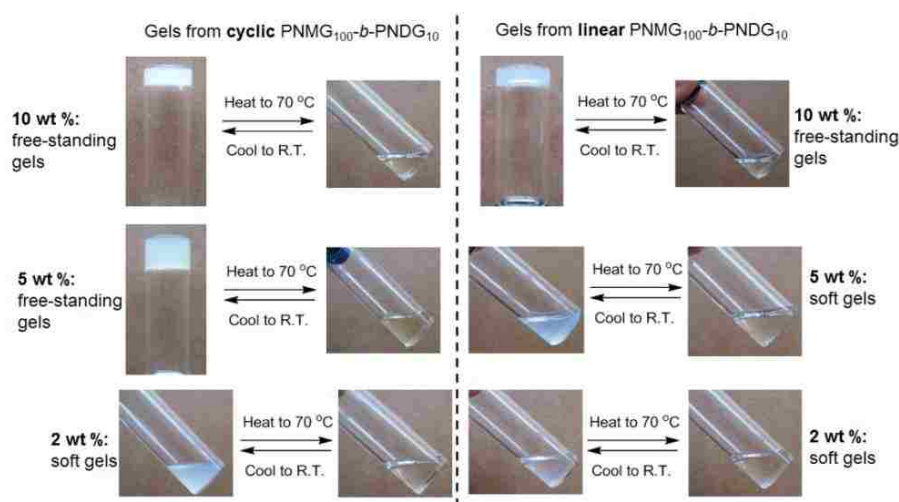


**Figure 2.24.** Thermo-responsive gelation from *c/l*-PNMG<sub>100</sub>-*b*-PNDG<sub>10</sub> diblock copolymers in methanol at a concentration of 2, 5, and 10 wt %.

### 2.3.3.2 Viscoelastic properties of gels

Viscoelastic properties of the gels were studied by rheological measurements. Figure 2.25 shows dynamic storage modulus ( $G'$ ) and loss modulus ( $G''$ ) of gels from  $c$ -PNMG<sub>100</sub>- $b$ -PNDG<sub>10</sub> in methanol at a concentration of 2, 5, or 10 wt % as a function of angular frequency within the linear viscoelastic region ( $\gamma = 1.0$  %) at 25 °C. As can be seen, in all concentration ranges, the storage modulus ( $G'$ ) is higher than the loss modulus ( $G''$ ), indicative of a solid-like behavior. The dynamic moduli of the gels ( $G'$  and  $G''$ ) dramatically increases by two orders of magnitude as the gel concentration increase from 2 wt % to 5 wt %, indicating transition from soft to hard gels. The  $G'$  and  $G''$  of the gels at 5 wt % and 10 wt % are comparable in all frequency ranges, suggesting similar stiffness of the gels at those two concentrations. To examine the effect of solvent evaporation during experiment on  $G'$  and  $G''$ , these moduli were measured for gels from cyclic copolymers at 5 wt % at 10 °C. It was found that  $G'$  and  $G''$  at 10 °C is close to those at 25 °C, indicating the solvent evaporation did not affect the moduli of the gels at 25 °C.

To further probe architectural (i.e., cyclic or linear) effect on the formation and properties of gels, gels from  $l$ -PNMG<sub>100</sub>- $b$ -PNDG<sub>10</sub> copolymers were prepared. As previously shown in Figure 2.24,  $l$ -PNMG<sub>100</sub>- $b$ -PNDG<sub>10</sub> copolymers in methanol can also form free-standing gels but they require a higher concentration (10 wt %) than their cyclic counterparts. Figure 2.26 (A) and (B) show  $G'$  and  $G''$  of gels from  $c$ -PNMG<sub>100</sub>- $b$ -PNDG<sub>10</sub> and  $l$ -PNMG<sub>100</sub>- $b$ -PNDG<sub>10</sub> at a concentration of 5 wt % and 2 wt %, respectively. As can be seen in Figure 2.26 (A),  $G'$  of gels from cyclic copolymers is more than 20 times than that from the linear ones at a frequency of 10 ( $\text{rad}\cdot\text{s}^{-1}$ ), indicating that cyclic copolymers make harder gels than linear ones. Figure 2.26 (A) further shows frequency-dependency of  $G'$  and  $G''$  of the gels. Those moduli decrease gradually

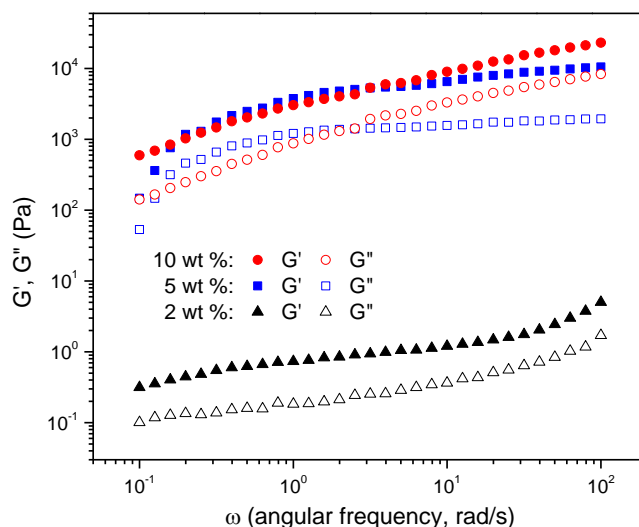


**Figure 2.25.** Storage modulus ( $G'$ ) and loss modulus ( $G''$ ) of gels from  $c$ -PNMG<sub>100</sub>- $b$ -PNDG<sub>10</sub> diblock copolymers in methanol (2, 5 or 10 wt %) as a function of angular frequency ( $\omega$ ) at a strain amplitude of  $\gamma = 1.0$  % at 25 °C.

from high frequency to low frequency, and decrease sharply from  $0.5 \text{ rad}\cdot\text{s}^{-1}$ . This indicates that the gels from cyclic or linear copolypeptides are not true “permanent” gels with “infinite” relaxation time.<sup>101</sup> Instead, they are “transient” gels showing “finite” relaxation time. That is, the gels may lose their physical networking at long time scales or at low frequencies. These rheological results suggest that the gelation is oriented by transient networking between cylindrical micelles formed from the copolymers. Additionally, Figure 2.27 (A) shows rheological data from strain sweep experiment. Figure 2.27 (B) shows elastic stress ( $\sigma' = G'\gamma$ ) of the gels as a function of strain, which was calculated by the rheological data of the strain sweep experiment. As can be seen in Figure 2.27 (B), the yield stress, or maximum stress of gels from cyclic copolymers is around 200 Pa, while that from the linear ones is about 8 Pa, indicating that harder gels formed from cyclic polymers than linear ones at identical composition and concentration. This is in agreement with our empirical observations showing that gels from cyclic copolymers are stiffer than those from linear ones.

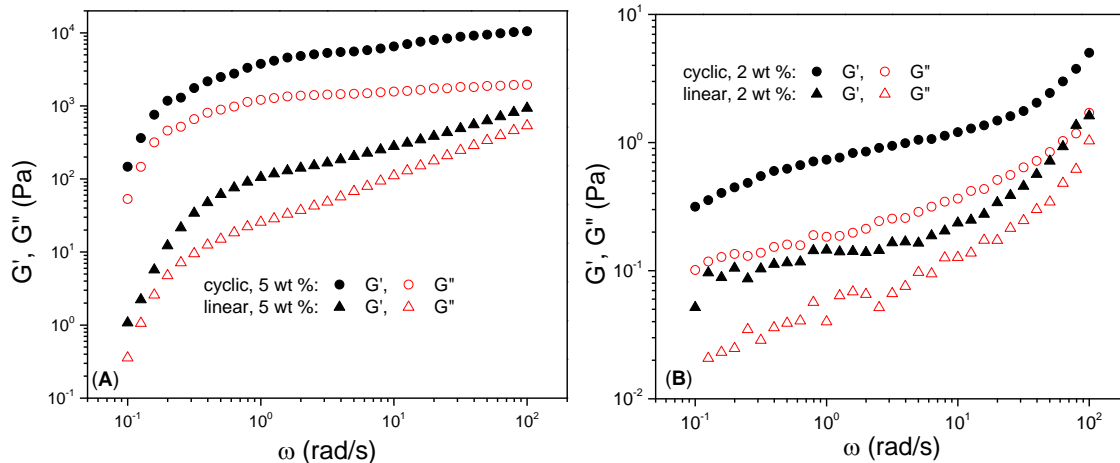


**Figure 2.26.**  $G'$  and  $G''$  of gels from  $c/l$ -PNMG<sub>100</sub>- $b$ -PNDG<sub>10</sub> diblock copolymers in methanol at a concentration of (A) 5 wt % and (B) 2 wt % as a function of angular frequency ( $\omega$ ) at a strain amplitude of  $\gamma = 1.0$  % at 25 °C.

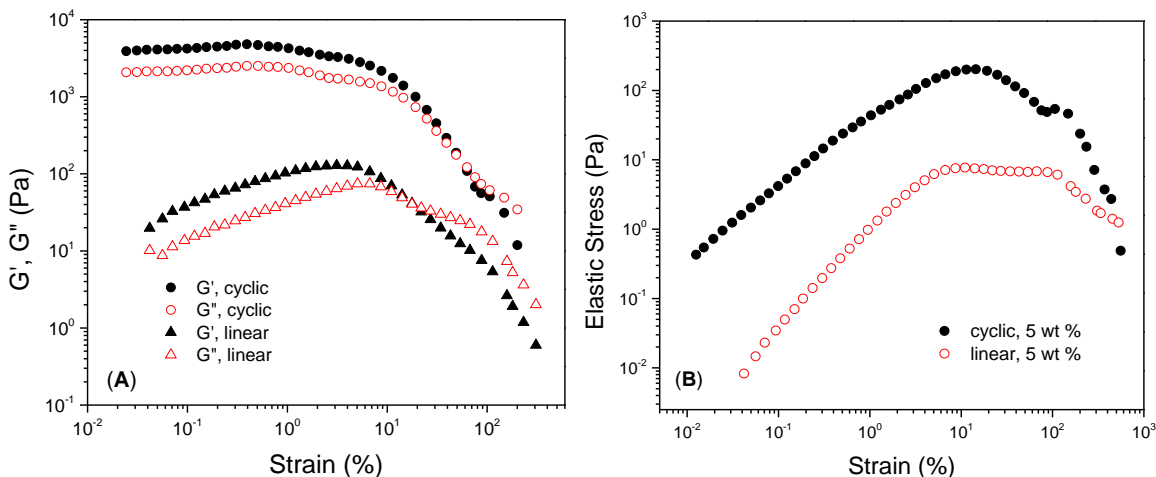


**Figure 2.27.** (A) Storage modulus ( $G'$ ) and loss modulus ( $G''$ ) of gels from  $c$ -PNMG<sub>100</sub>- $b$ -PNDG<sub>10</sub> diblock copolymers in methanol (5 wt %) as a function of strain amplitude ( $\gamma_0$ ) at a frequency of 10 ( $\text{rad}\cdot\text{s}^{-1}$ ) at 25 °C, (B) the calculated elastic stress ( $\sigma' = G'\gamma$ ) as a function of strain.

Additionally, steady-shear rheological data of the gels from  $c/l$ -PNMG<sub>100</sub>- $b$ -PNDG<sub>10</sub> in methanol (2 or 5 wt %) are shown in Figure 2.28. As can be seen in Figure 2.28 (A), the apparent viscosity of the gels decreases, as shear rate increases, indicating shear thinning of the gels. This is consistent with our observations showing that gels from  $c$ -PNMG<sub>100</sub>- $b$ -PNDG<sub>10</sub> at a concentration of 5 wt % gradually become a free-flowing liquid upon vigorous shaking.

Additionally, Figure 2.28 (B) shows complicated shear stress versus shear rate. Gels formed by physical networking or transient crosslinking may show this complicated shear stress trend, as gels deform and then the network structures are reorganized under shear.<sup>84</sup>

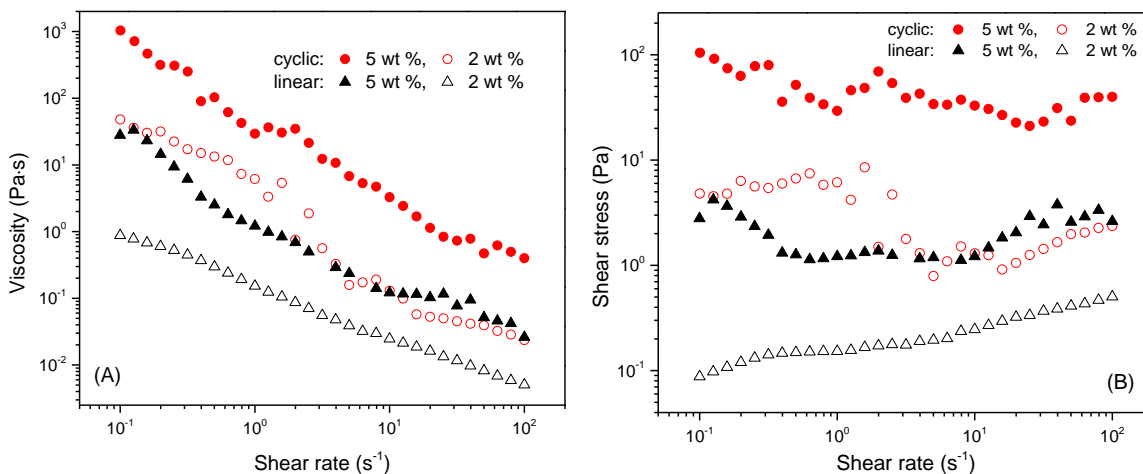


**Figure 2.28.** Steady-state flow rheological data of gels from cyclic or linear PNMG<sub>100</sub>-*b*-PNDG<sub>10</sub> diblock copolymers in methanol (2 wt or 5 wt %).

### 2.3.3.3 Variable-temperature <sup>1</sup>H NMR analysis of gels

Variable-temperature <sup>1</sup>H NMR studies were conducted for gels from cyclic or linear diblock copolypeptoids from 10 °C to 65 °C in order to gain insight into any temperature-induced change of solvation and solution morphology. Figure 2.29 (A) and (B) show <sup>1</sup>H NMR spectra of gels from *c*-PNMG<sub>100</sub>-*b*-PNDG<sub>10</sub> and *l*-PNMG<sub>100</sub>-*b*-PNDG<sub>10</sub> in CD<sub>3</sub>OD at 5 wt % at 25, 45, and 65 °C, respectively. Figure 2.30 shows the ratio of integration from methyl protons of PNDGs (*a* in Figure 2.29) to that from methyl protons of PNMGs (*b* in Figure 2.29) in gels from cyclic or linear PNMG<sub>100</sub>-*b*-PNDG<sub>10</sub> as a function of temperature, and sigmoidal fits from experimental data. Figure 2.31 shows the full <sup>1</sup>H NMR spectra of gels from *c*-PNMG<sub>100</sub>-*b*-PNDG<sub>10</sub> at 25, 45, and 65 °C. Figure 2.30 reveals a sigmoidal dependence of the ratio of integration of PNDG methyl protons to that of PNMG methyl protons, suggesting a two-state transition with a transition temperature at 47 °C for gels from cyclic copolymers. This transition

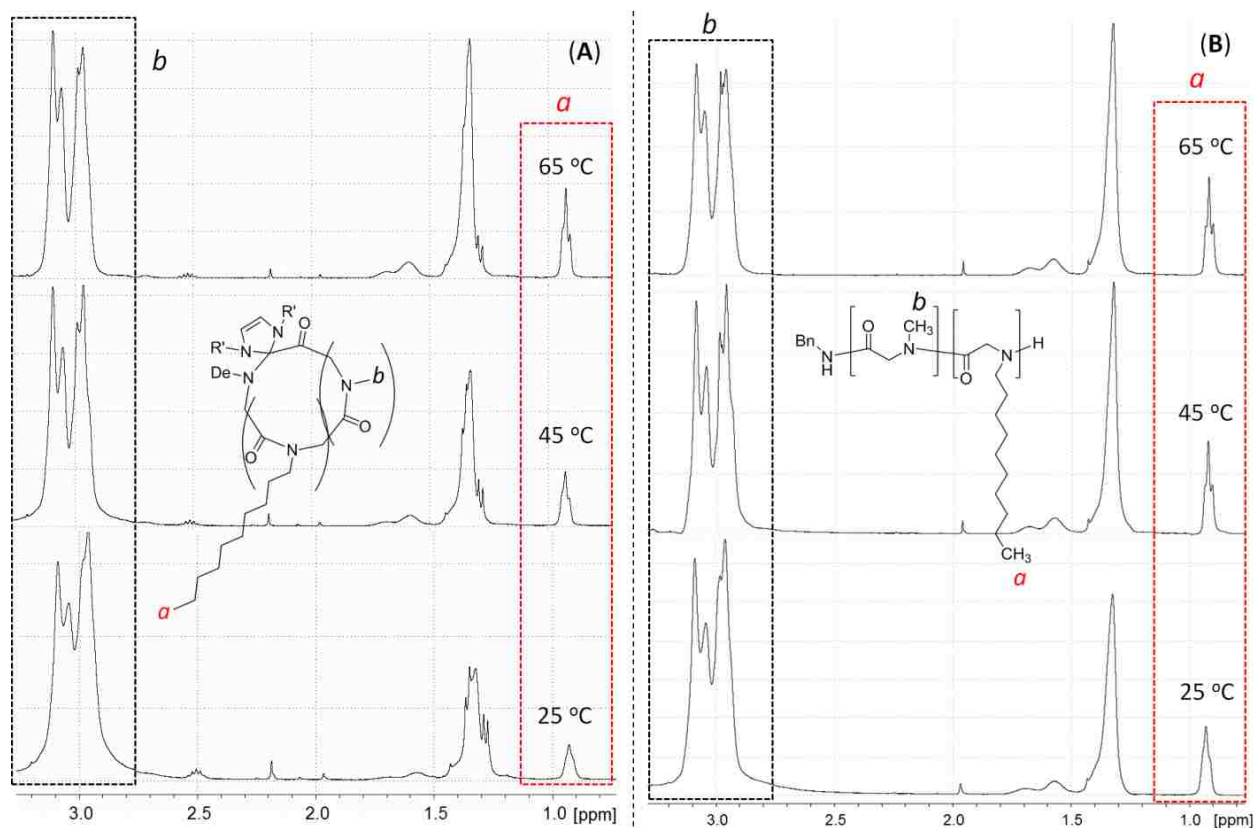


**Figure 2.29.**  $^1\text{H}$  NMR spectra of gels from (A)  $c\text{-PNMG}_{100}\text{-}b\text{-PNDG}_{10}$  and (B)  $l\text{-PNMG}_{100}\text{-}b\text{-PNDG}_{10}$  in  $\text{CD}_3\text{OD}$  (5 wt %) at 25, 45, and 65  $^\circ\text{C}$ .

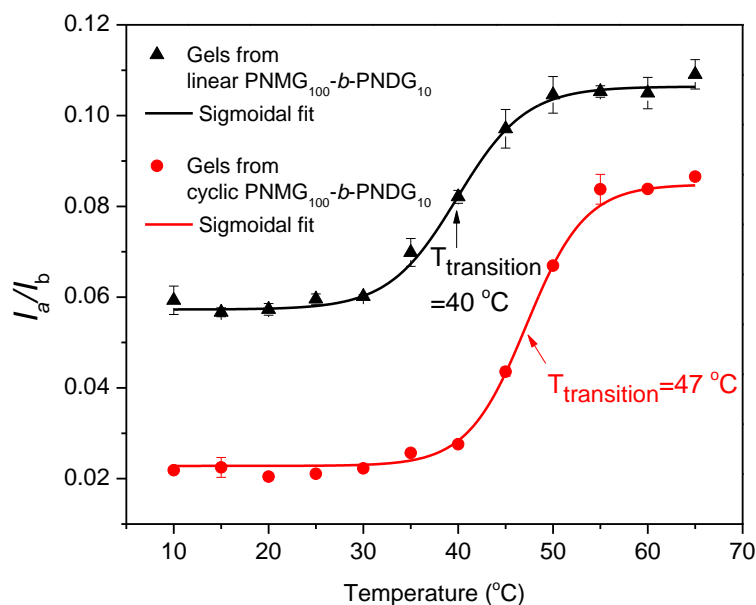


**Figure 2.30.** The ratio of integration of methyl protons of PNDGs ( $a$  in Figure 2.29) to that of methyl protons of PNMGs ( $b$  in Figure 2.29) in gels from cyclic or linear  $\text{PNMG}_{100}\text{-}b\text{-PNDG}_{10}$  as a function of temperature, and sigmoidal fits from experimental data.

is similar to the one observed for the diluted copolypeptoid/methanol solution (0.2 wt %) shown in Figure 2.23. As the temperature increases from 10 to 65 °C, the ratio of integration of PNDG methyl protons to that of PNMG methyl protons of *c*-PNMG<sub>100</sub>-*b*-PNDG<sub>10</sub> increases from 0.022 to 0.086, suggesting enhanced solvation and mobility of the PNDG segments upon heating. Consistently, we observe that the opaque free-standing gels become a flowing liquid at the transition temperature upon heating. This transition in solvation and mobility of PNDG segments can be attributed to any transitions of self-assembled structures formed from the copolymers from low to high temperature. Thermo-responsive morphological transitions in gels as well as in dilute solution are under investigation.

Additionally, Figure 2.30 shows that gels from *l*-PNMG<sub>100</sub>-*b*-PNDG<sub>10</sub> also exhibit a two-state transition upon heating. Sigmoidal fitting of the ratio of integration of PNDG methyl protons relative to PNMG methyl protons versus temperature gives a transition temperature at 40 °C, which is lower than that of gels from cyclic copolymers. Figure 2.30 further shows that the integration of PNDG methyl protons relative to that of PNMG methyl protons for the linear copolymers is larger than that for cyclic copolymers at all temperature ranges. The major difference lies in that the PNDG segments of the linear polypeptoids appear to be more solvated and mobile than those of the cyclic counterparts both in the sol and gel states. The difference in the level of solvation for the PNDG segments between cyclic and linear copolymers may result from different degree of crystalline packing of the core-forming hydrophobic PNDG segments in methanol. This may result in different rheological properties of gels from cyclic copolymers with those from linear copolymers.

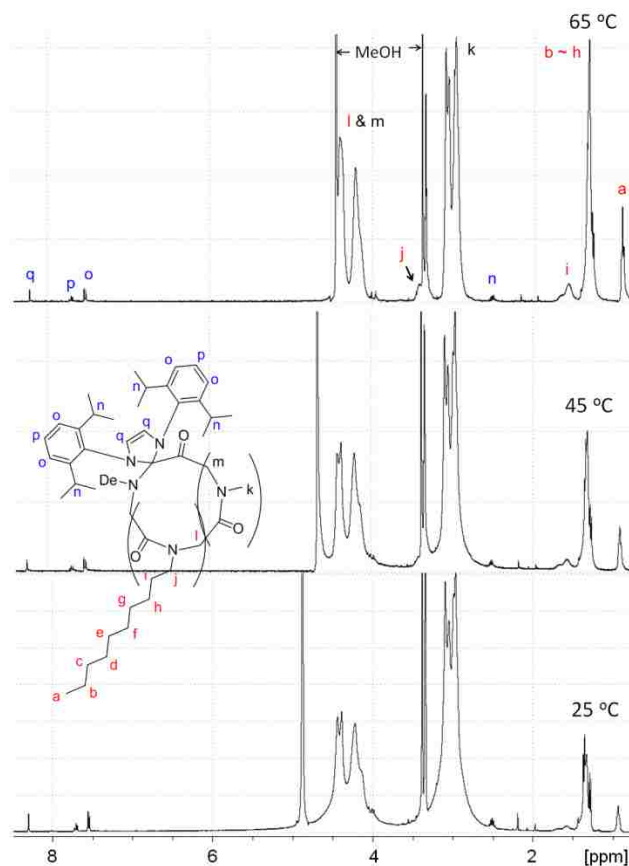


**Figure 2.31.** Full  $^1\text{H}$  NMR spectra of gels from *c*-PNMG<sub>100</sub>-*b*-PNDG<sub>10</sub> diblock copolymers in CD<sub>3</sub>OD (5 wt %) at 25 (bottom), 45, and 65 °C.

#### 2.3.3.4 POM of gels

To investigate the formation of any crystallites in the gels from cyclic PNMG<sub>100</sub>-*b*-PNDG<sub>10</sub> at 5 wt %, the gels were analyzed by POM at room temperature and 55 °C (Figure 2.32). Birefringent crystals were observed in the free-standing gels at room temperature, and those crystals disappeared upon heating to 55 °C when the gels become a free-flowing liquid. The crystals were shown to reform upon cooling to room temperature from 60 °C in one hour, followed by occurrence of gelation. These results clearly indicate that the physical gelation of *c*-PNMG<sub>100</sub>-*b*-PNDG<sub>10</sub> in methanol is driven by the crystallization of the PNDG segments in the copolypeptides.



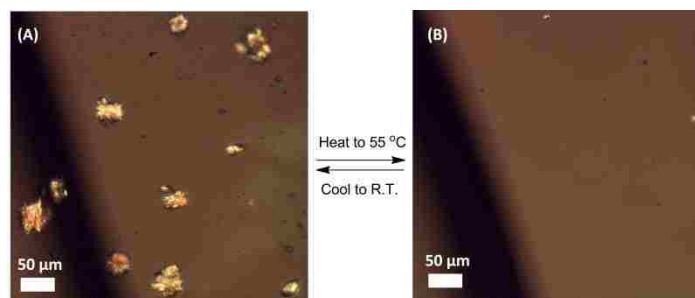


**Figure 2.32.** POM images of gels from *c*-PNMG<sub>100</sub>-*b*-PNDG<sub>10</sub> diblock copolymers in methanol (5 wt %) (A) at room temperature and (B) at 55 °C.

### 2.3.3.5 DSC of gels

Thermo-reversible gelation of *c*-PNMG<sub>100</sub>-*b*-PNDG<sub>10</sub> in methanol (10 wt %) has also been investigated by DSC (Figure 2.33). For this experiment, gels were hermetically sealed in an aluminum pan. As the sample was heated from 10 to 65 °C, an endothermic first-order transition was observed at 55 °C with an enthalpic change ( $\Delta H_m$ ) of 15.8 (0.5) J·g<sup>-1</sup> and a broad transition window ( $T = 16$  °C), suggesting dissolution of the gels. In the cooling cycle (rate = 2 °C·min<sup>-1</sup>), no exothermic peaks were observed, suggesting that sufficient time is required to induce crystallization and gelation. The observed enthalpic change is consistent with that for the melting of the cylindrical micelles in diluted methanol solution (Figure 2.22), suggesting the crystallization-driven gelation in the concentrated solution. The mass of the gels remain unchanged before and after the DSC experiment, suggesting that the endothermic peak did not result from solvent evaporation. For comparison, a solid sample of *c*-PNMG<sub>100</sub>-*b*-PNDG<sub>10</sub> was analyzed by DSC, showing neither endothermic nor exothermic peaks during heating and cooling cycles. This clearly suggests that a certain phase-separated morphology is required to promote the crystallization of the PNDG segment. While the gel morphology has not been unambiguously characterized, it clearly facilitates the crystallization of the PNDG segments, whereas the solid state morphology may inhibit the event.

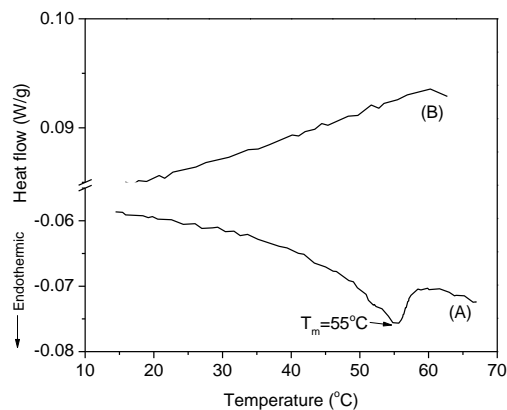


**Figure 2.33.** DSC of *c*-PNMG<sub>100</sub>-*b*-PNDG<sub>10</sub> diblock copolymer gels in methanol (10 wt %) (A) during first heating, and (B) during first cooling.

### 2.3.3.6 WAXS of gels

Gels from the cyclic or linear copolymers were studied by WAXS to examine the presence of any crystalline domains. Figure 2.34 shows WAXS data of gels from *c/l*-PNMG<sub>100</sub>-*b*-PNDG<sub>10</sub> diblock copolymers at 10 wt %. As can be seen in Figure 2.34 (A), the dominant peaks at  $q$  of  $0.089 \text{ \AA}^{-1}$  ( $d = 70 \text{ \AA}$ ) and at  $q$  of  $0.26 \text{ \AA}^{-1}$  ( $d = 24 \text{ \AA}$ ) were observed for gels from cyclic copolymers. The peak indicating domain spacing of  $70 \text{ \AA}$  is smaller than of the diameter of spherical ( $d = 103 \text{ \AA}$ ) and cylindrical ( $d = 122 \text{ \AA}$ ) micelles from the copolymers in dilute solution, determined by cryo-TEM (Figure 2.19). The peak indicating domain spacing of  $24 \text{ \AA}$  involve the distance between two decyl side chains, as observed in the WAXS of the *c*-PNDG solid (Figure 2.13). Figure 2.34 (B) shows that gels from the linear copolymers still show the peak at  $q$  of  $0.089 \text{ \AA}^{-1}$ , but the intensity of the peak is lower than that of gels from cyclic copolymers. Furthermore, gels from linear copolymers show the peak at  $q$  of  $0.26 \text{ \AA}^{-1}$  with much lower intensity than those from cyclic ones. This indicates that core-forming, semi-crystalline PNDG segments from cyclic copolymers crystallized more than those from linear ones. Higher degree of crystallinity in gels from cyclic copolymers may result in their lower degree of solvation of PNDG segments in gels than that of linear ones, which was presented in Figure 2.30.

This higher degree of crystallinity may increase the interfacial tension between PNDG cores and PNMG coronas of cyclic copolymers. This may result in more chances for the copolymers to form cylindrical micelles than linear ones, leading to their harder gels due to increased networking among cylindrical micelles.

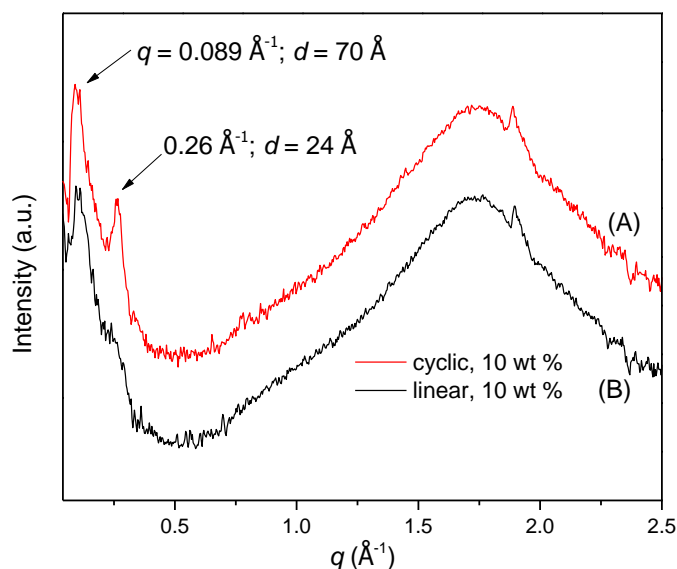


**Figure 2.34.** WAXS diffractograms of gels from (A) *c*-PNMG<sub>100</sub>-*b*-PNDG<sub>10</sub> and (B) *l*-PNMG<sub>100</sub>-*b*-PNDG<sub>10</sub> in methanol at 10 wt %.

### 2.3.3.7 SAXS of gels

To investigate the origin of different viscoelastic properties of gels from cyclic PNMG<sub>100</sub>-*b*-PNDG<sub>10</sub> from those from their linear counterparts, the gels were analyzed by SAXS. Figure 2.35 (A) shows SAXS data of gels from cyclic or linear copolymers. As can be seen, at low  $q$  region ( $q < 0.03 \text{ \AA}^{-1}$ ), the slope in the plot of  $\log I(q)$  as a function of  $\log q$  approaches -1. Particles with a cylindrical or rod-like shape may have higher intensity than those with a spherical shape, as the slope in the plot of  $I(q)$  as a function of  $q$  changes from 0 for spheres to -1 for rods.<sup>81</sup> Also, the intensity of the gels from cyclic copolymers is higher than that from linear ones. This SAXS data suggests that the cyclic copolymers in gels are more likely to form cylindrical micelles than their linear analogs.

Additionally, from small-angle X-ray or neutron scattering experiment, one may determine the cross-sectional radius of gyration ( $R_c$ ) for gels composed of rigid rods by the following Guinier equation<sup>102-104</sup>

$$I(q)q = 2\Phi_{vol}(\pi R_c \Delta\rho)^2 \exp\left(-\frac{q^2 R_c^2}{2}\right) \quad (2.1)$$

, where  $\Phi_{vol}$  is the volume fraction of the rigid rods and  $\Delta\rho$  is contrast in electron density of X-ray scattering between the rods and the surrounding medium. The plot of  $\ln[I(q)q]$  as function of  $q^2$  (the Guinier plot) will provide  $R_c$  of gels of rigid rods. Figure 2.35 (B) shows the Guinier plot of the SAXS data.  $R_c$  of the gels was determined from the slope of the plot in the Guinier region ( $q < 0.03 \text{ \AA}^{-1}$ ). It is noted that the Guinier plot for both gels from cyclic copolymers and linear copolymers become flat at high  $q$  value region. The origin of this is under current investigation. As can be seen,  $R_c$  [7 (0.9) nm] of gels from linear copolymers is smaller than  $R_c$  [10 (1.6) nm] of gels from cyclic copolymers. This reveals that the contribution of cylindrical micelles in the gels from cyclic copolymers to the total intensity in X-ray scattering in the Guinier region is higher than that from linear ones, resulting in a higher  $R_c$  value. This suggests that cyclic copolymers favor to form cylindrical micelles more than linear ones, which may result from higher degree of crystallinity of the gels from cyclic copolymers (Figure 2.34). The radius ( $r$ ) of the cylindrical micelles can be calculated from the following relation for rigid rods:  $r = R_c\sqrt{2}$ .<sup>105</sup> The calculated diameter of cylindrical micelles in gels from the cyclic copolymers is 28 (3) nm, which is the combined length of the core diameter and corona diameter of the micelles. This is comparable with the diameter of cores (12.2 nm) of the cylindrical micelles determined by cryo-TEM of dilute solution of the copolymers (Figure 2.19). Also, the calculated diameter of cylindrical micelles in gels from the linear copolymers is 20 (2) nm. As a result, WAXS and SAXS data suggest that the formation of harder gels from cyclic copolymers is contributed to more

possibility for their formation of cylindrical micelles and thus to more transient networking of the cylindrical micelles from cyclic copolymers than linear ones.

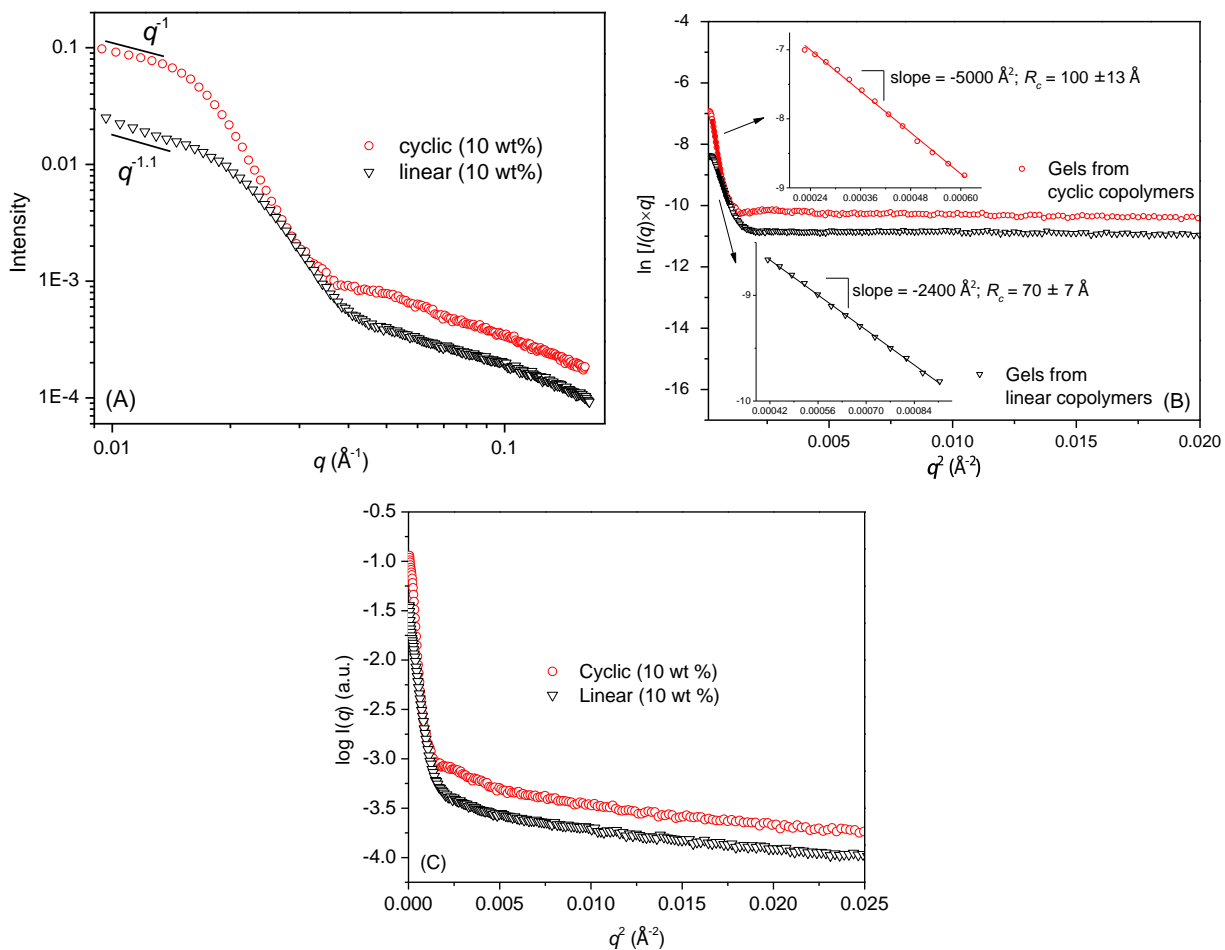


**Figure 2.35.** (A) SAXS diffractograms of gels from cyclic or linear PNMG<sub>100</sub>-*b*-PNDG<sub>10</sub> (10 wt % in methanol), (B) the Guinier plot ( $\ln[I(q)q]$  as a function of  $q^2$ ) of the SAXS data of gels from the copolymers. (The inset graphs are the linear fits of the data in the Guinier region,  $q < 0.03 \text{ \AA}^{-1}$ ), and (C) the plot of  $\log I(q)$  as a function of  $q^2$ .

### 2.3.3.8. Variable-time WAXS and SAXS analyses of gels

To confirm crystallization-driven gelation from PNMG-*b*-PNDG copolymers, WAXS and SAXS studies on the gels from cyclic copolymers at different times after heating the gels to 70 °C and cooling to room temperature. Figure 2.36 (A) shows WAXS data of the gels from cyclic copolymers after 15 m, 40 m, 2 h, and 20 h. The peak indicating the domain spacing of 24 Å is observed even after 15 m after cooling to room temperature from 70 °C, when free-standing

gels are not formed yet. The peak intensity of the domain spacing of  $24 \text{ \AA}$  increases from 15 m to 40 m and to 2 h. This WAXS data reveal that crystallization of the PNDG blocks of the copolymers precedes the gelation from the copolymers. Figure 2.36 (B) shows SAXS data of gels from cyclic copolymers after 10 m, 70 m, and 20 h at room temperature. The slope in the plot of  $\log I(q)$  as a function of  $\log q$  is 0.3 of the gels after 10 m and 70 m, when the free-standing gels are not formed yet. This suggests that the particles formed from the copolymers are not cylinders. After 20 h, the slope in the plot approaches -1, suggesting that cylindrical particles exist in the gels from the copolymers. Time-dependent studies of WAXS and SAXS of gels suggest that crystallization from the copolymers occurs before forming cylindrical micelles and gels from the copolymers, supporting crystallization-driven gelation from the copolymers.

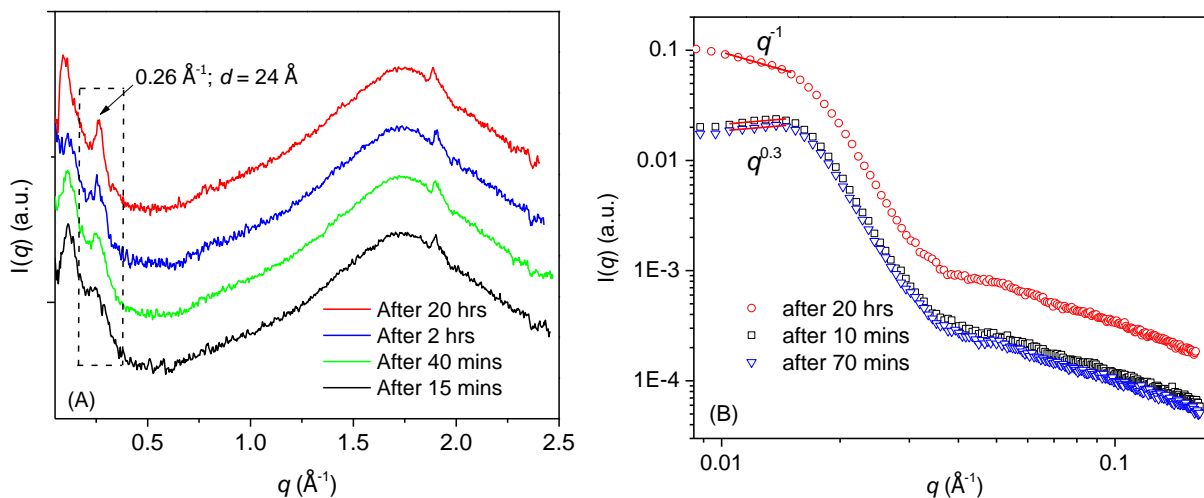


**Figure 2.36.** (A) WAXS diffractograms of gels from  $c$ -PNMG<sub>100</sub>- $b$ -PNDG<sub>10</sub> in methanol (10 wt %) after 15 m, 40 m, 2 h and 20 h (B) SAXS diffractograms after 10 m, 70 m and 20 h after heating to 70 °C and cooling to room temperature.

### 2.3.3.9 AFM of gels

Fibrillar or cylindrical structures in the gels from cyclic or linear PNMG<sub>100</sub>- $b$ -PNDG<sub>10</sub> were confirmed by AFM analysis. Figure 2.37 and 2.38 show AFM images of gels from the cyclic (1 wt %) and linear (5 wt %) copolymers, respectively. The formation of fibrils and their

bundles is clearly observed, and the diameter of the individual fibril was measured to be  $31 \pm 6$  nm for both gel from the cyclic and linear copolymers. The fibrils are twisted or aligned side by side to form bundles of various diameters. The average diameters of the bundles were  $56 \pm 12$  nm and  $120 \pm 56$  nm, and the average heights of the bundles were  $6.5 \pm 2.9$  nm and  $3.2 \pm 1.1$  nm for gels from cyclic and linear copolymers, respectively. It appears that gels from cyclic copolymers contain a substantially higher density of bundles than gels from linear copolymers with identical polymer concentration.

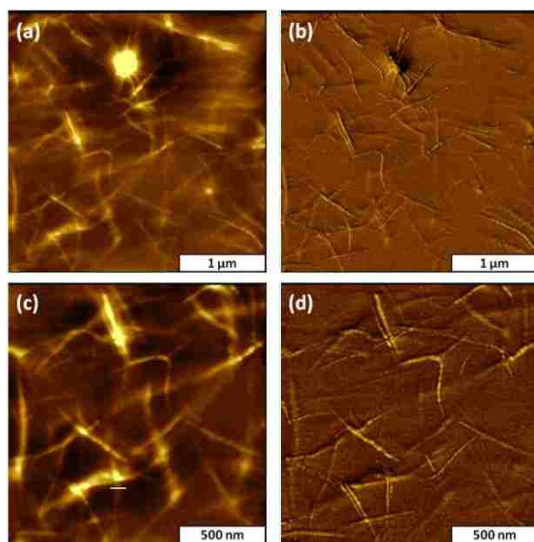


**Figure 2.37.** Gels from cyclic  $\text{PNMG}_{100}\text{-}b\text{-PNDG}_{10}$  (1 wt %) viewed with tapping-mode AFM. (a) Topograph  $3 \times 3 \mu\text{m}^2$ ; and (b) corresponding phase image. (c) Zoom-in topograph ( $1.5 \times 1.5 \mu\text{m}^2$ ) and (d) corresponding phase image.

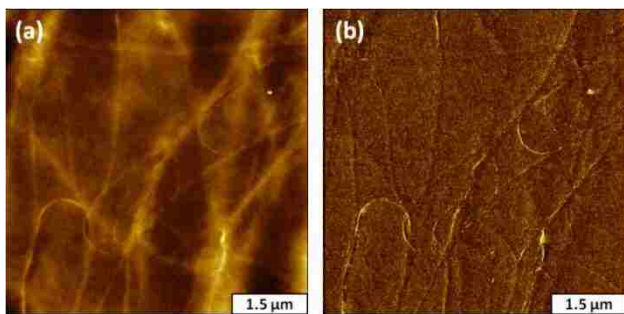


**Figure 2.38.** Gels from linear  $\text{PNMG}_{100}\text{-}b\text{-PNDG}_{10}$  (5 wt %) viewed with tapping-mode AFM. (a) Topograph  $6 \times 6 \mu\text{m}^2$ ; (b) corresponding phase image.

### 2.3.3.10 Effect of crystallization of core-forming hydrophobic segments on the gelation

To examine the effect of crystallization of core-forming, solvophobic blocks in polypeptoid copolymers on the gelation, cyclic poly(*N*-methyl-glycine)<sub>100</sub>-*b*-poly(*N*-2-ethyl-1-hexyl-glycine)<sub>15</sub> (*c*-PNMG<sub>100</sub>-*b*-PNEHG<sub>15</sub>) diblock copolymers were synthesized, and their gelation was tested. For this examination, 2-ethyl-1-hexyl-NCA monomers and cyclic poly(*N*-2-ethyl-1-hexyl-glycine)s (PNEHGs) were also synthesized. The procedures for the synthesis of 2-ethyl-1-hexyl-NCA and cyclic or linear PNEHGs are presented in section 4.2.1. The crystallization of solvophobic PNEHGs was significantly reduced by the asymmetrically-branched side chains, as observed by DSC and WAXS analyses. Details about melting and crystallization of cyclic or linear PNEHGs are presented in section 4.3.3. Gelation of *c*-PNMG<sub>100</sub>-*b*-PNEHG<sub>15</sub> diblock copolymers composed of hydrophobic PNEHGs with reduced crystallinity was tested in methanol at a concentration of 10 wt %. As can be seen in Figure 2.39, *c*-PNMG<sub>100</sub>-*b*-PNEHG<sub>15</sub> does not form gels. This result suggests that the crystallization of solvophobic, core-forming PNDG segments is critical for the formation of gels, and further supports crystallization-driven gelation from PNMG-*b*-PNDGs.

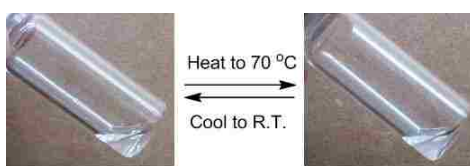


**Figure 2.39.** Poly(*N*-methyl-glycine)<sub>100</sub>-*b*-poly(*N*-2-ethyl-1-hexyl-glycine)<sub>15</sub> diblock copolymers in methanol at 10 wt %.

### 2.4 Notes

1. Cryo-TEM and light scattering experiments were conducted by Dr. Thomas Smart at the University of Delaware.
2. SAED experiments were conducted by Dr. Jihua Chen at Oak Ridge National Laboratory.
3. AFM experiments were conducted by Lu Lu.



## CHAPTER 3. CYCLIC TRIBLOCK TERPOLYPEPTOIDS: SYNTHESIS AND SELF-ASSEMBLY

### 3.1 Introduction

Triblock terpolymers have attracted much attention, because one may achieve more complex nanostructures in solution or in a solid state than those from diblock copolymers.<sup>106</sup> Primary variables to affect self-assembly of block copolymers in the solid state and thus their final morphologies include polymer topology, block length (degrees of polymerization), and interaction parameters ( $\chi$ ) between any two components.<sup>107</sup> Increasing the number of blocks into the architecture of a diblock copolymer expands the complexity of variables, such as the interaction parameters. In an AB-type diblock copolymer, only  $\chi_{AB}$ , an interaction parameter between A and B block can be considered. On the other hand, in an ABC-type triblock terpolymer, parameters between any two blocks ( $\chi_{AB}$ ,  $\chi_{BC}$ , and  $\chi_{AC}$ ) are considered to determine their final morphologies. In solution, in addition to the interactions between different blocks, interactions between each block with a solvent and kinetics of self-assembly are additional parameters that contribute to the complexity of the solution morphology. For example, if the A block is solvophilic, and the B and C blocks are solvophobic with varying degrees of solvophobicities, core-forming B and C blocks may phase-separate to form discrete nano-size domains inside the cores of the micelles, which generates multi-compartment micelles.<sup>108,109</sup> ABC-type linear triblock terpolymers possessing a simple architecture have been extensively studied on their synthesis and formation of multi-compartment micelles.<sup>108,110,111</sup> Kubowicz et al.<sup>108</sup> synthesized poly(4-methyl(4-vinylbenzyl)morpholinium chloride)-*b*-poly(styrene)-*b*-poly(pentafluorophenyl-4-vinyl benzyl ether) (PVBM-PS-PVBFP) by three consecutive RAFT polymerizations using dithiobenzoate as a chain transfer agent. In their study, PVBM was charged with cations, and thus hydrophilic. The two hydrophobic and incompatible blocks,

PVBFP with fluorinated side chains and PS, were selected to induce phase-separation in the cores of the micelles. They observed that the copolymer forms micelles with raspberry-like cores composed of small domains with a diameter of about 3 nm of fluorinated PVBFP chains and relatively large domains with a diameter of about 15 nm of PS chains in water.<sup>108,112</sup>

Synthesis and solution self-assembly of non-linear ABC triblock terpolymers, such as miktoarm star terpolymers, hyperbranched star-block terpolymers,<sup>113</sup> and cyclic triblock terpolymers, have been of growing interest, since such complex topologies may lead to the formation of more complex and unique nanostructures than those obtained from linear triblock terpolymers. Among them, the synthesis of complex nanostructures from ABC miktoarm star terpolymers have been mostly reported.<sup>106</sup> For example, Hillmyer, Lodge, and their co-workers<sup>114-116</sup> reported synthesis of mixed-arm ( $\mu$ ) star triblock terpolymers, composed of a hydrophilic poly(ethylene oxide) (PEO, O), a saturated polyethylene (PEE, E) and a hydrophobic, lipophobic poly(perfluoropropylene oxide) (PFPO, F) ( $\mu$ -EOF) block. PEE-*b*-PEO diblock copolymers were first synthesized by anionic polymerization with a protected hydroxyl group, which was then coupled with PFPO possessing a terminal acid chloride group.<sup>114</sup> Self-assembly of the synthesized  $\mu$ -EOF terpolymers with various block copolymer compositions in aqueous solution was studied by cryo-TEM. The specific architecture of the terpolymers lead to the formation of multi-compartment micelles with segmented cores, as mutually incompatible, hydrophobic E and F chains were connected to the hydrophilic O chain at a single point.<sup>116</sup> By tuning the relative chain length of these blocks, they observed a variety of nanostructures from ellipsoidal micelles, segmented worm-like micelles, and bilayer-like micelles to nanostructured vesicles.<sup>115,116</sup> Multi-compartment micelles with segregated, hydrophobic cores were further

utilized to simultaneously store two distinct, hydrophobic dyes of pyrene in the PEE-rich domain and 1-naphthyl perfluoroheptanyl ketone (NFH) in the PFPO-rich domain.<sup>117</sup>

Synthesis of cyclic ABC-type triblock terpolymers in a controlled manner, however, has rarely been reported, and thus their self-assembly in solution or in the solid state was not widely explored. This may result from the limitation in solubility of multi-block copolymers, possible self-assembly of diblock copolymer precursors during polymerization, and difficulty in cyclization of linear trifunctional precursors. Pantazis et al.<sup>118</sup> reported the synthesis of cyclic poly(styrene)-*b*-poly(isoprene)-*b*-poly(methyl methacrylate) (PS-*b*-PI-*b*-PMMA) triblock terpolymers by intramolecular amidation of linear  $\alpha,\omega$ -amino acid precursors under high dilution conditions. The linear precursors were prepared by sequential, anionic polymerization of S, I, and MMA monomers using an amine-generating initiator and carboxylic acid-generating terminator. In their study, the synthesis of cyclic terpolymers with varying copolymer compositions, and their self-assembly in solution were not reported. Additionally, the synthesis and self-assembly of a peptidomimetic cyclic triblock terpolymer with various side groups have not been reported. Thus, it is of special interest to investigate the synthesis of such triblock terpolypeptoids in a controlled manner, and to study the self-assembly in solution. In this study, we present the synthesis of cyclic triblock terpolypeptoids with controlled molecular weights and copolymer compositions by sequential, zwitterionic ring-opening polymerizations of NCA monomers. This expands our studies on the synthesis of cyclic diblock copolypeptoids via NHC-mediated zwitterionic ring-opening polymerization presented in section 2.1. Initial work of the self-assembly of the synthesized copolymers is also presented.

Section 3.2 presents experimental results on the synthesis of cyclic poly(*N*-methylglycine)-*b*-poly(*N*-allyl-glycine)-*b*-poly(*N*-benzyl-glycine) (PNMG-PNAG-PNBnG) triblock

terpolypeptoids by sequential addition of methyl-NCA, allyl-NCA, and benzyl-NCA. The PNBnG block is selected as the most hydrophobic segment, while the PNAG block is less hydrophobic than PNBnG, and PNMG block is the hydrophilic segment. The allyl groups may provide potential sites to bind with other functional groups such as thiols by click chemistry. Cyclic PNMG-PNAG-PNBnG triblock terpolypeptoids with a variety of compositions were prepared. NMR spectroscopy and SEC analysis were utilized to characterize the synthesized terpolymers.

Section 3.3 presents the synthesis of cyclic [poly(*N*-ethyl-glycine)-*ran*-poly(*N*-butyl-glycine)]-*b*-poly(*N*-methyl-glycine)-*b*-poly(*N*-decyl-glycine) ([P(NEG-*ran*-NBG)]-PNMG-PNDG) triblock terpolypeptoids. This copolymer is particularly interesting because it is composed of thermo-responsive P(NEG-*ran*-NBG) copolymers as one of the building blocks. More specifically, Lahasky et al.<sup>66</sup> reported that random copolymers composed of hydrophilic PNEG and hydrophobic PNBG exhibit reversible, phase transitions with tunable cloud point temperatures ( $T_{cps}$ ) ranging from 20 to 60 °C. That is, the copolymers in water become hydrophobic upon heating. They revealed that the  $T_{cps}$  can be controlled by changing the copolymer compositions and architectures (i.e. cyclic and linear). Thermo-responsive polymers as one of the blocks for ABC-type triblock terpolymers may play an important role to induce micellization and micellar aggregation at different temperatures. For example, Zhou et al.<sup>119</sup> reported that linear poly(ethylene-*alt*-propylene)-*b*-poly(ethylene oxide)-*b*-poly(*N*-isopropylacrylamide) (PEP-PEO-PNIPAM) triblock terpolymers composed of thermo-responsive PNIPAM polymers as one of the blocks form well-defined micelles with hydrophobic PEP chains as cores and PEO-PNIPAM chains as coronas below the lower critical solution temperature (LCST) of PNIPAM. Above the LCST, the copolymer form larger, micellar

aggregates, as studied by DLS and cryo-TEM. Furthermore, they reported that the copolymers form thermo-reversible hydrogels at elevated concentrations of 1 to 5 wt %.<sup>86</sup> Inspired by their work, cyclic [P(NEG-*ran*-NBG)]-PNMG-PNDG triblock terpolypeptoids were prepared by NHC-mediated ring-opening polymerization via sequential addition of a mixture of ethyl-NCA and butyl-NCA, methyl-NCA, and decyl-NCA. Initial studies on their self-assembly in water by DLS and TEM are also presented.

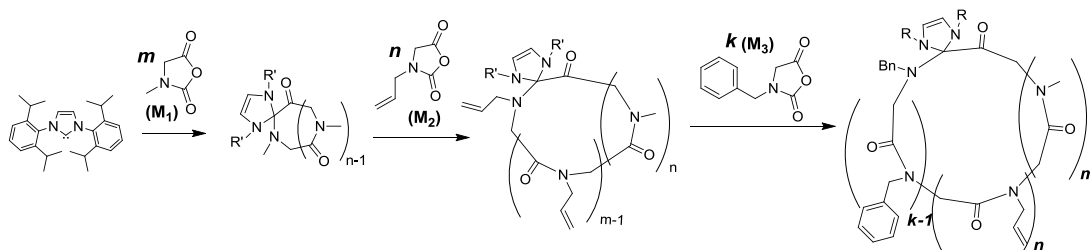
### 3.2 Cyclic poly(*N*-methyl-glycine)-*b*-poly(*N*-allyl-glycine)-*b*-poly(*N*-benzyl-glycine) triblock terpolypeptoids

#### 3.2.1 Experimental

Cyclic triblock terpolypeptoids were synthesized by NHC-mediated ring-opening polymerization via sequential addition of corresponding monomers. Allyl-NCA and benzyl-NCA monomers were synthesized by adapting the procedure described in section 2.1.1.3 and 2.1.2.1 by using allylamine and benzylamine as the starting material. Scheme 3.1 shows a synthetic procedure to prepare cyclic PNMG-PNAG-PNBnG triblock terpolymers. A representative procedure to prepare the terpolymers with various compositions starting from one batch (i.e.  $[M_1]_0:[M_2]_0:[M_3]_0:[NHC]_0 = 25:25:25:1$  starting from  $[M_1]_0:[NHC]_0 = 25:1$ ) is presented as follows. In the glovebox, methyl-NCA ( $M_1$ , 55 mg, 0.48 mmol,  $[M_1]_0 = 0.4$  M) was dissolved in 1200  $\mu$ L of anhydrous benzonitrile. A known volume of NHC/THF stock solution (247  $\mu$ L, 19  $\mu$ mol, 77 mM,  $[M_1]:[NHC]_0 = 25:1$ ) was added to the monomer solution. Polymerization was conducted at room temperature for 20 h under nitrogen. The aliquots (130  $\mu$ L) were taken for NMR and SEC analyses to determine the conversion of polymerization and molecular weights of PNMGs. Then the polymerization solution was divided by two in volume (650  $\mu$ L), and transferred to two vials. A known volume of allyl-NCA ( $M_2$ ), allyl-NCA/benzonitrile stock solution (285  $\mu$ L, 0.8 M, 33 mg of allyl-NCA,  $[M_1]_0:[M_2]_0 = 25:25$ ) and 285  $\mu$ L of benzonitrile

were added to one of the two vials. Polymerization was further conducted at 40 °C for 20 h. The aliquots (130  $\mu$ L) after the second polymerization were taken for NMR and SEC analyses. After cooling the solution to room temperature, the polymerization solution was divided by two in volume (610  $\mu$ L) in the glove box. Then a known volume of benzyl-NCA ( $M_3$ ), benzyl-NCA/benzonitrile (300  $\mu$ L, 0.4 M, 23 mg of benzyl-NCA,  $[M_1]_0:[M_2]_0:[M_3]_0= 25:25:25$ ) was added to one of the vials. Polymerization was further conducted at 70 °C for 48 h. The aliquots (130  $\mu$ L) after the third polymerization were taken for NMR and SEC analyses. Final products of triblock terpolymers were obtained as yellowish powder after precipitating in cold diethyl ether, filtering, and drying under vacuum (28 mg, 75 % yield). Instrumental conditions for SEC and  $^1\text{H}$  NMR are described in section 2.1.1.

**Scheme 3.1.** Synthetic procedure to prepare cyclic PNMG-PNAG-PNBnG triblock terpolymers.



### 3.2.2 Results and discussion

#### 3.2.2.1 Synthesis of cyclic PNMG-PNAG-PNBnG triblock terpolymers with controlled chain length and compositions

Figure 3.1 shows  $^1\text{H}$  and  $^{13}\text{C}\{^1\text{H}\}$  NMR spectra of cyclic  $\text{PNMG}_{144}\text{-PNAG}_{25}\text{-PNBnG}_{25}$  triblock terpolymers. The NMR spectra show that the synthesized polymers possess polypeptoid backbones and three distinct side groups from PNMG, PNAG, and PNBnG blocks, respectively. Also,  $^1\text{H}$  NMR spectrum of the copolymer indicates that the NHC moiety remains attached on the polymer backbones, which suggests that the polymer chains were expanded via NHC-mediated ring-opening polymerization. The conversion of each polymerization reaction reached

100 %, as revealed by  $^1\text{H}$  NMR spectroscopy of the aliquots taken from polymerization solution at each step. Additionally, Table 3.1 shows the molecular weights and compositions of the synthesized, cyclic PNMG-PNAG-PNBnG triblock terpolymers with various ratios of monomers to the initiator (NHC), as determined by  $^1\text{H}$  NMR spectroscopy. The molecular weights and compositions of the terpolymers can be controlled by altering the ratio of monomers to NHC. In most cases, the experimentally-determined degree of polymerization of each block agrees well with calculated, theoretical values based on the feed ratio of monomers and conversion.

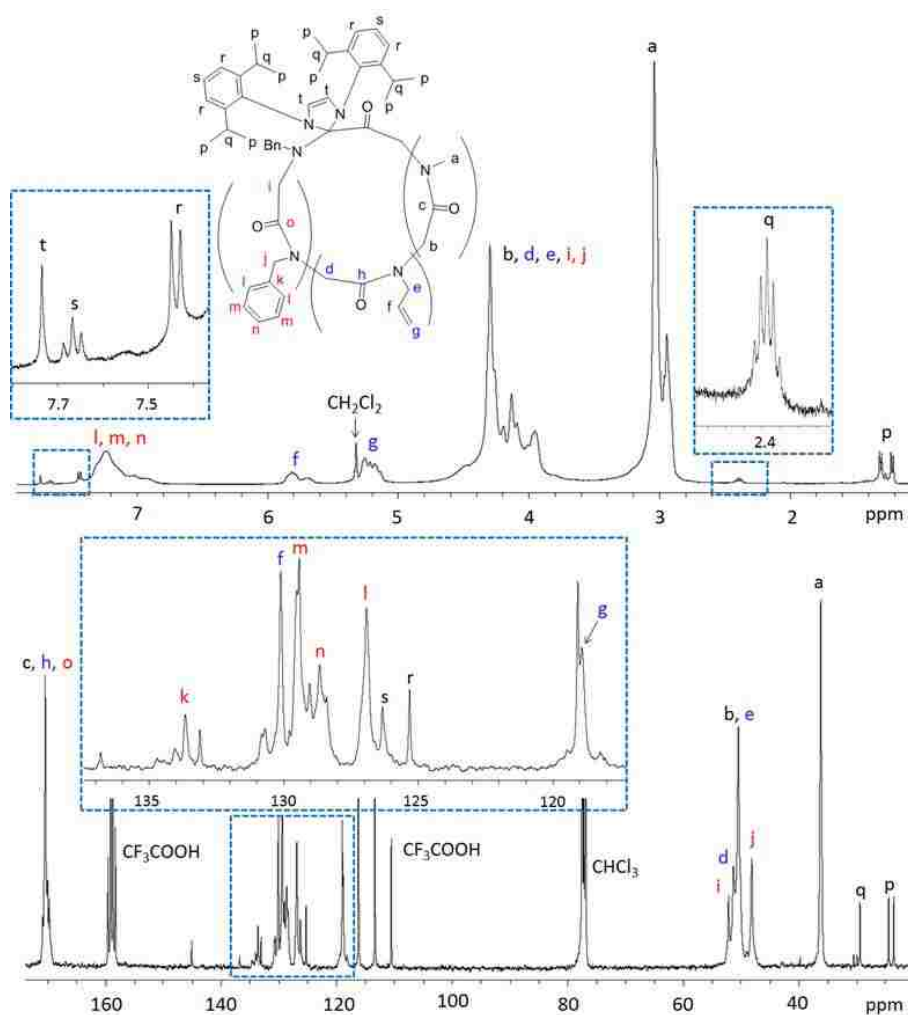


**Figure 3.1.**  $^1\text{H}$  and  $^{13}\text{C}\{^1\text{H}\}$  NMR spectra of cyclic  $\text{PNMG}_{144}\text{-PNAG}_{25}\text{-PNBnG}_{25}$  triblock terpolymers in  $\text{CDCl}_3/\text{CF}_3\text{COOD}$ .

**Table 3.1.** Compositions and molecular weights of cyclic PNMG-PNAG-PNBnG triblock terpolymers.<sup>a</sup>

Entry #	[M <sub>1</sub> ] <sub>0</sub> : [M <sub>2</sub> ] <sub>0</sub> : [M <sub>3</sub> ] <sub>0</sub> : [NHC] <sub>0</sub>	Copolypeptoid Composition <sup>b</sup>
1	10 : 10 : 10 : 1	PNMG <sub>10</sub> -PNAG <sub>11</sub> -PNBnG <sub>10</sub>
2	25 : 10 : 5 : 1	PNMG <sub>24</sub> -PNAG <sub>9</sub> -PNBnG <sub>3</sub>
3	25 : 10 : 25 : 1	PNMG <sub>24</sub> -PNAG <sub>10</sub> -PNBnG <sub>23</sub>
4	25 : 25 : 10 : 1	PNMG <sub>24</sub> -PNAG <sub>25</sub> -PNBnG <sub>9</sub>
5	25 : 25 : 25 : 1	PNMG <sub>24</sub> -PNAG <sub>26</sub> -PNBnG <sub>23</sub>
6	50 : 3 : 3 : 1	PNMG <sub>54</sub> -PNAG <sub>3</sub> -PNBnG <sub>2</sub>
7	50 : 25 : 25 : 1	PNMG <sub>54</sub> -PNAG <sub>25</sub> -PNBnG <sub>23</sub>
8	50 : 50 : 50 : 1	PNMG <sub>55</sub> -PNAG <sub>54</sub> -PNBnG <sub>49</sub>
9	100 : 5 : 5 : 1	PNMG <sub>104</sub> -PNAG <sub>6</sub> -PNBnG <sub>4</sub>
10	100 : 25 : 25 : 1	PNMG <sub>94</sub> -PNAG <sub>23</sub> -PNBnG <sub>21</sub>
11	100 : 50 : 50 : 1	PNMG <sub>94</sub> -PNAG <sub>48</sub> -PNBnG <sub>45</sub>
12	100 : 83 : 100 : 1	PNMG <sub>104</sub> -PNAG <sub>79</sub> -PNBnG <sub>82</sub>
13	150 : 20 : 20 : 1	PNMG <sub>144</sub> -PNAG <sub>25</sub> -PNBnG <sub>25</sub>

<sup>a</sup>. All polymerizations were conducted in dry benzonitrile. <sup>b</sup>. The numbers in subscripts correspond to DP<sub>n</sub> as determined by <sup>1</sup>H NMR. DP<sub>n</sub> of the PNMG block was determined by <sup>1</sup>H NMR. The relative DP<sub>n</sub> of PNAG and PNBnG blocks were determined by <sup>1</sup>H NMR.

Figure 3.2 shows SEC traces from the polymers obtained after sequential polymerization of methyl-NCA, allyl-NCA, and benzyl-NCA, respectively. Cyclic PNMG-*b*-PNAG diblock copolymers exhibit lower retention time than cyclic PNMG, and cyclic PNMG-PNAG-PNBnG triblock terpolymers exhibit lower retention time than cyclic PNMG-PNAG. This indicates that the hydrodynamic volumes of the polymers after each polymerization increased, and thus their chains have expanded. This suggests that the architecture of triblock terpolymers was achieved via sequential addition of three, distinct monomers.



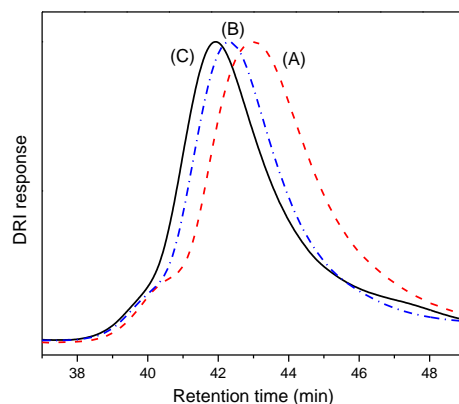


**Figure 3.2.** SEC traces of (A) cyclic PNMG<sub>144</sub>, (---), (B) cyclic PNMG<sub>144</sub>-*b*-PNAG<sub>25</sub> diblock copolymers (---), and (C) cyclic PNMG<sub>144</sub>-PNAG<sub>25</sub>-PNBnG<sub>25</sub> triblock terpolymers (—).

### 3.3 Cyclic [poly(*N*-ethyl-glycine)-*ran*-poly(*N*-butyl-glycine)]-*b*-poly(*N*-methyl-glycine)-*b*-poly(*N*-decyl-glycine) triblock terpolypeptoids

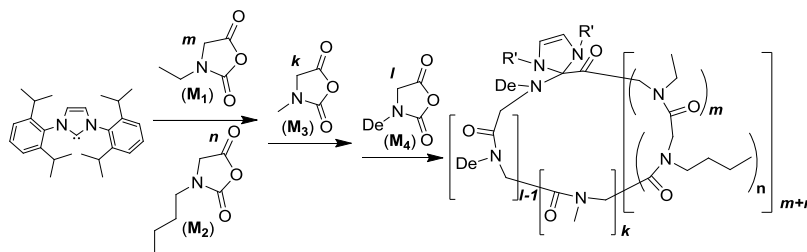
#### 3.3.1 Experimental

##### 3.3.1.1 Synthesis of cyclic [P(NEG-*ran*-NBG)]-PNMG-PNDG triblock terpolymers

Scheme 3.2 shows a synthetic procedure to prepare [P(NEG-*ran*-NBG)]-PNMG-PNDG triblock terpolymers by NHC-mediated ring opening polymerization via sequential addition of the corresponding NCA monomers. A procedure to prepare cyclic [P(NEG<sub>20</sub>-*ran*-NBG<sub>15</sub>)]-PNMG<sub>48</sub>-PNDG<sub>10</sub> is presented as follows. In the glovebox, ethyl-NCA (M<sub>1</sub>, 86 mg, 0.67 mmol, [M<sub>1</sub>]<sub>0</sub> = 0.4 M) was dissolved in 1100 μL of anhydrous acetonitrile, and butyl-NCA (M<sub>2</sub>, 70 mg, 0.45 mmol) was separately dissolved in 560 μL of anhydrous acetonitrile. These two monomer solutions were combined together, and stirred. A known volume of NHC/THF stock solution (560 μL, 45 μmol, 80 mM, [M<sub>1</sub>]:[M<sub>2</sub>]:[NHC]<sub>0</sub> = 15:10:1) was added to the solution of ethyl-NCA and butyl-NCA solution. Polymerization was conducted at 50 °C for 20 h under nitrogen. The aliquots (130 μL) were taken for NMR and SEC analyses to determine the conversion of polymerization and molecular weights of the polymer. Then a solution of methyl-NCA (M<sub>3</sub>, 150 mg, 0.3 mmol, [M<sub>1</sub>]:[M<sub>2</sub>]:[M<sub>3</sub>]:[NHC]<sub>0</sub> = 15:10:30:1) in 2700 μL of acetonitrile was added to the polymerization solution, and the second polymerization was conducted at room temperature for

20 h under nitrogen. Aliquots (130  $\mu\text{L}$ ) were taken for NMR and SEC analyses to determine the conversion of polymerization and the molecular weights of [P(NEG-*ran*-NBG)]-PNMG diblock copolymers. Finally, a solution of decyl-NCA ( $M_4$ , 73 mg, 0.3 mmol,  $[M_1]:[M_2]:[M_3]:[M_4]:[\text{NHC}]_0 = 15:10:30:7:1$ ) was added to the polymerization solution. The third polymerization was conducted at room temperature for 20 h. Aliquots (130  $\mu\text{L}$ ) were taken for NMR and SEC analyses. Final products were obtained as yellowish powder after precipitating in cold hexane and followed by cold diethyl ether, filtering, and drying under vacuum (175 mg, 67 % yield). Instrumental conditions for SEC and  $^1\text{H}$  NMR are described in section 2.1.1.

**Scheme 3.2.** Synthetic procedure to prepare cyclic [P(NEG-*ran*-NBG)]-PNMG-PNDG triblock terpolymers.



### 3.3.1.2 Sample preparation for DLS and TEM

An aqueous solution of triblock copolymers was prepared by “thin film hydration,” as reported by Zhou et al.<sup>119</sup> Dry polymers were directly dissolved in dichloromethane in a vial. The solvent was removed by evaporation in the air at room temperature, and followed by vacuum. Thin film of the polymer formed on the surface of the vial. Nanopure water was then added, and this solution was stirred at room temperature for one month before characterization. For DLS experiments, an aqueous solution ( $1.0 \text{ mg}\cdot\text{mL}^{-1}$ ) was prepared by diluting the concentrated solution which was filtered through a 20 nm filter (Anotop 25). The hydrodynamic radius ( $R_h$ ) of polymers in water was measured at temperatures from 25 to 65  $^\circ\text{C}$ . DLS experiments were

conducted using Malvern Zetasizer Nano-zs (Zen3600). The He-Ne laser operating at 633 nm was utilized, and light scattered by the sample was detected at an external angle of 173 ° for backscatter and at 12.8 ° for forward-scatter. Data from three measurements were recorded with at least 10 runs. At each temperature, the sample was equilibrated for at least 10 min. For samples from the TEM experiment, a dilute, aqueous solution of the terpolymers (about 5 µL) was deposited on the Formvar carbon-supported films with copper grids (Ted Pella, Inc.) The excess solution was removed using filter paper, and the TEM sample was dried in the air. TEM samples were negatively stained with uranyl formate aqueous solution (1 wt %) for 30 seconds. TEM images were collected by utilizing a JEOL 100CX instrument with an acceleration voltage of 80 kV.

### **3.3.2 Results and discussion**

#### **3.3.2.1 Synthesis and characterization of thermo-responsive triblock terpolypeptoids**

Figure 3.3 shows  $^1\text{H}$  NMR spectrum of  $[\text{P}(\text{NEG}_{20}\text{-ran-NBG}_{15})]\text{-PNMG}_{48}\text{-PNDG}_{10}$  triblock terpolymers in  $\text{CDCl}_3$ . It shows that the synthesized triblock terpolymers possess the desired polypeptoid backbone, four distinct side groups from  $\text{P}(\text{NEG-ran-NBG})$ ,  $\text{PNMG}$ , and  $\text{PNDG}$  chains. Additionally, the NHC moieties remain attached to the copolymer backbone, which suggests NHC-mediated chain extensions of polymers. NMR analysis of the aliquots of polymerization solution further revealed that the conversion after each polymerization reaction reached 100 %. Additionally, Table 3.2 shows the composition and molecular weights of cyclic  $[\text{P}(\text{NEG-ran-NBG})]\text{-PNMG-PNDG}$  triblock terpolymers, as determined by  $^1\text{H}$  NMR spectroscopy. The experimentally-determined  $\text{DP}_n$ s of the terpolymers are higher than the theoretical values. This may result from limited solubility of polymers after adding methyl-NCA and decyl-NCA monomers in the reaction medium.

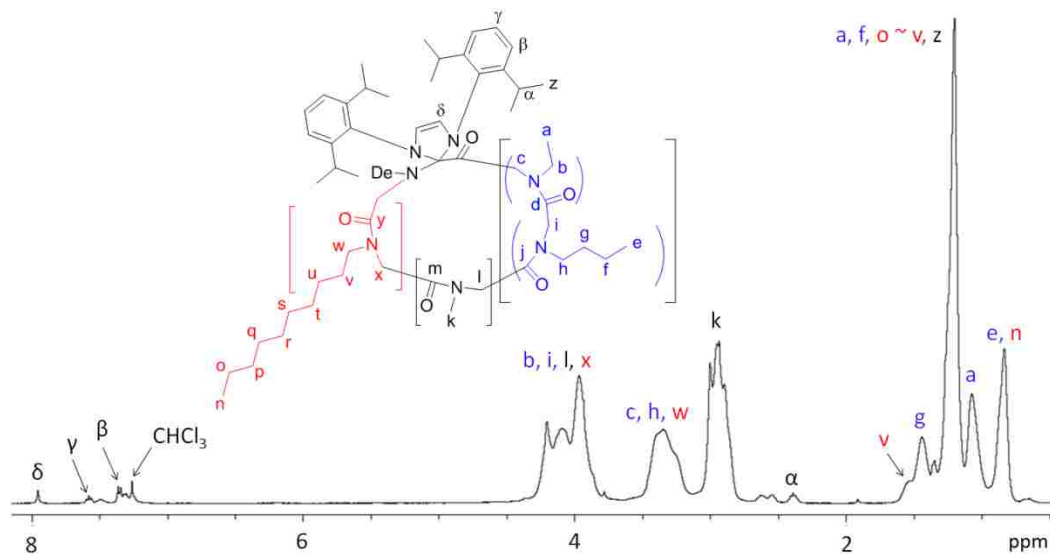


**Figure 3.3.**  $^1\text{H}$  NMR spectrum of  $[\text{P}(\text{NEG}_{20}\text{-ran-NBG}_{15})]\text{-PNMG}_{48}\text{-PNDG}_{10}$  triblock terpolymers in  $\text{CDCl}_3$ .

**Table 3.2.** Compositions and polymer MWs of cyclic  $[\text{P}(\text{NEG}\text{-ran-NBG})]\text{-PNMG-PNDG}$  triblock terpolymers.<sup>a</sup>

Entry #	$[\text{M}_1]_0:[\text{M}_2]_0:[\text{M}_3]_0:[\text{M}_4]_0:[\text{NHC}]_0$	Copolypeptoid composition <sup>b</sup>
1	15 : 10 : 15 : 3 : 1	$[\text{P}(\text{NEG}_{20}\text{-ran-NBG}_{15})]\text{-PNMG}_{16}\text{-PNDG}_5$
2	15 : 10 : 30 : 7 : 1	$[\text{P}(\text{NEG}_{20}\text{-ran-NBG}_{15})]\text{-PNMG}_{48}\text{-PNDG}_{10}$
3	30 : 18 : 80 : 10 : 1	$[\text{P}(\text{NEG}_{47}\text{-ran-NBG}_{21})]\text{-PNMG}_{128}\text{-PNDG}_{13}$

<sup>a</sup> All polymerizations were conducted in dry acetonitrile. <sup>b</sup> The numbers in subscripts correspond to  $\text{DP}_n$  as determined by  $^1\text{H}$  NMR.  $\text{DP}_n$  of the  $\text{P}(\text{NEG}\text{-ran-NBG})$  was determined by  $^1\text{H}$  NMR. The relative  $\text{DP}_n$  of PNMG and PNDG blocks were determined by  $^1\text{H}$  NMR.

Figure 3.4 shows SEC traces of  $\text{P}(\text{NEG}_{47}\text{-ran-NBG}_{21})$ ,  $[\text{P}(\text{NEG}_{47}\text{-ran-NBG}_{21})]\text{-PNMG}_{128}$ , and  $[\text{P}(\text{NEG}_{47}\text{-ran-NBG}_{21})]\text{-PNMG}_{128}\text{-PNDG}_{13}$ , respectively. The SEC traces shift to lower retention time, as adding methyl-NCA, followed by decyl-NCA monomers to the polymerization solution of  $\text{P}(\text{NEG}\text{-ran-NBG})$ , which indicates increased hydrodynamic volume after each

polymerization. This reveals that the polymer chains are extended by sequential addition of distinct monomers, which suggests the architecture of triblock copolymers of the final product.

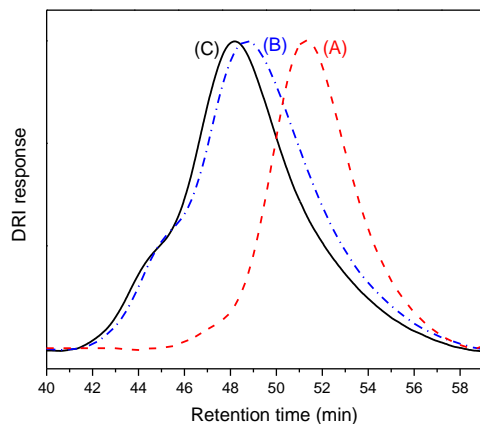


**Figure 3.4.** SEC traces of (A) cyclic P(NEG<sub>47</sub>-ran-NBG<sub>21</sub>) (---), (B) [P(NEG<sub>47</sub>-ran-NBG<sub>21</sub>)]-PNMG<sub>128</sub>(---), and (C) [P(NEG<sub>47</sub>-ran-NBG<sub>21</sub>)]-PNMG<sub>128</sub>-PNDG<sub>13</sub> triblock terpolymers (—).

### 3.3.2.2 Micellar aggregation from cyclic [P(NEG<sub>20</sub>-ran-NBG<sub>15</sub>)]-PNMG<sub>16</sub>-PNDG<sub>5</sub> triblock terpolymers

The morphologies of cyclic [P(NEG<sub>20</sub>-ran-NBG<sub>15</sub>)]-PNMG<sub>16</sub>-PNDG<sub>5</sub> triblock terpolymers in water were investigated by TEM. Figure 3.5 shows a TEM image of cast film from aqueous solution of cyclic [P(NEG<sub>20</sub>-ran-NBG<sub>15</sub>)]-PNMG<sub>16</sub>-PNDG<sub>5</sub> triblock terpolymers (1.0 mg·mL<sup>-1</sup>) at room temperature. The copolymers form worm-like micelles with a diameter of 9.3 nm (1.4 nm) and with various lengths up to a micron, as determined by using ImageJ software. Also, spherical, cylindrical, and other-shaped micelles are formed, revealing that the shape and size of the micelles at room temperature are not uniform.

The micellization and micellar aggregation of the cyclic triblock terpolymers in water at different temperatures was further examined by DLS. Figure 3.6 shows distribution of the apparent hydrodynamic radius ( $R_h$ ) from cyclic [P(NEG<sub>20</sub>-ran-NBG<sub>15</sub>)]-PNMG<sub>16</sub>-PNDG<sub>5</sub> triblock terpolymers in water as a function of temperature from 25 to 65 °C. Figure 3.6 (A), (B), and (C) show  $R_h$  distribution upon heating, cooling, and reheating after aging for 2 days at room

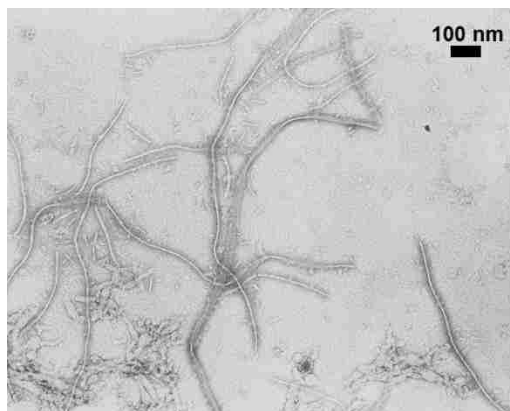


**Figure 3.5.** TEM image from cast film prepared from aqueous solution of cyclic  $[P(\text{NEG}_{20}\text{-ran-NBG})_{15}]$ -PNMG<sub>16</sub>-PNDG<sub>5</sub> triblock terpolymer ( $1.0 \text{ mg}\cdot\text{mL}^{-1}$ ) at room temperature. (A TEM sample was negatively stained with uranyl formate aqueous solution.)

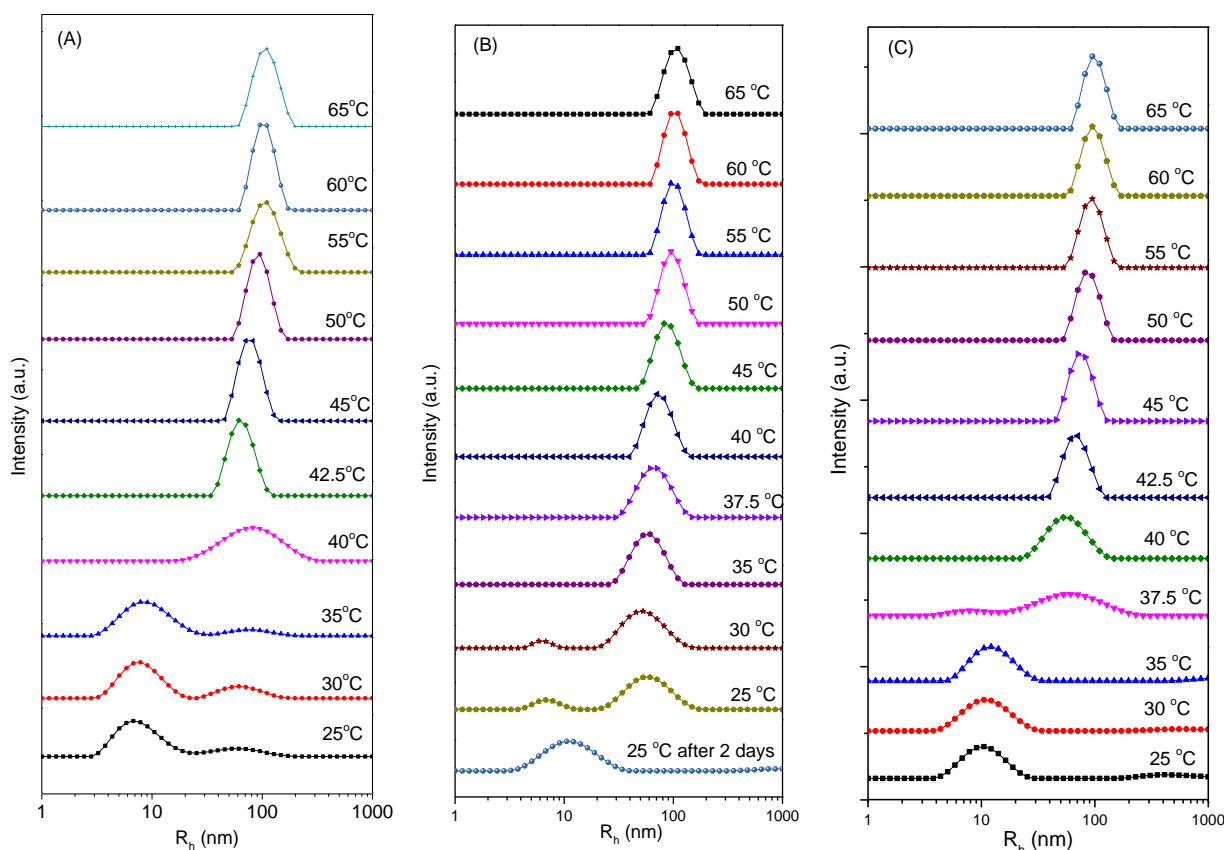


**Figure 3.6.** Apparent micelle size distributions of cyclic  $P(\text{NEG}_{20}\text{-ran-NBG})_{15}$ -PNMG<sub>16</sub>-PNDG<sub>5</sub> triblock copolymers in water ( $1.0 \text{ mg}\cdot\text{mL}^{-1}$ ) (A) while heating after filtering through a 20 nm filter, (B) cooling, and (C) reheating after aging for 2 days at room temperature.

temperature, respectively. Figure 3.7 summarizes the  $R_h$  and polydispersity index (PDI, particle size distribution) of the copolymers as a function of temperature. As can be seen in Figure 3.5

and 3.6, the copolymers may form micelles with  $R_h$  less than 20 nm with relatively broad distributions from 25 to 35 °C. A transition from relatively small micelles ( $R_h < 20$  nm) with broad distributions to large micelles ( $R_h > 70$  nm) with narrow distributions occurs between 35 °C to 45 °C. The size of the micelles dramatically increases to 70 to 120 nm above 45 °C with narrow distributions (PDI < 0.1). Upon further heating from 45 to 65 °C,  $R_h$  of the micelles gradually increases while keeping narrow distributions. As pointed out earlier in this chapter, Lahasky et al.<sup>66</sup> reported that cyclic P(NEG-*ran*-NBG) copolymers with PNEG molar fraction of around 0.6 exhibit  $T_{cp}$  around 35 °C. Thus, the transition in size and size distributions of the micelles from the copolymers may result from the change of hydrophobicity of the P(NEG-*ran*-NBG) block above its  $T_{cp}$ . DLS and TEM results reveal that the triblock copolymer forms micelles with relatively broad size distributions composed of both cylindrical micelles and spherical micelles below the  $T_{cp}$  of the P(NEG-*ran*-NBG) block (e.g. 25 °C). DLS results suggest that the triblock terpolymer forms well-defined, larger aggregates above the  $T_{cp}$  (e.g. 50 °C). This suggest that the micelles formed below  $T_{cp}$  may reorganize to form large micellar aggregates above  $T_{cp}$ .

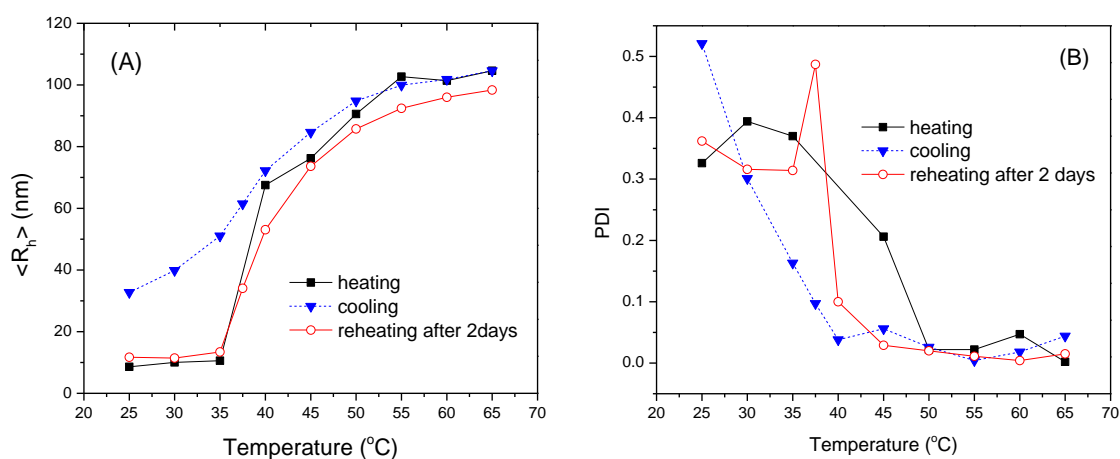


**Figure 3.7.** (A)  $R_h$  and (B) PDI (broadness of  $R_h$  distribution) of cyclic [P(NEG<sub>20</sub>-*ran*-NBG)<sub>15</sub>]-PNMG<sub>16</sub>]-PNDG<sub>5</sub> triblock terpolymer micelles as a function of temperature.

## CHAPTER 4. CRYSTALLIZATION AND MELTING BEHAVIOR OF CYCLIC OR LINEAR POLYPEPTOIDS WITH VARIOUS ALKYL SIDE CHAINS

### 4.1 Introduction

Incorporation of flexible, alkyl side chains to polymer main chains have been of great interest, as it enables tuning of the polymer physical properties such as crystallinity, melting point, or solubility, while maintaining structures and functions of the polymer backbones. Along with the altered properties of the polymers, crystallization and melting behavior of the side chains have been widely studied. As early as 1954, Greenburg et al.<sup>120</sup> reported side chain crystallization of polymethacrylates and polyacrylates with *n*-alkyl side chains containing 12 to 18 carbons. Later, crystallization and crystalline structures of rigid-rod polymers bearing alkyl pendent groups were extensively investigated, as the introduction of flexible side chains could improve the solubility and reduce melting temperatures of the rigid-rod polymers.<sup>121-124</sup> Watanabe et al.<sup>124</sup> studied side chain crystallization and thermotropic behavior of  $\alpha$ -helical polypeptides, poly( $\gamma$ -alkyl L-glutamates), with various flexible *n*-alkyl side chains. They reported that melting temperatures of the side chains increase from -24 to 62 °C, as the length of the side chains increases from decyl (10 carbons) to octadecyl (18 carbons) groups. Along with the side chain melting, these polymers with decyl or longer side chains showed behavior of thermotropic cholesteric liquid crystals, as the long flexible side chains behaved like a solvent. Studies on side chain crystallization were further extended to alkyl side chains attached to rigid-rod polymers including aromatic polyamides,<sup>125,126</sup> aromatic polyesters,<sup>127-130</sup> poly(3-*n*-alkylthiophenes),<sup>131-134</sup> N-alkylated polyanilines,<sup>135</sup> and polymaleimides.<sup>136</sup> These studies revealed that the *n*-alkyl side chain crystallization was observed from dodecyl (12 carbons) or longer side chains and it leads to packing rigid-rod main chains into ordered lamellae.<sup>127</sup> Additionally, Lee et al.<sup>122</sup> reported side chain melting transitions from semi-flexible, comb-like



hydroxypropylcellulose with 12 and 18 carbons of side chains at 45 °C and 56 °C as well as isotropic transitions at 106 °C and 115 °C, respectively. More recently, crystallization of shorter side chains than dodecyl groups was reported from poly(3-alkylthiophene). Pankaj et al.<sup>137</sup> reported side chain crystallization from regio-random poly(3-alkylthiophenes) with *n*-alkyl side chains of 6 – 12 carbons. Wu et al.<sup>138</sup> further reported side chain melting transitions around 50 – 60 °C for regio-regular poly(3-alkylthiophene) with hexyl side groups, poly(3-hexylthiophene) (P3HP), as evidenced by variable-temperature WAXS. Most recently, Yuan et al.<sup>139</sup> reported the melting transitions of the hexyl side chains as well as the main chains for poly(3-hexylthiophene) films at 54 and 223 °C, respectively. They demonstrated that the methyl groups from the side chains become disordered after the first melting transition, “solid-to-solid phase transition,” as revealed by temperature-dependent infrared spectroscopy. However, crystallization and melting from shorter side chains than hexyl groups, i.e. butyl side groups, bonded to polymer backbones have rarely been reported.

In section 2.1, crystalline structures and melting behavior of cyclic poly(*N*-decylglycine)s (*c*-PNDG)s, polypeptoids with *n*-decyl side chains (10 carbons), were presented. It was revealed that the decyl side chains of *c*-PNDGs are well organized, as the primary peak and multiple order reflections were observed in the WAXS spectrum. Furthermore, two melting transitions of the *c*-PNDGs at 72-79 °C ( $T_{m,1}$ ) and 166-177 °C ( $T_{m,2}$ ) were observed by DSC. The first melting transition, ( $T_{m,1}$ ) was not observed for the oligomeric peptoids.<sup>48</sup> The  $T_{m,1}$  was attributed to the melting of highly-ordered pendent groups. To have a better understanding of the melting and crystallization of polypeptoids with *n*-alkyl side chains, we expanded our studies by varying the length of *n*-alkyl side chains while keeping the length of main chains identical. More specifically, a series of cyclic poly(*N*-*n*-alkyl-glycine)s were synthesized with various *n*-alkyl

chains, i.e. ethyl, *n*-butyl, *n*-hexyl, *n*-octyl, *n*-decyl, *n*-dodecyl, or *n*-tetradecyl groups by NHC-mediated ring-opening polymerization of corresponding *N*-*n*-alkyl-*N*-carboxyanhydride (*n*-alkyl-NCA) monomers. Their linear counterparts were synthesized by using benzylamine as an initiator. Melting and crystallization behaviors were studied by DSC. Crystalline structures were studied by WAXS and domain spacing of the crystallites was correlated to the length of *n*-alkyl side chains. In addition to polypeptoids with linear *n*-alkyl side chains, polypeptoids with branched side chains were synthesized and characterized to study the effect of branching on the melting and crystallization of polypeptoids. This chapter further presents effects of the architecture of polymer backbones (i.e. cyclic or linear) and side structures (i.e. linear and branched) of polypeptoids on their melting and crystallization behaviors.

## 4.2 Experimental

### 4.2.1 Synthesis of monomers and their NMR spectra

The synthesis of *N*-*n*-alkyl NCAs, (*N*-ethyl NCA, *N*-*n*-butyl NCA, *N*-*n*-hexyl NCA, *N*-*n*-octyl NCA, *N*-*n*-decyl NCA, *N*-*n*-dodecyl NCA, and *N*-*n*-tetradecyl NCAs) was conducted by adapting a procedure reported by Guo et al.<sup>9</sup> using commercially available primary amines (e.g., *n*-alkylamines, ethylamine, butylamine, hexylamine, octylamine, decylamine, dodecylamine, and tetradecylamine). The synthetic scheme to prepare NCAs is shown in section 2.1.2. Synthesis of *N*-ethyl NCAs were reported by Lahasky et al.,<sup>66</sup> *N*-*n*-butyl NCAs by Guo et al.,<sup>9</sup> and *N*-*n*-decyl NCAs was reported by Lee et al.<sup>140</sup>

***N*-*n*-hexyl NCA** <sup>1</sup>H NMR ( $\delta$  in CDCl<sub>3</sub>, ppm): 0.86 (t, CH<sub>3</sub>(CH<sub>2</sub>)<sub>3</sub>CH<sub>2</sub>CH<sub>2</sub>-, 3H); 1.29 (m, CH<sub>3</sub>(CH<sub>2</sub>)<sub>3</sub>CH<sub>2</sub>CH<sub>2</sub>-, 6H); 1.56 (m, CH<sub>3</sub>(CH<sub>2</sub>)<sub>3</sub>CH<sub>2</sub>CH<sub>2</sub>-, 2H); 3.37 (t, CH<sub>3</sub>(CH<sub>2</sub>)<sub>3</sub>CH<sub>2</sub>CH<sub>2</sub>-, 2H); 4.09 (s, -COCH<sub>2</sub>-) (Figure 4.1 (A)).

***N-n-octyl-NCA***  $^1\text{H}$  NMR ( $\delta$  in  $\text{CDCl}_3$ , ppm): 0.85 (t,  $\text{CH}_3(\text{CH}_2)_5\text{CH}_2\text{CH}_2-$ , 3H); 1.25-1.29 (m,  $\text{CH}_3(\text{CH}_2)_5\text{CH}_2\text{CH}_2-$ , 10H); 1.56 (m,  $\text{CH}_3(\text{CH}_2)_5\text{CH}_2\text{CH}_2-$ , 2H); 3.36 (t,  $\text{CH}_3(\text{CH}_2)_5\text{CH}_2\text{CH}_2-$ , 2H); 4.08 (s,  $-\text{COCH}_2-$ ) (Figure 4.1 (B)).

***N-n-dodecyl-NCA***  $^1\text{H}$  NMR ( $\delta$  in  $\text{CDCl}_3$ , ppm): 0.86 (t,  $\text{CH}_3(\text{CH}_2)_9\text{CH}_2\text{CH}_2-$ , 3H); 1.25-1.31 (m,  $\text{CH}_3(\text{CH}_2)_9\text{CH}_2\text{CH}_2-$ , 18H); 1.59 (m,  $\text{CH}_3(\text{CH}_2)_9\text{CH}_2\text{CH}_2-$ , 2H); 3.39 (t,  $\text{CH}_3(\text{CH}_2)_9\text{CH}_2\text{CH}_2-$ , 2H); 4.08 (s,  $-\text{COCH}_2-$ ). (Figure 4.1 (C)).

***N-n-tetradecyl-NCA***  $^1\text{H}$  NMR ( $\delta$  in  $\text{CDCl}_3$ , ppm): 0.85 (t,  $\text{CH}_3(\text{CH}_2)_{11}\text{CH}_2\text{CH}_2-$ , 3H); 1.23-1.31 (m,  $\text{CH}_3(\text{CH}_2)_{11}\text{CH}_2\text{CH}_2-$ , 18H); 1.56 (m,  $\text{CH}_3(\text{CH}_2)_{11}\text{CH}_2\text{CH}_2-$ , 2H); 3.35 (t,  $\text{CH}_3(\text{CH}_2)_{11}\text{CH}_2\text{CH}_2-$ , 2H); 4.08 (s,  $-\text{COCH}_2-$ ) (Figure 4.1 (D)).

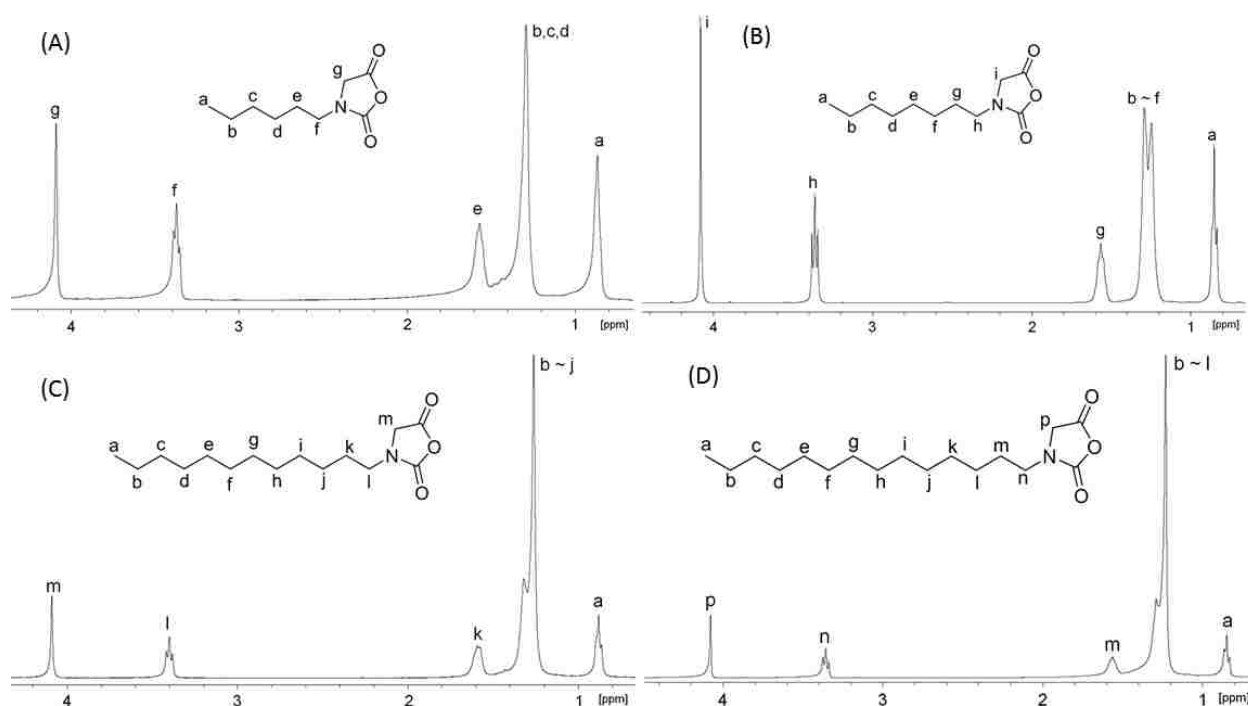
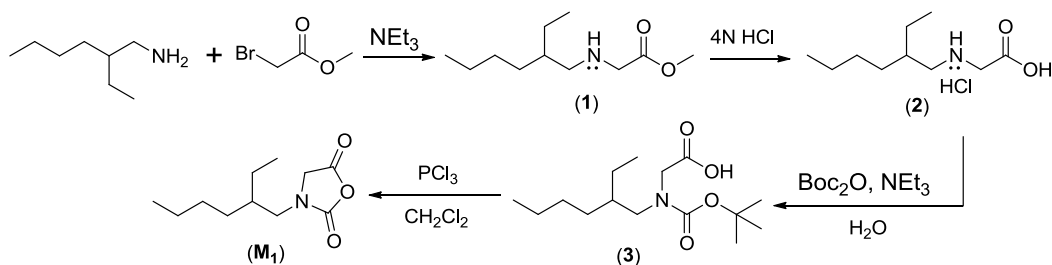


**Figure 4.1.**  $^1\text{H}$  NMR spectra of (A) hexyl-NCA, (B) octyl-NCA, (C) dodecyl-NCA, and (D) tetradecyl-NCA in  $\text{CDCl}_3$ .

***N-2-ethyl-1-hexyl NCA*** Branched NCAs, 2-ethyl-1-hexyl-NCAs, were synthesized by the procedure reported by Guo et al.<sup>45</sup> by starting with 2-ethyl-1-hexylamine and methylbromoacetate. Scheme 4.1 shows the synthetic procedure to prepare it.

**Scheme 4.1.** Synthetic procedure to prepare 2-ethyl-1-hexyl NCAs.



### Synthesis of (2-ethyl-1-hexylamino)acetate (1)

In a round bottom flask, 2-ethyl-1-hexylamine (6.55 mL, 40 mmol) was stirred with Et<sub>3</sub>N (6.1 mL, 44 mmol) in 50 mL of ethyl acetate at room temperature. Methylbromoacetate (4.5 mL, 48 mmol) was added to this solution. This mixture was heated to 55 °C and stirred for 24 h. The mixture was cooled down to room temperature and 30 mL of distilled water was added to the suspension. The organic layer was separated, washed with NaCl solution (15 %), and dried with anhydrous MgSO<sub>4</sub>. Then 2-ethyl-1-hexylamino-acetic acid methyl ester (1) was obtained as clear oil after filtering and removing the solvent (7.9 g, 97 % yield). <sup>1</sup>H NMR (δ in CDCl<sub>3</sub>, 400 MHz, ppm): 0.81 (m, CH<sub>3</sub>(CH<sub>2</sub>)<sub>3</sub>CH(C<sub>2</sub>H<sub>5</sub>)CH<sub>2</sub>- & CH<sub>3</sub>(CH<sub>2</sub>)<sub>3</sub>CH((CH<sub>2</sub>)(CH<sub>3</sub>))CH<sub>2</sub>-, 6H); 1.24 (m, CH<sub>3</sub>(CH<sub>2</sub>)<sub>3</sub>CH(C<sub>2</sub>H<sub>5</sub>)CH<sub>2</sub>-, 6H); 1.32 (m, CH<sub>3</sub>(CH<sub>2</sub>)<sub>3</sub>CH((CH<sub>2</sub>)(CH<sub>3</sub>))CH<sub>2</sub>-, 2H); 1.67 (m, CH<sub>3</sub>(CH<sub>2</sub>)<sub>3</sub>CH(C<sub>2</sub>H<sub>5</sub>)CH<sub>2</sub>-, 1H); 2.42 & 2.43 (s, CH<sub>3</sub>(CH<sub>2</sub>)<sub>3</sub>CH(C<sub>2</sub>H<sub>5</sub>)CH<sub>2</sub>N-, 2H); 3.33 & 3.46 (-NHCH<sub>2</sub>CO-, 2H); 3.61 & 3.62 (s, H<sub>3</sub>CO-, 3H) (Figure 4.2 (A)).

### Synthesis of (2-ethyl-1-hexylamino)acetatic acid hydrochloride (2)

The compound **1** (7.9 g, 39 mmol) was stirred with 4N HCl solution (30 mL) at 55 °C for 24 h. The solvent was removed under vacuum. Recrystallization in methanol followed by diethyl ether at -20 °C was conducted to obtain white, fine powder (5.2 g, 60 % yield). <sup>1</sup>H NMR (δ in DMSO, 400 MHz, ppm): 0.84 (m, CH<sub>3</sub>(CH<sub>2</sub>)<sub>3</sub>CH(C<sub>2</sub>H<sub>5</sub>)CH<sub>2</sub>- & CH<sub>3</sub>(CH<sub>2</sub>)<sub>3</sub>CH((CH<sub>2</sub>)(CH<sub>3</sub>))CH<sub>2</sub>-, 6H); 1.24 (m, CH<sub>3</sub>(CH<sub>2</sub>)<sub>3</sub>CH(C<sub>2</sub>H<sub>5</sub>)CH<sub>2</sub>-, 6H); 1.32 (m, CH<sub>3</sub>(CH<sub>2</sub>)<sub>3</sub>CH((CH<sub>2</sub>)(CH<sub>3</sub>))CH<sub>2</sub>-, 2H); 1.71 (m, CH<sub>3</sub>(CH<sub>2</sub>)<sub>3</sub>CH(C<sub>2</sub>H<sub>5</sub>)CH<sub>2</sub>-, 1H); 2.83 & 3.15 (s,

$\text{CH}_3(\text{CH}_2)_3\text{CH}(\text{C}_2\text{H}_5)\text{CH}_2\text{N}^-$ , 2H); 3.82 & 4.17 (s,  $-\text{NHCH}_2\text{CO}-$ , 2H); 9.14 ppm (s,  $\text{HNHCl}$ ) (Figure 4.2 (B)).

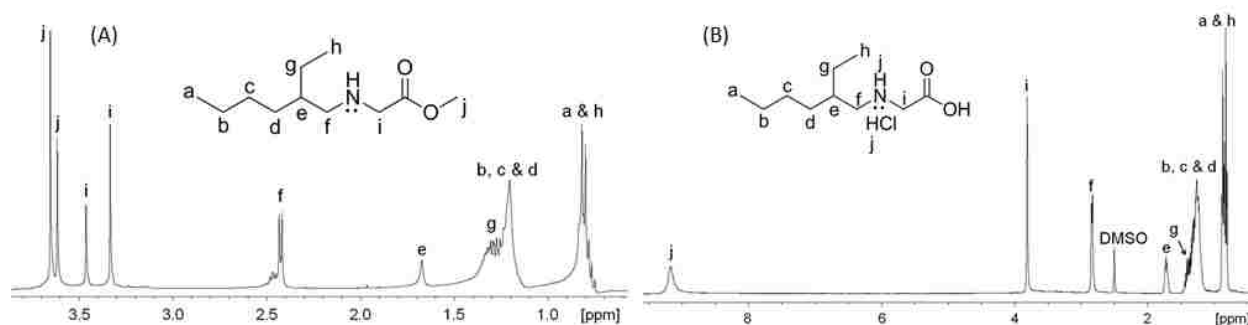


**Figure 4.2.**  $^1\text{H}$  NMR spectra of (A) (2-ethyl-1-hexylamino)acetate (1) and (B) (2-ethyl-1-hexylamino)acetic acid hydrochloride (2).

### Synthesis of 2-(*N,N*-*tert*-butoxycarbonyl(2-ethyl-1-hexyl)amino)acetic acid (3).

A mixture of **2** (5 g, 22 mmol), di-*tert*-butyl dicarbonate (12 g, 55 mmol) and triethylamine (15 mL, 110 mmol) in distilled water (100 mL) was stirred at 40 °C for 20 h. The reaction mixture was extracted with hexane (2×70 mL) to remove any unreacted di-*tert*-butyl dicarbonate. The aqueous phase was separated, acidified with aqueous HCl (50 mL, 4 M), and extracted with ethyl acetate (3×70 mL). Then, the organic phase was separated, washed with brine, and dried over anhydrous  $\text{MgSO}_4$ . Subsequent filtration and solvent removal afforded clear oil (5.3 g, 84 % yield).  $^1\text{H}$  NMR ( $\delta$  in  $\text{CDCl}_3$ , 400 MHz, ppm): 0.84 (m,  $\text{CH}_3(\text{CH}_2)_3\text{CH}(\text{C}_2\text{H}_5)\text{CH}_2-$  &  $\text{CH}_3(\text{CH}_2)_3\text{CH}((\text{CH}_2)(\text{CH}_3))\text{CH}_2-$ , 6H); 1.25 (m,  $\text{CH}_3(\text{CH}_2)_3\text{CH}(\text{C}_2\text{H}_5)\text{CH}_2-$  &  $\text{CH}_3(\text{CH}_2)_3\text{CH}((\text{CH}_2)(\text{CH}_3))\text{CH}_2-$ , 8H); 1.40 & 1.45 (s,  $-(\text{CH}_3)_3$ , 9H); 1.50 (m,  $\text{CH}_3(\text{CH}_2)_3\text{CH}(\text{C}_2\text{H}_5)\text{CH}_2-$ , 1H); 3.16 (m,  $\text{CH}_3(\text{CH}_2)_3\text{CH}(\text{C}_2\text{H}_5)\text{CH}_2\text{N}^-$ , 2H); 3.85 & 3.96 ( $-\text{NHCH}_2\text{CO}-$ , 2H).

### Synthesis of 2-ethyl-hexyl-NCA ( $\text{M}_1$ )

Compound **3** (5.2 g, 18 mmol) was dissolved in anhydrous  $\text{CH}_2\text{Cl}_2$  (120 mL) under a nitrogen atmosphere. The solution was cooled to 0 °C and phosphorous trichloride (2.4 mL, 27

mmol) was added dropwise. The reaction mixture was stirred at room temperature for 2 h, and the volatiles were removed under vacuum. Inside the glovebox, the solid residue was extracted with anhydrous  $\text{CH}_2\text{Cl}_2$  (20 mL) and filtered. The filtrate was concentrated as clear, viscous liquid. The product was purified by distillation using sublimation apparatus at  $70\text{ }^\circ\text{C}$  (4.5 g, 57 % yield).  $^1\text{H}$  NMR ( $\delta$  in  $\text{CDCl}_3$ , 400 MHz, ppm): 0.89 (m,  $\text{CH}_3(\text{CH}_2)_3\text{CH}(\text{C}_2\text{H}_5)\text{CH}_2-$  &  $\text{CH}_3(\text{CH}_2)_3\text{CH}((\text{CH}_2)(\text{CH}_3))\text{CH}_2-$ , 6H); 1.24 (m,  $\text{CH}_3(\text{CH}_2)_3\text{CH}(\text{C}_2\text{H}_5)\text{CH}_2-$ , 6H); 1.32 (m,  $\text{CH}_3(\text{CH}_2)_3\text{CH}((\text{CH}_2)(\text{CH}_3))\text{CH}_2-$ , 2H); 1.58 (m,  $\text{CH}_3(\text{CH}_2)_3\text{CH}(\text{C}_2\text{H}_5)\text{CH}_2-$ , 1H); 3.29 (m,  $\text{CH}_3(\text{CH}_2)_3\text{CH}(\text{C}_2\text{H}_5)\text{CH}_2\text{N}-$ , 2H); 4.08 (s,  $-\text{COCH}_2-$ , 2H).  $^{13}\text{C}\{^1\text{H}\}$  NMR ( $\delta$  in  $\text{CDCl}_3$ , 100 MHz, ppm): 10.5 ( $\text{CH}_3(\text{CH}_2)_3\text{CH}((\text{CH}_2)(\text{CH}_3))\text{CH}_2-$ ); 14.2 ( $\text{CH}_3(\text{CH}_2)_3\text{CH}(\text{C}_2\text{H}_5)\text{CH}_2-$ ); 23.1 ( $\text{CH}_3\text{CH}_2(\text{CH}_2)_2\text{CH}(\text{C}_2\text{H}_5)\text{CH}_2-$ ); 23.8 ( $\text{CH}_3\text{CH}_2\text{CH}_2\text{CH}_2\text{CH}(\text{C}_2\text{H}_5)\text{CH}_2-$ ); 28.6 ( $\text{CH}_3(\text{CH}_2)_3\text{CH}((\text{CH}_2)(\text{CH}_3))\text{CH}_2-$ ); 30.5 ( $\text{CH}_3(\text{CH}_2)_2\text{CH}_2\text{CH}(\text{C}_2\text{H}_5)\text{CH}_2-$ ); 37.7 ( $\text{CH}_3(\text{CH}_2)_3\text{CH}(\text{C}_2\text{H}_5)\text{CH}_2-$ ); 47.6 ( $\text{CH}_3(\text{CH}_2)_3\text{CH}(\text{C}_2\text{H}_5)\text{CH}_2-$ ); 49.7 ( $-\text{COCH}_2-$ ); 152.6 ( $-\text{NCOOCO}-$ ); 165.8 ( $-\text{NCOOCO}-$ ). (Figure 4.3)

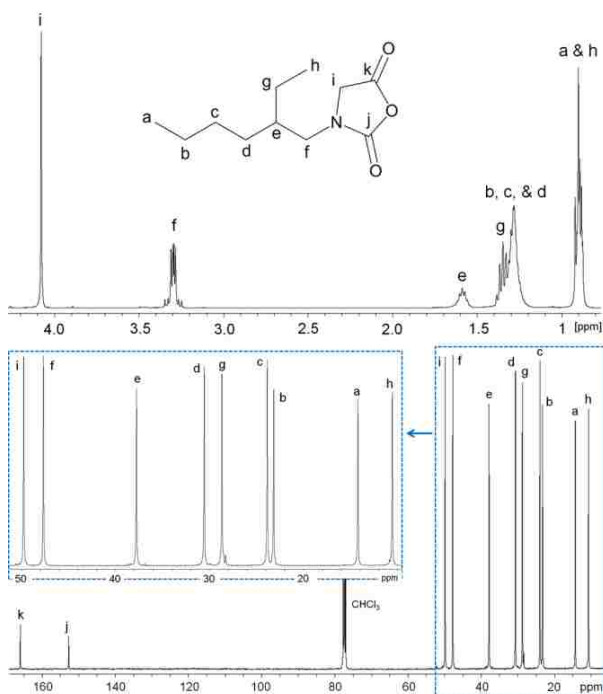
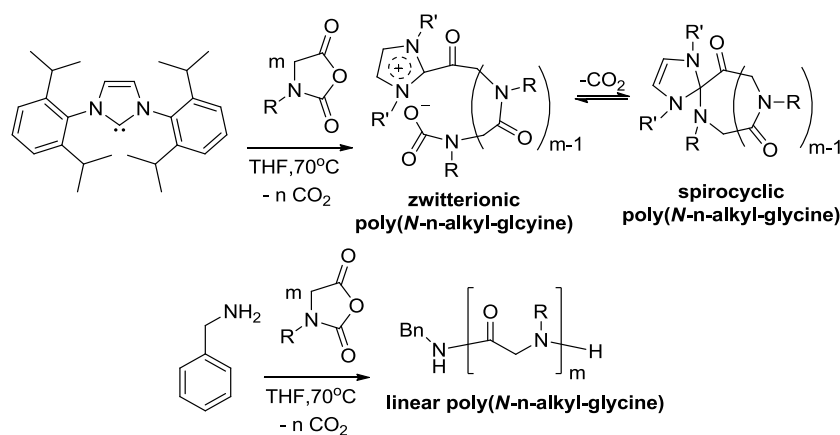


**Figure 4.3.**  $^1\text{H}$  and  $^{13}\text{C}\{^1\text{H}\}$  NMR spectra of 2-ethyl-1-hexyl-NCA in  $\text{CDCl}_3$ .

#### 4.2.2 Synthesis of cyclic or linear poly(*N*-alkyl-glycine)s

Cyclic poly(*N*-alkyl glycine)s were synthesized by NHC-mediated ring-opening polymerization of corresponding NCA monomers, as presented in sections 2.1.1.4 and 2.1.2.1 (Scheme 4.2).<sup>9,66,141</sup> Linear poly(*N*-alkyl glycine)s were synthesized using benzylamine as an initiator (Scheme 4.2). Table 4.1 summarizes polypeptoids with various alkyl side chains presented in this chapter. The molar ratio of monomers to NHC,  $[M]_0:[NHC]_0$ , was kept as 100 in this study. All polymerizations were conducted in THF at 70 °C for 24 h. After polymerization, PNEGs, PNBGs, PNHGs, and PNOGs were precipitated in cold hexane, and PNEHG, PNDG, PNDDG, and PNTG were precipitated in cold methanol. Polymers were obtained as pale yellow solids after filtering and drying under vacuum.

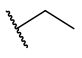
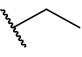
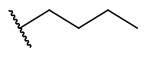
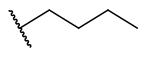
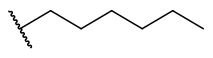
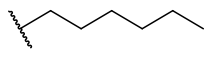
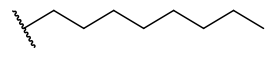
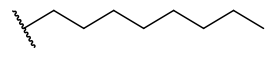
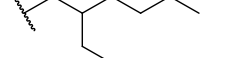
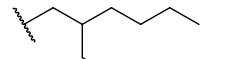
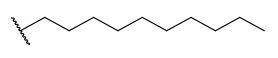
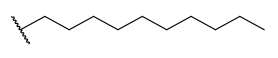
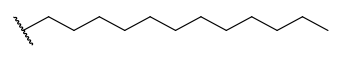
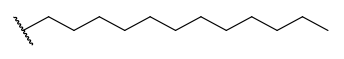
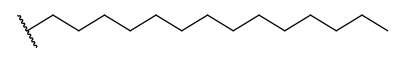
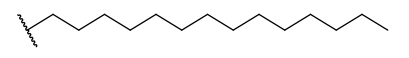
**Scheme 4.2.** Synthesis of cyclic or linear poly(*N*-*n*-alkyl-glycine)s.



R = ethyl, *n*-butyl, *n*-hexyl, *n*-octyl, *n*-decyl, *n*-dodecyl, *n*-tetradecyl, or 2-ethyl-1-hexyl group

The following example is a representative procedure to synthesize cyclic poly(*N*-2-ethyl-1-hexyl-glycine)s (*c*-PEHGs). In the glovebox, *N*-2-ethyl-1-hexyl NCA (M, 100 mg, 0.47 mmol,  $[M]_0=0.4$  M) was dissolved in anhydrous THF (1110  $\mu$ L). A known volume of NHC/THF stock solution (60  $\mu$ L, 4.7  $\mu$ mol, 77.2 mM,  $[M]:[NHC]_0 = 100:1$ ) was added to the monomer solution.

**Table 4.1.** Alkyl side chains of polypeptoids studied in chapter 4.

Polypeptoids	Abbreviation	Side chain ( <i>R</i> )	$n^a$	$DP_n^b$
<b>cyclic poly(<i>N</i>-ethyl-glycine)</b>	<b><i>c</i>-PNEG</b>		<b>2</b>	<b>100</b>
linear poly( <i>N</i> -ethyl-glycine)	<i>l</i> -PNEG		2	100
<b>cyclic poly(<i>N</i>-butyl-glycine)</b>	<b><i>c</i>-PNBG</b>		<b>4</b>	<b>100</b>
linear poly( <i>N</i> -butyl-glycine)	<i>l</i> -PNBG		4	100
<b>cyclic poly(<i>N</i>-hexyl-glycine)</b>	<b><i>c</i>-PNHG</b>		<b>6</b>	<b>100</b>
linear poly( <i>N</i> -hexyl-glycine)	<i>l</i> -PNHG		6	100
<b>cyclic poly(<i>N</i>-octyl-glycine)</b>	<b><i>c</i>-PNOG</b>		<b>8</b>	<b>100</b>
linear poly( <i>N</i> -octyl-glycine)	<i>l</i> -PNOG		8	100
<b>cyclic poly(<i>N</i>-2-ethyl-1-hexyl-glycine)</b>	<b><i>c</i>-PNEHG</b>		<b>8</b>	<b>100</b>
Linear poly( <i>N</i> -2-ethyl-1-hexyl-glycine)	<i>l</i> -PNEHG		8	100
<b>cyclic poly(<i>N</i>-decyl-glycine)</b>	<b><i>c</i>-PNDG</b>		<b>10</b>	<b>100</b>
linear poly( <i>N</i> -decyl-glycine)	<i>l</i> -PNDG		10	100
<b>cyclic poly(<i>N</i>-dodecyl-glycine)</b>	<b><i>c</i>-PNDDG</b>		<b>12</b>	<b>100</b>
linear poly( <i>N</i> -dodecyl-glycine)	<i>l</i> -PNDDG		12	100
<b>cyclic poly(<i>N</i>-tetradecyl-glycine)</b>	<b><i>c</i>-PNTG</b>		<b>14</b>	<b>70</b>
linear poly( <i>N</i> -tetradecyl-glycine)	<i>l</i> -PNTG		14	70

<sup>a</sup> $n$  is number of carbon of side chains (*R*). <sup>b</sup>Number average degree of polymerization ( $DP_n$ ) was determined by <sup>1</sup>H NMR.



Polymerization was allowed to proceed at 70 °C for 24 h under nitrogen and then quenched by the addition of cold methanol. The white precipitate was collected and washed with ample methanol to remove any unreacted monomer or initiator. Drying under vacuum yielded yellowish, sticky solid (48 mg, 60% yield).  $^1\text{H}$  NMR ( $\delta$  in  $\text{CDCl}_3$ , 400 MHz, ppm): 0.85 (m,  $\text{CH}_3(\text{CH}_2)_3\text{CH}(\text{C}_2\text{H}_5)\text{CH}_2^-$  &  $\text{CH}_3(\text{CH}_2)_3\text{CH}((\text{CH}_2)(\text{CH}_3))\text{CH}_2^-$ , 6H); 1.24 (m,  $\text{CH}_3(\text{CH}_2)_3\text{CH}(\text{C}_2\text{H}_5)\text{CH}_2^-$ , 6H); 1.38 (m,  $\text{CH}_3(\text{CH}_2)_3\text{CH}((\text{CH}_2)(\text{CH}_3))\text{CH}_2^-$ , 2H); 1.65 (m,  $\text{CH}_3(\text{CH}_2)_3\text{CH}(\text{C}_2\text{H}_5)\text{CH}_2^-$ , 1H); 3.19 (m,  $\text{CH}_3(\text{CH}_2)_3\text{CH}(\text{C}_2\text{H}_5)\text{CH}_2\text{N}^-$ , 2H); 4.34 (s,  $-\text{COCH}_2^-$ , 2H).  $^{13}\text{C}\{^1\text{H}\}$  NMR ( $\delta$  in  $\text{CDCl}_3$ , 100 MHz, ppm): 10.3 ( $\text{CH}_3(\text{CH}_2)_3\text{CH}((\text{CH}_2)(\text{CH}_3))\text{CH}_2^-$ ); 13.9 ( $\text{CH}_3(\text{CH}_2)_3\text{CH}(\text{C}_2\text{H}_5)\text{CH}_2^-$ ); 23.1 ( $\text{CH}_3\text{CH}_2(\text{CH}_2)_2\text{CH}(\text{C}_2\text{H}_5)\text{CH}_2^-$ ); 23.5 ( $\text{CH}_3\text{CH}_2\text{CH}_2\text{CH}_2\text{CH}(\text{C}_2\text{H}_5)\text{CH}_2^-$ ); 28.4 ( $\text{CH}_3(\text{CH}_2)_3\text{CH}((\text{CH}_2)(\text{CH}_3))\text{CH}_2^-$ ); 30.3 ( $\text{CH}_3(\text{CH}_2)_2\text{CH}_2\text{CH}(\text{C}_2\text{H}_5)\text{CH}_2^-$ ); 38.5 ( $\text{CH}_3(\text{CH}_2)_3\text{CH}(\text{C}_2\text{H}_5)\text{CH}_2^-$ ); 49.4 ( $\text{CH}_3(\text{CH}_2)_3\text{CH}(\text{C}_2\text{H}_5)\text{CH}_2^-$ ); 53.7 ( $-\text{COCH}_2^-$ ); 171.0 ( $-\text{NCOCH}_2^-$ ) (Figure 4.4).

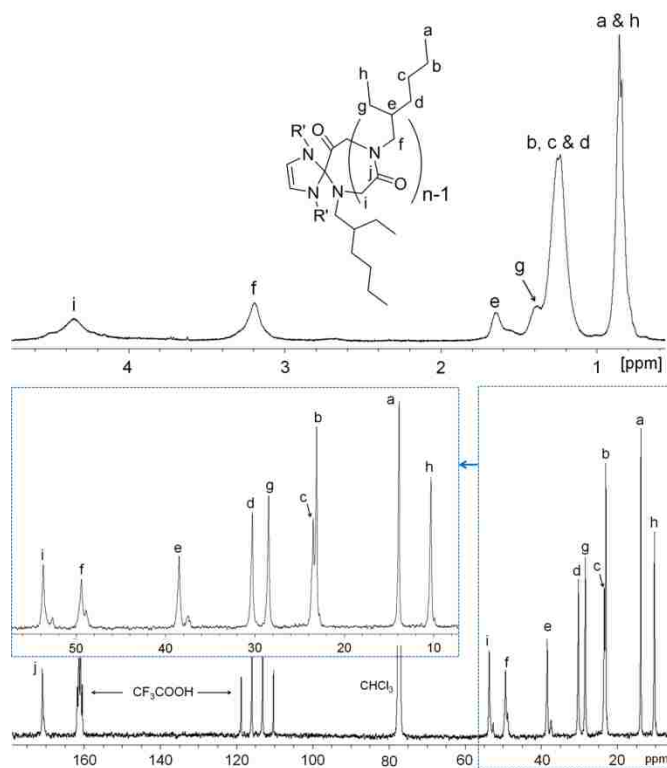


**Figure 4.4.**  $^1\text{H}$  and  $^{13}\text{C}\{^1\text{H}\}$  NMR spectra cyclic poly(*N*-2-ethyl-1-hexyl-glycine)s in  $\text{CDCl}_3$ .

Cyclic PNBGs and PNDGs were previously reported by Guo et al.<sup>142</sup> and Lee et al.<sup>141</sup>, respectively.

**Cyclic PNEGs** <sup>1</sup>H NMR ( $\delta$  in CDCl<sub>3</sub>, 400 MHz, ppm): 0.87 (CH<sub>3</sub>CH<sub>2</sub>-, 3H); 3.45 (CH<sub>3</sub>CH<sub>2</sub>-, 2H); 4.02 (-COCH<sub>2</sub>-, 2H) (Figure 4.5 (A)).

**Cyclic PNHGs** <sup>1</sup>H NMR ( $\delta$  in CDCl<sub>3</sub>, ppm): 0.86 (CH<sub>3</sub>(CH<sub>2</sub>)<sub>3</sub>CH<sub>2</sub>CH<sub>2</sub>-, 3H); 1.27 (CH<sub>3</sub>(CH<sub>2</sub>)<sub>3</sub>CH<sub>2</sub>CH<sub>2</sub>-, 6H); 1.50 (CH<sub>3</sub>(CH<sub>2</sub>)<sub>3</sub>CH<sub>2</sub>CH<sub>2</sub>-, 2H); 3.35 (CH<sub>3</sub>(CH<sub>2</sub>)<sub>3</sub>CH<sub>2</sub>CH<sub>2</sub>-, 2H); 4.00 (-COCH<sub>2</sub>-, 2H) (Figure 4.5 (B)).

**Cyclic PNOGs** <sup>1</sup>H NMR ( $\delta$  in CDCl<sub>3</sub>, ppm): 0.86 (CH<sub>3</sub>(CH<sub>2</sub>)<sub>5</sub>CH<sub>2</sub>CH<sub>2</sub>-, 3H); 1.27 (CH<sub>3</sub>(CH<sub>2</sub>)<sub>5</sub>CH<sub>2</sub>CH<sub>2</sub>-, 10H); 1.50 (CH<sub>3</sub>(CH<sub>2</sub>)<sub>5</sub>CH<sub>2</sub>CH<sub>2</sub>-, 2H); 3.35 (CH<sub>3</sub>(CH<sub>2</sub>)<sub>5</sub>CH<sub>2</sub>CH<sub>2</sub>-, 2H); 4.00 (-COCH<sub>2</sub>-, 2H) (Figure 4.5 (C)).

**Cyclic PNDDGs** <sup>1</sup>H NMR ( $\delta$  in CDCl<sub>3</sub>, ppm): 0.87 (CH<sub>3</sub>(CH<sub>2</sub>)<sub>9</sub>CH<sub>2</sub>CH<sub>2</sub>-, 3H); 1.24 (CH<sub>3</sub>(CH<sub>2</sub>)<sub>9</sub>CH<sub>2</sub>CH<sub>2</sub>-, 18H); 1.51 (CH<sub>3</sub>(CH<sub>2</sub>)<sub>9</sub>CH<sub>2</sub>CH<sub>2</sub>-, 2H); 3.35 (CH<sub>3</sub>(CH<sub>2</sub>)<sub>9</sub>CH<sub>2</sub>CH<sub>2</sub>-, 2H); 4.00 (-COCH<sub>2</sub>-, 2H) (Figure 4.6 (A)).

**Cyclic PNTGs** <sup>1</sup>H NMR ( $\delta$  in CDCl<sub>3</sub>, ppm): 0.86 (CH<sub>3</sub>(CH<sub>2</sub>)<sub>11</sub>CH<sub>2</sub>CH<sub>2</sub>-, 3H); 1.26 (m, CH<sub>3</sub>(CH<sub>2</sub>)<sub>11</sub>CH<sub>2</sub>CH<sub>2</sub>-, 18H); 1.58 (CH<sub>3</sub>(CH<sub>2</sub>)<sub>11</sub>CH<sub>2</sub>CH<sub>2</sub>-, 2H); 3.27 (CH<sub>3</sub>(CH<sub>2</sub>)<sub>11</sub>CH<sub>2</sub>CH<sub>2</sub>-, 2H); 4.30 (-COCH<sub>2</sub>-, 2H) (Figure 4.6 (B)).

The following example is a representative procedure to synthesize linear poly(*N*-2-ethyl-1-hexyl-glycine)s (*c*-PEHGs). In the glovebox, *N*-2-ethyl-1-hexyl NCA (M, 60 mg, 0.28 mmol, [M]<sub>0</sub>=0.4 M) was dissolved in anhydrous THF (670  $\mu$ L). A known volume of NHC/THF stock solution (30  $\mu$ L, 2.8  $\mu$ mol, 91.6 mM, [M]:[NHC]<sub>0</sub> = 100:1) was added to the monomer solution. The rest of the synthetic procedures are identical with those for cyclic analogs. Final product was obtained as white solid after filtration and drying under vacuum (30 mg, 63 % yield).

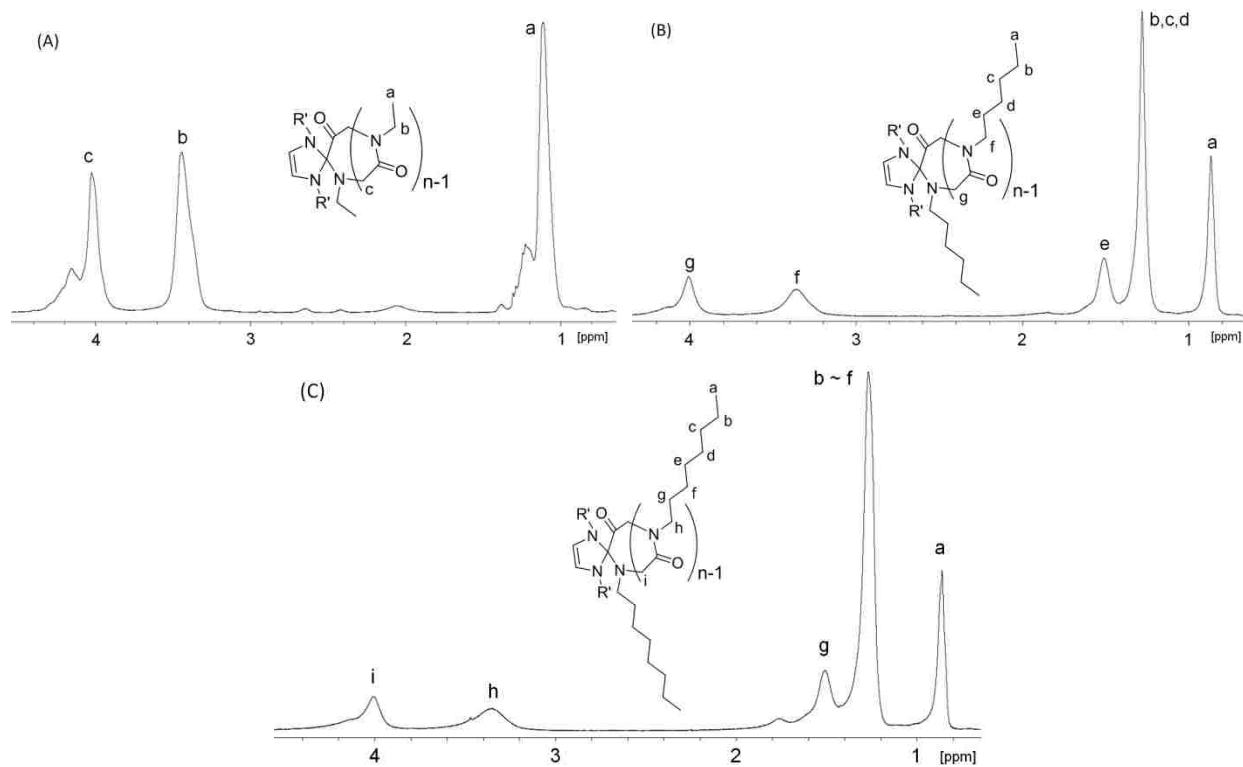


**Figure 4.5.**  $^1\text{H}$  NMR spectra of (A) *c*-PNEG, (B) *c*-PNHG, and (C) *c*-PNOG in  $\text{CDCl}_3$ .

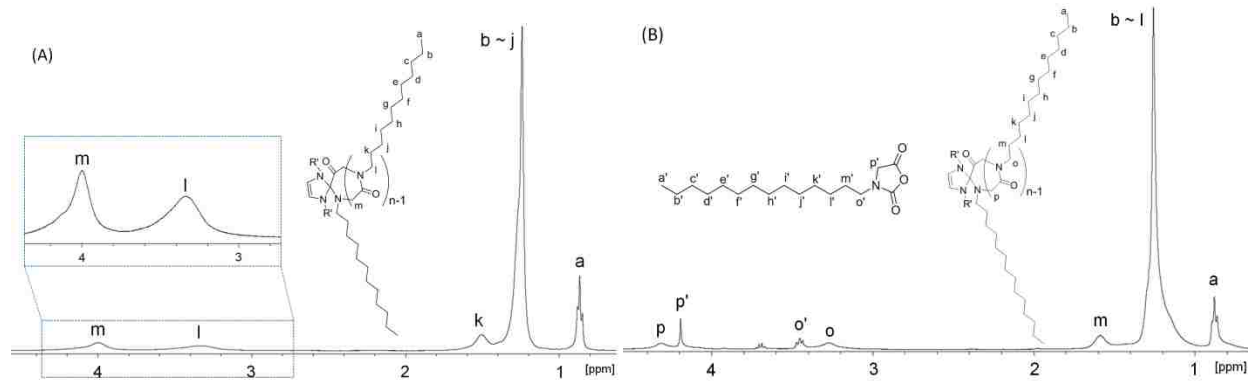


**Figure 4.6.**  $^1\text{H}$  NMR spectra of (A) *c*-PNDDG and (B) *c*-PNTG in  $\text{CDCl}_3$ .

### 4.2.3 Instrumentations and sample preparation for characterization

#### Differential scanning calorimetry (DSC)

DSC studies of cyclic or linear polypeptoids with various *n*-alkyl side chains were conducted using a TA DSC 2920 calorimeter under nitrogen. Powder samples sealed into the aluminum pans were first heated from room temperature up to  $250\text{ }^\circ\text{C}$  at  $10\text{ }^\circ\text{C min}^{-1}$ , cooled to -

50 °C at 5 °C min<sup>-1</sup>, and second heated to 250 °C at 10 °C min<sup>-1</sup>. For cyclic or linear PNBGs, we used a cooling system with liquid nitrogen to cool the sample to -150 °C at 5 °C min<sup>-1</sup>. Heat flow as watts (W) was recorded during heating and cooling cycles, and normalized by the mass (g) of samples.

### **Wide angle X-ray scattering (WAXS)**

Powder polymers as prepared were sealed in a glass ampule under vacuum (< 50 mmHg), and annealed in an oil bath above the second melting temperature (or isotropic melting temperature,  $T_{m,2}$ ) measured by DSC for 20 h. For example, *c*-PNOGs were annealed at 210 °C ( $T_{m,2} = 187$  °C). Above  $T_{m,2}$ , all powder samples were melted to isotropic liquid. To study structures of the polymers at different temperatures, powder samples were also annealed between  $T_{m,1}$ , and  $T_{m,2}$ , then cooled slowly to room temperature in an oil bath. Information of instruments was detailed in section 2.1.1.2.

### **Thermogravimetric analysis (TGA)**

TGA of cyclic or linear polypeptoids was conducted using a TA TGA 2950 under nitrogen at the heating rate of 10 °C min<sup>-1</sup>. The decomposition temperature of the polymers was determined from the onset points of weight loss.

## **4.3 Results and discussion**

### **4.3.1 DSC of cyclic or linear polypeptoids with various *n*-alkyl side chains**

This section presents melting and crystallization behavior of cyclic or linear polypeptoids with various *n*-alkyl side chains, ethyl, butyl, hexyl, octyl, decyl, dodecyl, and tetradecyl groups studied by DSC. All thermal analysis data from DSC including melting temperature ( $T_m$ ), crystallization temperature ( $T_c$ ), enthalpy change during melting ( $\Delta H_m$ ) and crystallization ( $\Delta H_c$ ), decomposition temperature ( $T_d$ ), and glass transition temperature ( $T_g$ ) are summarized in Table

4.2. Figure 4.7 shows DSC endotherms of cyclic [(A) through (G)] and linear [(H) through (N)] polypeptoids with various side chains during second heating, respectively. Figure 4.8 shows DSC exotherms of cyclic [(A) through (G)] and linear [(H) through (N)] polypeptoids during cooling, respectively. As can be seen in Figure 4.7 (A) and (H), *c*-PNEGs and *l*-PNEGs, polypeptoids with ethyl pendent groups do not have any endothermic transitions during heating. Instead, *c*-PNEGs and *l*-PNEGs show a glass transition at 108 °C and 96 °C. Figure 4.8 (A) and (H) further show that *c*-PNEGs and *l*-PNEGs do not have any exothermic transitions during cooling. These results suggest that cyclic or linear polypeptoids with ethyl side chains are amorphous.

However, two, distinct endothermic transitions as well as two corresponding exothermic transitions were observed from cyclic and linear polypeptoids with *n*-alkyl side chains of *n*-butyl (4 carbons) through *n*-tetradecyl (14 carbons) side groups. Figure 4.7 (B) shows endotherms of *c*-PNBGs during second heating. As can be seen, *c*-PNBGs have  $T_{m,1}$  at -65 °C and  $T_{m,2}$  at 230 °C. Additionally, Figure 4.7 (I) shows that *l*-PNHGs have  $T_{m,1}$  at -65 °C and  $T_{m,2}$  at 227 °C. Figure 4.8 (B) further shows exotherms of *c*-PNBGs, which have  $T_{c,1}$  at -110 °C and  $T_{c,2}$  at 199 °C. *l*-PNHGs have  $T_{c,1}$  at -116 °C and  $T_{c,2}$  at 196 °C, as shown in Figure 4.8 (I). Low-temperature transitions ( $T_{m,1}$  and  $T_{c,1}$ ) are attributed to melting and crystallization of side chains, and high-temperature transitions ( $T_{m,2}$  and  $T_{c,2}$ ) main chains. Both melting and crystallization transitions from side chains at -65 °C and -110 °C, respectively were rarely reported from polymers with short side groups as *n*-butyl one. Watanabe et al.<sup>124</sup> reported a melting transition of side chain crystallites with 10 carbons of poly( $\gamma$ -alkyl <sub>L</sub>-glutamates) at -24 °C. Rosales et al.<sup>48</sup> reported a melting transition of oligo-peptoids (15-mers) with butyl side chains at around 175 °C, but a melting temperature at lower temperature than 175 °C was not reported in their study. Our DSC

**Table 4.2.** DSC results of cyclic or linear polypeptoids with various alkyl side chains: melting temperature ( $T_m$ ), crystallization temperature ( $T_c$ ), enthalpy change during melting ( $\Delta H_m$ ), enthalpy change during crystallization ( $\Delta H_c$ ), decomposition temperature ( $T_d$ ), and glass transition temperature ( $T_g$ ).

	$T_{m,1}$ (°C)	$T_{m,2}$ (°C)	$\Delta H_{m,1}$ (J/g)	$\Delta H_{m,2}$ (J/g)	$T_{c,1}$ (°C)	$T_{c,2}$ (°C)	$\Delta H_{c,1}$ (J/g)	$\Delta H_{c,2}$ (J/g)	$T_d$ (°C)	$T_g$ (°C)
<b><i>c</i>-PNEG</b>	-	-	-	-	-	-	-	-	<b>339</b> (2)	<b>108</b>
<i>l</i> -PNEG	-	-	-	-	-	-	-	-	332 (2)	96
<b><i>c</i>-PNBG</b>	<b>-65</b> (2)	<b>230</b> (1)	<b>4</b> (1)	<b>63</b> (4)	<b>-110</b> (3)	<b>199</b> (1)	<b>12</b> (1)	<b>62</b> (3)	<b>338</b> (4)	-
<i>l</i> -PNBG	-65 (1)	225 (3)	5 (1)	48 (1)	-116 (3)	195 (2)	11 (2)	55 (3)	331 (1)	-
<b><i>c</i>-PNHG</b>	<b>29</b> (2)	<b>204</b> (1)	<b>15</b> (2)	<b>63</b> (2)	<b>-18</b> (1)	<b>174</b> (1)	<b>20</b> (2)	<b>56</b> (2)	<b>347</b> (3)	-
<i>l</i> -PNHG	29 (3)	194 (4)	17 (1)	57 (2)	-15 (2)	168 (5)	20 (1)	54 (2)	346 (2)	-
<b><i>c</i>-PNOG</b>	<b>53</b> (5)	<b>187</b> (1)	<b>21</b> (3)	<b>53</b> (1)	<b>23</b> (3)	<b>152</b> (1)	<b>22</b> (2)	<b>51</b> (1)	<b>349</b> (2)	-
<i>l</i> -PNOG	52 (4)	180 (2)	26 (3)	50 (3)	26 (2)	143 (1)	28 (2)	48 (2)	340 (4)	-
<b><i>c</i>-PNEHG</b>	-	<b>186</b> (2)	-	<b>7</b> (1)	-	<b>173</b> (1)	-	<b>5</b> (1)	<b>355</b> (2)	-
<i>l</i> -PNEHG	-	181 (2)	-	7 (1)	-	172 (1)	-	7 (1)	349 (3)	-
<b><i>c</i>-PNDG</b>	<b>77</b> (2)	<b>174</b> (1)	<b>36</b> (1)	<b>53</b> (1)	<b>48</b> (2)	<b>143</b> (1)	<b>40</b> (1)	<b>51</b> (1)	<b>356</b> (3)	-
<i>l</i> -PNDG	74 (2)	169 (2)	37 (1)	42 (2)	<b>50</b> (1)	<b>135</b> (1)	<b>36</b> (2)	<b>41</b> (1)	336 (3)	-
<b><i>c</i>-PNDDG</b>	<b>90</b> (1)	<b>166</b> (1)	<b>37</b> (3)	<b>46</b> (1)	<b>61</b> (2)	<b>138</b> (1)	<b>39</b> (1)	<b>43</b> (1)	<b>349</b> (3)	-
<i>l</i> -PNDDG	84 (1)	157 (1)	41 (2)	37 (2)	63 (3)	123 (2)	39 (4)	37 (1)	343 (3)	-
<b><i>c</i>-PNTG</b>	<b>100</b> (1)	<b>140</b> (1)	<b>49</b> (4)	<b>18</b> (1)	<b>89</b> (1)	<b>105</b> (2)	<b>43</b> (2)	<b>13</b> (1)	<b>304</b> (6)	-
<i>l</i> -PNTG	100 (1)	139 (1)	53 (6)	25 (2)	87 (1)	110 (1)	46 (3)	20 (1)	304 (6)	-

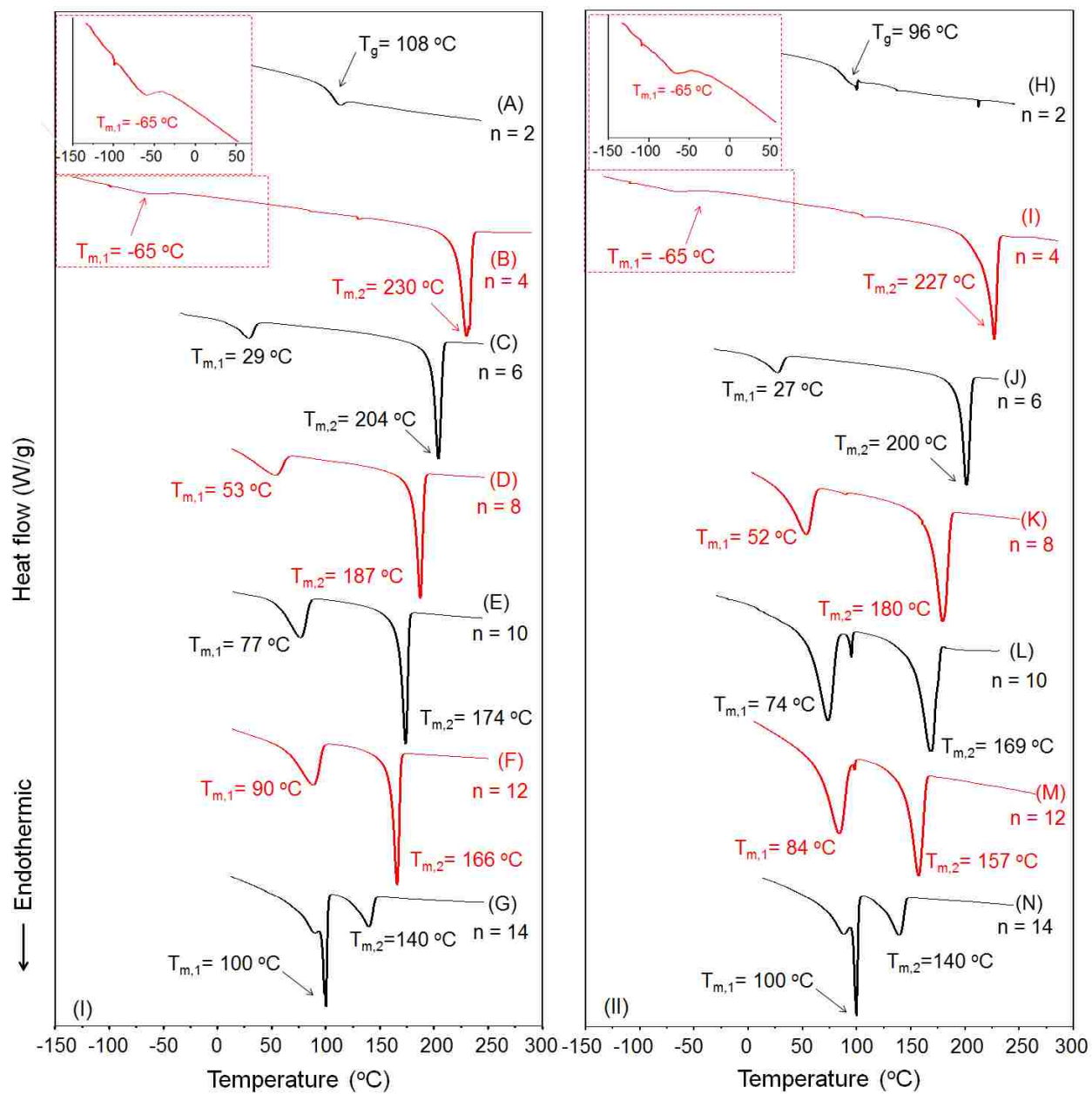


**Figure 4.7.** DSC thermograms of (I) cyclic or (II) linear poly(*N*-*n*-alkyl-glycine)s during second heating (*n* in the Figure is the number of carbons on *n*-alkyl side chains).

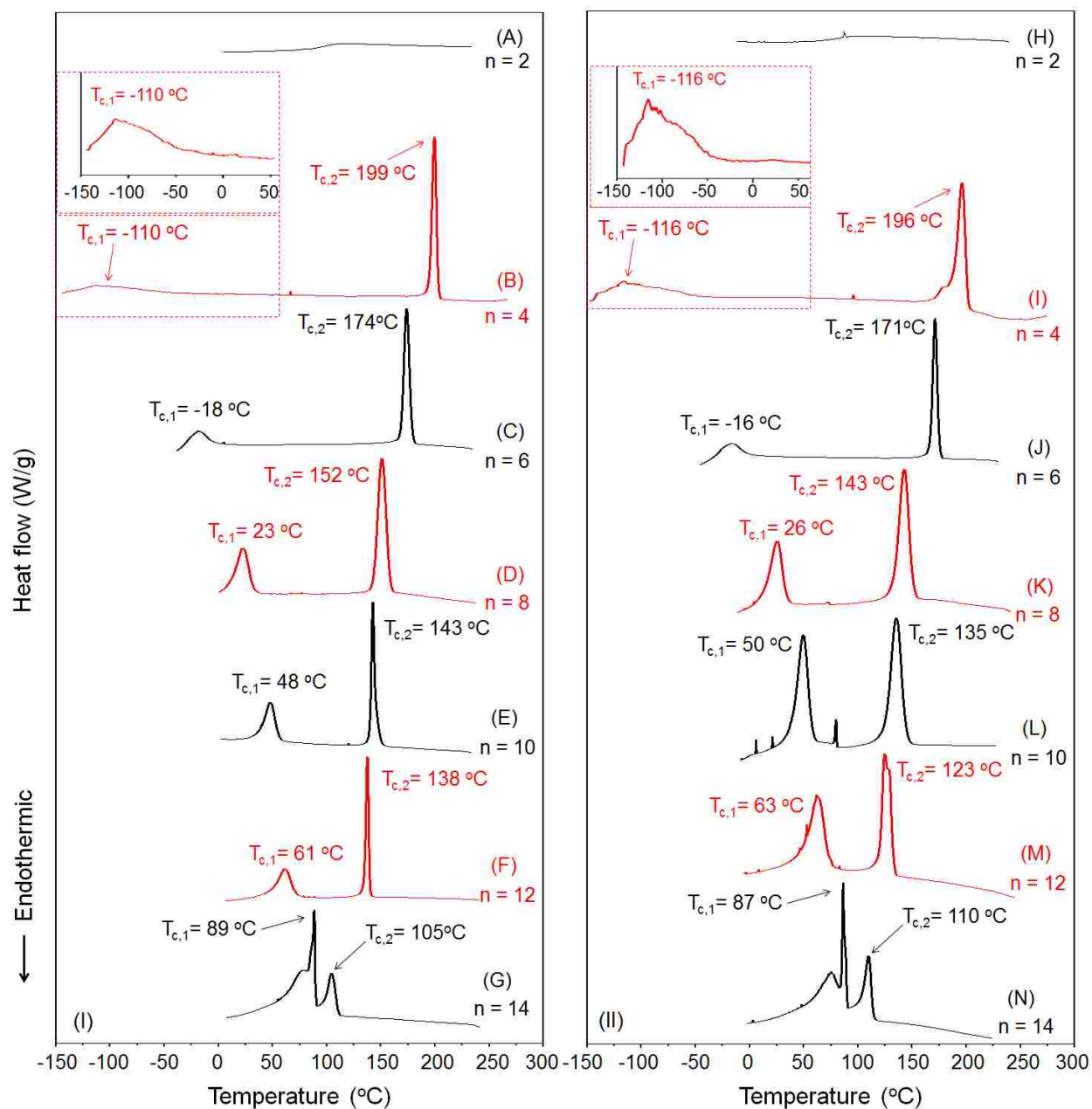


**Figure 4.8.** DSC thermograms of (I) cyclic or (II) linear poly(*N-n*-alkyl-glycine)s during first cooling (*n* in the Figure is the number of carbons on *n*-alkyl side chains).



results suggest that even butyl side chains on polypeptoid backbones can be crystallized and these crystallites can be melted. The low-temperature melting temperature ( $T_{m,1}$ ) at  $-65\text{ }^{\circ}\text{C}$  was observed when the PNBG samples in the pans were cooled down to  $-150\text{ }^{\circ}\text{C}$ , which is below the lower-temperature crystallization temperature.

Figure 4.7 (C) shows endotherms of *c*-PNHGs, which have  $T_{m,1}$  at  $29\text{ }^{\circ}\text{C}$  and  $T_{m,2}$  at  $204\text{ }^{\circ}\text{C}$ . Figure 4.7 (J) shows that *l*-PNHGs have  $T_{m,1}$  at  $27\text{ }^{\circ}\text{C}$  and  $T_{m,2}$  at  $200\text{ }^{\circ}\text{C}$ . As the number of carbons in the alkyl side chain of cyclic or linear polypeptoids increases from 4 to 6,  $T_{m,1}$  increased by  $94\text{ }^{\circ}\text{C}$  from  $-65$  to  $29\text{ }^{\circ}\text{C}$ , and  $T_{m,2}$  decreased by  $26\text{ }^{\circ}\text{C}$  from  $230$  to  $204\text{ }^{\circ}\text{C}$ . Additionally, Figure 4.8 (C) shows exotherms of *c*-PNHGs, which have  $T_{c,1}$  at  $-18\text{ }^{\circ}\text{C}$  and  $T_{c,2}$  at  $174\text{ }^{\circ}\text{C}$ . Figure 4.8 (J) shows that *l*-PNHGs have  $T_{c,1}$  at  $-16\text{ }^{\circ}\text{C}$  and  $T_{c,2}$  at  $171\text{ }^{\circ}\text{C}$ .  $T_{c,1}$  increased by  $92\text{ }^{\circ}\text{C}$  and  $T_{c,2}$  decreased by  $25\text{ }^{\circ}\text{C}$  from *c*-PNBGs to *c*-PNHGs. Both the low-temperature melting transition around  $30\text{ }^{\circ}\text{C}$  and crystallization transition at around  $-15\text{ }^{\circ}\text{C}$  have been rarely reported from relatively short, hexyl side chains bonded to polymer backbones. The low-temperature melting temperature ( $T_{m,1}$ ) at  $27\text{ }^{\circ}\text{C}$  or  $29\text{ }^{\circ}\text{C}$  was observed when the PNBG samples in the pans were cooled down to  $-50\text{ }^{\circ}\text{C}$ , which is below the lower-temperature crystallization temperature.

Figure 4.7 (D) shows endotherms of *c*-PNOGs, which have  $T_{m,1}$  at  $53\text{ }^{\circ}\text{C}$  to  $T_{m,2}$  at  $187\text{ }^{\circ}\text{C}$ . Figure 4.7 (K) shows that *l*-PNOGs have  $T_{m,1}$  at  $52\text{ }^{\circ}\text{C}$  and  $T_{m,2}$  at  $180\text{ }^{\circ}\text{C}$ . When the hexyl side chains of *c*-PNOGs were replaced by octyl side chains,  $T_{m,1}$  increased by  $24\text{ }^{\circ}\text{C}$  from  $29\text{ }^{\circ}\text{C}$  to  $53\text{ }^{\circ}\text{C}$ , and  $T_{m,2}$  increased by  $17\text{ }^{\circ}\text{C}$ . Additionally, Figure 4.8 (D) shows exotherms of *c*-PNOGs, which have  $T_{c,1}$  at  $23\text{ }^{\circ}\text{C}$  and  $T_{c,2}$  at  $152\text{ }^{\circ}\text{C}$ . Figure 4.8 (K) shows that *l*-PNOGs have  $T_{c,1}$  at  $26\text{ }^{\circ}\text{C}$  and  $T_{c,2}$  at  $143\text{ }^{\circ}\text{C}$ .  $T_{c,1}$  increased by  $41\text{ }^{\circ}\text{C}$ , and  $T_{c,2}$  decreased by  $22\text{ }^{\circ}\text{C}$  from *c*-PNHGs to *c*-PNOGs. These results suggest that crystalline packing of the octyl side chains are enhanced

relative to that of the hexyl groups, and the crystalline packing of the polypeptoid main chains with octyl side groups are diminished relative to the crystalline packing of those with hexyl groups. This change of melting and crystallization transitions reveals that the crystallization of the polypeptoid side chain and main chains are coupled; the length of side chain affects crystallization and melting of the main polypeptoid chains.

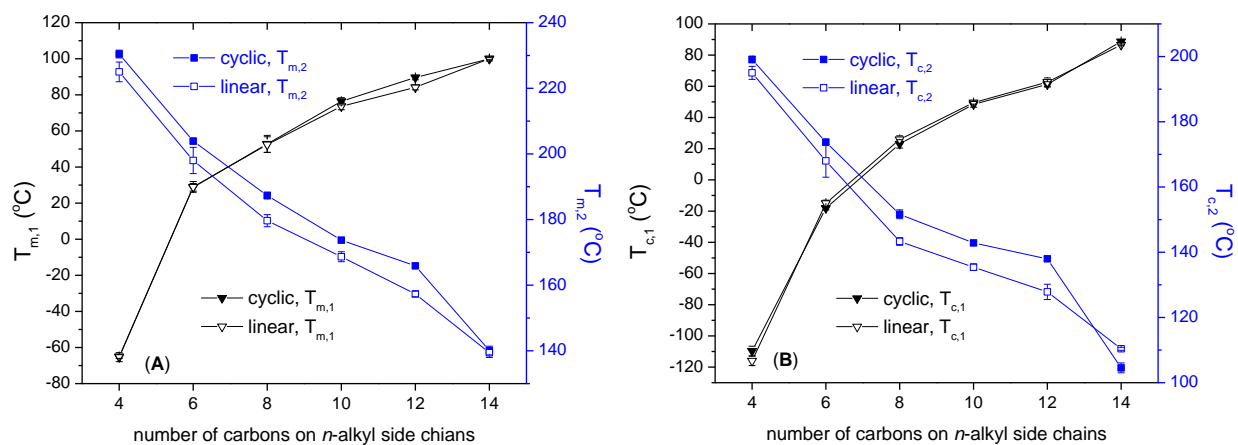
Figure 4.7 (E), (F) and (G) show endotherms of cyclic PNDGs, PNDDGs, and PNTGs, respectively. As can be seen,  $T_{m,1}$  increased from 77 °C, 90 °C, to 100 °C from cyclic polypeptoids with decyl, dodecyl, and tetradecyl side chains.  $T_{m,2}$  decreased from 174 °C, 166 °C, to 140 °C from those polymers, respectively. Figure 4.8 (E), (F) and (G) show exotherms of cyclic PNDGs, PNDDGs, and PNTGs.  $T_{c,1}$  increased from 48 °C, 61 °C to 89 °C, and  $T_{c,1}$  decreased from 143 °C, 138 °C to 105 °C from cyclic polypeptoids with decyl, dodecyl, and tetradecyl side chains. Additionally, Figure 4.7 (L), (M), and (N) show that  $T_{m,1}$  increased from 74 °C, 84 °C, to 100 °C, and  $T_{m,2}$  decreased from 169 °C, 157 °C, to 139 °C from *l*-PNDGs, *l*-PNDDGs, to *l*-PNTGs. Figure 4.8 (L), (M), and (N) shows that  $T_{c,1}$  increased from 50 °C, 63 °C to 87 °C, and  $T_{c,2}$  decreased from 135 °C, 123 °C to 110 °C from the linear polypeptoids. These results suggest that the crystalline packing of alkyl side chains are enhanced, resulting in higher melting points, as the length of the alkyl side groups increases from decyl to tetradecyl groups. On the other hand, longer side chains of polypeptoids may inhibit efficient packing of polypeptoid main chains, resulting in lower melting points.

Additionally, Figure 4.7 (G) and (N) show that the first endothermic peak of *c*-PNTGs and *l*-PNTGs at 100 °C became very sharp, compared to first endothermic peaks from other polypeptoids with shorter side chains than tetradecyl. The enthalpy change ( $\Delta H_m$ ) for this transition increased from 37 J·g<sup>-1</sup> to 49 J·g<sup>-1</sup> from *c*-PNDDGs to *c*-PNTGs. On the other hand,

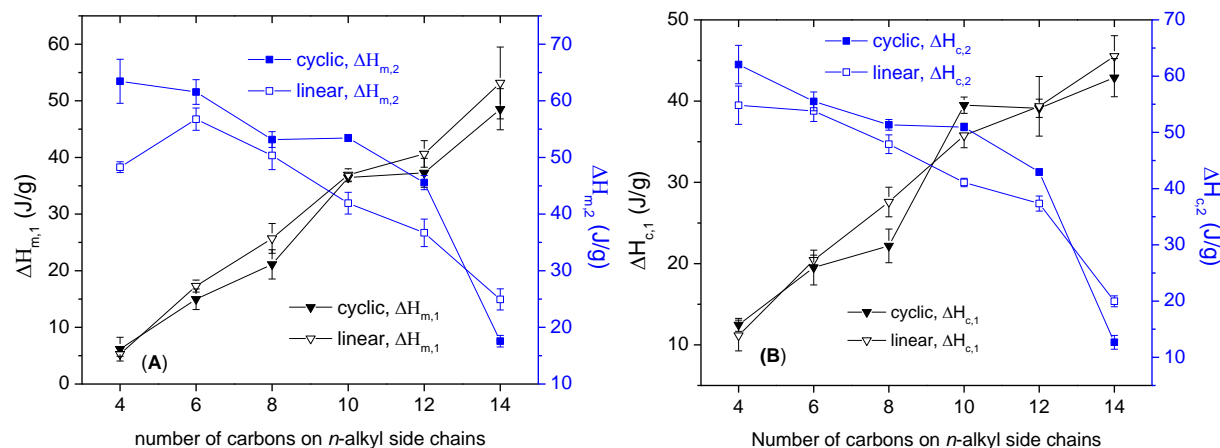
the second endothermic peak of *c*-PNTGs and *l*-PNTGs at 140 °C became smaller in intensity, in contrast to the sharp second endothermic peaks of other polypeptoids with shorter side chains than tetradecyl ones. The enthalpy change ( $\Delta H_m$ ) for this transition decreased from 46 J·g<sup>-1</sup> to 18 J·g<sup>-1</sup> from *c*-PNDDGs to *c*-PNTGs. These results reveal that crystallization of side chains is most enhanced for tetradecyl side chains, and crystallization of main chains is most inhibited. These results further suggest that one may control melting and crystallization temperatures of side chains as well as of main polypeptoid chains by altering the length of alkyl side chains.

Figure 4.9 (A) and (B) summarize the melting and crystallization temperatures as a function of the number of carbons on the alkyl side chains. As can be seen in Figure 4.9 (A),  $T_{m,2}$  decreases from 230 °C of *c*-PNBGs to 140 °C of *c*-PNTGs.  $T_{m,1}$  increases from -67 °C of *c*-PNBGs to 100 °C of *c*-PNTGs. Additionally, Figure 4.9 (B) shows that  $T_{c,2}$  decreases from 199 °C of PNBGs to 105 °C of PNTGs and  $T_{c,1}$  increases from -110 °C of PNBGs to 85 °C of PNTGs. The enthalpy changes during melting and crystallization show similar trends with the transition temperatures. Figure 4.10 (A) and (B) show the enthalpy change during the melting and crystallization as a function of the number of carbons on alkyl side chains, respectively. As can be seen in Figure 4.10 (A), enthalpy change during second heating ( $\Delta H_{m,2}$ ) decreases from 63 J·g<sup>-1</sup> of *c*-PNBGs to 18 J·g<sup>-1</sup> of *c*-PNTGs. Enthalpy change during first heating ( $\Delta H_{m,1}$ ) increases from 4 J·g<sup>-1</sup> of *c*-PNBGs to 49 J·g<sup>-1</sup> of *c*-PNTGs. Additionally, Figure 10 (B) shows that enthalpy change during second crystallization ( $\Delta H_{c,2}$ ) decreases from 62 J·g<sup>-1</sup> of *c*-PNBGs to 13 J·g<sup>-1</sup> of *c*-PNTGs, and enthalpy change during first crystallization ( $\Delta H_{c,1}$ ) increases from 12 J·g<sup>-1</sup> of *c*-PNBGs to 43 J·g<sup>-1</sup> of *c*-PNTGs. These trends of the melting and crystallization behavior strongly suggest that the first melting ( $T_{m,1}$ ) and crystallization ( $T_{c,1}$ ) transitions are attributed to the side chain melting and packing, and the second transitions ( $T_{m,2}$  and  $T_{c,2}$ ) to the main chain melting

and packing. The gradual decrease of  $T_{m,2}$ ,  $\Delta H_{m,2}$ ,  $T_{c,2}$ , and  $\Delta H_{c,2}$  with longer  $n$ -alkyl side chains suggests that the main chain packing is interrupted as the side chain becomes longer. At the same time, the longer side chains are more efficiently packed, which supports their gradual increase of  $T_{m,1}$ ,  $\Delta H_{m,1}$ ,  $T_{c,1}$ , and  $\Delta H_{c,1}$ . As a result, it is evident that the crystallization of main chains is coupled with that of side chains; the crystalline packing of alkyl side chains affects that of the polypeptoid main chains.



**Figure 4.9.** (A)  $T_{m,1}$  and  $T_{m,2}$ , and (B)  $T_{c,1}$  and  $T_{c,2}$  of cyclic or linear poly( $N$ - $n$ -alkyl-glycine)s with various  $n$ -alkyl side chains.



**Figure 4.10.** (A)  $\Delta H_{m,1}$  and  $\Delta H_{m,2}$ , and (B)  $\Delta H_{c,1}$  and  $\Delta H_{c,2}$  of cyclic or linear poly( $N$ - $n$ -alkyl-glycine)s with various  $n$ -alkyl side chains.

#### 4.3.1.1 Effect of architecture of polymers, i.e. cyclic or linear on melting and crystallization of polypeptoids

Linear poly(*N*-*n*-alkyl-glycine)s were synthesized using benzylamine as an initiator, and their thermal properties were compared with those of cyclic ones. The degree of polymerization of cyclic and linear ones was set to be identical at 100 with that of cyclic counterparts. In Figure 4.9 (A) and (B), melting and crystallization temperatures of cyclic polypeptoids were plotted along with those of linear ones as a function of the number of carbons on *n*-alkyl side chains. Figure 4.9 (A) shows that the  $T_{m,2}$ s of cyclic polymers is higher than those of linear ones by at least 5 °C regardless of the number of carbons on side chains, except for PNTGs. On the other hand,  $T_{m,1}$ s from cyclic polymers are close to those from the linear ones. Additionally, Figure 4.9 (B) shows that cyclic polymers have higher  $T_{c,2}$ s than those of their linear counterparts.  $T_{c,1}$ s of cyclic polymers are close to those from linear ones. The second melting temperatures are affected by the architecture of the main chains, i.e. cyclic or linear, whereas the first melting temperatures are not affected by the architecture of the main chains. These DSC results support that the second melting transitions result from the main chain packing, and the first melting transitions from the side chain packing. The higher melting temperatures of cyclic polymers may be attributed to more compact packing of the polymer chains without chain ends than linear counterparts.

In Figure 4.10 (A) and (B), the enthalpy changes during melting ( $\Delta H_m$ ) and crystallization ( $\Delta H_c$ ) of linear polypeptoids were plotted along with those of the cyclic analogs as a function of the number of carbon on *n*-alkyl side chains. As can be seen in Figure 4.10 (A) and Table 4.2, the enthalpy change during the second melting transition ( $\Delta H_{m,2}$ ) decreased from 63 J·g<sup>-1</sup> to 18 J·g<sup>-1</sup> for *c*-PNBG through *c*-PNTTG, and from 48 J·g<sup>-1</sup> to 25 J·g<sup>-1</sup> for *l*-PNBG through *l*-PNTG. Also, the enthalpy change during the first melting transition ( $\Delta H_{m,1}$ ) increased from 4

$\text{J}\cdot\text{g}^{-1}$  to  $49 \text{ J}\cdot\text{g}^{-1}$  for *c*-PNBG through *c*-PNTTG, and from  $5 \text{ J}\cdot\text{g}^{-1}$  to  $53 \text{ J}\cdot\text{g}^{-1}$  for *l*-PNBG through *l*-PNTG. Additionally, Figure 4.10 (B) and Table 4.2 show that the enthalpy change during the second crystallization transition ( $\Delta H_{c,2}$ ) decreased  $62 \text{ J}\cdot\text{g}^{-1}$  to  $13 \text{ J}\cdot\text{g}^{-1}$  for *c*-PNBG through *c*-PNTTG, and  $55 \text{ J}\cdot\text{g}^{-1}$  to  $20 \text{ J}\cdot\text{g}^{-1}$  for *l*-PNBG through *l*-PNTG. These results further support that the low-temperature transitions result from the crystallization of side chains, and the high-temperature transitions from that of main chains. Additionally, Figure 4.10 (A) shows that  $\Delta H_{m,2}$  of cyclic polypeptoids is higher than that of linear ones, except PNTGs. However,  $\Delta H_{m,1}$  of cyclic polypeptoids is lower than their linear counterparts. This reveals that the polypeptoid architectures, i.e. cyclic or linear, have a similar effect on enthalpy change during melting and crystallization. Also, Figure 4.10 (B) shows that  $\Delta H_{c,2}$  of cyclic polypeptoids is higher than linear one, except for PNTGs. No clear trends were observed between the cyclic and linear polypeptoids for the first crystallization transition ( $\Delta H_{c,1}$ ). This indicates that melting and crystallization behavior of side chains are not affected by the architecture of the main chains, i.e. cyclic and linear.

#### 4.3.2 WAXS of cyclic or linear polypeptoids with various *n*-alkyl side chains

Crystalline structures of cyclic or linear polypeptoids with various alkyl side chains were studied by WAXS, and their crystalline domain spacing was determined from peaks from WAXS data by Bragg's law. Figure 4.11 shows WAXS diffractograms of cyclic polypeptoids with various alkyl side chains, which were annealed above  $T_{m,2}$  (the melting point of the main chains). For comparison, WAXS data of one the linear polypeptoid samples, *l*-PNDGs, was collected, and compared with that of *c*-PNDGs. WAXS of *l*-PNDGs was exactly same with that of *c*-PNDGs. Figure 4.11 (A) shows WAXS data of *c*-PNEGs. There are no featured peaks observed from *c*-PNEGs, indicating that ethyl pendent groups are not well-organized on an angstrom

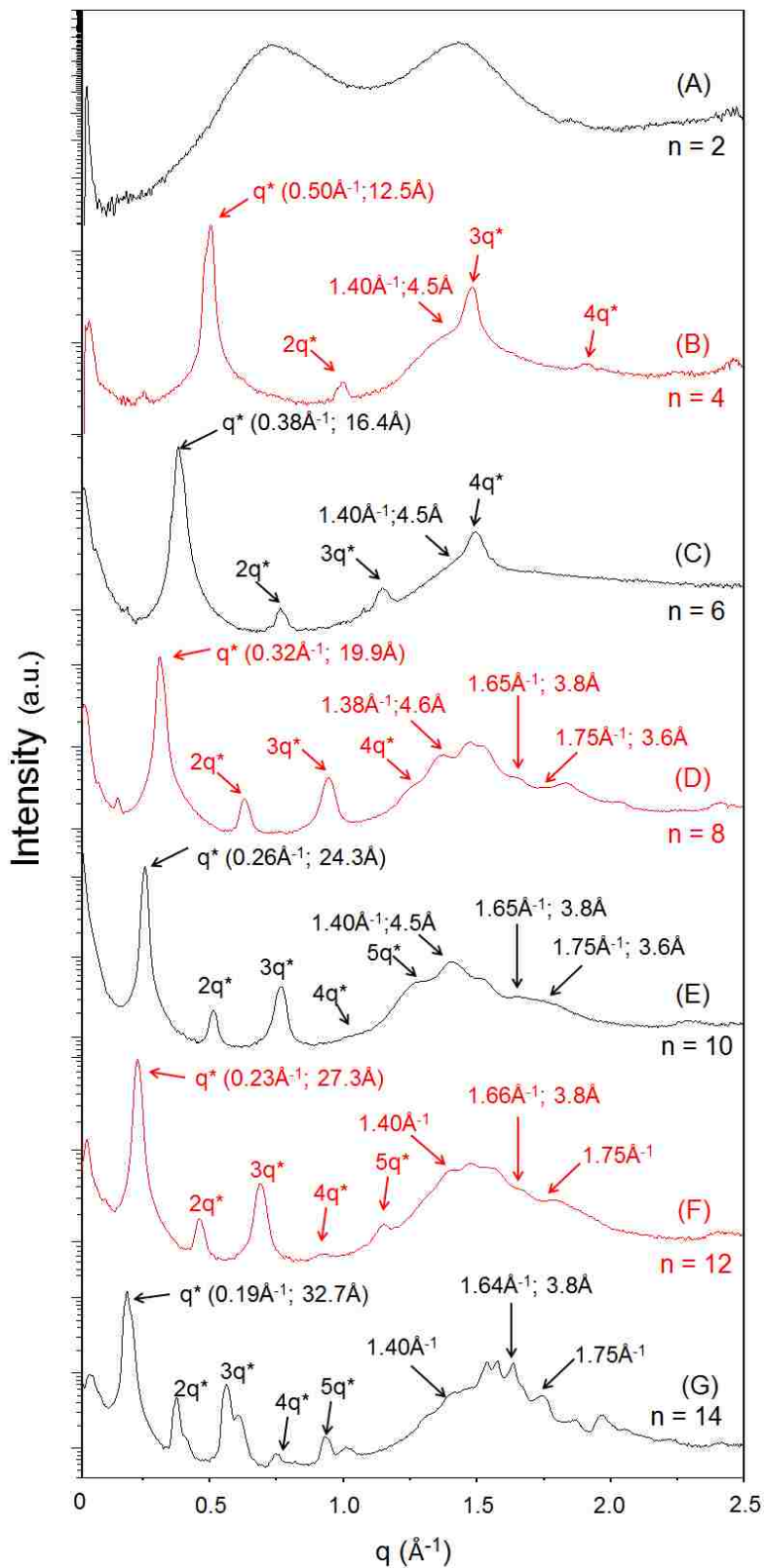


**Figure 4.11.** WAXS diffractograms of cyclic poly(*N*-*n*-alkyl-glycine)s (*n* is the number of carbons on the side chains).

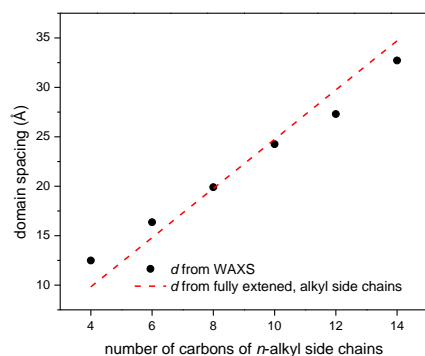
length scale and thus not crystalline. The WAXS data agrees with DSC data of PNEGs, showing no transitions for melting and crystallization. This suggests that ethyl side chains are not long enough to be crystallized. Furthermore, WAXS and DSC data suggest that short, ethyl side chains hinder the crystallization of the main, polypeptoid chains. Figure 4.11 (B) through (G) show WAXS data of cyclic polypeptoids with butyl or longer side chains. As can be seen, strong peaks of the primary peak ( $q^*$ ) and multiple order reflections of  $2q^*$ ,  $3q^*$ ,  $4q^*$ , and even  $5q^*$  were observed from cyclic polypeptoids with  $n$ -butyl side chains to  $n$ -tetradecyl. This indicates that polypeptoids with butyl or longer side chains are highly crystalline and well-organized. This WAXS data agrees well with DSC results from cyclic or linear polypeptoids that revealed polypeptoids with butyl or longer side groups have two melting transitions as well as two crystallization transitions. The domain spacing between side chains was determined from the position of the primary peak,  $q^*$ . The position of  $q^*$  shifts to lower values as the side chains become longer from butyl to tetradecyl one, indicating the domain spacing increases. Figure 4.11 (B) shows WAXS data of  $c$ -PNBGs. The strong, primary peak ( $q^*$ ) is observed at  $q$  of  $0.5 \text{ \AA}^{-1}$  (domain spacing  $d = 12.5 \text{ \AA}$ ), and the multiple reflections were observed at  $2q^*$ ,  $3q^*$ , and  $4q^*$ , which indicates that even butyl side chains bonded to polypeptoid backbones are well-organized. Another peak is observed at  $q$  of  $1.40 \text{ \AA}^{-1}$  ( $4.5 \text{ \AA}$ ), which is commonly observed in peptoids as the distance between adjacent peptoid chains.<sup>47,48</sup> Figure 4.11 (C) shows WAXS data of  $c$ -PNHGs. The primary peak  $q^*$  is observed at  $q$  of  $0.38 \text{ \AA}^{-1}$  ( $16.4 \text{ \AA}$ ), and the multiple order reflections were observed at  $2q^*$ ,  $3q^*$ , and  $4q^*$ , which indicates that hexyl side chains are well-organized. The peak indicating the interchain arrangement is also observed at  $q$  of  $1.40 \text{ \AA}^{-1}$  ( $4.5 \text{ \AA}$ ).



Figure 4.11 (D) shows WAXS data of *c*-PNOGs. The strong, primary peak ( $q^*$ ) is observed at  $0.32 \text{ \AA}^{-1}$  ( $19.9 \text{ \AA}$ ) and the multiple order reflections are also observed. In section 2.1.2.1, the crystalline packing of *c*-PNDGs was proposed based on orthorhombic unit cells,  $a$  ( $=4.5 \text{ \AA}$ ) as the interchain distance,  $b$  ( $=3.6 \text{ \AA}$ ) as the distance between adjacent repeating units, and  $c$  ( $=24 \text{ \AA}$ ) as the distance between two decyl side chains.<sup>141</sup> Peaks from orthorhombic unit cells were observed at  $q$  of  $1.40 \text{ \AA}^{-1}$  ( $4.5 \text{ \AA}$ ) and  $q$  of  $1.75 \text{ \AA}^{-1}$  ( $3.6 \text{ \AA}$ ) in *c*-PNOGs. This suggests that *c*-PNOGs have the identical crystalline structures proposed for *c*-PNDGs. Furthermore, another peak at  $q$  of  $1.65 \text{ \AA}^{-1}$  ( $3.8 \text{ \AA}$ ) is observed from PNOGs. This domain spacing was reported from triclinic unit cells in *n*-paraffin crystals or low molecular weight *n*-alkanes.<sup>122,124</sup> It was widely studied that octyl or longer *n*-alkyl side chains bonded to rigid-rod or semi-rigid polymer backbones were packed into *n*-paraffine-like crystals.<sup>124</sup> Thus, WAXS data of *c*-PNOGs suggests that possible crystalline structures of *c*-PNOGs include orthorhombic, triclinic unit cells, or other types of crystallites. Figure 4.11 (E) shows WAXS data of *c*-PNDGs, which was presented in section 2.1.2.1. In addition to peaks from orthorhombic unit cells, a peak at  $q$  of  $1.65 \text{ \AA}^{-1}$  ( $3.8 \text{ \AA}$ ) was observed, suggesting *n*-paraffin-like crystallites of triclinic unit cells. Figure 4.11 (F) shows WAXS data of *c*-PNDDGs. The strong, primary peak ( $q^*$ ) was observed at  $q$  of  $0.23 \text{ \AA}^{-1}$  ( $27.3 \text{ \AA}$ ), and the multiple reflections at  $2q^*$ ,  $3q^*$ ,  $4q^*$ , and  $5q^*$  were also observed. In addition to the peaks originating from orthorhombic unit cells at  $q$  of  $1.40 \text{ \AA}^{-1}$  ( $4.5 \text{ \AA}$ ) and  $1.75 \text{ \AA}^{-1}$  ( $3.6 \text{ \AA}$ ), a peak at  $q$  of  $1.65 \text{ \AA}^{-1}$  ( $3.8 \text{ \AA}$ ) was observed, suggesting that *n*-paraffin-like crystallites of triclinic unit cells exist. Finally, Figure 4.11 (G) shows WAXS data of *c*-PNTGs. The strong, primary peak ( $q^*$ ) was observed at  $q$  of  $0.19 \text{ \AA}^{-1}$  ( $32.7 \text{ \AA}$ ), and multiple order reflections at  $2q^*$ ,  $3q^*$ ,  $4q^*$ , and  $5q^*$  were also observed. In addition to the peaks originated from orthorhombic unit cells at  $q$  of  $1.41 \text{ \AA}^{-1}$  ( $4.5 \text{ \AA}$ ) and  $1.75 \text{ \AA}^{-1}$  ( $3.6 \text{ \AA}$ ), a peak at  $q$  of  $1.65 \text{ \AA}^{-1}$  ( $3.8$

Å) was observed, suggesting their *n*-paraffin-like crystallites of triclinic unit cells. Additionally, other peaks are observed besides those assigned, suggesting other crystalline structures formed from *c*-PNTGs.

In Figure 4.12, domain spacing from cyclic polypeptoids with various side chains was plotted as a function of number of carbons on the *n*-alkyl side chains, and compared with double length of fully-extended alkyl side chains. Domain spacing from cyclic polypeptoids with octyl or decyl side chains agrees well with the theoretical domain spacing. Domain spacing from butyl or hexyl groups is shorter than the theoretical one, and domain spacing from dodecyl or tetradecyl groups is longer. This can be attributed to the fact that the outer part of longer side chains is more flexible than that of shorter side chains.<sup>124</sup> Thus, dodecyl or tetradecyl side chains may be folded, resulting in shorter domain spacing than spacing length in full-extended conformation of side chains.



**Figure 4.12.** Domain spacing (*d*) calculated from the primary peak (*q*\*) of WAXS experiment as a function of the number of carbons on *n*-alkyl side chains. The straight line indicates double length of fully extended alkyl side chains.

### 4.3.3 Effect of branching of side groups on melting and crystallization of polypeptoids

This section presents the effect of branched side chains on the melting and crystallization behaviors of the main polypeptoid chains as well as on those of alkyl side chains. Figure 4.13 (A) shows DSC endotherms of *c*-PNEHG, which have branched 2-ethyl-1-hexyl side chains

composed of 8 carbons. It was compared with that of *c*-PNHGs with *n*-hexyl side groups and *c*-PNOGs with *n*-octyl side groups. As can be seen, *c*-PNEHGs have only one melting transition at 186 °C with  $\Delta H_m$  of 7 J·g<sup>-1</sup>. On the other hand, *c*-PNHGs have two melting transitions at 29 °C and 204 °C with  $\Delta H_m$  of 15 J·g<sup>-1</sup> and 63 J·g<sup>-1</sup>, respectively. *c*-PNOGs also have two melting transitions at 53 °C and 187 °C with  $\Delta H_m$  of 21 J·g<sup>-1</sup> and 53 J·g<sup>-1</sup>, respectively. These results suggest that branched, side chains of polypeptoids rarely crystallized and they significantly inhibit the crystallization of the main polypeptoid chains. Figure 4.13 (B) shows WAXS data of the three polypeptoids. A strong but broad primary peak at  $q$  of 0.54 Å<sup>-1</sup> (11.6 Å) was observed from *c*-PNEHGs, but the multiple reflections were not observed. Additionally, peaks at  $q$  of 1.40 Å<sup>-1</sup> (4.5 Å) and 1.75 Å<sup>-1</sup> (3.6 Å) from orthorhombic unit cells were not observed. This indicates that 2-ethyl-1-hexyl side chains of polypeptoids are not well ordered. This is in contrast to PNHGs and PNOGs where multiple higher order reflection peaks were observed, consistent with their highly ordered crystalline structures. Furthermore, the domain spacing ( $d = 11.6$  Å) of *c*-PNEHGs decreased, compared to that of *c*-PNHGs ( $d = 16.4$  Å) and cyclic PNOGs ( $d = 19.9$  Å), indicating that branched, side chains adopt much more flexible conformations, which allows for the reduced domain spacing of polypeptoid crystals formed from main chain crystallization.

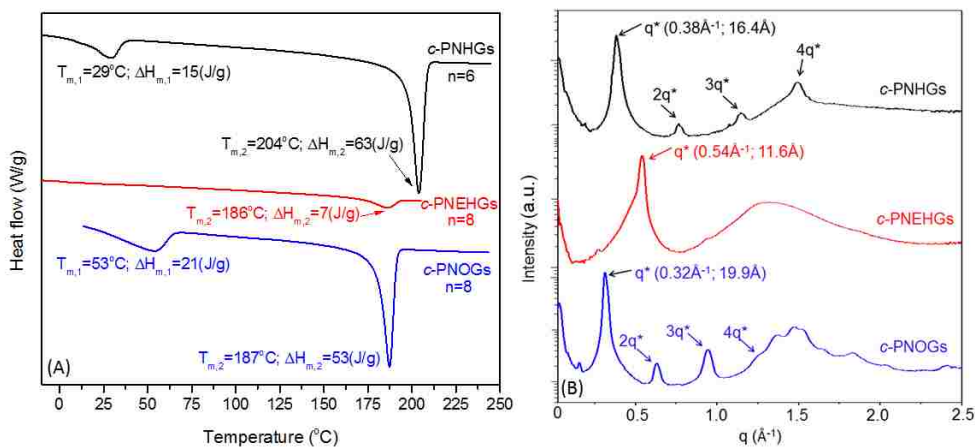


**Figure 4.13.** (A) DSC thermograms and (B) WAXS diffractograms of cyclic PNEHGs along with those of PNHGs and PNOGs, respectively.

#### 4.3.4 Effect of annealing temperature on molecular packing of polypeptoids

To probe any possible molecular packing of polypeptoids at different temperature ranges, polypeptoids were annealed between  $T_{m,1}$  and  $T_{m,2}$ , or above  $T_{m,2}$ , cooled to room temperature (c.a.  $5\text{ }^{\circ}\text{C}\cdot\text{min}^{-1}$ ), and studied by WAXS. This experiment was design such that the mobility of the main polypeptoid chains as well as side chains can be different at those two temperature ranges, and thus it may result in different crystalline packing. Figure 4.14 (A) shows WAXS of *c*-PNOGs annealed at  $150\text{ }^{\circ}\text{C}$  (between  $T_{m,1}$  and  $T_{m,2}$ ) and at  $210\text{ }^{\circ}\text{C}$  (above  $T_{m,2}$ ), respectively. When *c*-PNOGs were annealed above  $T_{m,2}$  ( $187\text{ }^{\circ}\text{C}$ ), the main polypeptoid chains as well as side chains were melted, and the solid sample became an isotropic liquid. Upon cooling to room temperature, both main and side chains may become well-organized, as multiple peaks were observed from WAXS studies. On the other hands, when *c*-PNOGs are annealed between  $T_{m,1}$  and  $T_{m,2}$ , the sharp primary peak at  $0.32\text{ \AA}^{-1}$  become broad and reduced in intensity. Peaks of multiple reflections become very weak. Additionally, the intensity of the peaks at  $1.38\text{ \AA}^{-1}$  and  $1.75\text{ \AA}^{-1}$  corresponding to the interchain distances and distances between adjacent repeating units decreased. *c*-PNTGs show similar results of WAXS at different temperature ranges. Figure 4.14 (B) shows WAXS of *c*-PNTGs annealed at  $120\text{ }^{\circ}\text{C}$  (between  $T_{m,1}$  and  $T_{m,2}$ ), and  $170\text{ }^{\circ}\text{C}$  (above  $T_{m,2}$ ), respectively. When *c*-PNTGs are annealed between  $T_{m,1}$  and  $T_{m,2}$ , the intensity of the primary peak and its multiple reflections decreased, compared to that from *c*-PNTGs annealed above  $T_{m,2}$ . Additionally, the peaks at  $1.40\text{ \AA}^{-1}$  and  $1.75\text{ \AA}^{-1}$  became very weak.

Based on those WAXS results, possible molecular packing of polypeptoids at different temperature ranges is proposed. Figure 4.15 shows schematic illustration for proposed molecular packing of polypeptoids (A) below  $T_{m,1}$ , (B) between  $T_{m,1}$  and  $T_{m,2}$ , and (C) above  $T_{m,2}$ . Below

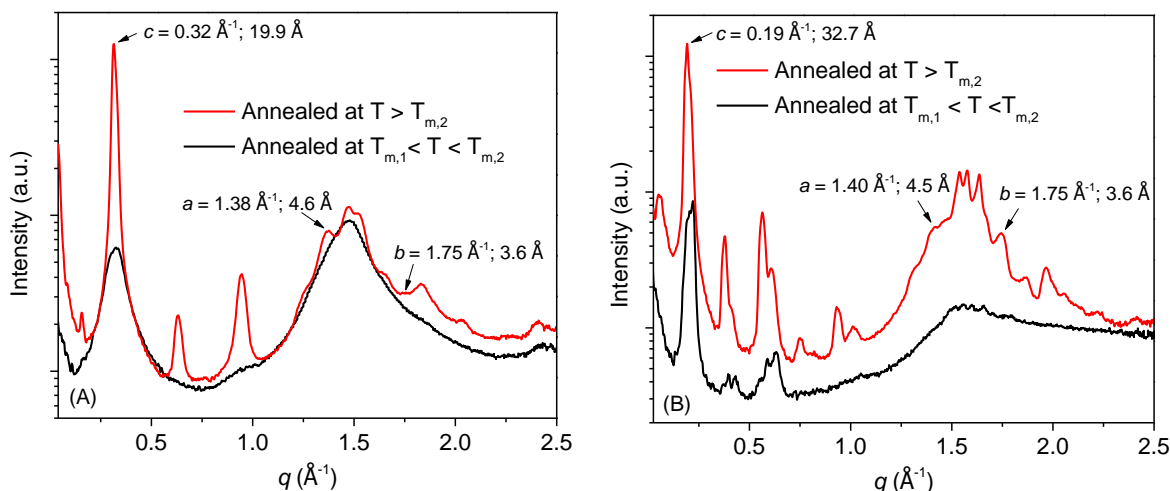


**Figure 4.14.** (A) WAXS diffractograms of *c*-PNOGs annealed at 150 °C ( $T_{m,1} < T < T_{m,2}$ ) or 210 °C ( $T > T_{m,2}$ ), and (B) of *c*-PNTGs annealed at 120 °C ( $T_{m,1} < T < T_{m,2}$ ) or 170 °C ( $T > T_{m,2}$ ).

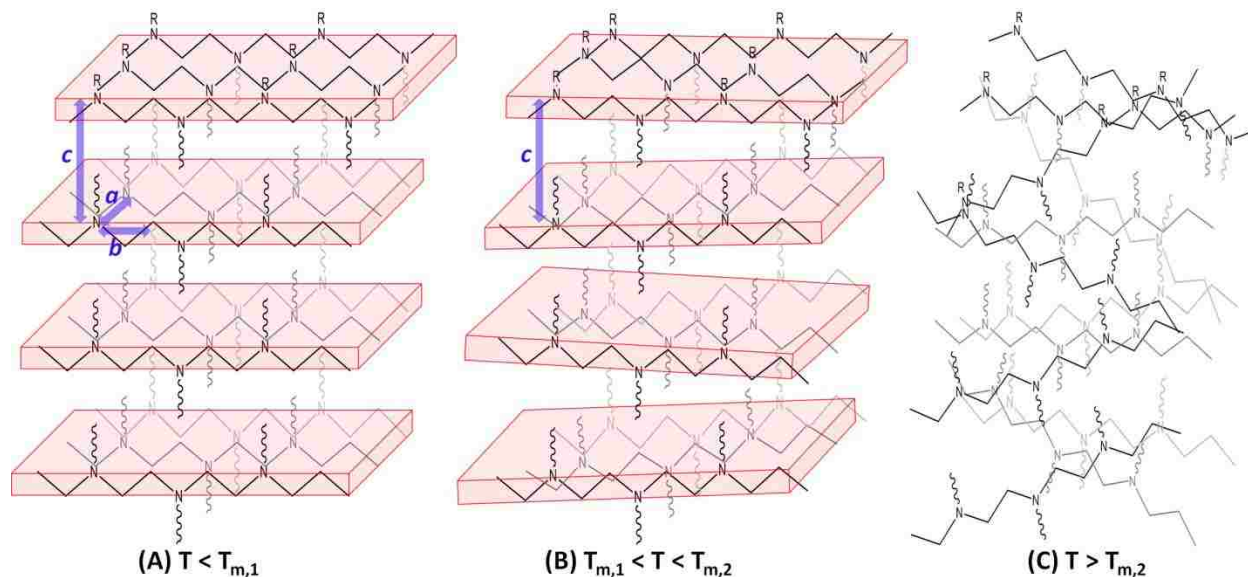


**Figure 4.15.** Schematic illustration of molecular packing of polypeptoid chains (A) below  $T_{m,1}$ , (B) between  $T_{m,1}$  and  $T_{m,2}$ , and (C) above  $T_{m,2}$ .

$T_{m,1}$ , polypeptoid chains are packed into layers, which are separated from each other by the distance ( $c$  in Figure 4.15) of two side chains.<sup>127</sup> Those layers are well-organized, as the primary peak and the multiple reflections are observed by WAXS. In the layer, each polymer chain is well-aligned by the distance of 4.5 Å ( $a$  in Figure 4.15). Additionally, the distance of 3.6 Å

between adjacent repeating units in the polymer chain ( $b$  in Figure 4.15) is also well-established below  $T_{m,1}$ , as illustrated in Figure 4.15 (A).

At temperature between  $T_{m,1}$  and  $T_{m,2}$ , the mobility of the alkyl, pendent groups of polypeptoids increases, and they become disordered or melted. As the side chains become more mobile and disordered, the arrangement of the crystalline packing of polymer chains in the layer become disordered, as evidenced by the disappearance of the diffraction peaks corresponding  $a$  and  $b$  spacing (Figure 4.15). However, WAXS data reveals that the mobility of side chains does not disorder the arrangement between those layers. Instead, those layers may become distorted, while keeping the interlayer distances, as illustrated in Figure 4.15 (B). This is evidenced by the broadening of the primary peak ( $c$ ) and the significant weakening of the higher order reflections. Additionally, the positions of the primary peak shift to higher  $q$  values from  $0.32 \text{ \AA}^{-1}$  ( $19.9 \text{ \AA}$ ) to  $0.33 \text{ \AA}^{-1}$  ( $19.3 \text{ \AA}$ ) for  $c$ -PNOGs and from  $0.19 \text{ \AA}^{-1}$  ( $32.7 \text{ \AA}$ ) to  $0.22 \text{ \AA}^{-1}$  ( $28.6 \text{ \AA}$ ) for PNTGs from temperature below  $T_{m,2}$  to that between  $T_{m,1}$  and  $T_{m,2}$ . This suggests that the distance between the layers decreased, as the side chains become disordered. Finally, at temperature above  $T_{m,2}$ , all crystallites are melted to isotropic liquid and all the ordered arrays of the polymer chains are disordered as well as packing of polymer chains in the layer, as illustrated in Figure 4.15 (C).

#### 4.3.5 Decomposition temperatures of cyclic or linear polypeptoids

Thermal stability of cyclic or linear polypeptoids with various alkyl side chains was studied by TGA. Decomposition temperatures of polypeptoids analyzed in this study are summarized in Table 4.2, and plotted as a function of the number of carbons on the alkyl side chains in Figure 4.16 (A). Figure 4.16 (B) shows representative TGA of  $c$ -PNDGs and  $l$ -PNDGs. As can be seen, cyclic or linear polypeptoids maintain their thermal stability up to  $300 \text{ }^\circ\text{C}$ , which is above the glass transition for PNEGs or the second melting (or isotropic transition) for other

polypeptoid samples. The fairly broad temperature window between the melting and decomposition enables one to thermally process the polypeptoids with alkyl side chains from ethyl to tetradecyl groups.<sup>48</sup> Additionally, cyclic polypeptoids have higher decomposition temperatures than linear counterparts except PNHGs and PNTTGs, suggesting thermal stability of polypeptoids is affected by polymer architecture.

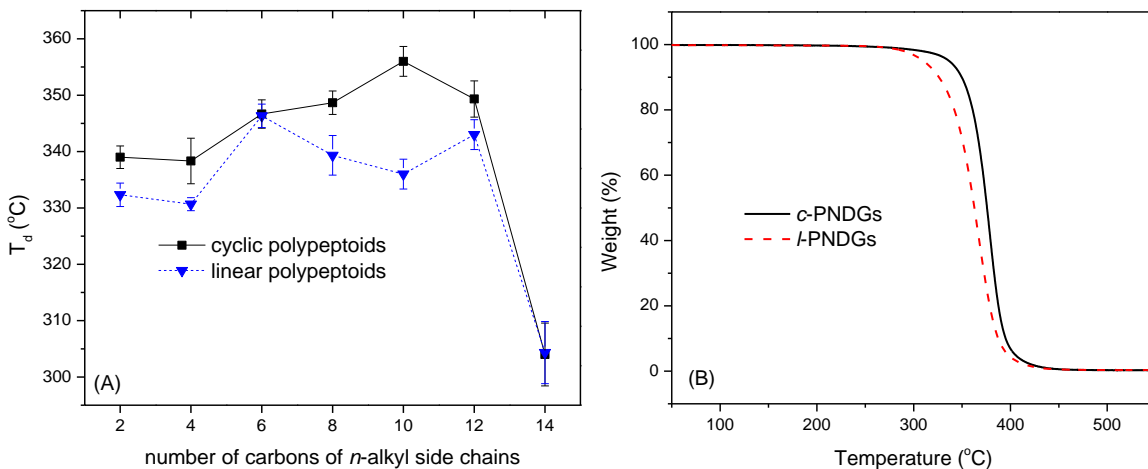


**Figure 4.16.** (A) Decomposition temperature ( $T_d$ ) of cyclic or linear polypeptoids with  $n$ -alkyl side chains as a function of the number of carbons on the side chains, (B) TGA of  $c$ -PNDGs and  $l$ -PNDGs.

## CHAPTER 5. CONCLUSIONS AND FUTURE WORK

It was demonstrated that NHC mediates the zwitterionic polymerization of decyl-NCA to afford *c*-PNDG with controlled molecular weights of polypeptoids and narrow PDI in section 2.1. The reaction exhibits characteristics of a controlled polymerization and has been successfully extended toward the synthesis of amphiphilic cyclic block copolypeptoids (i.e., *c*-PNMG-*b*-PNDG) by sequential addition of monomers. While the exact composition of the block copolypeptoids appears to deviate somewhat from the theoretical values, the relative PNMG and PNDG content in the amphiphilic block copolypeptoids can be adjusted by controlling the ratio of initial monomers to NHC and the conversion of polymerization. The synthesis of these block copolypeptoids sets the foundation for systematic investigations of their self-assembly properties in solution and in the solid state.

This new class of cyclic amphiphilic block copolymers exhibits a strong tendency toward aggregation, forming discrete supramolecular assemblies. Section 2.2 presented the self-assembly of cyclic or linear PNMG-*b*-PNDG diblock copolypeptoids in dilute methanol solution. The particular amphiphilic diblock copolypeptoid, PNMG<sub>105</sub>-*b*-PNDG<sub>10</sub>, forms spherical micelles which evolve to cylindrical micelles. SAED and microDSC studies on the copolymers in dilute solution reveal that the formation of cylindrical micelles is attributed to crystallization of core-forming, hydrophobic PNDG segments. Variable-temperature <sup>1</sup>H NMR spectroscopic analysis of the diluted copolymer solution also suggests morphological changes of the self-assembled structures upon heating. Cryo-TEM at high temperature would be important to reveal morphologies formed from the copolymers in methanol at high temperature. Our current investigations also include studies on self-assembly of the copolymers with different compositions in different solvents. For example, cyclic PNMG<sub>70</sub>-*b*-PNDG<sub>70</sub> diblock copolymers



form arrays of vesicle-like micelles with a diameter of about 150 nm in a mixture of methanol and chloroform (v:v, 1:3), revealed by TEM. Additionally, it would be important to expand this work to studies on self-assembly of the copolymers in aqueous solution for potential biological applications. The self-assembly of amphiphilic block copolypeptoids provides a means to access novel peptidomimetic materials of variable length scales and dynamics that are potentially useful for various biomedical applications, such as drug delivery carriers or bioactive coatings.

The PNMG-*b*-PNDG diblock copolymers further exhibit interesting macroscopic properties. Section 2.3 presents thermo-reversible gelation from the copolymers in methanol at an elevated concentration of 5 wt % or 10 wt %. Rheological studies show that cyclic copolypeptoids produce harder gels than their linear counterparts. Variable-temperature NMR studies on the gels suggest that temperature-induced reversible gelation is related to the transition of self-assembled morphologies formed from the copolymers upon heating. WAXS or SAXS of gels suggest that the formation of harder gels from cyclic copolymers is caused by more favors for them to form cylindrical micelles than linear ones and thus more transient networking among the cylindrical micelles. The formation of more cylindrical micelles may result from higher degree of crystallinity of cyclic copolymers in gels than linear ones, as revealed by WAXS analysis. Variable-temperature WAXS and SAXS experiments are current concerns to further probe the origin of formation and dissolution of gels upon cooling and heating. Additionally, neutron scattering would be a good tool to investigate self-assembled morphologies formed from the copolymers in gels. Finally, developing thermo-reversible hydrogels from amphiphilic block copolypeptoids is of our particular interest.

Chapter 3 presents initial work on the synthesis of cyclic triblock terpolypeptoids by NHC-mediated ring-opening polymerization via sequential addition of corresponding NCA

monomers. NMR spectroscopy shows that cyclic PNMG-PNAG-PNBnG and [P(NEG<sub>20</sub>-*ran*-NBG)<sub>15</sub>]-PNMG<sub>16</sub>-PNDG<sub>5</sub> with a NHC moiety attached to the copolymer backbone are successfully synthesized. SEC analysis suggests the triblock copolymer architecture of those synthesized polymers, as it shows that the polymer chains are extended by sequential addition of distinct monomers. Self-assembly of [P(NEG<sub>20</sub>-*ran*-NBG)<sub>15</sub>]-PNMG<sub>16</sub>-PNDG<sub>5</sub> with in water was studied. TEM and DLS results suggest that micelles with broad size distribution are formed below the  $T_{cp}$  of P(NEG<sub>20</sub>-*ran*-NBG)<sub>15</sub> blocks, and those micelles reorganize to form well-defined, micellar aggregates above the  $T_{cp}$ . Cryo-TEM would provide detailed and direct morphologies of this copolymer in water at different temperatures. Additionally, it would be interesting to study the effect of such parameters of polymer architecture, i.e. cyclic or linear, and molecular weights of the copolymers on their final morphologies in water.

Chapter 4 presents systematic studies on crystallization and melting behavior of cyclic or linear polypeptoids with various alkyl side chains. DSC results reveal that polypeptoids possessing butyl or longer, pendent groups have two distinct melting transitions. A low-temperature melting point ( $T_{m,1}$ ) of the polypeptoids increased and high-temperature melting point ( $T_{m,2}$ ) decreased, as the length of the side chains increased.  $T_{m,1}$  is attributed to side chain melting, and  $T_{m,2}$  to main chain melting. Additionally, DSC analysis reveals that cyclic polypeptoids have higher  $T_{m,2}$  than their linear counterparts, suggesting that polymer architecture affects the melting and crystallization of polypeptoids main chains. WAXS studies further reveal that polypeptoids with butyl or longer alkyl side chains are well ordered. Their molecular packing is proposed such that polymer chains are arranged in the layers, and the layers are separated by the distance of side chains. The arrangement of the polymers in the layer can be distorted between  $T_{m,1}$  and  $T_{m,2}$ , as the mobility of the side chains increases. DSC and WAXS on

polypeptoids with branched side chains further suggest that asymmetrically branched side chains strongly inhibit the crystallization of polypeptoids. In this study, it was found that crystallization and melting properties of this, peptidomimetic polymer are strongly affected by length and structure of alkyl side chains. Our studies may provide a guideline to control the melting and crystallization of polypeptoids by varying alkyl side chains.

## REFERENCES

- (1) Dulbecco, R.; Vogt, M. *Proc. Natl. Acad. Sci. U. S. A.* **1963**, *50*, 236-243.
- (2) Vinograd, J.; Lebowitz, J.; Radloff, R.; Watson, R.; Laipis, P. *Proc. Natl. Acad. Sci. U. S. A.* **1965**, *53*, 1104.
- (3) Zimm, B. H.; Stockmayer, W. H. *J. Chem. Phys.* **1949**, *17*, 1301.
- (4) Douglas, J. F.; Freed, K. F. *Macromolecules* **1984**, *17*, 2344-2354.
- (5) Ohta, Y.; Masuoka, K.; Takano, A.; Matsushita, Y. *Phys. B* **2006**, *385*, 532-534.
- (6) Semlyen, E. *Cyclic polymers*; Springer Verlag, 2001.
- (7) Bielawski, C. W.; Benitez, D.; Grubbs, R. H. *Science* **2002**, *297*, 2041-2044.
- (8) Culkin, D.; Jeong, W.; Csihony, S.; Gomez, E.; Balsara, N.; Hedrick, J.; Waymouth, R. *Angew. Chem. Int. Ed.* **2007**, *46*, 2627-2630.
- (9) Guo, L.; Zhang, D. *J. Am. Chem. Soc.* **2009**, *131*, 18072-18074.
- (10) Minatti, E.; Borsali, R.; Schappacher, M.; Deffieux, A.; Soldi, V.; Narayanan, T.; Putaux, J.-L. *Macromol. Rapid Commun.* **2002**, *23*, 978-982.
- (11) Minatti, E.; Viville, P.; Borsali, R.; Schappacher, M.; Deffieux, A.; Lazzaroni, R. *Macromolecules* **2003**, *36*, 4125-4133.
- (12) Putaux, J.-L.; Minatti, E.; Lefebvre, C.; Borsali, R.; Schappacher, M.; Deffieux, A. *Faraday Discuss.* **2005**, *128*, 163-178.
- (13) Honda, S.; Yamamoto, T.; Tezuka, Y. *J. Am. Chem. Soc.* **2010**, *132*, 10251-10253.
- (14) Shin, E. J.; Jeong, W.; Brown, H. A.; Koo, B. J.; Hedrick, J. L.; Waymouth, R. M. *Macromolecules* **2011**, *44*, 2773-2779.
- (15) Nasongkla, N.; Chen, B.; Macaraeg, N.; Fox, M. E.; Fréchet, J. M. J.; Szoka, F. C. *J. Am. Chem. Soc.* **2009**, *131*, 3842-3843.
- (16) Chen, B.; Jerger, K.; Fréchet, J. M. J.; Szoka Jr, F. C. *J. Controlled Release* **2009**, *140*, 203-209.
- (17) Raskatov, J. A.; Hargrove, A. E.; So, A. Y.; Dervan, P. B. *J. Am. Chem. Soc.* **2012**, *134*, 7995-7999.
- (18) Laurent, B. A.; Grayson, S. M. *Chem. Soc. Rev.* **2009**, *38*, 2202-2213.

- (19) Geiser, D.; Höcker, H. *Macromolecules* **1980**, *13*, 653-656.
- (20) Laurent, B. A.; Grayson, S. M. *J. Am. Chem. Soc.* **2006**, *128*, 4238-4239.
- (21) Kricheldorf, H. R.; Lee, S.-R. *Macromolecules* **1995**, *28*, 6718-6725.
- (22) Bielawski, C. W.; Benitez, D.; Grubbs, R. H. *J. Am. Chem. Soc.* **2003**, *125*, 8424-8425.
- (23) Boydston, A. J.; Holcombe, T. W.; Unruh, D. A.; Frechet, J. M. J.; Grubbs, R. H. *J. Am. Chem. Soc.* **2009**, *131*, 5388-5389.
- (24) Boydston, A. J.; Xia, Y.; Kornfield, J. A.; Gorodetskaya, I. A.; Grubbs, R. H. *J. Am. Chem. Soc.* **2008**, *130*, 12775-12782.
- (25) Simon, R. J.; Kania, R. S.; Zuckermann, R. N.; Huebner, V. D.; Jewell, D. A.; Banville, S.; Ng, S.; Wang, L.; Rosenberg, S.; Marlowe, C. K. *Proc. Natl. Acad. Sci.* **1992**, *89*, 9367-9371.
- (26) Miller, S. M.; Simon, R. J.; Ng, S.; Zuckermann, R. N.; Kerr, J. M.; Moos, W. H. *Bioorg. Med. Chem. Lett.* **1994**, *4*, 2657-2662.
- (27) Miller, S. M.; Simon, R. J.; Ng, S.; Zuckermann, R. N.; Kerr, J. M.; Moos, W. H. *Drug Dev. Res.* **2004**, *35*, 20-32.
- (28) Hara, T.; Durell, S. R.; Myers, M. C.; Appella, D. H. *J. Am. Chem. Soc.* **2006**, *128*, 1995-2004.
- (29) Kwon, Y.; Kodadek, T. *J. Am. Chem. Soc.* **2007**, *129*, 1508-1509.
- (30) Zuckermann, R. N.; Kerr, J. M.; Kent, S. B. H.; Moos, W. H. *J. Am. Chem. Soc.* **1992**, *114*, 10646-10647.
- (31) Fowler, S. A.; Blackwell, H. E. *Org. Biomol. Chem.* **2009**, *7*, 1508-1524.
- (32) Waley, S. G.; Watson, J. *J. Am. Chem. Soc.* **1948**, *70*, 2299-2300.
- (33) Waley, S.; Watson, J. *Proc. R. Soc. A Mathematical and Physical Sciences* **1949**, *199*, 499-517.
- (34) Zhang, Y.; Wang, G.; Huang, J. *J. Polym. Sci., Part A: Polym. Chem.*
- (35) Fetsch, C.; Grossmann, A.; Holz, L.; Nawroth, J. F.; Luxenhofer, R. *Macromolecules* **2011**, *44*, 6746-6758.
- (36) Zhang, D.; Lahasky, S. H.; Guo, L.; Lee, C.-U.; Lavan, M. *Macromolecules* **2012**, *45*, 5833-5841.

- (37) Sun, H.; Zhang, J.; Liu, Q.; Yu, L.; Zhao, J. *Angew. Chem. Int. Ed.* **2007**, *46*, 6068-6072.
- (38) Jia, L.; Sun, H.; Shay, J. T.; Allgeier, A. M.; Hanton, S. D. *J. Am. Chem. Soc.* **2002**, *124*, 7282-7283.
- (39) Lin, S.; Zhang, B.; Skoumal, M. J.; Ramunno, B.; Li, X.; Wesdemiotis, C.; Liu, L.; Jia, L. *Biomacromolecules* **2011**, *12*, 2573-2582.
- (40) Liu, G.; Jia, L. *Angew. Chem. Int. Ed.* **2006**, *45*, 129-131.
- (41) Chai, J.; Liu, G.; Chaicharoen, K.; Wesdemiotis, C.; Jia, L. *Macromolecules* **2008**, *41*, 8980-8985.
- (42) Shah, N. H.; Butterfoss, G. L.; Nguyen, K.; Yoo, B.; Bonneau, R.; Rabenstein, D. L.; Kirshenbaum, K. *J. Am. Chem. Soc.* **2008**, *130*, 16622-16632.
- (43) Wu, C. W.; Sanborn, T. J.; Zuckermann, R. N.; Barron, A. E. *J. Am. Chem. Soc.* **2001**, *123*, 2958-2963.
- (44) Wu, C. W.; Sanborn, T. J.; Huang, K.; Zuckermann, R. N.; Barron, A. E. *J. Am. Chem. Soc.* **2001**, *123*, 6778-6784.
- (45) Guo, L.; Li, J.; Brown, Z.; Ghale, K.; Zhang, D. *J. Pept. Sci.* **2011**, *96*, 596-603.
- (46) Murnen, H. K.; Rosales, A. M.; Jaworski, J. N.; Segalman, R. A.; Zuckermann, R. N. *J. Am. Chem. Soc.* **2010**, *132*, 16112-16119.
- (47) Nam, K.; Shelby, S.; Choi, P.; Marciel, A.; Chen, R.; Tan, L.; Chu, T.; Mesch, R.; Lee, B.; Connolly, M. *Nat. Mater.* **2010**, *9*, 454-460.
- (48) Rosales, A.; Murnen, H.; Zuckermann, R.; Segalman, R. *Macromolecules* **2010**, *43*, 5627-5636.
- (49) Bates, F. S.; Fredrickson, G. H. *Annu. Rev. Phys. Chem.* **1990**, *41*, 525.
- (50) Bates, F. S.; Fredrickson, G. *Phys. Today. February 1999*, *32* **2000**, 38.
- (51) Eastwood, E.; Viswanathan, S.; O'brien, C.; Kumar, D.; Dadmun, M. *Polymer* **2005**, *46*, 3957-3970.
- (52) Hiemenz, P.; Lodge, T. *Polymer Chemistry*; 2nd ed.; CRC Press, 2007.
- (53) Israelachvili, J. N. *Intermolecular and surface forces: revised third edition*; Academic press, 2011.

- (54) Rodriguez-Hernandez, J.; Chécot, F.; Gnanou, Y.; Lecommandoux, S. *Prog. Polym. Sci.* **2005**, *30*, 691-724.
- (55) Jain, S.; Bates, F. S. *Macromolecules* **2004**, *37*, 1511-1523.
- (56) Hayward, R. C.; Pochan, D. J. *Macromolecules* **2010**, *43*, 3577-3584.
- (57) Cui, H.; Chen, Z.; Zhong, S.; Wooley, K. L.; Pochan, D. J. *Science* **2007**, *317*, 647-650.
- (58) Wang, X.; Guerin, G.; Wang, H.; Wang, Y.; Manners, I.; Winnik, M. *Science* **2007**, *317*, 644.
- (59) Lescanec, R. L.; Hajduk, D. A.; Kim, G. Y.; Gan, Y.; Yin, R.; Gruner, S. M.; Hogen-Esch, T. E.; Thomas, E. L. *Macromolecules* **1995**, *28*, 3485-3489.
- (60) Yin, R.; Hogen-Esch, T. E. *Macromolecules* **1993**, *26*, 6952-6957.
- (61) Zhu, Y.; Gido, S. P.; Iatrou, H.; Hadjichristidis, N.; Mays, J. W. *Macromolecules* **2002**, *36*, 148-152.
- (62) Eugene, D. M.; Grayson, S. M. *Macromolecules* **2008**, *41*, 5082-5084.
- (63) Poelma, J. E.; Ono, K.; Miyajima, D.; Aida, T.; Satoh, K.; Hawker, C. J. *ACS Nano* **2012**, *6*, 10845-10854.
- (64) Shin, S.; Yoo, B.; Todaro, L.; Kirshenbaum, K. *J. Am. Chem. Soc.* **2007**, *129*, 3218-3225.
- (65) Holub, J.; Jang, H.; Kirshenbaum, K. *Org. Lett.* **2007**, *9*, 3275-3278.
- (66) Lahasky, S. H.; Hu, X.; Zhang, D. *ACS Macro Lett.* **2012**, *1*, 580-584.
- (67) Arduengo III, A. J.; Krafczyk, R.; Schmutzler, R.; Craig, H. A.; Goerlich, J. R.; Marshall, W. J.; Unverzagt, M. *Tetrahedron* **1999**, *55*, 14523-14534.
- (68) Tang, H.; Zhang, D. *Biomacromolecules* **2010**, *11*, 1585-1592.
- (69) Li, X.; Guo, L.; Casiano-Maldonado, M.; Zhang, D.; Wesdemiotis, C. *Macromolecules* **2011**, *44*, 4555-4564.
- (70) Raynaud, J.; Absalon, C.; Gnanou, Y.; Taton, D. *J. Am. Chem. Soc.* **2009**, *131*, 3201-3209.
- (71) Cao, L.; Manners, I.; Winnik, M. *Macromolecules* **2002**, *35*, 8258-8260.
- (72) Gilroy, J. B.; Gädt, T.; Whittell, G. R.; Chabanne, L.; Mitchels, J. M.; Richardson, R. M.; Winnik, M. A.; Manners, I. *Nat Chem* **2010**, *2*, 566-570.

- (73) Massey, J. A.; Temple, K.; Cao, L.; Rharbi, Y.; Raez, J.; Winnik, M. A.; Manners, I. *J. Am. Chem. Soc.* **2000**, *122*, 11577-11584.
- (74) Wang, X.; Guerin, G.; Wang, H.; Wang, Y.; Manners, I.; Winnik, M. A. *Science* **2007**, *317*, 644-647.
- (75) Patra, S. K.; Ahmed, R.; Whittell, G. R.; Lunn, D. J.; Dunphy, E. L.; Winnik, M. A.; Manners, I. *J. Am. Chem. Soc.* **2011**, *133*, 8842-8845.
- (76) Petzetakis, N.; Dove, A. P.; O'Reilly, R. K. *Chem. Sci.* **2011**, *2*, 955-960.
- (77) Mathisen, H.; Norman, N. *Acta Chem. Scand.* **1972**, *26*, 3913-3916.
- (78) Tiktopulo, E. I.; Bychkova, V. E.; Ricka, J.; Ptitsyn, O. B. *Macromolecules* **1994**, *27*, 2879-2882.
- (79) Ding, Y.; Ye, X.; Zhang, G. *Macromolecules* **2005**, *38*, 904-908.
- (80) Robertson, A. D.; Murphy, K. P. *Chem. Rev.* **1997**, *97*, 1251-1268.
- (81) Blanz, A.; Verber, R.; Mykhaylyk, O. O.; Ryan, A. J.; Heath, J. Z.; Douglas, C. W. I.; Armes, S. P. *J. Am. Chem. Soc.* **2012**, *134*, 9741-9748.
- (82) Ferry, J. D. *Viscoelastic properties of polymers*; Wiley: New York, 1980; Vol. 3.
- (83) Appel, E. A.; del Barrio, J.; Loh, X. J.; Scherman, O. A. *Chem. Soc. Rev.* **2012**, *41*, 6195-6214.
- (84) Appel, E. A.; Loh, X. J.; Jones, S. T.; Biedermann, F.; Dreiss, C. A.; Scherman, O. A. *J. Am. Chem. Soc.* **2012**, *134*, 11767-11773.
- (85) Hoffman, A. *Adv. Drug Delivery Rev.* **2002**, *54*, 3-12.
- (86) Zhou, C.; Hillmyer, M. A.; Lodge, T. P. *J. Am. Chem. Soc.* **2012**, *134*, 10365-10368.
- (87) Weng, W.; Beck, J. B.; Jamieson, A. M.; Rowan, S. J. *Journal of the American Chemical Society* **2006**, *128*, 11663-11672.
- (88) Buerkle, L. E.; Rowan, S. J. *Chem. Soc. Rev.* **2012**, *41*, 6089-6102.
- (89) Jeong, B.; Kim, S.; Bae, Y. *Adv. Drug Delivery Rev.* **2002**, *54*, 37-54.
- (90) Peppas, N. A.; Hilt, J. Z.; Khademhosseini, A.; Langer, R. *Adv. Mater.* **2006**, *18*, 1345-1360.
- (91) Huynh, C. T.; Nguyen, M. K.; Lee, D. S. *Macromolecules* **2011**, *44*, 6629-6636.



- (92) He, C.; Kim, S. W.; Lee, D. S. *J. Controlled Release* **2008**, *127*, 189-207.
- (93) Ward, M. A.; Georgiou, T. K. *Polymers* **2011**, *3*, 1215-1242.
- (94) Mortensen, K.; Pedersen, J. S. *Macromolecules* **1993**, *26*, 805-812.
- (95) Jeong, B.; Bae, Y. H.; Lee, D. S.; Kim, S. W. *Nature* **1997**, *388*, 860-862.
- (96) Jeong, B.; Bae, Y. H.; Kim, S. W. *Macromolecules* **1999**, *32*, 7064-7069.
- (97) Kim, M. S.; Hyun, H.; Khang, G.; Lee, H. B. *Macromolecules* **2006**, *39*, 3099-3102.
- (98) Jiang, X.; Jin, S.; Zhong, Q.; Dadmun, M. D.; Zhao, B. *Macromolecules* **2009**, *42*, 8468-8476.
- (99) Nguyen, M. K.; Park, D. K.; Lee, D. S. *Biomacromolecules* **2009**, *10*, 728-731.
- (100) Nečas, D.; Klapetek, P. *Cent. Eur. J. Phys.* **2012**, *10*, 181-188.
- (101) Kumar, R.; Kalur, G. C.; Ziserman, L.; Danino, D.; Raghavan, S. R. *Langmuir* **2007**, *23*, 12849-12856.
- (102) Glatter, O.; Kratky, O. *In Small angle X-ray scattering*; Academic Press: London, 1982.
- (103) Guinier, A.; Fournet, G. *Small Angle Scattering of X-rays*; Wiley: New York, 1955.
- (104) Terech, P.; Coutin, A.; Giroud-Godquin, A. *J. Phys. Chem. B* **1997**, *101*, 6810-6818.
- (105) Li, Z.; Buerkle, L. E.; Orseno, M. R.; Streletzky, K. A.; Seifert, S.; Jamieson, A. M.; Rowan, S. J. *Langmuir* **2010**, *26*, 10093-10101.
- (106) Hadjichristidis, N.; Iatrou, H.; Pitsikalis, M.; Pispas, S.; Avgeropoulos, A. *Prog. Polym. Sci.* **2005**, *30*, 725-782.
- (107) Bates, F. S.; Hillmyer, M. A.; Lodge, T. P.; Bates, C. M.; Delaney, K. T.; Fredrickson, G. H. *Science* **2012**, *336*, 434-440.
- (108) Kubowicz, S.; Baussard, J. F.; Lutz, J. F.; Thünemann, A. F.; von Berlepsch, H.; Laschewsky, A. *Angew. Chem. Int. Ed.* **2005**, *44*, 5262-5265.
- (109) Sun, G.; Cui, H.; Lin, L. Y.; Lee, N. S.; Yang, C.; Neumann, W. L.; Freskos, J. N.; Shieh, J. J.; Dorshow, R. B.; Wooley, K. L. *J. Am. Chem. Soc.* **2011**, *133*, 8534-8543.
- (110) Marsat, J. N.; Heydenreich, M.; Kleinpeter, E.; Berlepsch, H.; Böttcher, C.; Laschewsky, A. *Macromolecules* **2011**.

- (111) Betthausen, E.; Drechsler, M.; Förtsch, M.; Schacher, F. H.; Müller, A. H. E. *Soft Matter* **2011**, *7*, 8880-8891.
- (112) Moughton, A. O.; Hillmyer, M. A.; Lodge, T. P. *Macromolecules* **2011**, *45*, 2-19.
- (113) Mao, J.; Ni, P.; Mai, Y.; Yan, D. *Langmuir* **2007**, *23*, 5127-5134.
- (114) Li, Z.; Hillmyer, M. A.; Lodge, T. P. *Macromolecules* **2004**, *37*, 8933-8940.
- (115) Li, Z.; Hillmyer, M. A.; Lodge, T. P. *Langmuir* **2006**, *22*, 9409-9417.
- (116) Li, Z.; Kesselman, E.; Talmon, Y.; Hillmyer, M. A.; Lodge, T. P. *Science* **2004**, *306*, 98.
- (117) Lodge, T. P.; Rasdal, A.; Li, Z.; Hillmyer, M. A. *J. Am. Chem. Soc.* **2005**, *127*, 17608-17609.
- (118) Pantazis, D.; Schulz, D. N.; Hadjichristidis, N. *J. Polym. Sci., Part A: Polym. Chem.* **2002**, *40*, 1476-1483.
- (119) Zhou, C.; Hillmyer, M. A.; Lodge, T. P. *Macromolecules* **2011**, *44*, 1635-1641.
- (120) Greenberg, S. A.; Alfrey, T. *J. Am. Chem. Soc.* **1954**, *76*, 6280-6285.
- (121) Ballauff, M. *Angew. Chem. Int. Ed.* **1989**, *28*, 253-267.
- (122) Lee, J. L.; Pearce, E. M.; Kwei, T. K. *Macromolecules* **1997**, *30*, 6877-6883.
- (123) Steuer, M.; Hörth, M.; Ballauff, M. *J. Polym. Sci., Part A: Polym. Chem.* **1993**, *31*, 1609-1619.
- (124) Watanabe, J.; Ono, H.; Uematsu, I.; Abe, A. *Macromolecules* **1985**, *18*, 2141-2148.
- (125) Ballauff, M.; Schmidt, G. F. *Makromol Chem-Rapid* **1987**, *8*, 93-97.
- (126) Kricheldorf, H. R.; Domschke, A. *Macromolecules* **1994**, *27*, 1509-1516.
- (127) Watanabe, J.; Harkness, B. R.; Sone, M.; Ichimura, H. *Macromolecules* **1994**, *27*, 507-512.
- (128) Duran, R.; Ballauff, M.; Wenzel, M.; Wegner, G. *Macromolecules* **1988**, *21*, 2897-2899.
- (129) Kricheldorf, H. R.; Domschke, A. *Macromolecules* **1996**, *29*, 1337-1344.
- (130) Rodriguez-Parada, J. M.; Duran, R.; Wegner, G. *Macromolecules* **1989**, *22*, 2507-2516.
- (131) Chen, S. A.; Ni, J. M. *Macromolecules* **1992**, *25*, 6081-6089.

- (132) Hsu, W. P.; Levon, K.; Ho, K. S.; Myerson, A. S.; Kwei, T. K. *Macromolecules* **1993**, *26*, 1318-1323.
- (133) Causin, V.; Marega, C.; Marigo, A.; Valentini, L.; Kenny, J. M. *Macromolecules* **2004**, *38*, 409-415.
- (134) Prosa, T. J.; Winokur, M. J.; Moulton, J.; Smith, P.; Heeger, A. J. *Macromolecules* **1992**, *25*, 4364-4372.
- (135) Zheng, W.-Y.; Levon, K.; Laakso, J.; Oesterholm, J.-E. *Macromolecules* **1994**, *27*, 7754-7768.
- (136) La Campa, D.; González, J.; Barrales-Rienda, J.; Ramos, J. G. *J. Polym. Sci., Polym. Phys.* **1980**, *18*, 2197-2207.
- (137) Pankaj, S.; Beiner, M. *Soft Matter* **2010**, *6*, 3506-3516.
- (138) Wu, Z.; Petzold, A.; Henze, T.; Thurn-Albrecht, T.; Lohwasser, R. H.; Sommer, M.; Thelakkat, M. *Macromolecules* **2010**, *43*, 4646-4653.
- (139) Yuan, Y.; Zhang, J.; Sun, J.; Hu, J.; Zhang, T.; Duan, Y. *Macromolecules* **2011**, *44*, 9341-9350.
- (140) Lee, C. U.; Smart, T. P.; Guo, L.; Epps III, T. H.; Zhang, D. *Macromolecules* **2011**, *44*, 9574-9585.

## VITA

Chang-Uk Lee was born in Busan, South Korea. He attended Pusan National University in Busan, South Korea, and received a B.S. degree in 2004 with a major in Polymer Science and Engineering. He then joined the graduate program in the Materials Science and Engineering Department at the University of Tennessee, Knoxville in August, 2004. He conducted graduate research in the Chemistry Department under the direction of Professor Mark Dadmun. He successfully defended his Master thesis in November, 2006, and received an M.S. degree with a major in Polymer Engineering in the Materials Science and Engineering Department in December, 2006. He then joined the graduate program for his Ph.D. degree in the Chemistry Department at Louisiana State University in August, 2008. He conducted graduate research under the supervision of Professor Donghui Zhang, and successfully defended this Ph.D. dissertation on March 28, 2013.